PHD

An evaluation of cold expansion methods used for improving the fatigue life of fastener holes in aerospace aluminum alloy 7075-T6

Chakherlou, Tajbakhsh Navid

Award date:
2002

Awarding institution:
University of Bath

An evaluation of cold expansion methods used for improving the fatigue life of fastener holes in aerospace aluminium alloy 7075-T6

Submitted by Tajbakhsh Navid Chakherlou

for the degree of

Doctor of Philosophy

of the University of Bath

2002

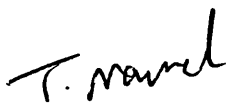

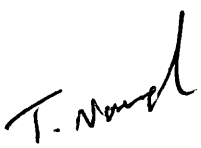

ProQuest LLC
789 East Eisenhower Parkway
P.O. Box 1346
Ann Arbor, MI 48106-1346

Summary

A theoretical study of the distribution of tangential residual stresses around a cold expanded hole has been carried out using FE analysis and their effect on fatigue life improvement has been investigated by fatigue testing.

In the theoretical study a number of FE models have been developed to simulate the expansion of a 5 mm diameter hole in aluminium alloy 7075-T6. In order to study the effect of different cold expansion methods on the tangential residual stress around the hole it was expanded using 2-D axisymmetric models loaded by uniform radial displacement, ballising and using a tapered pin.

Also the research has investigated the effect of a sleeve slit on the tangential residual stress distribution for three developed 3-D models. In these models cold expansion was simulated using a tapered pin with mating split sleeve, a tapered pin with parallel split sleeve and a taper pin without a sleeve. These 3-D FE models accurately simulated the cold expansion techniques that were practically performed. In addition to creating residual stress in the models, the distribution of longitudinal stress around the hole was studied due to a remote longitudinal load. To verify the validity of the simulations, the pin pushing forces were calculated and compared with their corresponding practical results.

In the experimental part of the study the holes in the 6.32 mm thick fatigue specimens were cold expanded with a nominal interference of 4.6% using three techniques as mentioned previously. The cold expanded specimens, and also the "as drilled" specimens were fatigue tested to investigate the efficiency of the techniques in improving fatigue life. Also the fractured sections of the specimens were studied after the fatigue tests to identify the fatigue crack initiation and propagation regions.

It was found that fatigue life improvement and also crack initiation and propagation were related to the tangential residual stress distribution which itself depends on the cold expansion method, the plate thickness and the interference amount.

Acknowledgement

I would like to sincerely thank the people who helped me during the last three years of my research especially my wife and my daughter who shared with me in the difficulties, also my parents who encouraged me constantly. Particular thanks must go to my supervisor, Dr. Jeff Vogwell, who has always been approachable and willing to advise.

Also thanks to John Fortune and John Perry, the Mechanical Engineering Workshop Technicians, who patiently prepared my test specimens. I would like to thank Chris Arnold and Richard Weston, Structural Lab. Technicians of the Engineering Department who instructed and helped me using the testing machines.

Also many thanks to Prof. G. W. Hunt, Head of Structural Mechanics and Biomechanics group, who helped by giving me scientific advise and arranging for me to use the Mechanical Engineering Department facilities.

Contents

List of Tables

List of Figures

Nomenclature

a	Hole radius, mm
b	Half of a holed plate width, mm
d	Ball or tapered pin displacement, mm
D	Hole diameter before cold expansion, mm
d_p	Nominal tapered pin diameter, mm
E	Elasticity Modulus, N/mm^2
f	A factor for contact element stiffness
h	Characteristic contact length, mm
I	Interference amount, %
KN	Normal contact stiffness, N/mm
KT	Sliding stiffness, N/mm
l	Tapered pin length, mm
L_b	Nominal mating sleeve length, mm
L_p	Nominal tapered pin length, mm
L1	A norm name
L2	A norm name
n	exponent of Ramberg-Osgood equation
N	Number of cycle for fatigue fracture
p	Pin pushing force or tensile force, kN
P_a	Mean load applied in fatigue tests, kN
P_{max}	Maximum applied force in fatigue tests, kN
P_{min}	Minimum applied force in fatigue tests, kN
r	Ball radius or maximum radius of a tapered pin, mm
r1	Contact washer inner radius, mm
r2	Contact washer outer radius, mm
S	Tangential residual stress, MPa
S_x	Longitudinal stress in 3-D models and radial stress in 2-D models, MPa
T	Plate thickness, mm
T_b	Nominal mating sleeve wall thickness, mm
t_s	Sleeve wall thickness, mm
x	Radial distance from a hole edge, mm
y	Distance from hole edge in 3-D models, mm

u_x Radial displacement, mm

u_z Axial displacement, mm

δ Axial displacement of pin and specimen elongation in simple tension test, mm

ΔD Hole diameter enlargement after cold expansion, mm

Δu Uniform radial displacement of a hole, mm

$\Delta\varepsilon$ Strain range at hole edge, mm/mm

λ Element side length, mm

μ Coefficient of friction, N/N

ν Poisson's ratio

σ_x Remote stress, MPa

Chapter 1

Introduction

Mechanical joints incorporating pins, bolts or rivets through drilled holes are used extensively in structures particularly in aircraft. The joints created by these fasteners not only are easy to assemble and disassemble but also are able to support loads that are applied. However, such connections have a major vulnerability to fatigue because of the presence of the hole causes a stress concentration and in addition, machining causes surface roughness.

One way to compensate for this vulnerability and thus increase fatigue life is to introduce beneficial compressive residual stress around the hole. This can be achieved by cold expansion, for example, by inserting an oversized ball or tapered pin through a hole to create a plastic region then allowing the surrounding elastic region of the hole to spring back from the expanded state. During this process, because the plastically yielded material now offers less stiffness, it is deformed smaller and leaves compressive tangential residual stress around the hole. In addition, the surface of hole can be smoothed which may have a positive effect on fatigue life improvement.

Compressive residual stress around the hole is very useful in resisting fatigue because it reduces the resultant stress when the plate undergoes a tensile load. This is shown in fig 1.1 for a plate with an "as drilled" hole and compared a plate that was drilled and

then cold expanded to create residual stresses. In the "as drilled" hole, the maximum tensile stress is at the critical hole edge position whereas in the cold expanded hole the magnitude of the maximum tensile stress is reduced.

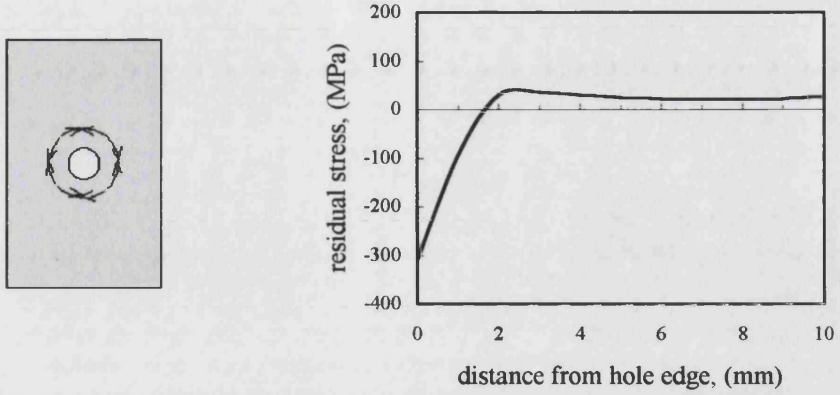

a) Tangential residual stress for a cold expanded hole

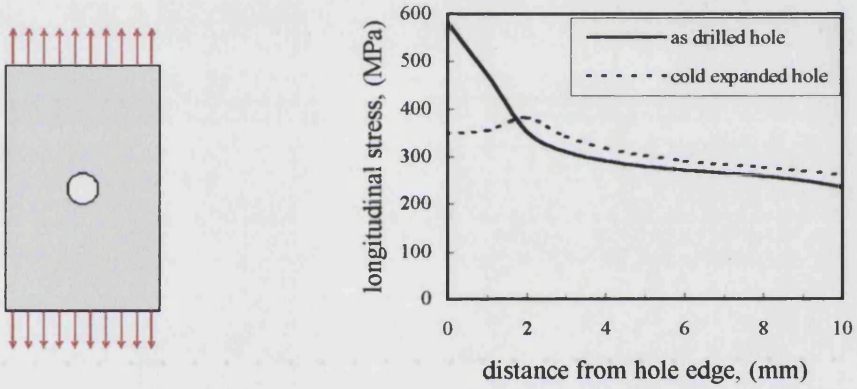

b) Holed plate under longitudinal load and stress distribution around hole

Fig 1.1: Effect of cold expansion in reducing stress at hole edge

Cold expansion can be achieved in several different ways. A common feature of most methods is to insert an oversized object from one side of the holed plate and remove from the other side. The main differences in methods relate to the shape of the oversized object and whether a sleeve is used in the hole during cold expansion. In most methods a tapered pin is used for the oversized object and in other methods a ball. Sometimes a lubricated solid or split sleeve is used to avoid direct pin contact because it is believed this causes surface damage to the hole.

Three different methods of cold expansion are shown schematically in fig 1.2. In the first method a ball is used (called ballising) [1, 2] whereas in the other two a tapered pin and parallel sleeve are used. These last two methods are almost the same and are used by two different companies. The method shown in fig 1.2 (b) is used by J.O. King. Inc. [3] and the method in fig 1.2 (c) is marketed by Fatigue Technology Inc. of Seattle, Washington [4]; it is called the FTI method and it is now used extensively in the aerospace industry.
Also there are other cold expansion methods such as the rolling burnish method and cold expanding by a pin without using a sleeve.

Despite cold expansion being widely used the full effects of the methods are not fully understood and this raises the following questions;

1) Does cold expansion always increase fatigue life and by how much?
2) What is the residual stress distribution around hole after cold expansion and is it uniform through the plate thickness?
3) Is residual stress distribution "method dependent"? For example, does cold expanding a hole by a ball or by a tapered pin produce different residual stress distributions?
4) What is the relation between the amount of interference and the resulting residual stress distribution?
5) Are residual stress distributions the same for different plate thicknesses?
6) Does friction have a negative or positive effect on the resulting tangential residual stress distribution and is it beneficial for fatigue life?
7) Is there any relation between fatigue life improvement and residual stress distribution?
8) What is the role of a sleeve and its slit on the residual stress distributions and pin pushing force?
9) Is there any relation between the tangential residual stress distribution and fatigue crack initiation and propagation?

There are answers to some of the above questions in technical publications and it is generally found that cold expansion does produce an improvement in fatigue life - which partly answers the first question only. In order to answer the second question mathematical, experimental and computational methods have been used by researchers to calculate or measure the residual stresses around a cold expanded hole.

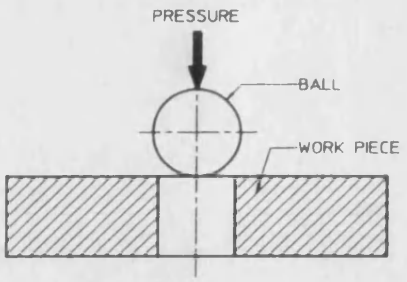

a) Ballising [1]

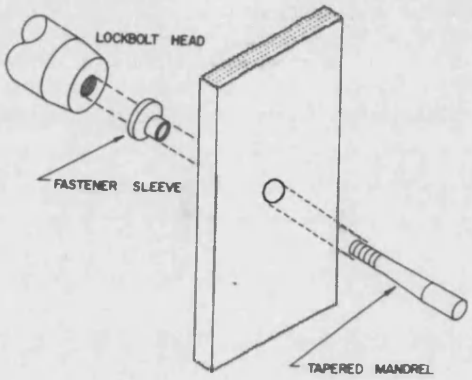

b) Tapered mandrel and sleeve used by J.O. King. Inc. [3]

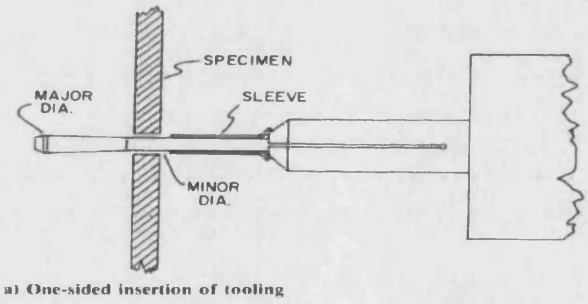

a) One-sided insertion of tooling

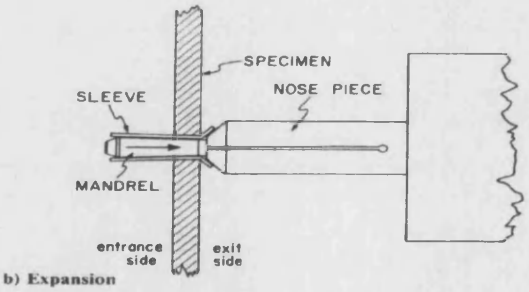

b) Expansion

c) Tapered mandrel and split sleeve used by FTI [4]

Fig 1.2: Different cold expansion methods

In calculating residual stresses mathematically a hole is assumed to be expanded by pressure or by radially displacing the hole, however, this assumption is far from what occurs in practice. In such calculations the holed plate is considered to be in a plane stress or plane strain state and different models are considered for different material stress-strain relationships (see Chapter 2). Another drawback of mathematical methods is that in considering small deformation theory for strains it avoids geometrical non-linearity. Small deformation theory is valid until about 5% of total strain, whereas, typically in cold expansion this strain is larger than 8% (depending on interference amount).

A second method of obtaining residual stresses is to use a fracture mechanic approach [5]. This method is practical but obtains only the average amount of residual stress in the plate thickness and so it does not give accurate local values or any information about residual stress variation through the plate thickness.

A third and practical method of measuring residual stress is proposed by Suchs [6, 7]. The residual stress distribution is measured for an area near the hole but not exactly at the hole edge. This method is considered better than the previous methods because it measures residual stresses through the plate thickness but is very expensive to apply.

A fourth method of calculating residual stresses is numerically using finite element analysis. This is a powerful technique and can cover different non-linearities and so it is not restricted to small deformations like mathematical methods. FE is less expensive than Suchs practical method and has the benefit of showing residual stress magnitudes at the hole edge.

In this research, FE modelling and experimental testing are carried out to answer most of the previously posed questions. In Chapter 3 residual stress distributions are determined for different cold expansion methods using axisymmetric models. These cold expansion methods are called uniform radial displacement, ballising and using a tapered pin. The uniform radial displacement model is the ideal situation and is chosen as a basis for comparing the other model results with. However, ballising and using a tapered pin are more practical methods (as will be described later). In Chapter

3 the effect of interference and plate thickness on the distribution of tangential residual stress is considered together with the cold expansion method. The models discussed in Chapter 3 have a support at the rim of the plate and are considered frictionless and sleeveless.

To cover the effects of plate support location, friction and using a sleeve on the distribution of residual stress, further models are described in Chapter 4. These models, like in chapter 3, are axisymmetric and are versions of cold expansion using a tapered pin. In addition to currently used methods of cold expansion, a new method (using tapered pin with mating sleeve) is also investigated.

Chapter 3 and Chapter 4 are concerned with simplified 2-D axisymmetric models, which give residual stress distributions quickly due to the small model sizes. However, such models have some disadvantages as mentioned later. To avoid the inherent disadvantages with axisymmetric models, 3-D models have been used also and are described in Chapter 5. In this chapter, which is a bridge between Chapters 3 and 4 and Chapter 6, three models of cold expansion (using a tapered pin with mating split sleeve, a tapered pin with parallel split sleeve and tapered pin without a sleeve) are investigated.

The experimental part of the research is included in Chapters 6 and 7 and these concentrate on practical cold expansion techniques and the fatigue tests. In Chapter 6 three cold expansion techniques (the ones in which their FE models were investigated in Chapter 5) are performed on aluminium alloy 7075-T6 holed plates using steel tapered pins and split sleeves. In addition, some mechanical property tests were carried out because their results were needed for the FE models and these are included in Chapter 6.

Having obtained the FE result for the distribution of tangential residual stress for the three techniques and performing them practically, fatigue tests were then carried out to investigate the efficiency of the various techniques in improving fatigue life. The fatigue test results for the specimens subjected to the three techniques together with "as drilled" fatigue specimens are given in Chapter 7 and the fatigue life improvements are compared. In addition, the fractured sections are examined to identify the crack initiation locations and propagation regions.

A general discussion of results and conclusions are given in Chapters 8 and 9 respectively.

It is found that cold expansion involves three nonlinearities - geometrical, material and boundary. Geometrical nonlinearity occurs due to large deformation and large strain [8-10], material nonlinearity is due to plasticity [11-20] and boundary nonelinearity due to interference [21-25]. In all models considered in this research the associative flow rule [12, 20] for the Von Mises yield criterion, which is called Prandtl-Reuss flow equation, is used. In this thesis, however except for some general features, these nonelinearity theories are not explained, although some references are made.

Chapter 2

A survey of previously conducted research into cold expansion of fastener holes

2.1) Introduction

A survey has been carried out of published research of cold expansion applied to fastener holes and shows the work in this area can be divided, for convenience, into four categories (although some of these categories overlapped with some of the research). These categories are:

1) Experimental fatigue life and crack retardation tests.
2) Experimental measurement of residual stresses and strains around a cold expanded hole.
3) Mathematical calculating of residual stresses.
4) Numerical modelling using the finite element method to evaluate residual stresses.

This chapter discusses the relevant research as categorised above.

2.2) Experimental research to show the benefit of cold expanded hole on fatigue life

Nopporn Chanawanich [3] studied the initiation and growth of fatigue cracks in 3 mm thick and 5 mm diameter cold expanded holes in aluminium 7075-T6 specimens.
He observed that with remote cyclic loading (causing local plasticity around the hole) a fatigue crack starts from just one edge of the hole edge in a non-cold worked specimen rather than starting simultaneously at both hole edges. However in the cold worked specimens, instead of a single crack, several cracks emanate from the hole

edges. These cracks start at the face where the cold expansion mandrel entered (entrance face) and developed though the plate thickness. During fatigue cracking the length of cracks at the exit face are shorter than at the mandrel entrance face.
In this research, in order to predict crack initiation, strains were measured at the hole edge using the Moiré technique in both cold expanded and non-cold expanded specimens. For predicting fatigue crack initiation life the method proposed by Smith and et al [26] was used. This is a strain based two-term power law as follows:

$$\frac{\Delta\varepsilon}{2} = .026(N)^{-.172} + 1.65(N)^{-1.29} \qquad 2.1$$

Nopporn Chanawanich's research showed that this law predicts fatigue life in non-cold worked specimens accurately, but predicts the fatigue life of cold worked specimen roughly an order of magnitude too large. Although this research shows that the cold working process affects crack growth rate but not crack initiation.

For improving the fatigue performance of a double-shear lap joint, experimental research has been conducted by L. Schwarmann [27]. In his research, different methods were investigated for preparing fastener holes (as used on airframe structures). The methods include the use of cylindrical and tapered fasteners, using clearance and interference fits in cold worked (cold expanded) and non-cold worked holes. Double-shear lap joints made from Al-alloy 2024-T3 were fatigue tested and the work concluded that:

- The installation of cylindrical fasteners with a clearance fit into non-cold-worked fastener holes should be avoided due to low fatigue life.
- Cold working of fastener holes or installing interference fit fasteners significantly improves fatigue performance.
- The improvement in fatigue life for cold worked holes under low alternating stress is greater than under higher alternating stress.

The effect on fatigue life of cold working as published by Schwarmann is shown in fig 2.1. In this figure the expansion interference λ=2.8% (later in this thesis I is used rather than λ) with no initial clearance μ=0%.

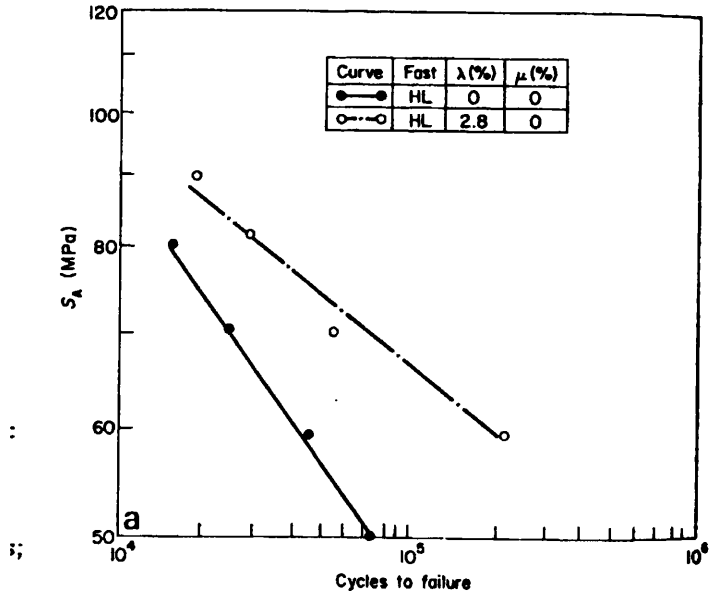

Fig 2.1: Influence of cold working on fatigue life as reported by Schwarmann [27]

Experimental work on fatigue properties of holes with residual stresses was carried out by M O Lai et al [2]. In this research residual stresses were induced in pre-machined holes using the ballising method in which a slightly oversized tungsten carbide ball was pushed (without rotation) through the holes (see fig 2.2).

The material used in their fatigue specimens was Assab 760 steel (a near equivalent to En 43). In this research a 4 mm diameter hole was drilled in 3 mm thick specimens and ballised with different interference amounts up to 3.5%.

The tangential residual stress was determined around the ballised hole using a fracture mechanics approach [5]. The residual stress distribution is shown in fig 2.3 for the cold expanded hole for three interference sizes (I=1%, 2.8%, 3.2%). According to this figure the compressive residual stress around the hole increases with increasing interference size.

Fatigue tests with a 20 kN mean load and 7.5 kN alternating load were conducted on both the ballised and unballised (i.e. as drilled) specimens. According to this research, in the ballised specimens the compressive tangential residual stress together with the improvement of the hole surface finish resulted in a significant increase in the fatigue life. As fig 2.4 shows, the fatigue life in the ballised hole specimen increases with increasing interference size.

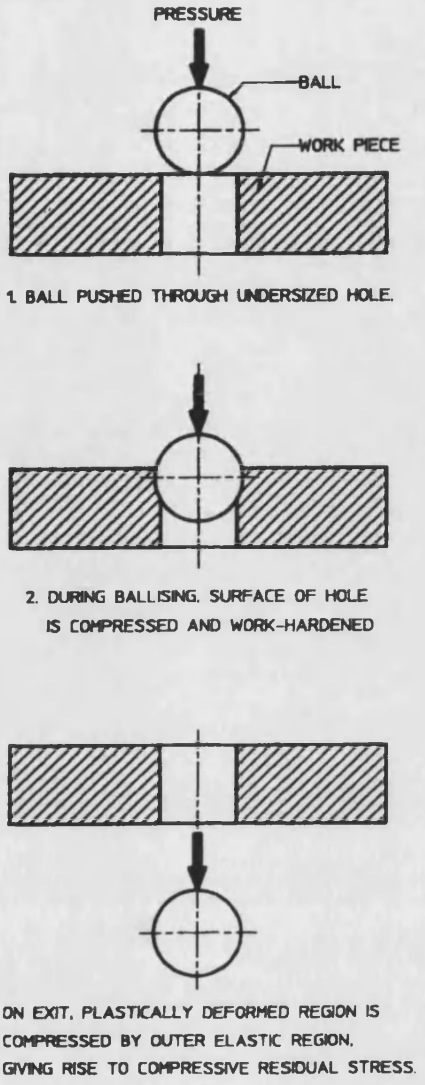

Fig 2.2: The ballising process [1]

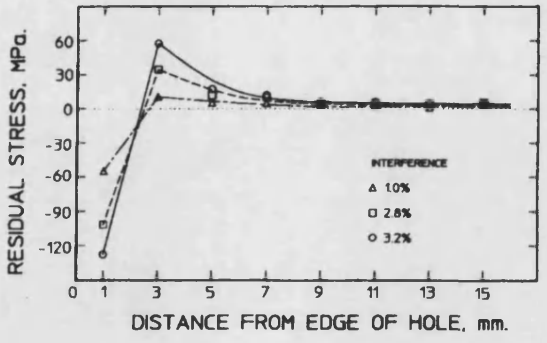

Fig 2.3: Tangential residual stress distribution around a ballised hole [1]

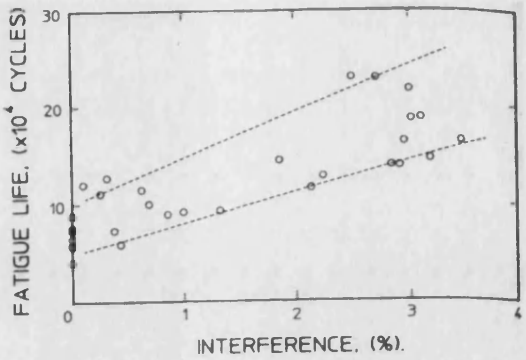

Fig 2.4: Fatigue lives of unballised and ballised holes with varying degree of interference [1]

Another piece of research carried out by M O Lai and Y H Siew [1] investigated how three different cold working processes (namely, shot peening, wet blasting and ballising) would affect the fatigue lives of holes. In this research the authors have used the same material and geometry specification for the specimens as their previously mentioned work.

According to this work, when the holes were cold worked by shot peening (with pressure from 138 kPa to 414 kPa) a fatigue life enhancement of about 30% to 100% was achieved. In the specimens that were cold worked by wet blasting (at pressure from 69 to 690 kPa) the fatigue life increased from 10% to 50%. The holes which were cold worked by ballising (with interferences between 1% to 3.3%) have shown that the fatigue life increases from about 60% to 220%.

In Lai and Siew research the tangential residual stresses around holes (as a result of the various cold working processes) were determined using the fracture mechanics approach. The results show that all of the three processes studied induced compressive residual stress fields at the hole surface. The tangential residual stress was compressive near the hole but it decreased and became tensile at a distance far from the hole surface.

The research also shows that compressive residual stress increases near the hole with increasing shot peening and wet blasting pressure. Also the magnitude increases with increasing interference size with ballising. For the range of pressure and interference size which the investigation considered, the compressive tangential residual stress magnitudes were greater due to ballising and lower due to wet blasting. This was clearly shown in the resulting fatigue lives of holed specimens with the same load as in their previous work.

2.3) Experimental research to measure the residual stresses and strains

Work to measure residual strains surrounding split sleeve cold expanded holes has been conducted by R. E. Link et al [4]. In this research, measurements of the residual displacement field surrounding cold expanded holes were made by using three optical techniques for strain analysis. The optical techniques used were Moiré interferometry (for areas far from the hole edge), Speckle photography and Micro-moiré (for areas near the hole edge).

The residual strain fields were computed from the displacement field data for two levels of cold expansion size (3% and 5%). Three typical hoop strain curves are shown in fig 2.5. The split sleeve cold expansion tests were carried out in 0.25 inch thick 7075-T651 aluminium alloy plates with hole diameters of 0.226 and 0.2308 inch.

The experimental results were compared with theoretical predictions of displacement and strain fields. The theory, which was used to compare with test results, was proposed by Nadai [31] who assumed elastic-perfect plastic behaviour for the material. The results show that the current theories do not accurately predict the residual strains. This maybe due to the three-dimensional nature of the split sleeve cold expansion process and the boundary condition of split sleeve.

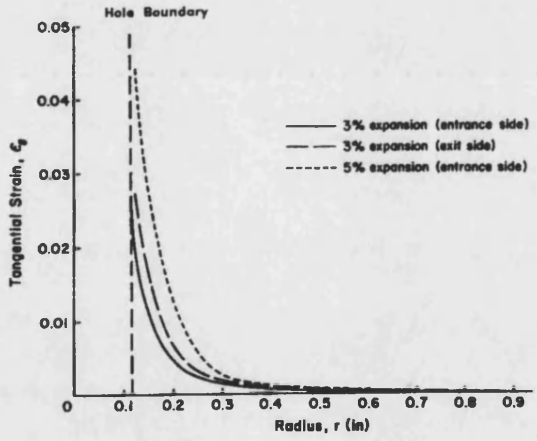

Fig 2.5: Tangential residual strains around cold expanded hole [4]

Another piece of experimental work was carried out by R. Herman [28] to measure residual stresses around a cold expanded hole. In this research aluminium alloy 6082

and aluminium-lithium alloy 8090 and 2091 were examined after 9 and 10 mm diameter holes were drilled and cold expanded by means of an oversized mandrel in plates with a thickness of 1.6 mm. The residual stresses (radial, axial and hoop) were measured by two techniques, neutron diffraction (ND) and the Sachs cutting method (SM). The ND technique is non-destructive and requires neutron diffraction facilities. The SM technique is destructive and is based on the removal of thin layers of material from the inside of the cold expanded hole while recording the apparent change in strains by the removal of the layer. With the SM technique the residual stresses were calculated using Hook's law to relate stresses and the measured strains around the hole.

In Hermans's research the stress analysed by ND (see fig 2.6) and SM (see fig 2.7) shows that the residual hoop stress is compressive near the hole and tensile far from the hole. However, the ND method underestimates the residual stress in comparison with the SM method near the hole.

According to Herman's research, in all alloys examined it was found that the improved fatigue performance was a function of the degree of expansion. All alloys exhibited a maximum expansion beyond which fatigue life deteriorated. He believed this was due to crack initiation during excessive hole enlargement exceeding the ultimate strength of the alloys. Crack initiation usually started from inside the fastener hole but was always perpendicular to the applied load.

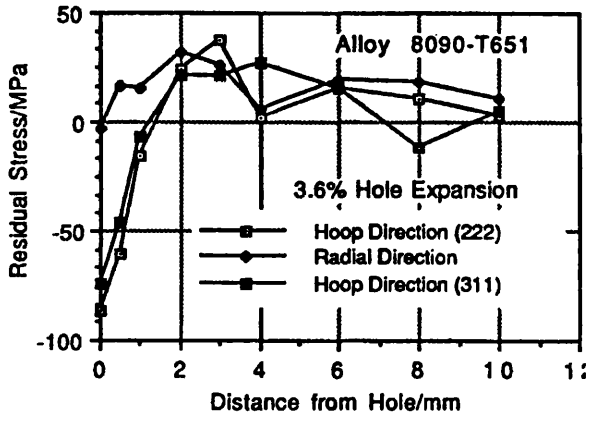

Fig 2.6: Stress distribution from cold expanding alloy 8090 by neutron diffraction [28]
(in this thesis hoop stress referred as tangential stress)

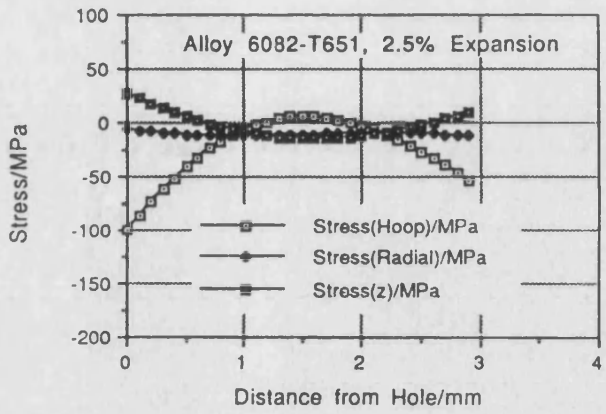

Fig 2.7: Stress distribution from cold expanding the alloy 6082 by the Sachs cutting method [28]

To measure the three-dimensional residual stress distribution around a split-sleeve used for cold expanding holes, A. T. Ozdemir et al [6] conducted experimental research. In this research the residual stress distribution around split sleeve cold expanded holes was measured using the Sachs method. The tests were conducted on 7050-T76 aluminium alloy plate with a thickness of 5 mm and with 9 mm diameter cold expanded holes. The research includes three cold expansion sizes (2%, 4% and 5%) and it was carried out using a tapered mandrel with a thin 0.2 mm pre-lubricated single slit sleeve (called the FTI method). In their research, in order to measure the relaxation of residual strains for the Sachs boring-out method, a 40 mm diameter washer was cut concentric to the cold expanded hole. The relaxation of the residual strains has been measured during material removal from the hole inside surface using strain gauges that were located in the hoop and transverse directions at the outer side of the washer. The residual stresses have been calculated from the residual strain relaxation using elastic material properties. The residual stress distributions have been determined through the plate thickness as well as the periphery of the hole and some are shown in figs 2.8 and 2.9. This experimental research shows that:

- The optimum cold expansion size using the FTI method is 4%.
- The residual stress distributions vary both through the thickness and around the periphery of cold expanded holes

- The smallest (absolute) peak compressive tangential residual stresses are near mandrel the entrance face (i.e. inlet).
- The weakest residual hoop stress distribution occurs at the hole edge by the location of the sleeve slit while the maximum compressive effect is at 90 degrees to this location. At the hole edge the split of the sleeve results in a local tensile residual stress.

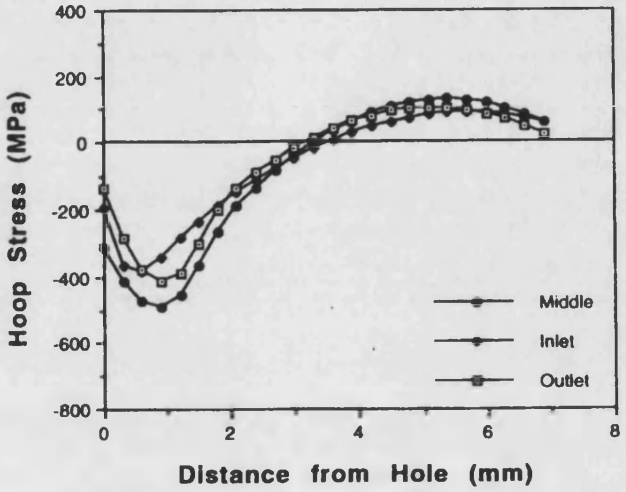

Fig 2.8: Residual hoop stress distributions for a 4% cold expanded hole [6]

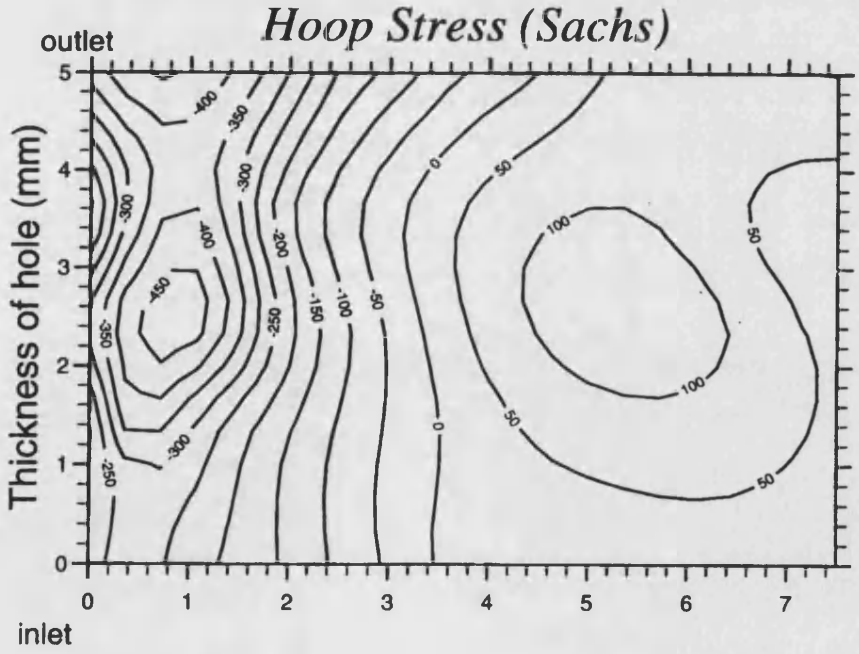

Fig 2.9: Contour map of residual hoop stresses (MPa) for a 4% expanded hole by Suchs. [6]

Ozdemir and Hermann [7] have also conducted research on the effect of the expansion technique and plate thickness on near-hole residual stresses and fatigue life of cold expanded holes. Residual stresses were produced at expanded holes (in several types of aluminium plate) by two different techniques: split sleeve (FTI) and roller burnishing (RB). The residual stresses have been determined using the destructive Sachs method. This research shows that the residual stress distribution (particularly in the vicinity of the hole) was different for the two cold expansion techniques although the cold expansion sizes were almost identical. The compressive residual hoop stress that was produced by the FTI method is more compressive (thus better) than the roller burnishing method near the hole surface. It was explained that this was because of the presence of a transverse friction force with the RB method that causes transverse plastic flow.

According to this practical work, after cold expansion, secondary reverse yielding causes stress relaxation and this reduces residual hoop stresses at the edge of the hole with a greater cold expansion size.

The authors stated that, "there is a cold expansion limit in which excessive cold expanding beyond that increase reverse yielding. S-N data revealed that no benefit was gained from expanding beyond this limit" (see figs 2.10 and 2.11). It was suggested that the reduction in the number of cycles to cause crack initiation, or more often to cause crack growth, was due to increased reversed yielding in the vicinity of the expanded hole. In this research the authors explain that with increasing thickness, the state of stress changes from plane stress to plane strain. Consequently, the residual stress produced after cold expansion become more compressive.

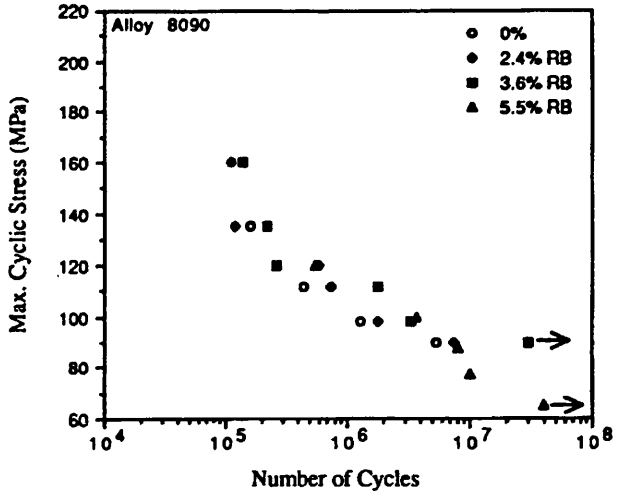

Fig 2.10: Improvement in fatigue life with roller burnishing expanded holes [7]

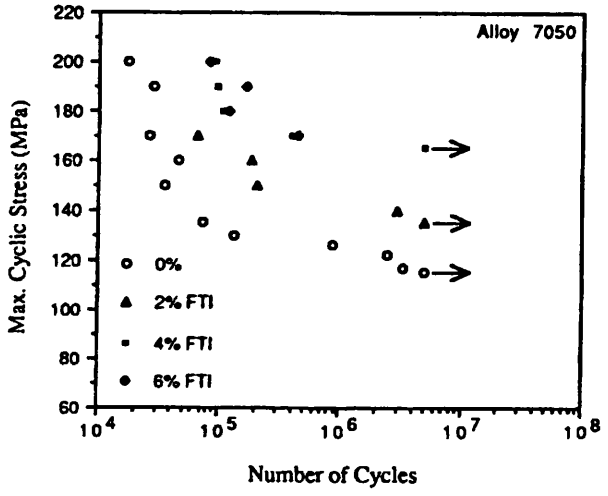

Fig 2.11: Improvement in fatigue life with split sleeve expanded holes presented by Ozdemir [7]

2.4) Mathematical research to calculate residual stress

Analysis of an infinite sheet having a circular hole under pressure was completed by Y. C. Hsu and R. G. Forman [29] In this mathematical study an elastic-plastic solution for the stresses around a hole (when subjected to pressure) was obtained using Von Mises deformation theory with a modified Ramberg-Osgood law for material stress and strain behaviour in simple tension (see fig 2.12). In this research, the sheet was considered orthotropic but isotropic in the radial plane (i.e. pressure direction). The

state of stress was considered plane stress and small deformation theory was used for the strain since displacements were considered to be small.

For the solution the authors separated the loaded sheet into two regions, one elastic and the other elastic plastic deformation region. The stress solution (for the elastic region) was obtained as a function of distance from the hole centre but the stress solution for the elastic-plastic deformation region is a function of a parameter α (see fig 2.13). There is no simple relation in the elastic-plastic region between the distance from the hole centre and the stress. Also the distance from the hole centre is itself a function of α, so stress components are related to distance from the hole centre by transcendental equations. After having obtained the solution for stress components, strain components have been obtained and the hole diameter enlargement was calculated corresponding to the applied pressure. In this research, by assuming that the material behaves elastically during unloading, the residual stresses also have been calculated (see fig 2.14).

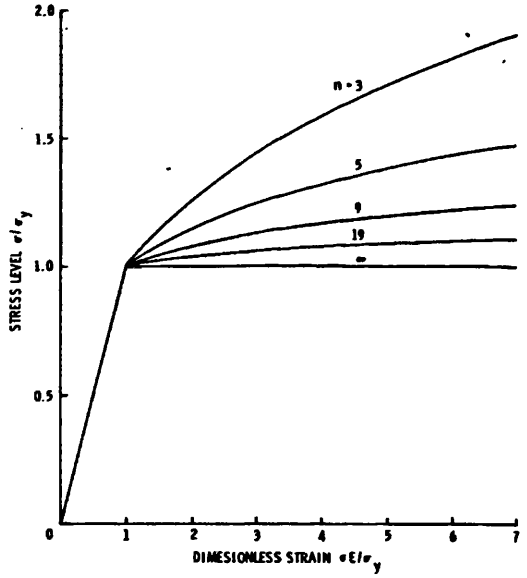

Fig 2.12: Ramberg-Osgood equation curves for material stress-strain behaviour [29]

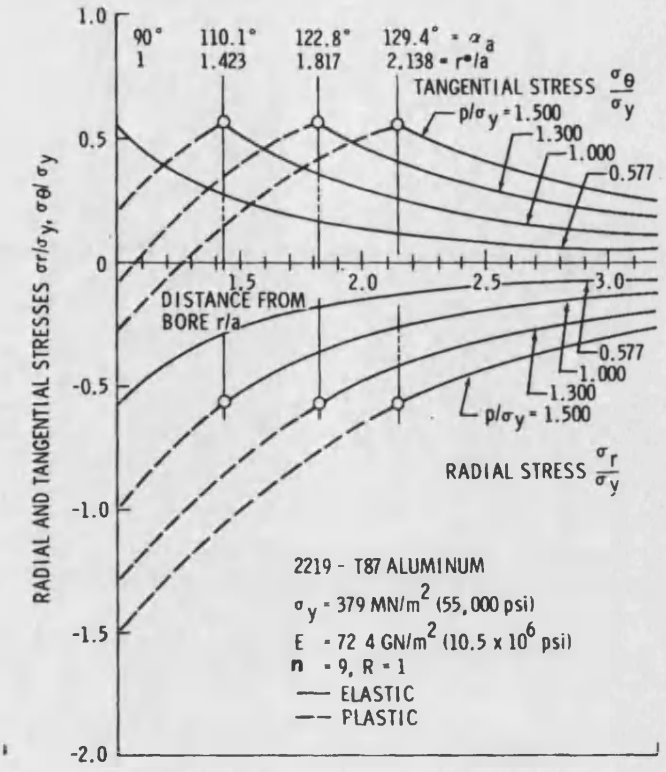

Fig 2.13: Stress distributions in a holed plate subjected to pressure [29]

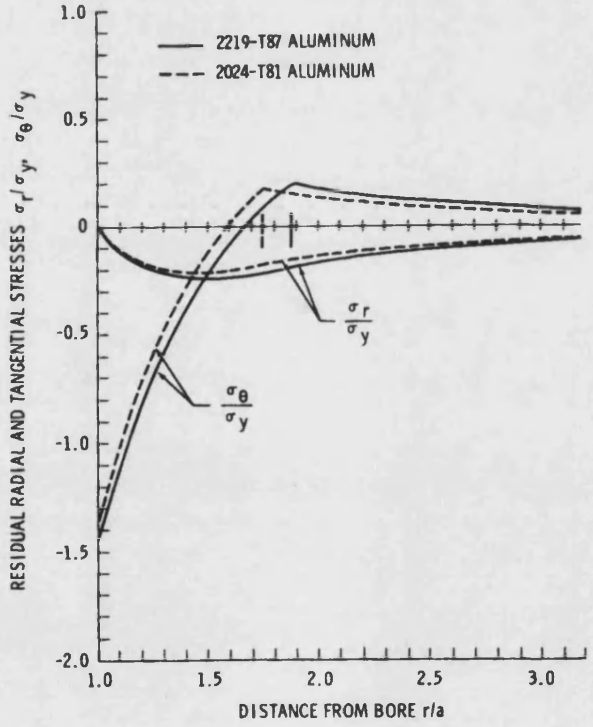

Fig 2.14:Residual radial and tangential stresses due to a radial expansion of 2% at a hole [29]

Guo Wanlin [30] also carried out a mathematical study of the elastic-plastic analysis of a finite sheet with a cold-worked hole. The solution for the residual stresses and strains in a circular sheet having a cold worked or interference fitted hole has been obtained. In this research the solution was obtained using the Von Mises deformation theory with a modified Ramberg-Osgood law (for the material σ-ε diagram). For simplicity the sheet was considered annular with an inner radius, a and outer radius, b. The solution for a finite sheet is very similar to that for an infinite sheet except that in the former case there is an extra boundary condition due to the sheet outer radius.

In this research the effect of exponent, n (of the stress-strain relation in Rambrg-Osgood equation), interference size, effect of b/a (ratio of outer radius to inner radius) and material properties of fitted pin to the hole have been studied. This mathematical work concluded that:

- The amount of compressive tangential residual stress increases rapidly with increasing interference amount (at low interference i.e. less than 2%), but increases slowly at high interference (see fig 2.15).
- For a given interference value the tangential residual stress at the hole edge increases quickly for b/a up to 6 but then changes slowly.
- For a given interference and b/a ratio, the tangential residual stress increases with E_0/E (ratio of imaginary hole plug modulus to sheet modulus) but it's increase is slow at high E_0/E
- For a given b/a, E_0/E and interference value the tangential residual stress increase with exponent, n.

In Guo Wanlin's research the mathematical solution for a circular sheet was compared with the solution for a rectangular sheet by 2-D finite element analysis and it was concluded that the difference is very small (see 2.16).

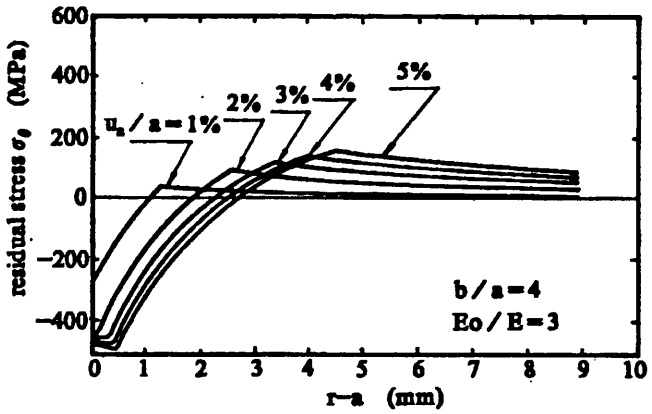

Fig 2.15: The effect of interference on residual stress distribution in LY12CZ aluminium plate [30]

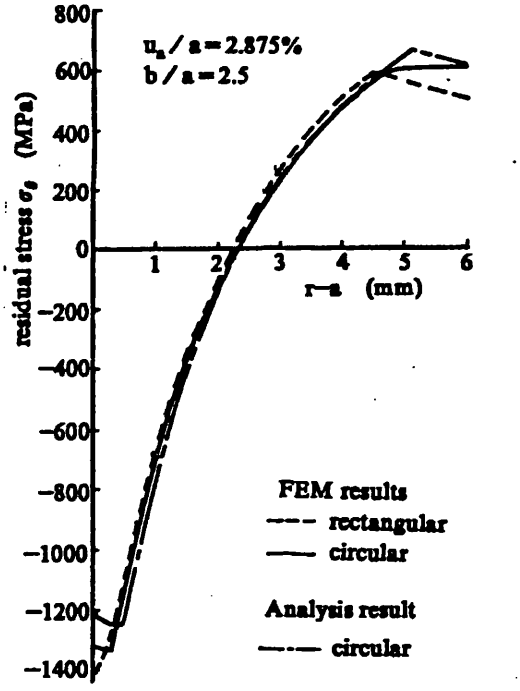

Fig 2.16: The distribution of residual stress in a high strength steel [30]

Many other mathematical theories have been developed to predict the residual stress distribution due to plastic hole enlargement in a sheet [31-37]. All of the theories assume that the deformation is radially symmetric and it is a result of a uniform pressure or displacement to the hole boundary large enough to cause yielding of the material adjacent to the hole wall. All of these theories only consider small

deformation. Five of the theories assume the material to be in a state of plane stress [31-35], while two assume a state of plane strain [36, 37]. The theories also make assumptions about the material behaviour. The theory proposed by Taylor [32], for example, assumes that the material is perfectly plastic whereas the theory of Nadai [31], Carter-Hanagud [36], Hoffman Sachs [37], Alexander-Ford [34] and Rich-Impellizzeri [35] assume that the material behaves in an elastic-perfectly plastic manner. Three of the theories [29, 30, 33] assume that material behaviour can be represented by a Ramberg-Osgood uniaxial stress-strain relation. The possibility of secondary compressive yielding occurring during elastic unloading is also addressed [31, 34, 35].

2.5) Using the finite element method to evaluate residual stresses

A part experimental and part analytical research to assess the residual stresses around cold-worked holes was carried out by M. Priest et al [38]. In the experimental part X-ray diffraction was employed to determine the residual stresses at a 4% cold expanded hole by a mandrel in a 6 mm thick 2024-T351 aluminium plate. Due to the limitation of the X-ray diffraction method, the radial and tangential residual stresses were measured only at the plate faces.

In the analytical part a two-dimensional axisymmetric finite element model was used. In the model the cold expansion process was carried out by uniform radial displacement of the hole. For plastic deformation of the plate both kinematic and isotropic hardening material properties have been used.

Experimental determination of residual stresses shows differences between the mandrel exit face and the entrance face (see fig 2.17). This result was attributed to the directional nature of cold working by the mandrel. The calculated residual stresses from the FE model and experimental measurements were different and this was thought to be due to the limitation of the X-ray diffraction technique, which needs large sampling areas.

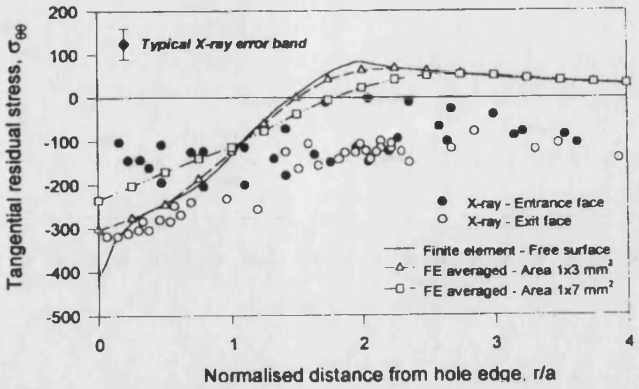

Fig 2.17: Comparison of X-ray measurements and integrated finite element prediction [38]

Analytical and finite element predictions of residual stresses in cold worked fastener holes were investigated by C. Poussard et al [39]. In this research 2-D finite element model were used to determine residual stress distribution around a 4% cold expanded hole. The finite element study was carried out on a 6.35 mm diameter hole in a 2024-T351 aluminium alloy plate with a thickness of 6 mm. In the analysis the plate was considered as different models: once in a plane stress state, then in a plane strain state and also it was considered annular in order to model it axisymmetrically.

In the simulations, small deformation theory was carried out to assess the influence of strain hardening and the role of reversed yielding on the residual stress distribution. According to the results, the different strain levels of hardening were not very influential, however, reversed yielding influenced the residual stress when isotropic or kinematic hardening was considered (see 2.18). Cold expansion, by a mandrel, was simulated by radial displacement in all geometrical models and it was concluded that:

- Plane stress and plane strain models predict different residual stresses around a hole.
- An axisymmetric model reveals that residual stress distributions through the thickness are not uniform and so neither a plane stress nor a plane strain model can predict satisfactorily the residual stress around a cold expanded hole.

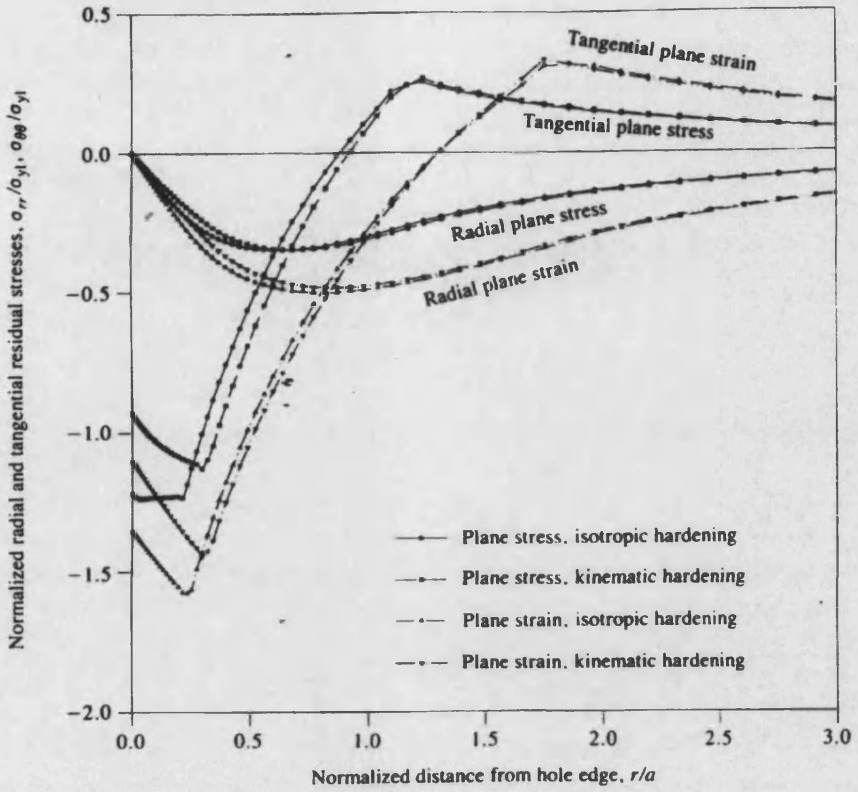

Fig 2.18: 2-D FE radial and tangential residual stress predictions [39]

A three-dimensional elastic-plastic finite element analysis of cold expansion of adjacent holes was studied by P. Papanikos et al [40]. It was conducted to evaluate the development and growth of the plastic zone and residual stresses resulting from the cold expansion of two adjacent holes. The finite element model was based on 7075-T651 aluminium plates with a thickness of 6.35 mm and holes with 2.87 mm radii. A steel mandrel with elastic behaviour was used to achieve a 3% cold expansion and elastic Coulomb friction with a coefficient μ=0.15 was assumed. The research concentrated on the effect of simultaneous and sequential cold expansion on the residual stresses around adjacent holes.

In the research the residual strain results (obtained using FE) compared well with existing experimental results using a split sleeve for cold expansion. This research concluded that:

- "The compressive residual stress varies across the thickness of the specimen, with the maximum being around mid-thickness and the minimum at the entry face.

- A decrease in the centre distance between expanded holes results in a decrease in the compressive residual stresses at the entry face of the work piece (plate)
- Sequential hole expansion results in lower compressive residual stresses at the exit face of the work piece (plate)."

M J Pavier et al [41] has also published results of a finite element simulation of the cold working process. In this research, two-dimensional axisymmetric finite element simulations have been completed for the cold working of a fastener hole with 3.175 mm radius in a 2024-T351 aluminium alloy plate with a 6 mm thickness. In this research both isotropic and kinematic hardening material property models were used. The models simulated the cold working process where an oversized mandrel was pulled through the fastener hole. The results of the simulation were compared with a simplified finite element model where the cold working process was reduced to applying a uniform radial expansion to the hole surface. It was shown that substantial differences exist between the finite element simulations. The mandrel simulation results showed that even tensile tangential residual stresses on the plate surface could occur after cold working (see fig 2.19), whereas the simplified radial displacement simulation shows only compressive ones. Further comparisons are made for the axial deformation of the plate by using the results of experimental measurements of the surface profile around a cold worked hole. There was good agreement between finite element results and experimental work.

2.6) Shortcomings of previous researches

This review of other researchers work has identified a number of shortfalls in gaining a full understanding of some of the important aspects of the cold expansion process. Some of these shortcomings are related to the effect of interference, plate thickness and cold expansion method on tangential residual stress distribution. So to cover these gaps these effects are investigated in Chapter 3 using the FE method for three interference amounts, three plate thicknesses and three different cold expansion methods. In previous works there was virtually no investigation about the plate support location and the effect of friction on the residual stress distributions. Also in all methods considered, the fastener holes are expanded incrementally across the plate

thickness but there was no method whereby the holes were expanded uniformly through the plate thickness. In Chapter 4, therefore, the effect of plate support and friction was studied alongside a newly proposed method to expand and allow a hole to spring back uniformly. To study more deeply the effect of a sleeve and it's slit on the tangential residual stress, 3-D models are developed in Chapter 5. These 3-D computer models are performed together with some mechanical tests (their results were required for FE simulations) in Chapter 6. In order to investigate the efficiency of the cold expansion techniques in improving life, fatigue tests are carried out and their results are presented in Chapter 7. To discuss the effect of the cold expansion method on tangential residual stress, the history of stresses and displacements are explained in Chapter 8.

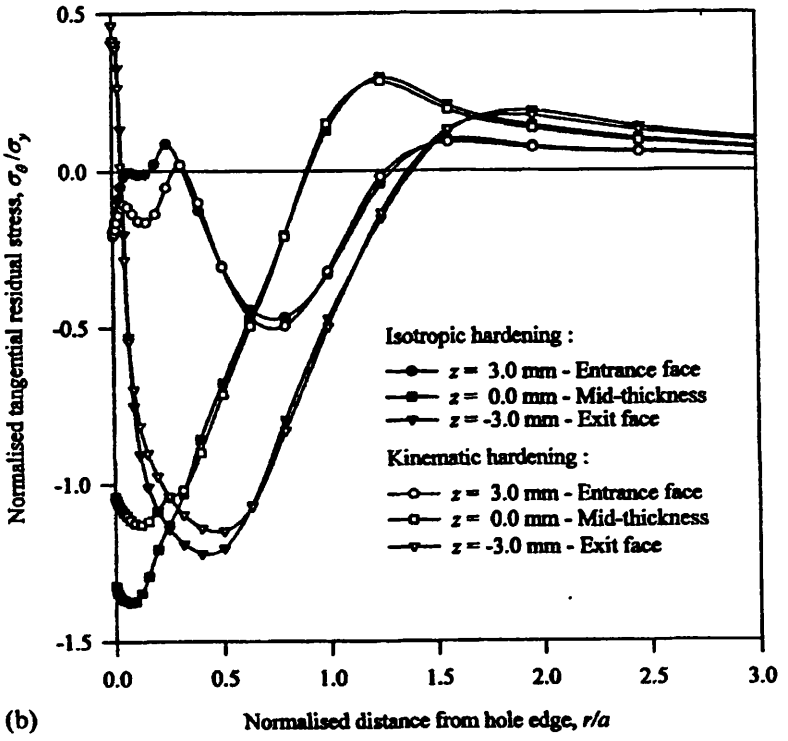

Fig 2.19: Residual stress distributions obtained from finite element simulation by Pavier [41].

Chapter 3

2-D Axisymmetric FE analysis for cold expansion

3.1) Introduction

A fastener hole in a plate is a vulnerable site for initiation and growth of fatigue cracks subjected to cyclic loading. A way of improving the fatigue life around a hole is to produce compressive tangential residual stress around the hole. To achieve this, load must be applied to expand the hole surface to create a plastic region locally around the hole. When the load is removed the yielding region results in compressive tangential residual stresses. Further from the hole tensile tangential residual stresses are produce to maintain balance.

To apply the load to the hole surface there are theoretical methods like applying internal pressure or uniform radial displacement to the hole surface. Unfortunately these methods face serious problems in practise. In the case of applying very high internal pressure it is possible with an analytical expression or in a finite element package but it is not possible to achieve this in practise. For example to produce a plastic region around a 5 mm diameter hole in Al-alloy 7075-T6 a typical pressure of 700 MPa (7000 bar) is needed but this cannot easily be applied in practise.

With uniform radial displacement of the fastener hole, although it is not as difficult as applying internal pressure, it still has its own problems (see Chapter 6). It appears from the literature survey that very few attempts have been made to use this method and where it has been used it is not considered to have been done so efficiently.

Because applying such high pressure is impractical and also because applying uniform radial displacement is very difficult, a method in which an oversized object (such as a ball or pin) is needed to be forced through the hole. This is called the cold expansion method (fig.3.1), and it is fundamentally different from the above methods. As the pin or ball enters the hole from one face and passes through the thickness then exits from the other face of the plate the hole expands incrementally. The fact that the hole neither expands nor springs back simultaneously after the cold expansion process is significantly different to what is considered in any mathematical assumption.

Calculating the residual stress mathematically around a cold expanded hole using a pin or a ball is analytically very difficult. However, the study can be carried out numerically using the finite element method. Consequently this chapter is concerned with using the finite element method to determine tangential residual stress around a cold expanded hole when a tapered pin or a ball is used. For comparison purpose the results for an ideal uniform radial displacement model of cold expansion has also been studied.

In addition to the effect of the cold expansion method on tangential residual stress the effect of the plate thickness and the amount of interference effect have been studied. This chapter also describes model validation for mesh size and involving non-linear parameters. For simplicity all the cold expansion models have been considered axisymmetric.

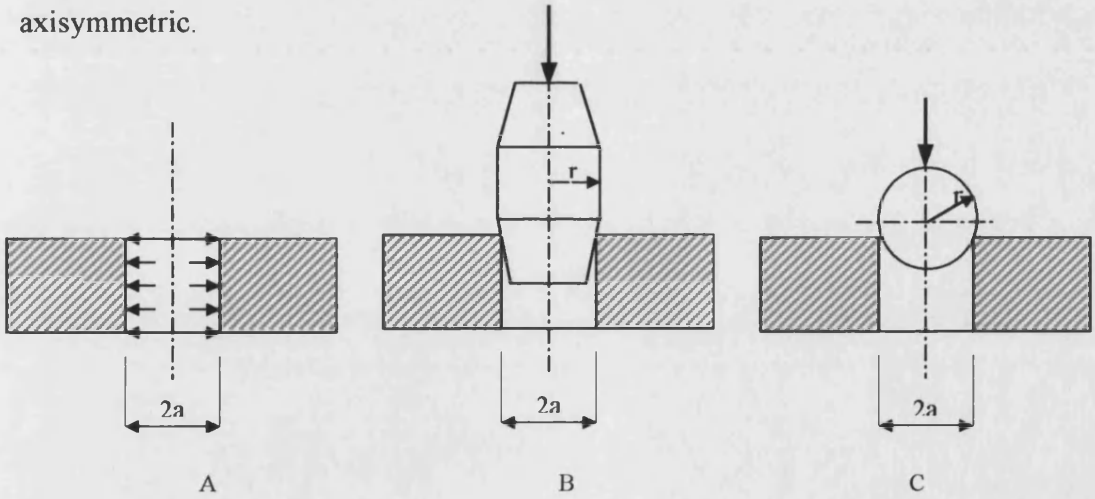

A: uniform radial displacement B: tapered pin without sleeve C: ballising

Fig 3.1: Theoretical A, practical methods (B and C) of a hole cold expansion

3.2) Models configuration

To study the effect of the cold expansion methods on tangential residual stress, three different models are studied using finite elements as shown in fig 3.1. These are:

1) Uniform radial displacement of a hole as an ideal model A
2) Cold expanding a hole by a tapered pin without sleeve, model B
3) Cold expanding a hole by a ball without sleeve, model C

Modelling the cold expansion process precisely is a complex task. The model should include friction between contacting surfaces, local plastic zone in the oversized pin or ball and the exact geometry of the holed plate. In this chapter to avoid complex models some assumptions have been made to simplify the models. The assumptions that have been made are that the contacting surface is considered frictionless and also that the ball or pin material is modelled as an elastic material. These assumptions will not affect the result much because in practise the coefficient of friction can be reduced by using a good lubricant, and local plasticity of the ball or pin takes place in a very small region or in region that is not of interest (such as the load point of application).

From geometry consideration the holed plate maybe square or rectangular. However, preliminary studies showed that for large b (i.e. $\frac{b}{a} \geq 10$ see fig 3.2) the corner or rectangular edges have very little effect on the distribution of tangential residual stress introduced by cold expansion process. So instead of considering a 3-D cubic model, which needs considerable hard disk space and long processing time, the plate can be considered as an annular one with inner diameter equal to the hole diameter and outer diameter equal to the plate width (fig 3.2). The annular plate can be treated as an axisymmetric model, which needs less hard disk space and much shorter processing time.

The magnitude of the compressive tangential residual stress near the hole for a give hole radius in a plate can depend on different parameters. These parameters include the amount of interference, the plate material, the plate thickness, the oversized object material and shape. Studying the effect of all of these parameters is a substantial task, so in this chapter the study has concentrated on the amount of interference and the

plate thickness in Al-alloy 7075-T6 for each of the three previously mentioned models.

For studying the effect of interference, levels (I=2%, 4%, 6%) were considered for each model. Unfortunately there is no unique convention to define the level of cold expansion in the hole. In some papers [6, 7] it has been defined as the diameter enlargement of the cold expanded hole over the initial hole diameter:

$$I = (\frac{\Delta D}{D}) \times 100 \qquad (3.1)$$

In which ΔD is the hole diameter enlargement after cold expansion and D is the hole initial diameter.

However, with this definition problems arise. The increase in hole diameter is not known either before carrying out the cold expansion or producing the results from the computer simulation. Even having the test and simulation results, no criterion has been defined for the hole diameter enlargement. Computer simulation (see Chapter 8) and experimental test results show that the hole diameter enlargement varies throughout the plate thickness. It is larger at the plate faces than in the middle. For such a definition there is an added practical problem in accurately measuring the diameter increase in a test. This is because measurement tools like a vernier calliper or a ball gauge are not suitable for this purpose, so to avoid these problems, the following definition has been used:

$$I = (\frac{r-a}{a}) \times 100 \qquad (3.2)$$

Where r is the largest radius of the oversized object and a is the hole radius.

In order to study the effect of plate thickness on tangential residual stress, three different plate thicknesses (T=2, 5, 10 mm) have been studied for each model. Most of the holed plates used in aircraft structures are within these ranges of thickness.

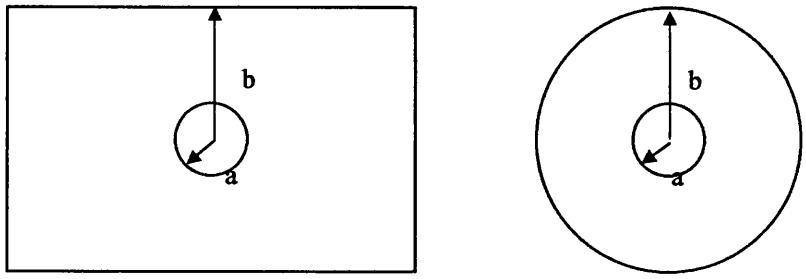

Fig 3.2: Choosing an annular rather than a rectangular plate

3.2.1) Uniform radial displacement of a hole (model A)

Plane stress and plane strain models have been considered for simplicity in the mathematical analysis and so they do not show the residual stress variation through the plate thickness. Although these models assume that the residual stress is uniform throughout the plate thickness, a plane stress state exists at the plate faces and a plane strain state exists in the middle. In order to show the variation of residual stress throughout the plate thickness an axisymmetric model is used instead of a plane stress or plane strain model (fig 3.3). The elements used for this model in the ANSYS package [58] have been axisymmetric Plane 42 and the model was constrained at the outer radius in the Z direction. Such a boundary condition is enough for a well-constrained axisymmetric model and avoids rigid motion of the model. As figure 3.3 shows, the model has been constrained in the Z direction in the lower surface as well. This is due to the symmetry of the model with respect to the X-axis so that just half of the model is needed for simulation. In this model the load has been achieved by applying uniform radial displacement (Δu) incrementally (see fig 3.3-b) at the hole inner surface nodes in one load step. These nodes have been released in another load step to create compressive tangential residual stress.

In this model the definition of cold expansion size is defined as:

$$I = (\frac{\Delta u}{a}) \times 100 \qquad (3.3)$$

Where a is the hole radius.

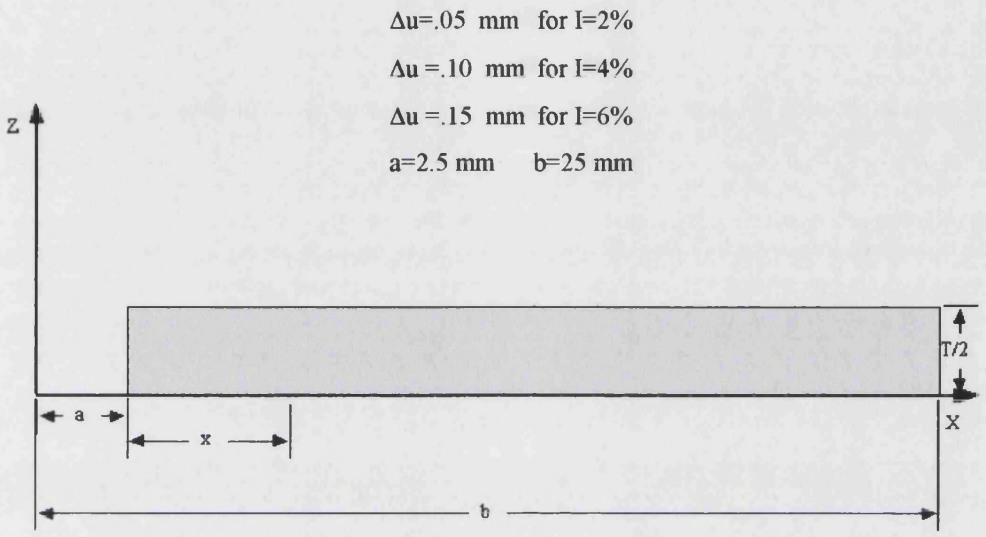

a) Projected surface

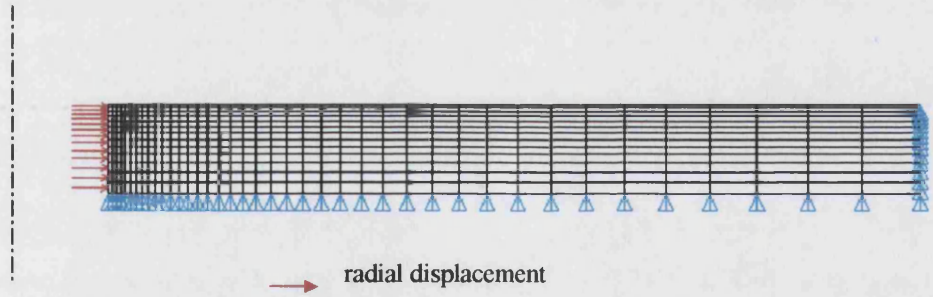

b) Axisymmetrical mesh

Fig 3.3: Uniform radial displacement model (A)

3.2.2) Cold expanding a hole using a tapered pin without a sleeve, model B

Cold expanding a hole by uniform radial displacement through the plate thickness is straightforward in theory but difficult to achieve in practise. A more practical method is to continuously push or pull of an oversized tapered pin through the hole. For the finite element model axisymmetric Plane 42 elements have been used for both the plate and the pin. This is the same as with model A. Also the plate is constrained in the Z direction at the outer radius as shown in fig. 3.4.

In practice, because of friction, a high force is necessary to push the pin through the hole consequently a support is needed for the plate near the hole. As the finite element model described in this chapter ignores the presence of friction, the pin pushing force is low and so supporting the plate at the outer edge is adequate. The effect of friction is however included in the model which is studied in the next chapter.

The pin is constrained in the X direction along its centre line. The top nodes of the pin are displaced incrementally in the -Z direction in order to push the pin through the hole.

During loading two different surfaces (the hole surface and the pin outer surface) contact together so in order to prevent penetration of the surfaces contact elements are needed. These are discussed in more detail in section 3.3. The contact elements rest on the solid elements (in this case Plane 42) in the contacting area during simulation of the model.

In this model the level of cold expansion is defined by equation 3.2.

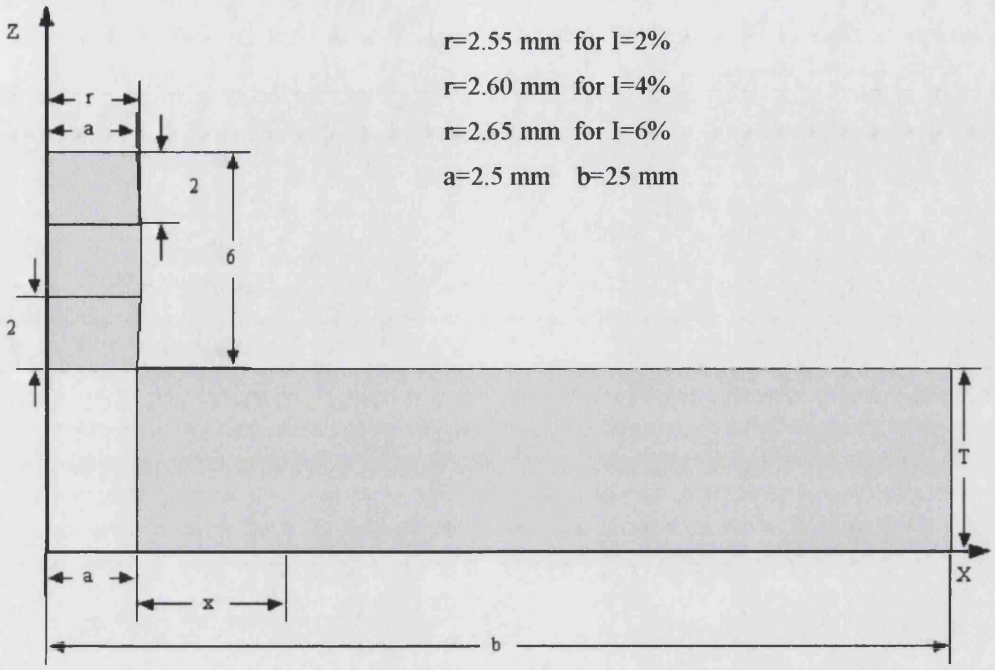

a) Projected surfaces

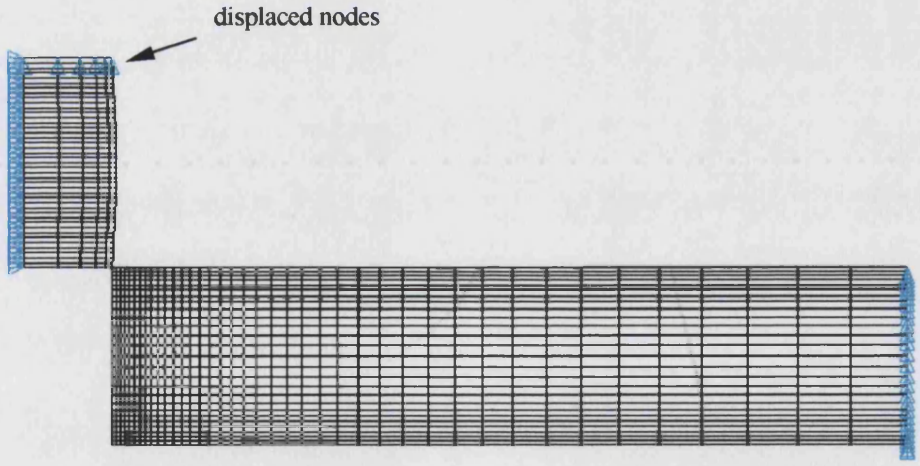

b) Axisymmetric mesh

Fig 3.4: Cold expanding a hole using a tapered pin without a sleeve, model B

3.2.3) Cold expanding a hole directly using a ball (ballising), model C

This model is very similar to model B except that a ball is used instead of a pin as the oversized object. The boundary condition in this model for the plate is the same as model B. The ball is constrained in the X direction at its centre line and pushed down by incrementally displacing its top node. The elements that have been used for this model are the same as model B. However contact elements have been used only for the half of the ball surface that is in contact with the hole in order to save CPU time and hard disk space (fig 3.5).
The cold expansion level in this model is the same as model B which is defined by equation 3.2.

3.3) Element type used

Two Ansys element types have been used in the previously mentioned models, these being Plane 42 (a 2-D structural solid element) and Contact 48 (a 2-D point-to-surface contact element). Each element type is discussed below in detail.

3.3.1) Plane 42 2-D structural solid element

Plane 42 is used in 2-D modelling of solid structures. It can be used either as a plane element (plane stress or plane strain) or as an axisymmetric element. The element is defined by four nodes having two degrees of freedom at each node: translation in the nodal x and y direction. The element has plasticity, stress stiffening, large deflection and large strain capability. Fig 3.6 shows the geometrical node location of this element.
The Ansys manual [42, 43] does not recommend the use of Plane 42 in the triangular form (fig 3.6) due to the increased stiffness of this element type. To prevent this, mapped area meshing is necessary. Mapped meshing requires that each area be defined as having four sides.

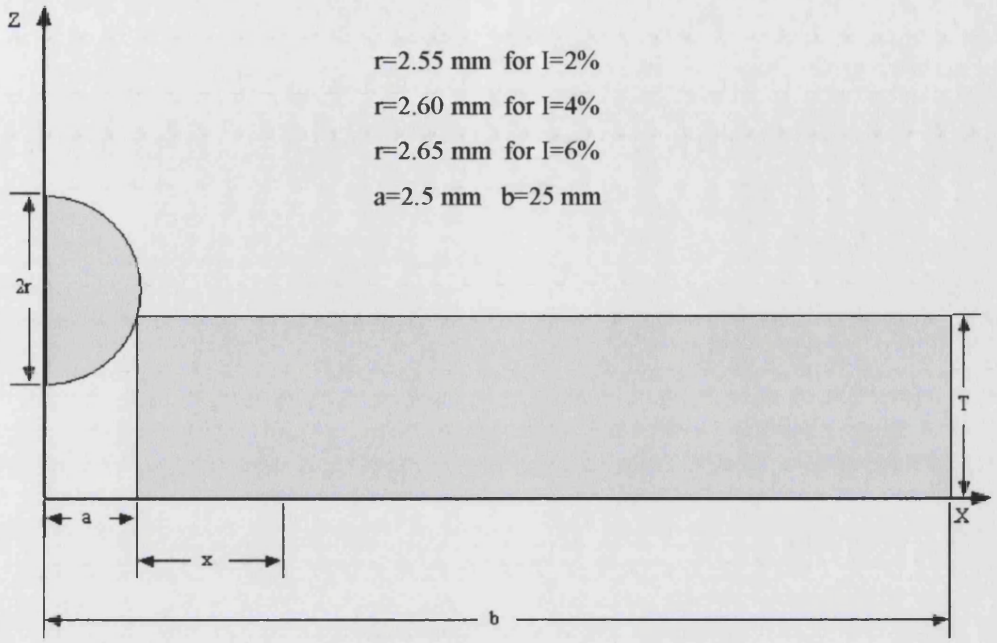

a) Projected surfaces

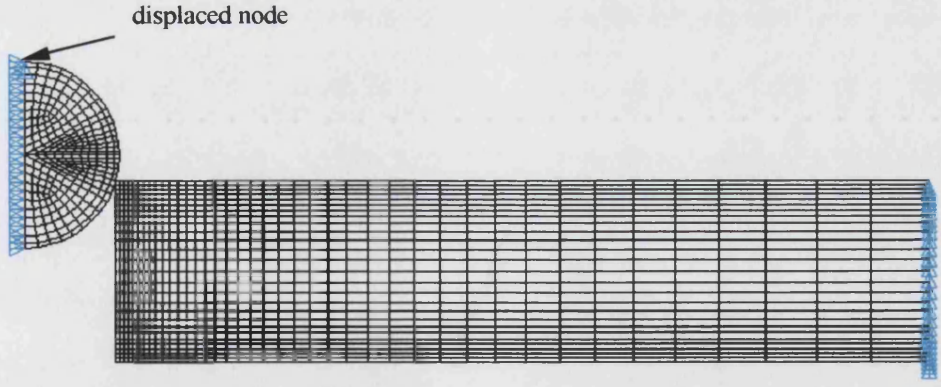

b) Axisymmetric mesh

Fig 3.5: Cold expanding a hole by a ball without a sleeve, model C

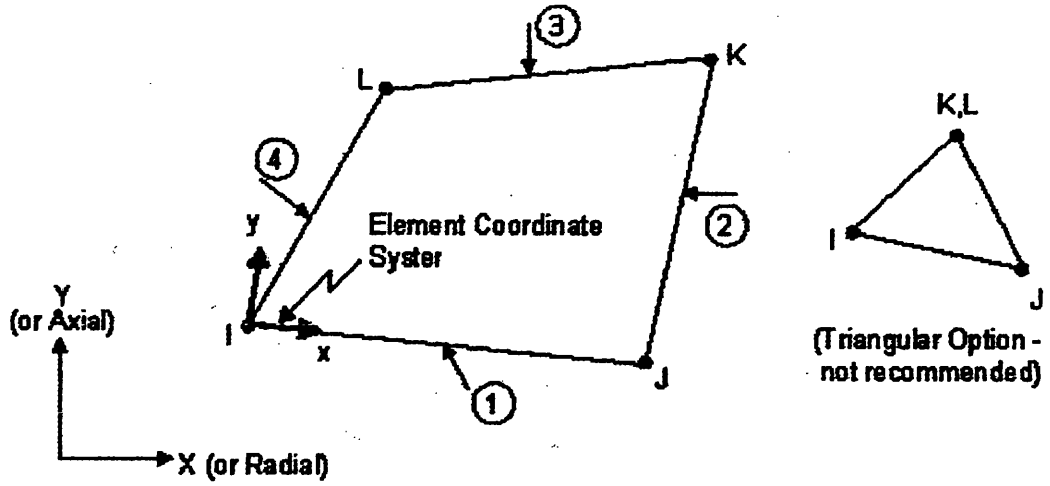

Fig 3.6: Plane 42 2-D structural solid element

In the modelling process a higher order element like the 8-node Plane 82 (which is a 2-D structural solid element) could be used. This element, though, has not been used because of the following reasons:

When plasticity occurs (as with cold expansion) calculations for stress and strain are based on the element integration points. In Ansys, a lower order element will provide the same number of integration points as a higher order element and will thus have the same accuracy for fewer DOFs and a smaller wave front (see fig 3.7).

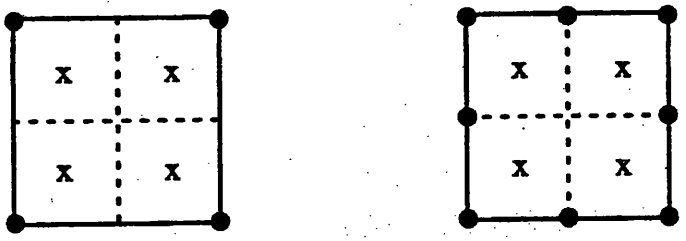

4 integration pts.
8 DOFs

Plane 42 element

4 integration pts.
16 DOFs

Plane 82 element

Fig 3.7: Integration points in Plane 42 and Plane 82 structural solid elements

When creating a contact element between mating surfaces which contain Plane 82, Ansys ignores the mid-side nodes on the target face of the element. The Ansys program for deformable surfaces (referred to as general contact in the package) has been developed for none mid-side node elements and so the Ansys User Guide recommend using general contact analysis for a surface having no mid-side nodes.

3.3.2) Contact 48 2-D point to surface contact element

The geometry and node locations are shown for the Contact 48 element in fig 3.8. The element geometry is a triangle with the base being a line between two nodes on one of the surfaces (called the target surface) and the opposing vertex being a node on the other surface (called the contact surface). The line on the target surface is called a target line and the nodes at the ends of the target line are called target nodes. The node on the contact surface that completes the triangle is called a contact node. The target line and the contact node of the element are displayed in fig 3.8. Nodes I and J define the target line, and node K is the contact node. The surface tangent vector is taken to be the unit vector that is tangent to the target line and pointing from I to J. The surface normal vector is defined to be the unit vector that is perpendicular to the target line and pointing to the left of the target line looking from I to J. Nodes I and J should be specified so that the target surface is on the right as you advance from node I to node J. Initially, node K may be far removed from nodes I and J, may be collinear with nodes I and J, or may have penetrated the target line. Contact occurs only when the normal projection (to the target line) of node K lies on the target line.

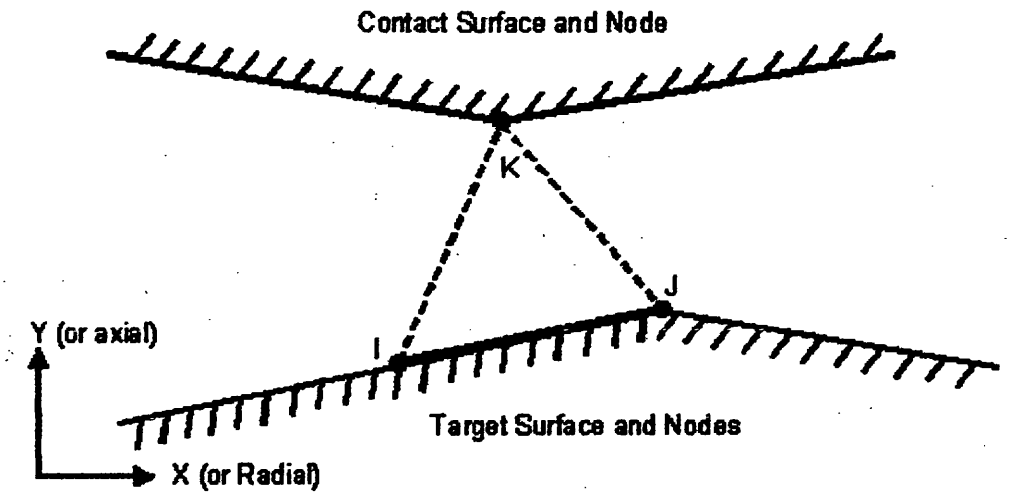

Fig 3.8: Ansys contact element type " Contact 48 " [43]

The normal contact stiffness, referred to as *KN* in the Ansys manual, is used in the penalty function method to determine contact forces [$8_{chap.\ 23}$]. *KN* (which has units of force/length) corresponds to a penalty stiffness that acts in the direction of the target surface normal. Its use enforces displacement compatibility by limiting the penetration of the target line by the contact node. A large value of *KN* is usually needed to enforce compatibility if the penalty function method is selected. A lower *KN* value can be used with the penalty function plus Lagrange multiplier method [8].

The absolute tolerance applied in the direction of the surface normal, TOLN, is used to determine if penetration compatibility is satisfied when the penalty function plus Lagrange multiplier method is used. Contact compatibility is considered to be satisfied if the contact node is within TOLN clearance on either side of the target line.

Real constant TOLS is used to add a small tolerance that will internally increase the length of the target (nodes I and J). Units for TOLS are percent (1.0 implies a 1.0% increase in the target length). TOLS is useful for problems where contact nodes (K) are likely to lie on the edge of targets (as at symmetry planes or for models generated in a node-to-node contact pattern). In these situations, the contact node may repeatedly "slip" off one target and on to another target or completely out of contact,

resulting in convergence difficulties from oscillations. A small value of TOLS will usually prevent this situation from occurring.

Real constant PINB specifies the pinball radius to be used in determining whether the contact node is in or near contact. The default is for the program to calculate the pinball radius based on the dimensions of the target. It is possible to specify other pinball radius if the initial interference in a model is larger than the target length (otherwise, this initial interference would go undetected since it is outside the pinball). In some case it is need to specify PINB if the contact node passes through the target surface with a displacement greater than the target length. However, using too large of a radius will increase the contact search time.

3.4) Properties of materials used

In cold expansion two different metals are used, steel for the pin (or ball) and aluminium alloy 7075-T6 for the holed plate.
In the simulation model, the steel is assumed to behave elastically. Although the elastic modulus for different steels varies between 200-210 GPa [44] a lower limit has been used here (see table 3.1). Choosing a higher value of elastic modulus for steel would only have a very negligible effect on the results.
Aluminium alloy 7075-T6 has been considered to behave as an elastic-plastic isotropic material. Although it shows a little anisotropy in its mechanical properties (E, ν), it is assumed to behave isotropically for simplicity.
A tension test was carried out on the aluminium alloy (described in Chapter 6) in the rolling direction and engineering stress-strain was calculated from the load-displacement curve and then converted to the true stress-strain diagram [44]. This graph is idealised in fig 3.9 for inputting to the Ansys material table; this can accept only 5 points. To take account of the Bauschinger effect, the kinematic hardening rule has been chosen in plasticity deformation theory [13].

Table 3.1: Material properties

	Elastic modulus, E	Poisson's ratio,ν
Steel	200 GPa	.3
Aluminium 7075-T6	71.5 GPa	.33

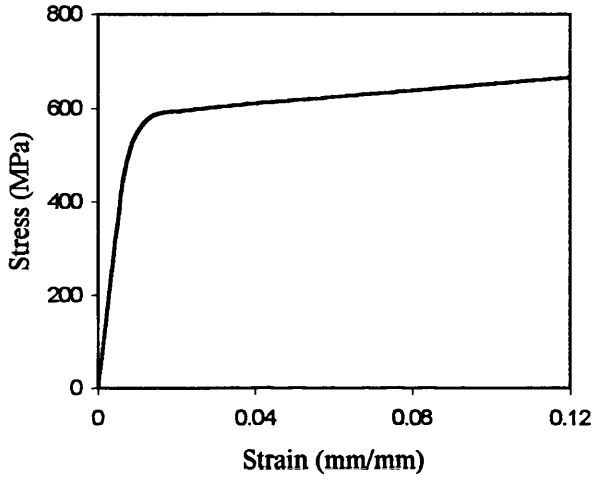

Fig 3.9: Stress-strain curve of aluminium alloy 7075-T6

3.5) Loading process

The elastic-plastic material behaviour is non-linear and path dependent. The final state of stresses and strains depends on the loading history so loading should be carried out in the same way they are applied to the models. In non-linear problems incremental loading is necessary for the accuracy of results.

In model A, loading and unloading has been carried out in two separate load steps. At first a radial displacement has been applied to the hole inner surface nodes in 40 sub-steps. That is, the load has been broken for 40 equal portions at the final radial displacement, Δu. The magnitude of Δu corresponding to interferences of I=2%, 4%, 6% are Δu=0.05, 0.1, 0.15 mm respectively. At the second load step (stage) unloading

has been carried out by releasing the radial displacement constraints from the inner hole surface nodes; these are the same nodes in which loading was applied at the first load step.

The loading for models B and C has been performed in one load step only. The pin (or ball) has been pushed (displaced) incrementally from the plate entrance side until it comes out the other side (exit face). Choosing the number of load sub-steps is very important, not only for result accuracy, but also for convergence of the equilibrium iteration during the solution process. When choosing a large load increment the pinball area (see section 3.3.2) may be passed over and cause equilibrium iteration convergence difficulties. The area where the contact node can be detected by the target surface is called the pinball area. This area equals the default area of 1.5L. Where L is the underneath Plane 42 element edge. By choosing a very small load increment the equilibrium iteration convergence problem can be avoided but running the models takes longer. Running models B and C in 5 mm thick plate has been carried out for the following numbers of sub-steps 80, 100, 120, 170, 200, 250 and 500. The results show that getting equilibrium iteration convergence is difficult using 120 sub-steps or less, especially for interferences of I=6%. Running models with sub-steps of 200 or more is unnecessary from the point of view of both result and equilibrium iteration. Before applying load to model B (or C), the pin (or ball) was initially positioned so that it touches the inner surface of the fastener hole at the entrance face. In model B (or C) to move the pin (or ball) through the hole, a displacement, d, is applied to the pin top face nodes and the ball top node in the -Z direction. The chosen displacements of d are:

$$d = l + T + .1 \qquad \text{for the pin} \qquad (3.4)$$

$$d = T + 2r\sin(\arccos(a/r)) + .1 \qquad \text{for the ball} \qquad (3.5)$$

In which l is the pin length, T is the plate thickness and r is the ball radius. A margin of 0.1 mm has been allowed to ensure that the pin (and ball) come out of the plate exit face completely.

3.6) Validation of models

To ensure that the calculated tangential residual stress around the cold expanded hole is accurate for models, the models, validity should be examined for parameters such as mesh density, loading sub-step number, contact stiffness in the case of models B and C and the equilibrium iteration convergence tolerance. To investigate the model validity, one parameter was allowed to change in each run while the other remained unchanged. The parameter was changed until convergence of the result was achieved. This process has been carried out in turn for all mentioned parameters.
In the following sub-section the validity of models for each parameter has been investigated.

3.6.1) Mesh density of models

In Ansys, at the pre-processing stage, to find a suitable mesh density the geometry of the holed plate was built and its parallel lines were divided for each model. The lines were divided such that near square shaped plane elements (with an aspect ratio of about one) would be possible in the map mesh. In model B the geometry of the pin was constructed using three quadrilateral areas descretised using map mesh [45] for reasonable mesh density.
In model C the outer portion of the ball was map meshed and the inner portion was free meshed. For including contact elements, the hole inner nodes and the pin (or ball) outer surface nodes have been chosen to construct symmetric contact elements (the nodes are both contact nodes and target nodes). With the contact elements a big number was considered for contact stiffness (KN=10^{10} N/m).
In the solution process of models B and C, an equilibrium iteration convergence tolerance of .001 has been applied for force criteria with the norm of the square root sum of the square (SRSS) see section 3.6.4. In model B and C, the pin (and ball) has been pushed through the hole in 200 or 400 sub-steps (see table 3.2).
In the post–process stage of Ansys, the results have been obtained and presented as graphs by sending the nodal solution to Excel to get best fit curves.

The process of refining the mesh (for the plate with near square shaped Plane 42 elements) continued several times for each model. The tangential residual stress result graph has been compared for each refined mesh with the previous one. This process showed that the plate needed more mesh refinement near the hole especially around the entrance and exit faces (see fig 3.10) so the mesh with square shaped elements was replaced by a logarithmic one. With this kind of mesh smaller elements can be created where they are needed without unnecessarily increasing the number of elements used; this would need more hard disk space and CPU time.

In model B the effect of mesh refinement on the tangential residual stress around the cold expanded hole for T=5 mm and I=6%, in three different planes are shown in fig 3.11 and fig 3.12. As the graphs show, the result has converged after the third mesh refinement for all three planes except in the very small area near the hole at the exit face of the plate. To overcome this problem further mesh refinement (especially by using a logarithmically varying mesh) continued near the hole at the exit face. Figure 3.12 shows that although the area (where the result did not converge) becomes smaller and smaller by refining the mesh, the problem still remained.

In order to compare the behaviour of tangential residual stress against mesh refinement in the corner nodes and the middle node at the hole surface, the result (for T=5 mm and I=6%) is shown in fig 3.13. The graph shows that refining the mesh has little effect on the result at the entrance corner and the middle node but it has a major effect on the exit face corner result. The tangential residual stress at the corner of the exit face changes from –450 MPa to 250 MPa when the element edge goes from 0.5 mm to 0.05 mm with mesh refinement.

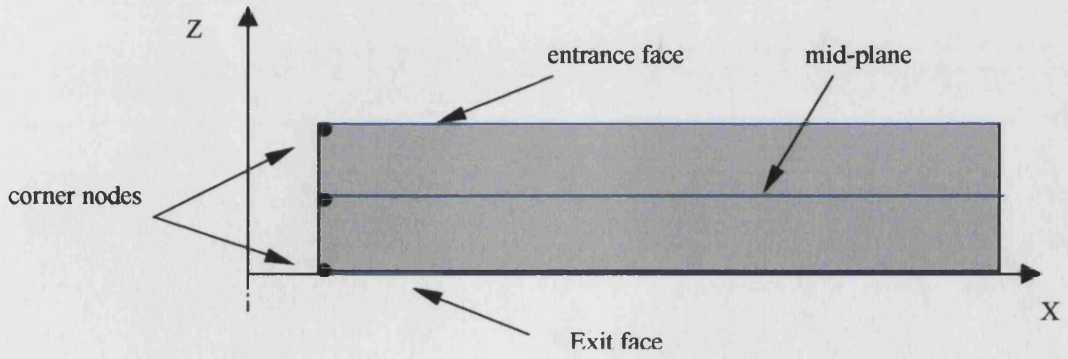

Fig 3.10: Different plane positions of plate in the models

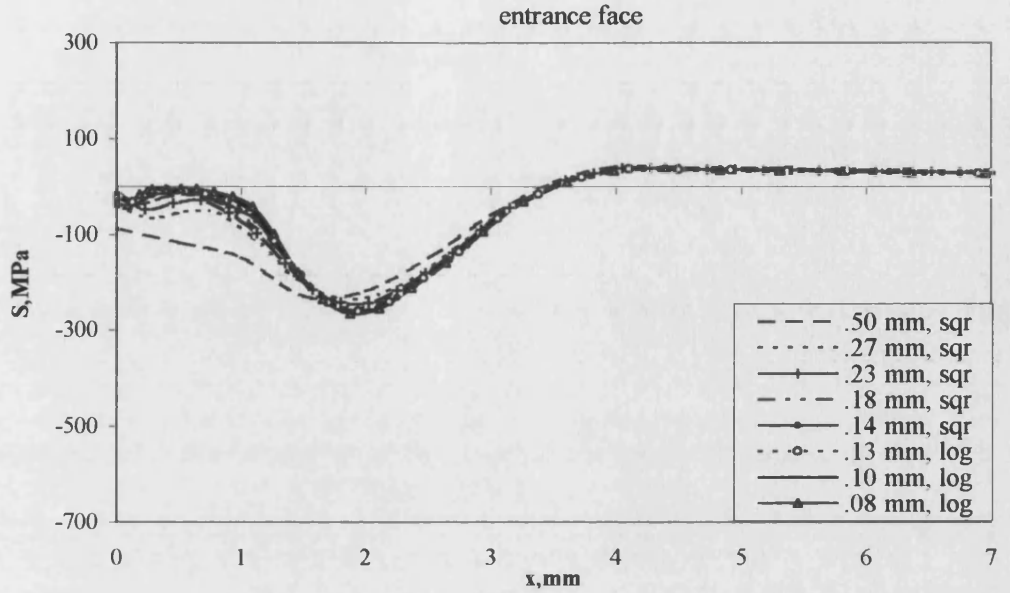

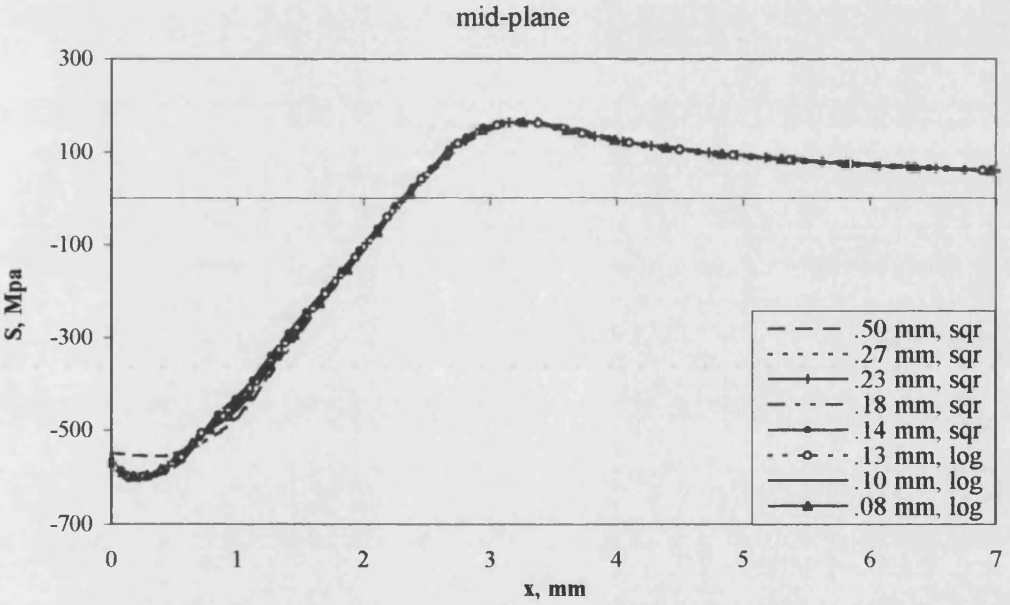

Fig 3.11: Effect of mesh refinement on tangential residual stress around the hole at entrance and mid-Plane for model B (for T=5 mm and I=6%)

Note: In the legend 'sqr' indicates all elements in the mesh are square and their side lengths are given. Also with the 'log' mesh the plate was divided into 40 divisions with different spacing and only the side length of the corner element at hole surface is shown.

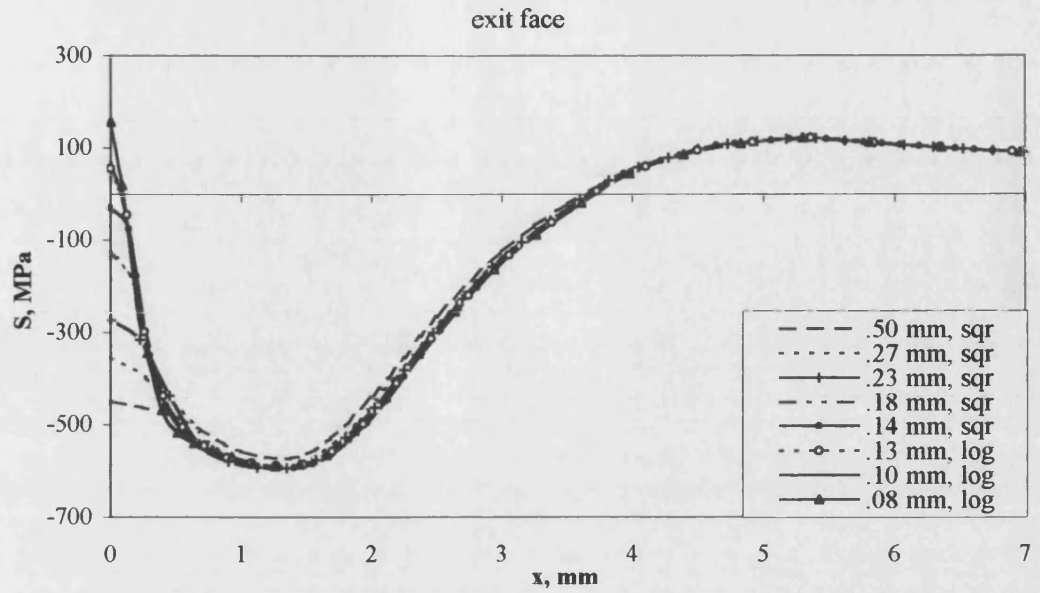

Fig 3.12: Effect of mesh refinement on tangential residual stress around the hole at exit face in model B (for T=5 mm and I=6%)

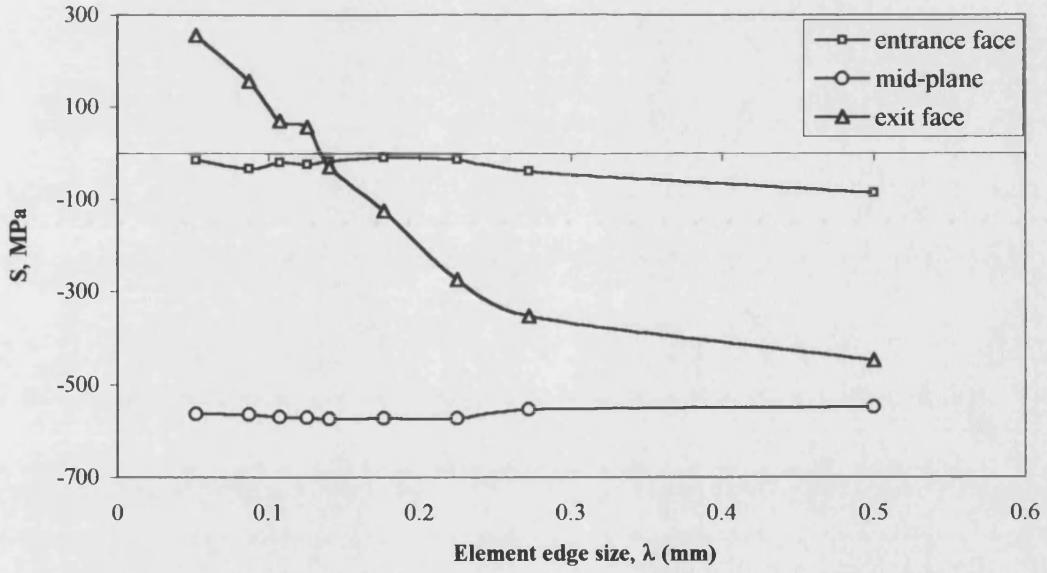

Fig 3.13: Variation of tangential residual stress at hole surface mid-plane node and corner nodes verse element edge for model B (for T=5 mm and I=6%)

3.6.2) Effect of loading sub-step number on model results

The importance of the loading process and loading sub-steps number was discussed in section 3.5. As an example, to show the effect of loading sub-steps number on tangential residual stress distribution for cold expanded hole in a plate with T=5 mm and I=6% at model B is shown as graphs in fig 3.14. The graphs show that the number of loading sub-steps has a small effect on the result at the entrance plane and the effect for the mid-plane and exit plane is so small that all the graphs coincide.
From fig 3.14 it can be deduced that loading sub-steps number has negligible effect on the result when the equilibrium iteration convergence is achieved in the solution process. The number of loading sub-steps used for the models is shown in table 3.2.

Table 3.2: Number of load sub-steps for models

	Interference, I (%)	Plate thickness, T (mm)		
		2	5	10
Model A	2	40	40	40
	4			
	6			
Model B	2	200	200	400
	4			
	6			
Model C	2	200	200	400
	4			
	6			

3.6.3) Contact stiffness value in models B and C

In order to deal with contacting surfaces with the finite element method a relationship must be established between the two contact areas otherwise the two areas will pass through each other. This relationship is established by specifying stiffness between

the two contacting areas and the amount of penetration between the two surfaces depends on the stiffness value. The higher the contact stiffness the better the compatibility, however, a higher value of contact stiffness leads to ill conditioning of the global stiffness matrix as well as convergence difficulties. Unfortunately there are only a few recommendations on how to choose an appropriate contact stiffness in Ansys manuals. One recommendation for choosing contact stiffness value for bulky solid is:

$$KN = fEh \qquad (3.6)$$

Where f is a factor between 1 and 100, E is elastic modulus of contacting material (the smaller one) and h is characteristic contact length (in the axisymmetric models it is the fastener hole radius). In both model B and C the KN value has been chosen to be 10^{10} N/m making f equal 56.

It is considered that the Ansys manual's recommendation for contact stiffness is a general one. However, this should be validated by testing the models results using different numbers for f and thus KN.

In order to check the validity and effect of contact stiffness on tangential residual stress due to cold expansion, the models have been run using five different values (these lie between 10^7 to 10^{11}N/m). As an example, fig 3.15 shows the result for cold expansion with I=6% in 5 mm thick plate for model B. The graph indicates that the tangential residual stress around the cold expanded hole is very sensitive to the contact stiffness value used. This sensitivity can be seen when considering that the tangential residual stress at the pin entrance face at the hole surface changes from -216.43 MPa to –20.3 MPa as KN changes from 10^7 to 10^{11} N/m.

Fig 3.15 shows that increasing the contact stiffness from 10^{10} to 10^{11} N/m has virtually no effect on the result. However, it increases the CPU time by increasing the cumulative equilibrium iteration number from 1248 to1657. Therefore KN=10^{10} N/m is good for achieving a valid result and also for saving CPU time as well.

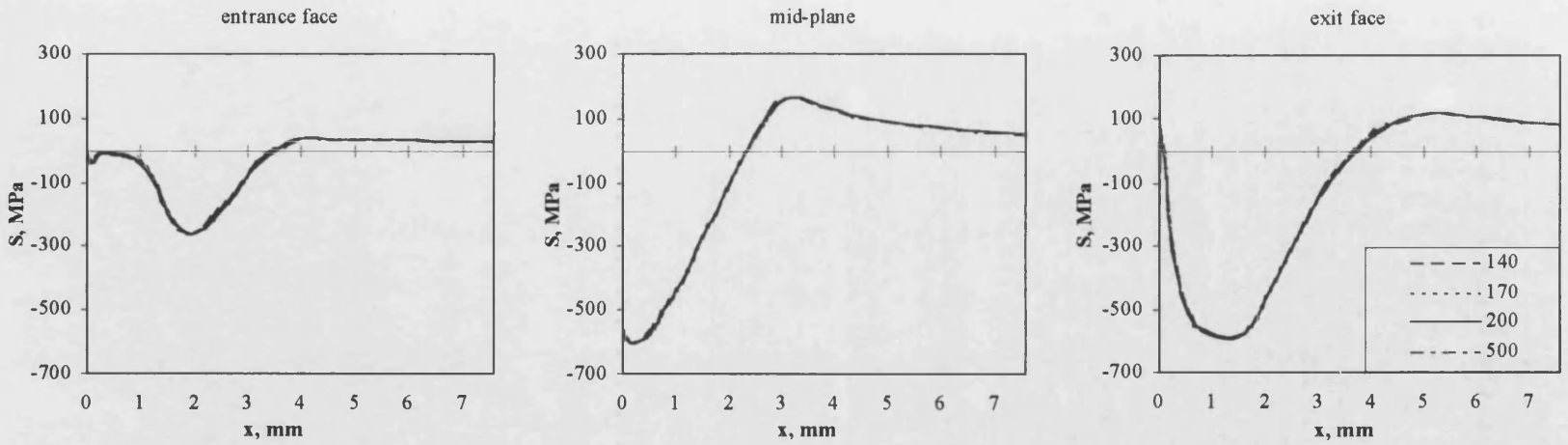

Fig 3.14: Loading sub-step number on tangential residual stress, S in model B (for T=5 mm and I=6%)

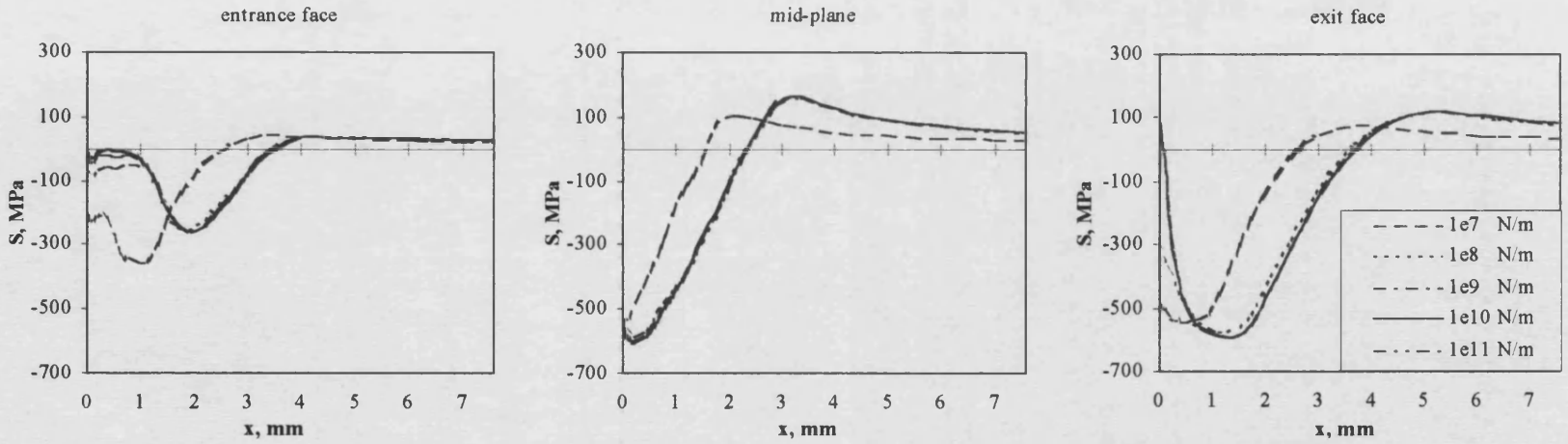

Fig 3.15: Effect of contact element stiffness effect on tangential residual stress, S in model B (for T=5 mm and I=6%)

3.6.4) Equilibrium iteration convergence tolerance in the models

In the solution process loading must be carried out incrementally to find the non-linear response of a model under load. Therefore, the final load is divided into several smaller loads and each of these smaller loads is applied to the model in sub-steps. In each sub-step the model must be examined to see if it is in equilibrium or not. To examine the equilibrium state criteria must be chosen to check that external and internal forces are in balance or almost in balance in the model. From mathematical considerations the external and internal forces of the model will never be exactly equal so there must be some tolerance between them. This tolerance in a non-linear problem is called "equilibrium convergence criteria" and affects the solution accuracy as well as efficiency. The tighter the tolerance the more accurate the results, but more iterations are needed. The tolerance in a non-linear solution could be based on force, displacement or energy. In the Ansys package only displacement-based and force-based equilibrium iteration convergence criteria are available. Although these two criteria can be used together or individually, mostly the force-based criterion is recommended [12].

In Ansys, three different "norms" have been defined for the equilibrium iteration convergence criteria. These are as followas:

L1 norm: $$\|\{R\}\|_1 = \Sigma|R_i| \qquad (3.7)$$

L2 norm: $$\|\{R\}\|_1 = \left(\Sigma R_i^2\right)^{1/2} \qquad (3.8)$$

Infinite norm: $$\|\{R\}\|_\infty = \max\left(|R_i|\right) \qquad (3.9)$$

where {R} is the residual force vector.

The equilibrium convergence criterion that has been used in the models is force-based and L2 norm has a tolerance of 0.001. Thus the solution is considered to converge if the square root sum of the squares (SRSS) of the residual forces is less than 0.1% of the applied force. As fig 3.16 shows, a tolerance of 0.001 is adequate for all models.

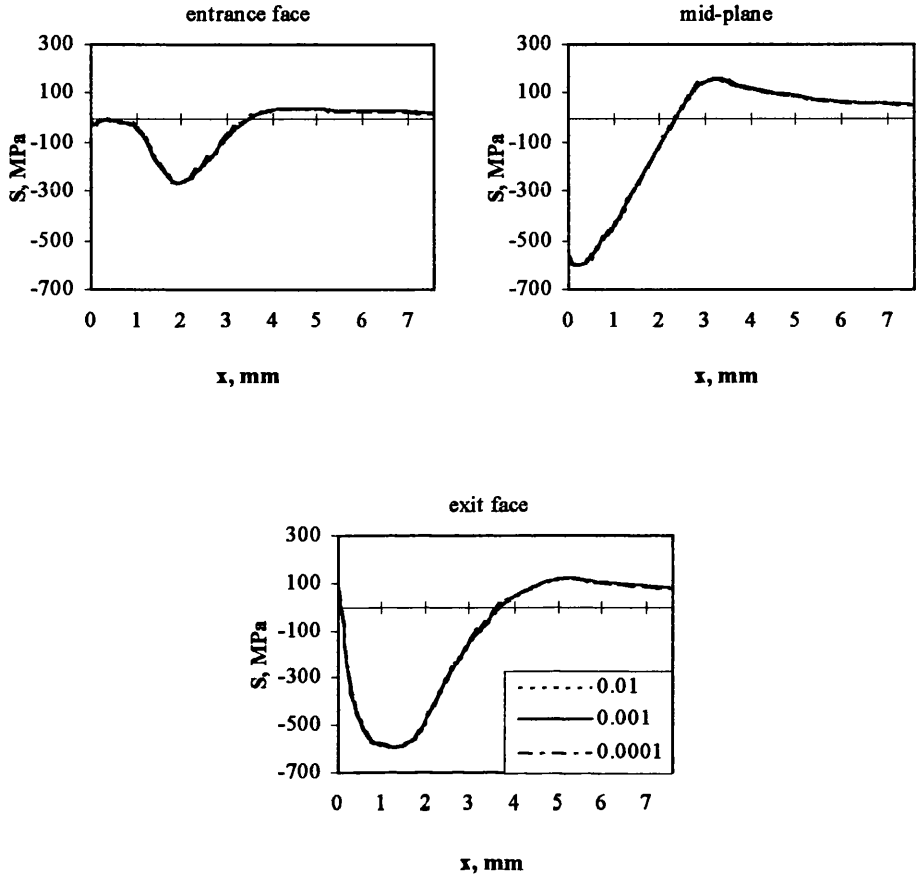

x is distance from hole edge

Fig 3.16: Effect of equilibrium iteration convergence tolerance on tangential residual stress, S (for model B for T=5 mm and I=6%)

3.7) Tangential residual stress discussion

In the section 3.6 the importance of mesh density, loading sub-steps number, contact element stiffness and equilibrium iteration convergence tolerance was discussed for the validity of the model results.

In this section the cold expansion results of the three previously mentioned models are discussed. For each model, the tangential residual stress of interest is plotted against the distance from the hole edge, x.

The data for the graphs have been extracted from the nodal solutions in the Ansys post-processing stage and input to the Excel package to produce the best fit curves. In order to compare the results (two sets with model A and three sets with models B and C) curves are presented in charts. Each chart corresponds to different cold expansion interference and different plate thickness.

The tangential residual stress varies through the plate thickness for all models. To display the variation of this stress through the plate thickness, the results of three planes are included. These planes are at the plate faces and at the middle of the plate. In models B and C the plate faces are defined as the entrance face (where the pin or ball approaches the hole) and the exit face (where the pin or ball comes out of plate face).

3.7.1) Uniform radial displacement (model A)

The tangential residual stress distributions for this model around the cold expanded hole for three interference and three plate thicknesses are shown in fig 3.17. This model is symmetrical about the mid-plane from both geometrical and load considerations and so the stress distribution will also be symmetrical about the mid-plane. Therefore the residual stress distribution would be identical at both plate faces. For this reason only the stress results of two planes (the plate faces and the mid-plane) are shown.

In model A the shapes of the tangential residual stress distributions are similar to those which are obtained when assuming plane stress and plane strain. As the graphs

in fig 3.17 show, the model predicts a large compressive tangential residual stress near the hole edge. Typically the tangential residual stress is compressive near the hole and becomes tensile at about 1.5-3.5 mm from the hole then reaches a maximum value. After its maximum tensile value the tangential residual stress reduces with radius and approaches zero at plate outer radius.

The magnitude of the tangential residual stress increases with radial displacement at the hole edge in both plate faces and mid-plane, but the rate of this increase lowers for the greater radial displacement. The uniform radial displacement model predicts a higher tangential residual stress for the hole edge at the mid-plane than at the plate faces. This behaviour can be explained as a plane stress state at the plate faces and almost as a plane strain state at the plate mid-plane. The plate faces have a plane stress state because there is no stress in the Z direction whereas there is nearly a plane strain state in the mid-plane because there is stress in the Z direction due to the material presence.

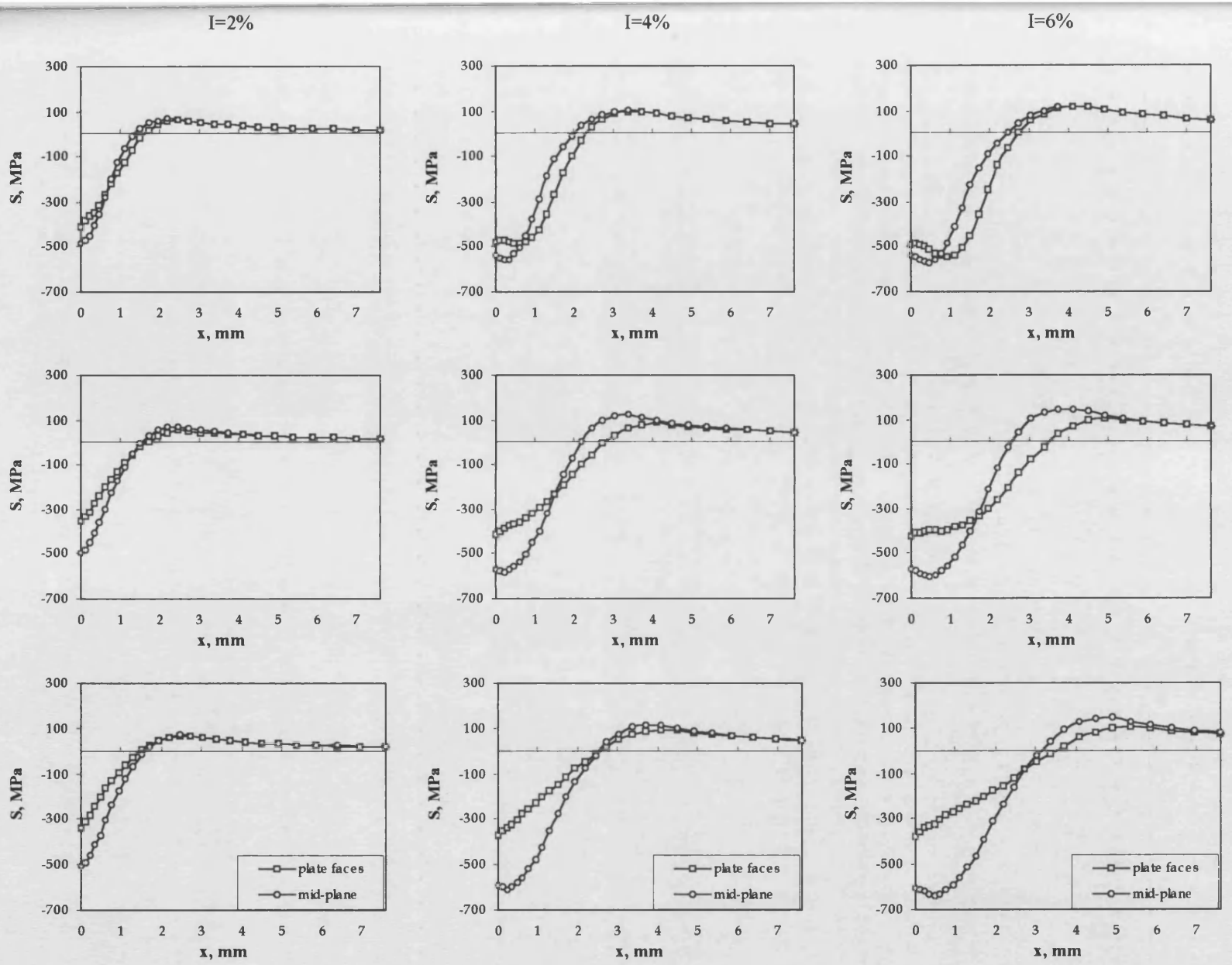

Fig 3.17: Tangential residual stress, S around hole for different plate thicknesses and cold expansion interferences for model A

3.7.2) Tapered pin without sleeve (model B)

The tangential residual stress results for different interference and plate thicknesses for this cold expansion model are presented in fig 3.18. The residual stress distributions are shown for three planes of the entrance face, the mid-plane and the exit face across the plate thickness. As shown in fig 3.18 the distribution of tangential residual stress around the hole is not uniform through the plate thickness. The tangential residual stress varies with the amount of interference and also the plate thickness.

At the entrance face the residual stresses are mostly compressive, however, at higher interference (4% and 6%) and in the 10 mm thick plate they become tensile. It is noted that the presence of tensile residual stress near the hole is in conflict with the described cold expansion aim.

The magnitude of compressive residual stress at the hole edge in the mid-plane is larger than at the plate faces and it increases with increasing plate thickness and interference from I=2% to I=4% and 6%.

The residual stress in the exit face is compressive and decreases with increasing interference and plate thickness. It is also positive in thicker plate and for I=4% and I=6% at the hole edge. However, the region in the exit face that has positive residual stress is very small in comparison with the entrance face. At the exit face the maximum compressive residual stress moves from the hole edge with I=2% to 1-1.5 mm from the hole edge with I=4%, and I=6% for all plate thicknesses.

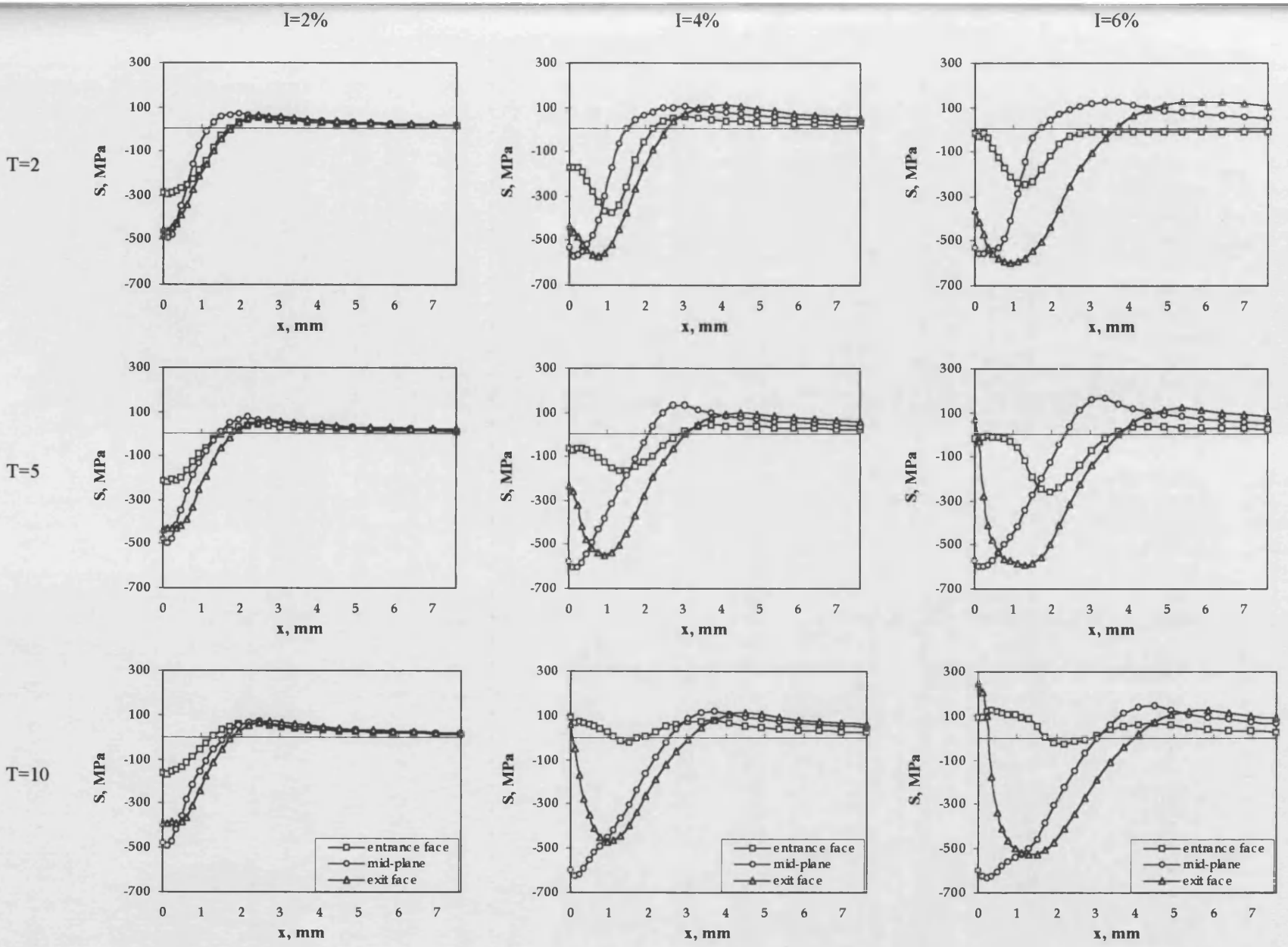

Fig 3.18: Tangential residual stress, S around hole for different plate thicknesses and cold expansion interferences for model B

3.7.3) Ballising (model C)

The tangential residual stress results around the hole for this model are shown in fig 3.19. The results include the effect of different cold expansion interference as with previous models and plate thicknesses. The tangential residual stress is shown for three planes through the plate thickness as with model B. As fig 3.19 shows, the tangential residual stress around the hole is different for the planes and like model B the stress distribution is not uniform through the plate thickness. Also the tangential residual stress of this model, like model B, depends not only on the cold expansion interference but also the plate thickness.

The tangential residual stress at the hole edge is tensile at the entrance face for all cold expansion interferences and plate thicknesses. This stress is different for the different plate thicknesses and cold expansion interferences and does not show any consistent trend. However, the area of tensile region around the hole increases with increasing cold expansion interference and plate thickness, for example, the tensile region at the entrance face changes from 0.3 mm (with I=2% and T=2 mm) to 1.6 mm (with I=6% and T=10 mm).

The tangential residual stress at the hole edge in the mid-plane is compressive for all cold expansion interferences and plate thicknesses. In the mid-plane compressive tangential residual stress at the hole edge does not change much with plate thickness or cold expansion interference.

Fig 3.19 also shows that the distribution of tangential residual stress around the hole at the exit face is slightly better than at the entrance face. At the exit face the tangential residual stress at the hole edge is compressive for different cold expansion interferences with a plate thickness of T=2 mm. With other plate thicknesses the tangential residual stress at the exit face is less tensile than at the entrance face. At the exit face the tensile region is smaller than at the entrance face. In this model the tangential residual stress at the exit face of the hole edge is worse with increasing cold expansion interference and plate thickness. However, there is a big compressive region a little distance from the hole edge.

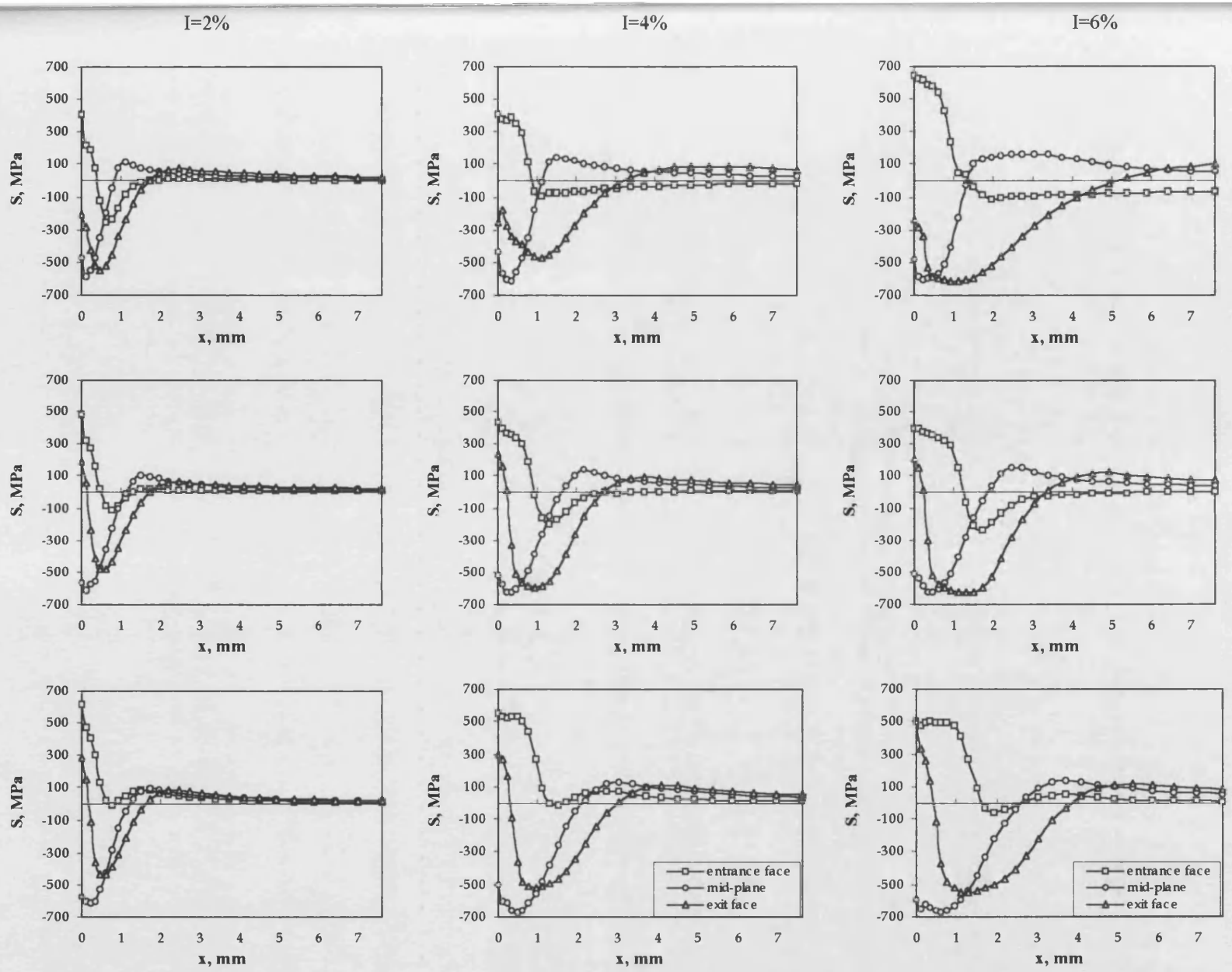

Fig 3.19: Tangential residual stress, S around hole for different plate thicknesses and cold expansion interferences in model C

Chapter 4

FE analysis of the effect of plate support, friction and sleeve

4.1) Introduction

In Chapter 3, three fundamentally different methods of cold expansion were introduced now this chapter considers other effects worthy of special attention. This chapter concentrates mainly on the tapered pin method (i.e. model B) rather than the uniform radial displacement and ballising methods (i.e. model A, C). This is done for two reasons, firstly model A is a theoretical model and it is very difficult to perform practically, and model C it has been shown, can produce tensile tangential residual stress, especially at the plate faces. Secondly, method B is a commonly used method of cold expansion and in the aerospace industry, for example, the FTI method has been used for more than thirty years [46].

In Chapter 3, the effect of interference and plate thickness on the tangential residual stress was investigated for model B. In this chapter the FE model descibed is made closer to the actual cold expansion process. For this purpose other parameters, which affect the tangential residual stress are considered. These include near hole support (model B_r), friction (model B_f) and sleeve (model B_s) which are all versions of model B. The effect of these parameters and additionally a novel method using a tapered pin and mating sleeve will be discussed in the following section.

4.2) Effect of near hole support (model B_r)

The initial FE model of the cold expansion method (model B) avoided local support effects on the distribution of tangential residual stress by supporting at the outer radius of the plate. This was done to show the effect of pin direction and compare it with the mathematical solutions which assume the plate to be either in the plane stress or plane strain state and cold expanding is carried out by applying pressure (or radial displacement) at the hole surface. In this section the effect of supporting the plate near the hole is discussed as it improves the model simulation.

4.2.1) A practical method for providing support

In practice, support is necessary for reacting the force needed for cold expansion and it can be provided by putting a ring (or washer) at the pin exit face of the plate. In the FTI method, the support is an integral part of the cold expanding tool and acts as a ring, which is located concentrically with the hole. The radial distance of the support from the hole centre and also the area of support is determined by choice of inner and outer radii for the ring.

In this section two different rings have been considered to investigate the support effect. The smaller ring has an inner radius, r1=2.5 mm and outer radius r2=3.7 mm and supports the plate just from the hole edge, and the bigger ring has r1=4.7 mm and r2=5.9 mm and supports the plate further from the hole (figs 4.1 and 4.2). Both the small ring and bigger ring have the same radial wall thickness of 1.2 mm.

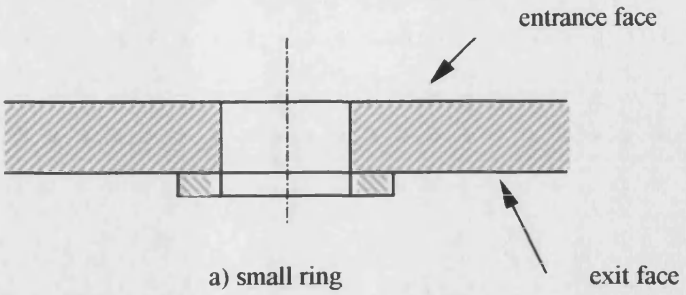

a) small ring

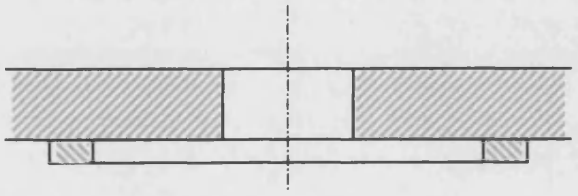

b) big ring

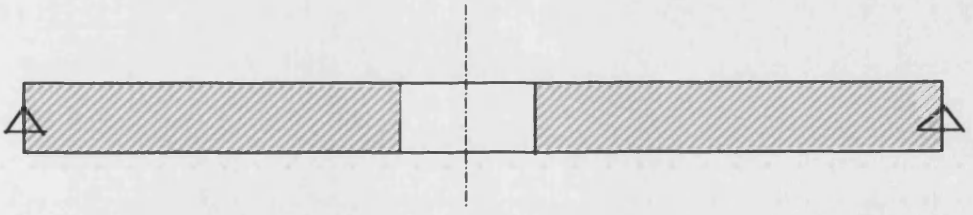

c) plate supported at its rim

Fig 4.1: Plate with different supports

4.2.2) FE models with near hole support

Model B_r is very similar to model B (see Chapter 3) except that there is an extra boundary condition due to the support ring. In practice the support ring is under axial compression during cold expansion so it deforms axially. However, for simplicity of the model the ring is assumed to be rigid and thus shows no axial deformation. This assumption will not affect the result much when the ring has a short axial thickness and is made from steel.

To include the ring support effect in the model, it appears that the nodes of the plate (which are in contact with the ring) need to be constrained in the Z direction. This is incorrect, because during the loading process (pushing the pin though the hole) some of these nodes would be in contact with the ring and some not, so to overcome this problem ground contact elements should be used instead of the support ring. The ground element (Contact 26 in Ansys) applies force to the nodes which are in contact with the ground surface otherwise it would not apply any force to the nodes (see sub-section 4.2.3).

This model, like model B, was carried out for three plate thicknesses and three interference amounts. Each set of near hole support models, B_r has been analysed once using the small ring and the other time using with the bigger ring.

With model B_r two load steps have been used instead of one as with model B. At the first load step the pin is pushed through the hole from the plate entrance face until it comes out from the plate exit face. At the second load step the cold expanded plate is removed from the ground element (i.e. from the ring surface). Although the effect of the second load step on the tangential residual stress is small for most of the time, it is necessary for the simulation.

In practice the only support is the ring (or washer) and this is simulated by using ground contact elements. This support is an unreliable constraint for a static model if the model does not include other constrained nodes this is especially so when the model loses contact with the ground. To have a well-constrained model, therefore, the plate has to be constrained at its outer radius (see fig 4.2).

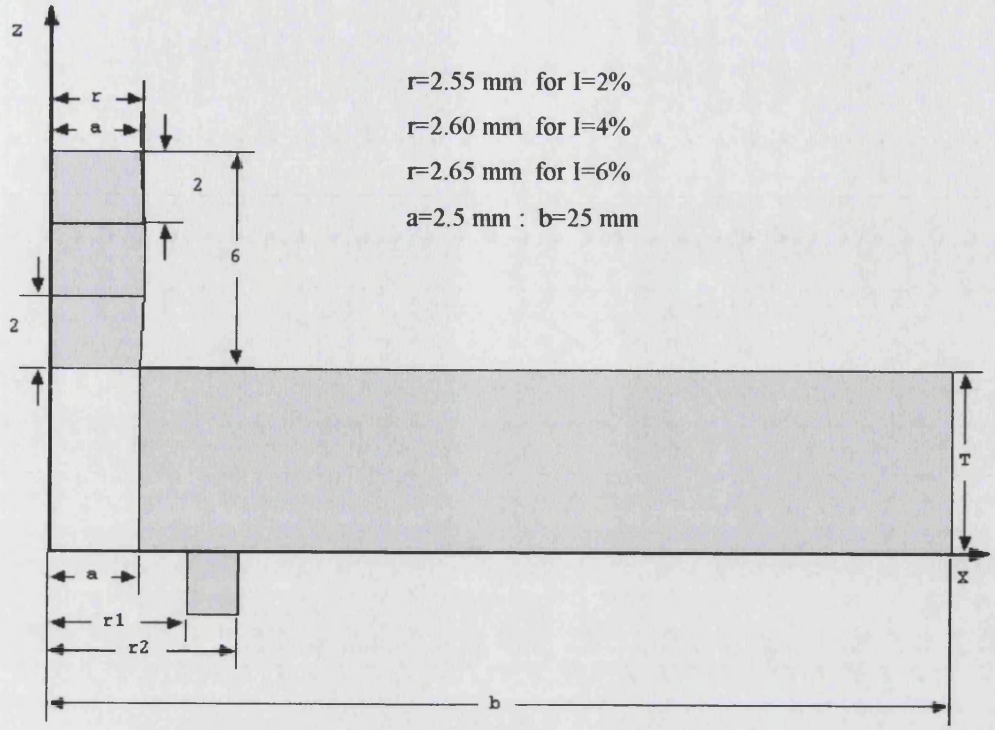

a) Projected surfaces

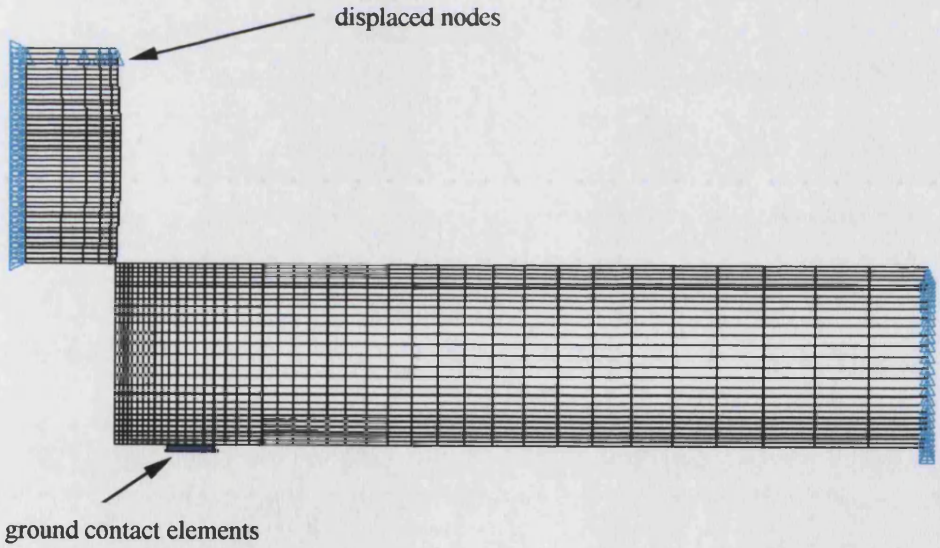

b) Axisymmetric mesh

Fig 4.2: Cold expanding a hole using a tapered pin with near hole support (model B_r)

4.2.3) Contact-26 element description

Contact 26 is a gap element representing a surface which will resist penetration by a node. The element is capable of supporting compression in the direction normal to the surface and also shear in the tangential direction (i.e. Coulomb friction). The element has two degrees of freedom at each node: translations in the nodal x and y directions. The surface may be straight or a circular arc and the surface may also be defined to move. Multiple elements may be defined to form a complex surface. The element may only be used to represent model-to-ground behaviour

The element may be initially preloaded in the normal direction or it may be given a gap specification. A specified stiffness acts in the normal direction when a node penetrates the surface.

The geometry, node locations and the co-ordinate system for this element are shown in fig 4.3. The element is defined by three nodes (I, J and K), surface constants (defining the surface curve), a normal stiffness (*KN*) (to JK), and sliding stiffness (along JK) for elastic Coulomb sliding (*KT*) although this is not included in model B_r.

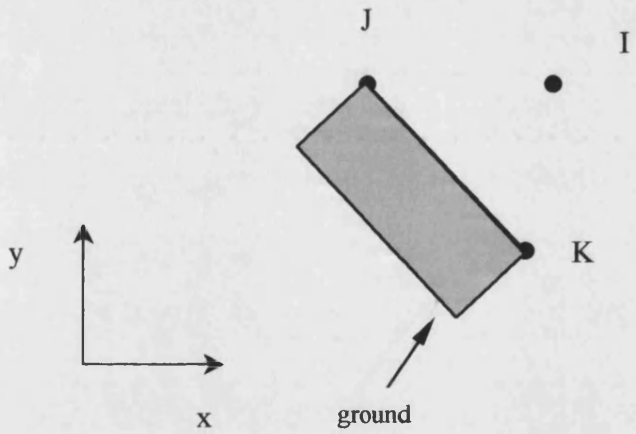

Fig 4.3: CONTAC26 2-D Point-to-Ground Contact Element

Node *I* is the active node associated with the flexible model. Nodes J and K are used to define the ends of the contact surface, which may be defined as moving by imposed

displacements. A flat surface is assumed to be rectangular having its width between nodes J and K in the x-y plane and a semi-infinite length to the right of the surface line (when viewed from node J to node K).

4.2.4) Discussion of results

The tangential residual stress results for the three plate thicknesses (2, 5 and 10 mm) are shown in figs 4.4 to 4.6. Each figure presents three cold expansion sizes in rows and three support locations in columns (the small ring is in first column and the bigger ring is in the second column). For comparison the results of model B, in which the model was supported at the farthest nodes from the hole (outer rim), have been added as a third column. Therefore each figure consists of nine charts and each chart includes three curves, which correspond to the plate entrance face, the mid-plane and the exit face. In each chart, like with chapter 3, the x- axis shows the distance from the hole edge and y-axis shows the tangential residual value.

4.2.4.1) Plate thickness of 2 mm

The results for this plate are shown in fig 4.4 and it shows that the tangential residual stress at the pin entrance face worsens when the support location moves from the hole edge to the plate rim. The support effect on the tangential residual stress is small for a small cold expansion size at entrance face but it is quite appreciable with larger cold expansion sizes (interference amount). This is understandable because the compressive tangential residual stress is reduced from 350 MPa (at the hole edge) in small ring support to 20 MPa when the plate is supported at the outer rim (for the I=6%). Such a result can be explained by a larger deflection occurring in the plate due to larger axial force transmitted from the pin with larger interference. As a result the hole experiences less interference at the entrance face in the case of outer rim support. Figure 4.4 shows also that the support location does not influence the distribution of tangential residual stress at the mid-plane.

The effect of support location on the tangential residual stress is small for small amount of interference at the exit face like the entrance face. However, with the larger interference, its effect for the exit face is opposite to its effect for the entrance face.

Therefore the farther the support (from the hole) the more compressive and thus the better tangential residual stress distribution at the hole edge in the exit face.

4.2.4.2) Plate thickness of 5 mm and 10 mm

The results for these plates are shown in fig 4.5 and fig 4.6. As these figures show the support location does not have any appreciable effect on the tangential residual stress distribution at the plate entrance faces and their mid-planes.

At the exit face, the effect of the support location is negligible on the tangential residual stress for I=2% with both plates. However, strictly speaking the support location has a mixed effect at the exit face for larger cold expansion sizes.

At the exit face in the 5 mm thick plate the residual stress with I=4% is improved at the hole edge when the support moves towards the outer rim, whereas, with I=6% the support position does not have much effect on the result.

For the 10 mm thick plate the tangential residual stress at the hole edge is worse. As figures 4.5 and 4.6 show there is some disruption in the exit face curves especially for I=4 % and I= 6% as this is due to presence of the contact elements, which replaced instead of the support rings.

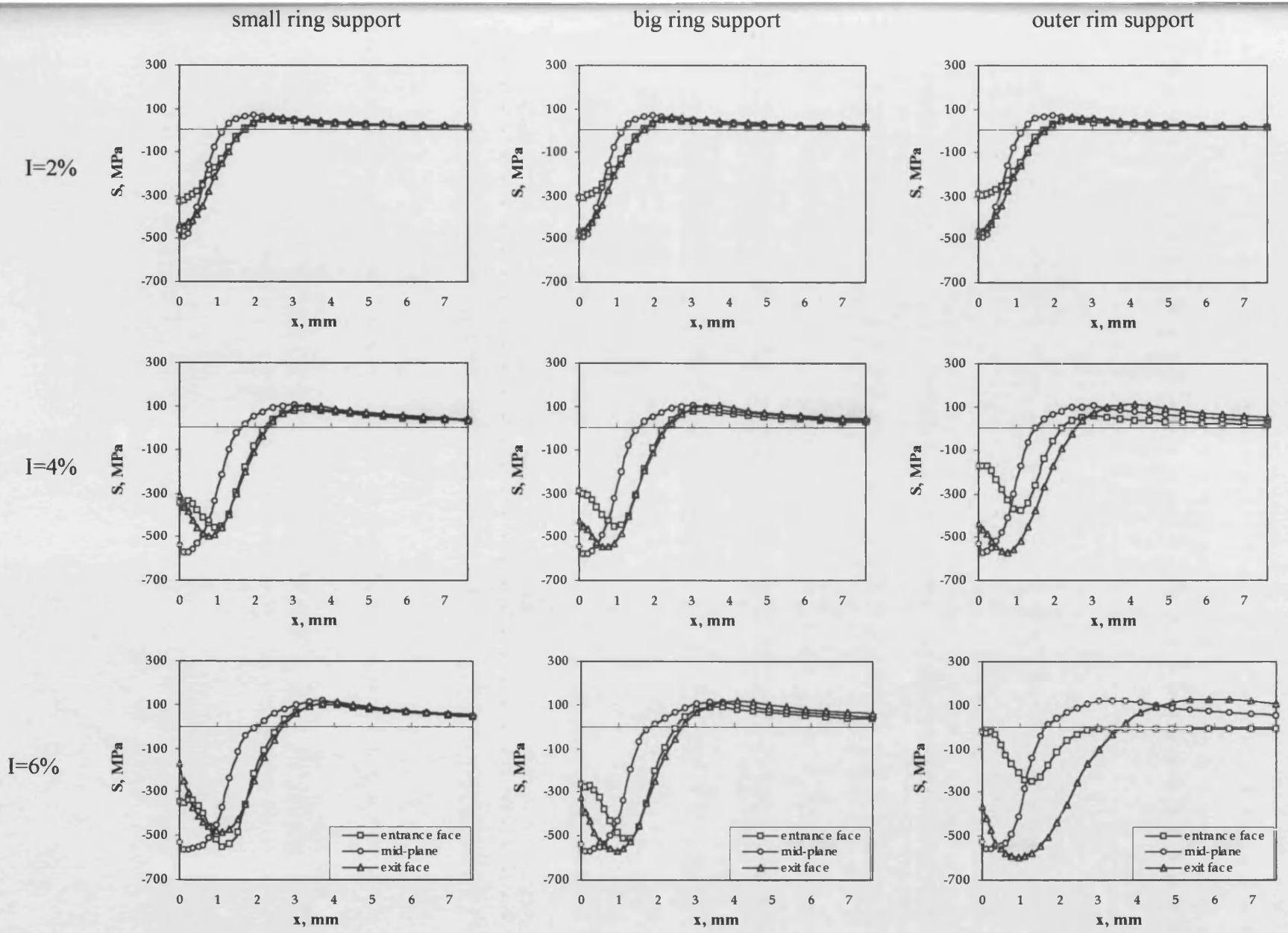

Fig 4.4: Tangential residual stress, S in model B_r for three supports and three interferences for 2 mm thick plate

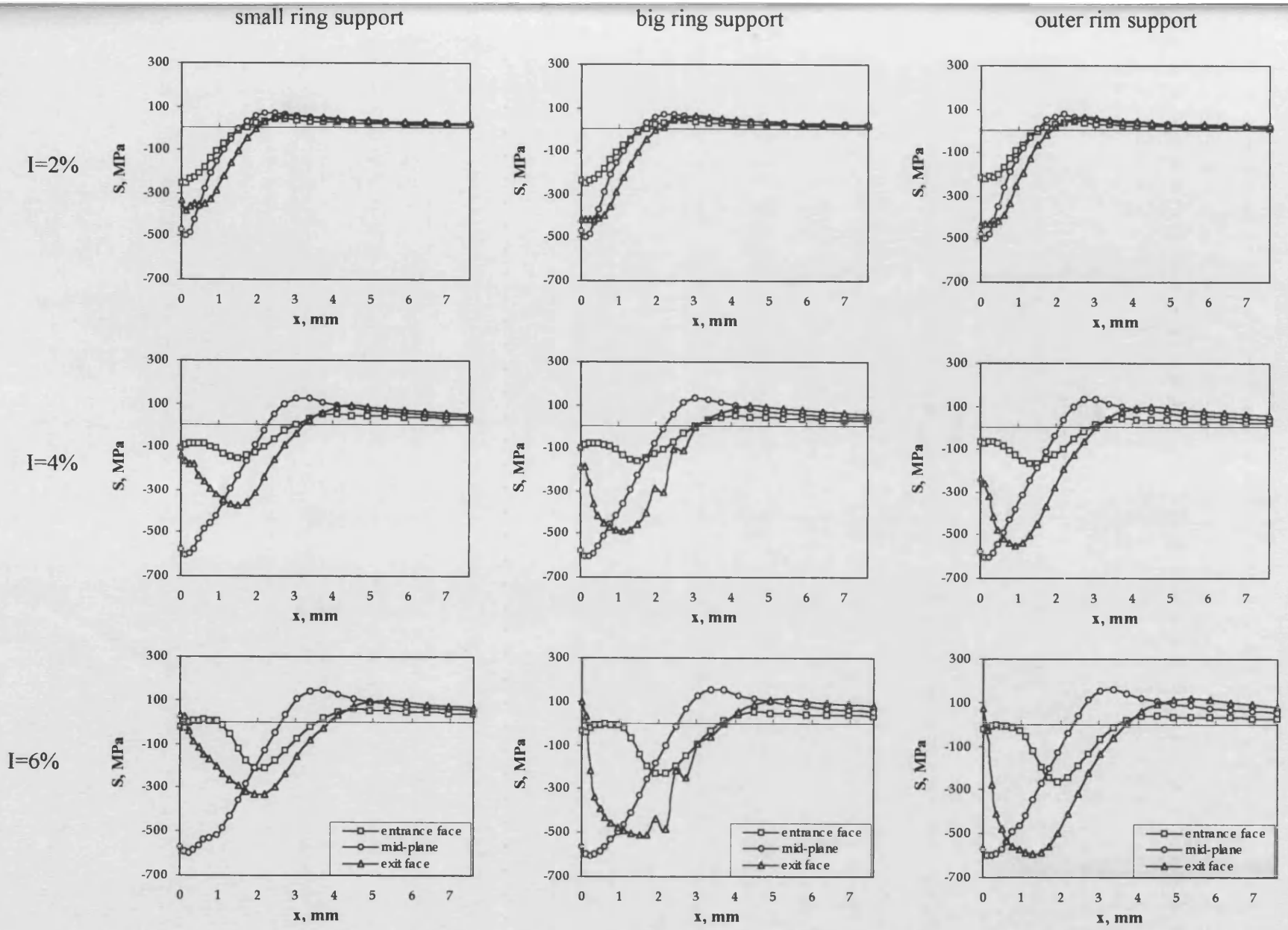

Fig 4.5: Tangential residual stress, S in model B_r for three supports and three interferences for 5 mm thick plate

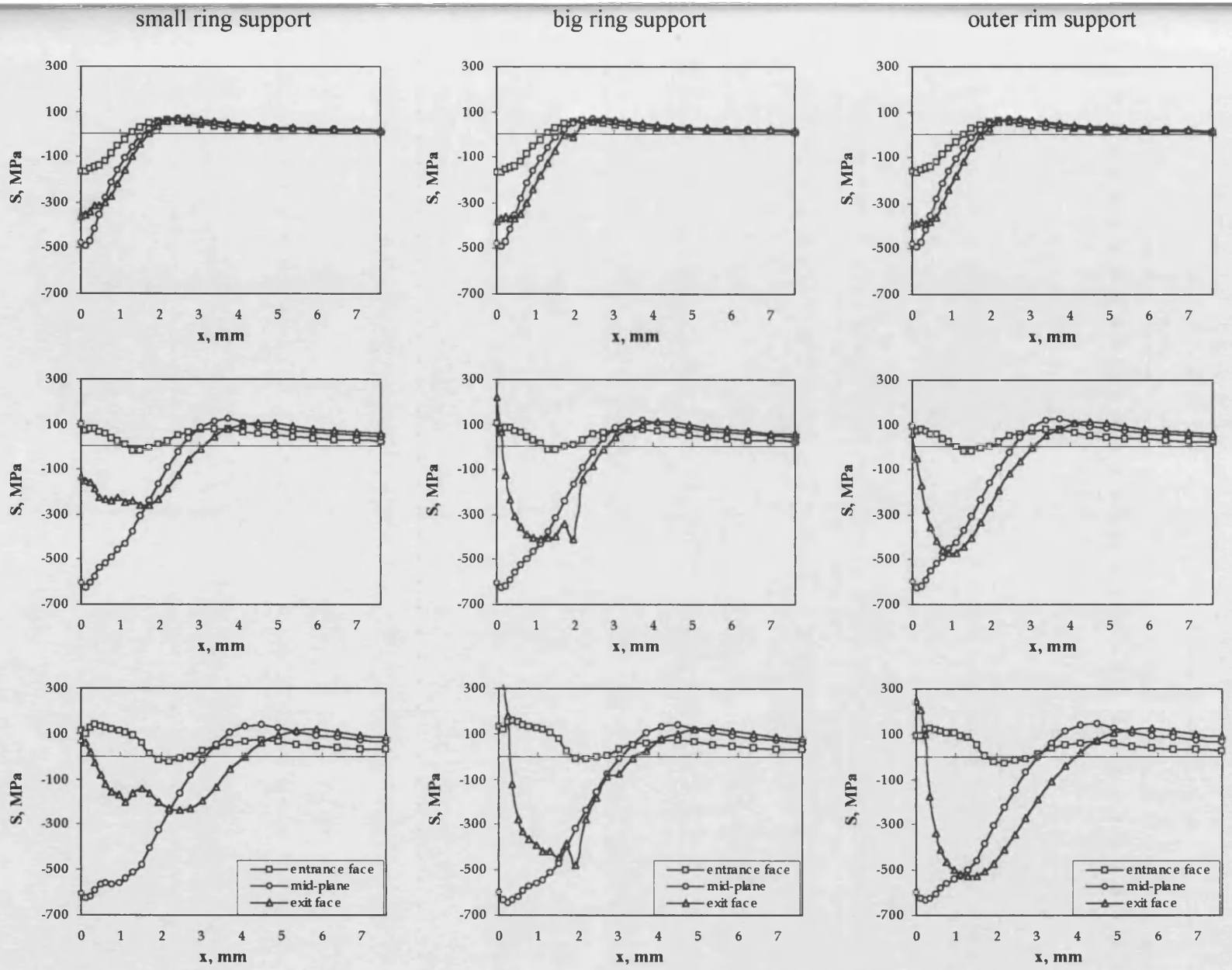

Fig 4.6: Tangential residual stress, S in model B_r for three supports and three interferences for 10 mm thick plate

4.3) Friction effect (model B_f)

Researchers have tried to minimise friction but without knowing fully the implication of whether it is desirable [4, 6, 7, 28]. In practise, friction can be reduced by using a good lubricant like molybdenum disulphide or Tallow. However, using lubricant never fully eliminates friction so it could still affect the residual stress around the hole. Therefore in an accurate simulation of cold expansion friction should be included. The reasons for reducing the coefficient of friction originated from two considerations. Firstly the rubbing may cause scratches and thus affect fatigue life so it should be minimised, secondly lower friction reduces the pushing force of the pin through the hole.

Unfortunately few papers report including friction in their cold expansion analysis or simulation and therefore there is only a vague idea that it has a negative effect on fatigue life. Even reporting experimental result papers that prove this assumption are rare.

In this section the effect of friction on the tangential residual stress is investigated. This is done to find if friction has a positive or a negative effect in producing favourable compressive tangential residual stress in a cold expanded hole.

4.3.1) FE of friction model B_f

This model is the same as model B_r but with friction included. The B_f model is used only for 5 mm thick plate for three cold expansion interferences and two support rings as described in sub-section 4.2.1. In order to investigate the friction effect on the tangential residual stress distribution two different values for coefficient of friction are considered between the contacting surfaces (μ= 0.15 and μ=0.30). Friction is included only between the steel pin and the aluminium plate. The effect of friction at the ring supports is considered negligible. The coefficient of friction for dry metal-to-metal contacting surfaces is quoted as between 0.15 and 0.3 [47] but will be smaller when lubricant is used.

In friction model B_f the coefficient of friction is given as a material property for the Contact 48 elements; these are capable of applying friction force to the plate at the hole surface and the pin surface. The available friction models in the Ansys package

are Rigid Coulomb and Elastic Coulomb. The Elastic Coulomb friction model has been applied to the B_f model because it is suitable for static analysis.

In model B_f away from the hole the same Plane 42 quadrilateral elements are used as for model B_r but near the hole region the triangular form of Plane 42 elements are used (see fig 4.7). This was done to avoid the element formation problem occurring during solution process; some of the hole surface elements can so deform that the quadrilateral shape elements can change to triangular and cause element mapping problem [48-52]. This difficulty occurs in problem involving plasticity and can be overcome by using: large quadrilateral elements or triangular form of elements.

Using large quadrilateral Plane 42 elements are not suitable near the hole for this model because they give an inaccurate result at the region of interest. Using triangular elements are suitable although these are not as accurate as the quadrilateral form. However, the accuracy problem has been improved by choosing a finer mesh.

With model B_f the material properties and loading process are the same as model B_r. In the loading process (pushing the pin though the plate hole) a larger number of sub-steps (500) were needed to get equilibrium iteration convergence.

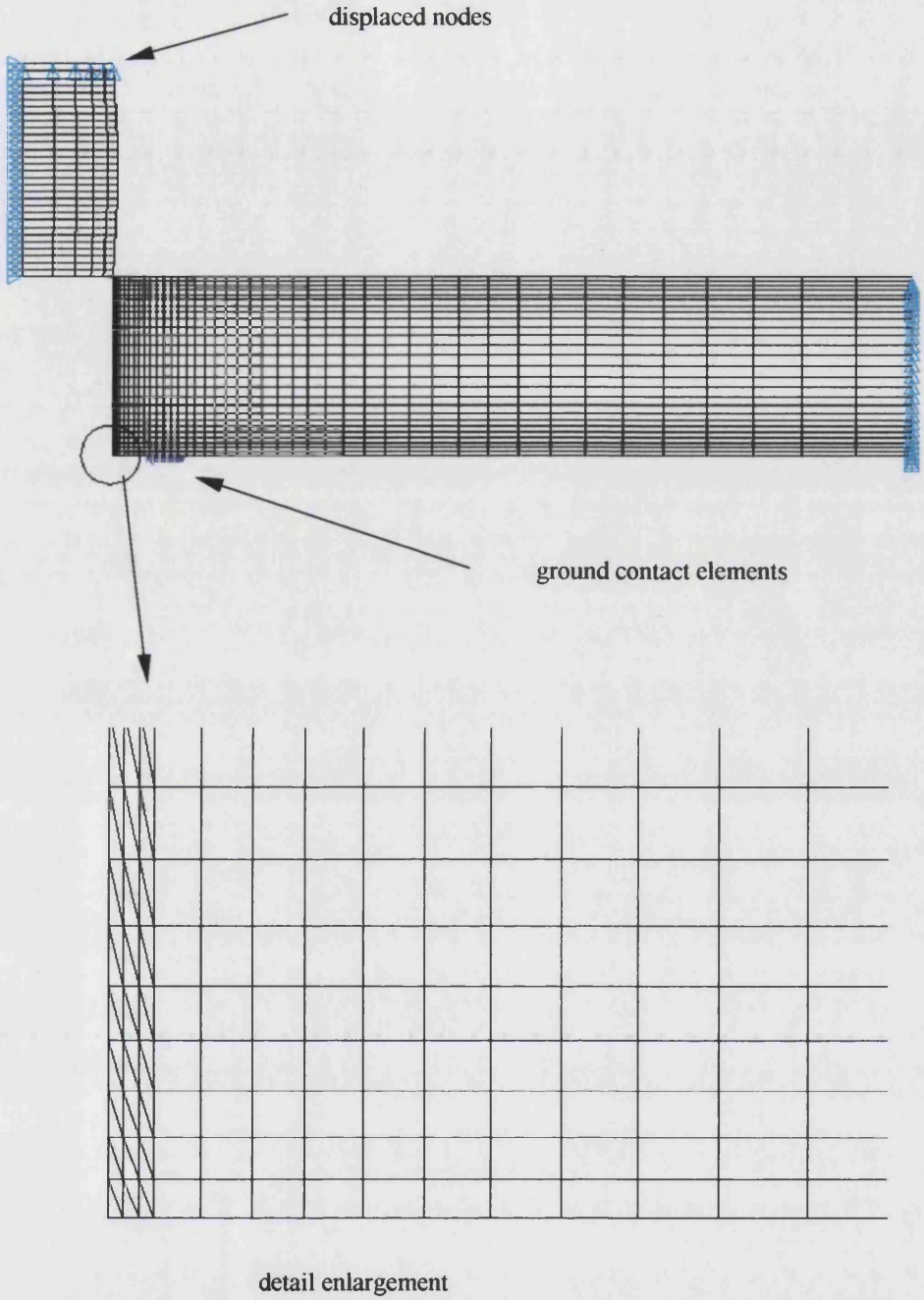

Fig 4.7: Position of triangular Plane 42 elements near the hole in friction model B_f

4.3.2) Discussion of results

In model B_f the combined effects of friction, cold expansion size and support location (i.e. using the small and big ring) on the tangential residual stress for 5 mm thick plate are shown in figs 4.8 and 4.9. In these figures, the tangential residual stress distribution for the frictionless (μ=0) model B_r for the 5 mm thick plate has been included for comparison with the model B_f.

The graphs in figs 4.8 and 4.9 have been arranged as arrays of a matrix in which common interference amounts are in rows and different coefficients of friction (μ) are in the columns. In these figures the tangential residual stress results verses distance from the hole edge are shown for three planes - the pin entrance face, the mid-plane and the exit face of the plate (like the previous models).

4.3.2.1) Big ring support

The tangential residual stress distribution for this friction model is shown in fig 4.8. It can be seen that the friction effect is more evident at the entrance face than at the mid-plane and exit face. For each interference amount the compressive tangential residual stress increases with increasing coefficient of friction at the hole edge of the entrance face. For I=2% the effect of friction is restricted only to the hole edge. However, for I= 4% and 6% the friction improves the tangential residual stress magnitude not only at the hole edge but also in the region far from the hole at entrance face. This is especially evident for I=6% and μ=0.3.

Comparing the frictionless model B_r and the friction included model B_f shows that friction has little effect on the tangential residual stress at the mid-plane. It improves it at the hole edge when I=2% but its effect for the larger interferences is negligible.

At the exit face, friction generally causes tensile tangential residual stress at the hole edge as shown in fig 4.8. However, the region that has tensile residual stress is very small and it is limited to the corner near of the hole surface only.

In model B_f (which is similar to model B_r) there are disruptions in the tangential residual stress curves at the exit face. This is because of the direct contact with the big ring support and this causes a local plastic region.

4.3.2.2) Small ring support

For model B_f the tangential residual stress results are presented in fig 4.9 for when the support is located from the hole edge using small ring. The results show that the tangential residual stress has been improved appreciably at the hole edge of the entrance face when friction is included in the model. As the graphs show, with the larger amount of interference and coefficient of friction, even the region that is 1.5 mm from the hole edge benefits from this improvement at the entrance face. Comparing the corresponding curves at the entrance face for the nine charts shown in figs 4.8 and 4.9, it shows that with the small ring the tangential residual stress has a better distribution than with the big ring. For example, with I=2% and μ=0.3 the tangential residual stress was –440 MPa using the big ring but –500 MPa at the hole edge using the small ring (see fig 4.10).

It is found that using the small ring support, as with the big ring support, does not change the distribution of tangential residual stress at the mid-plane. There is only a little increase in compressive tangential residual stress with increasing coefficient of friction for I=2% at the mid-plane. Comparing the results of residual stress at the mid-plane in fig 4.8 with fig 4.9 shows that the support position virtually does not affect the distribution of tangential residual stress.

The small ring support though has an appreciable effect on the distribution of tangential residual stress at the exit face of plate - especially in the hole edge. Unlike with the big ring support, with small ring support the exit side generally has compressive tangential residual at the hole edge.

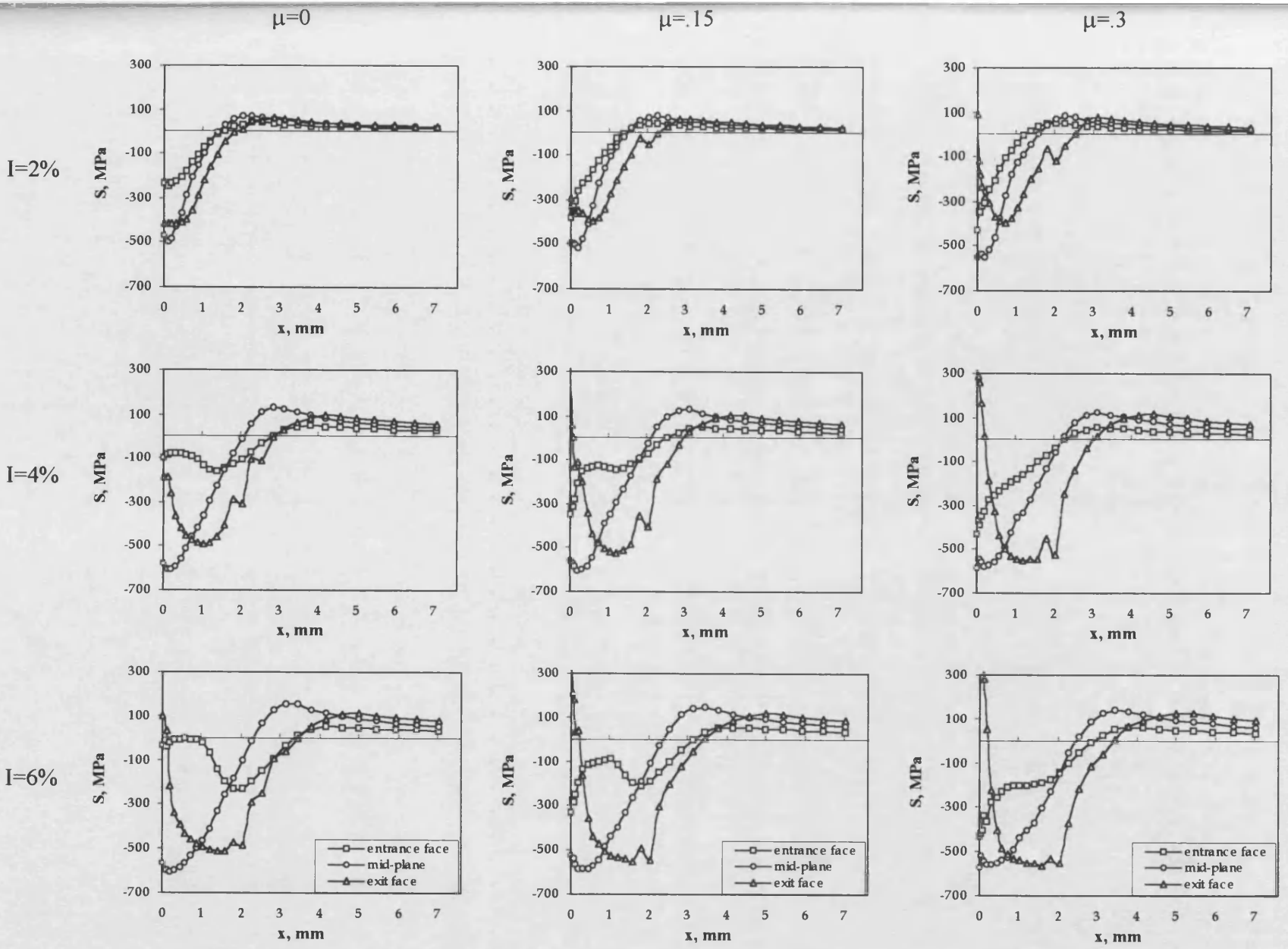

Fig 4.8: Tangential residual stress, S in model B_f for three coefficient of friction and three interferences with big ring support (in T=5 mm)

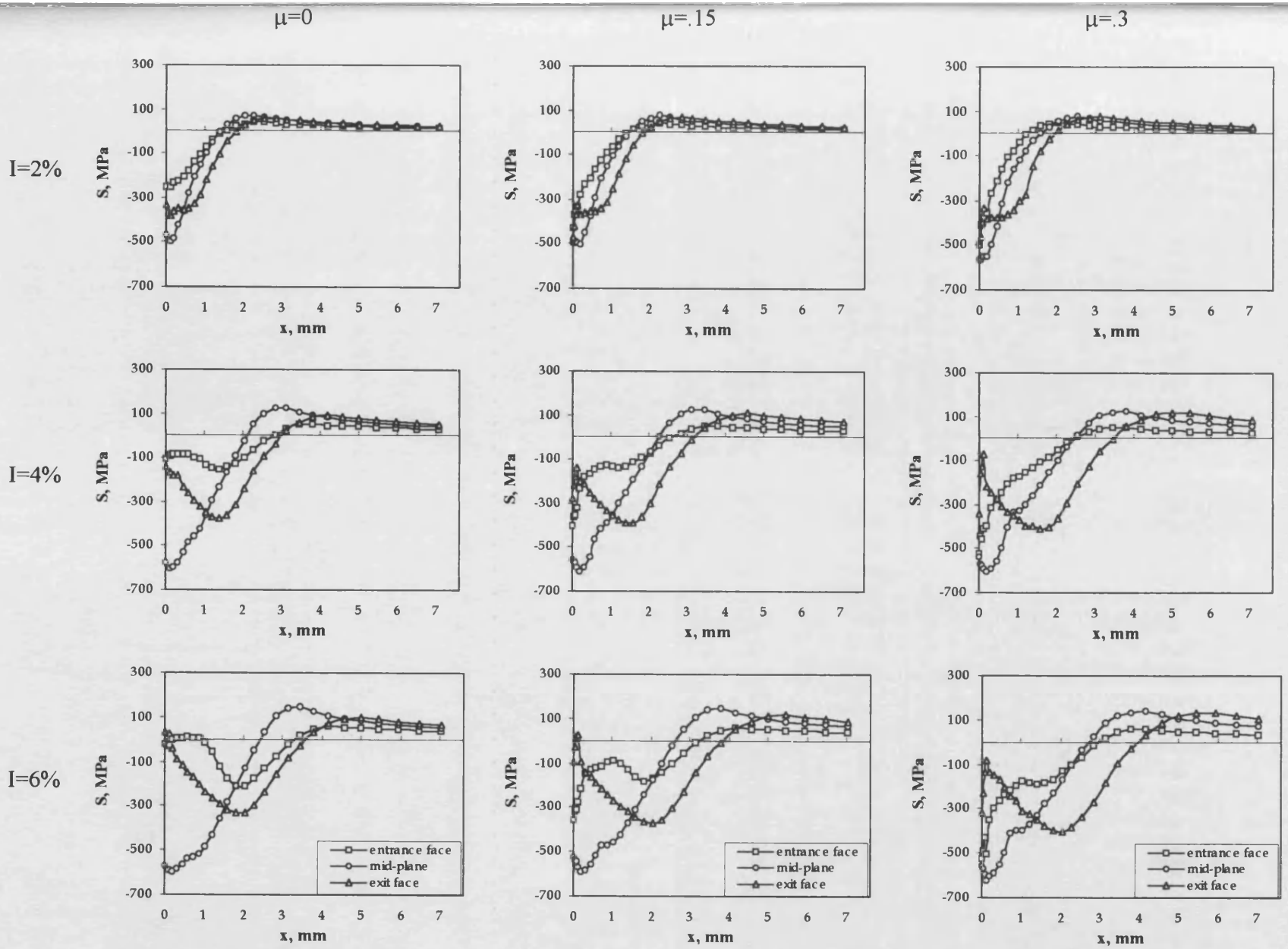

Fig 4.9: Tangential residual stress, S in model B_f for three coefficient of friction and three interferences with small ring support (in T=5 mm)

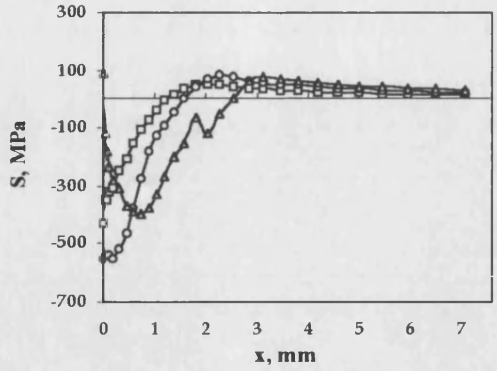

a) Using big ring

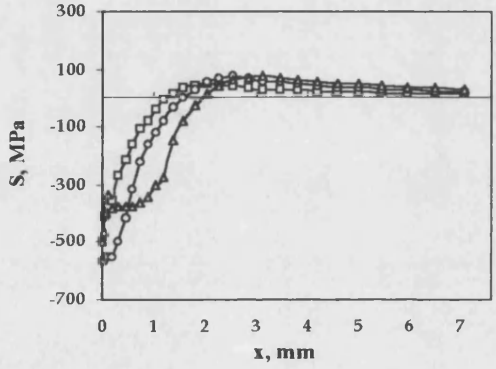

b) Using small ring

Fig 4.10: Comparison of tangential residual stress using big and small ring support

4.4) The effect of using a sleeve (model B_s)

In some cold expansion methods, for example the FTI method, a lubricated sleeve is used in the hole. The purpose of using a sleeve is to avoid the likelihood of hole surface damage that could be caused by friction between the pin and the hole [4, 6, 7, 28]. In the presence of a sleeve there is no direct contact between the pin and the hole therefore the rubbing effect due to the direct contact is eliminated.

Different wall thicknesses may be used for the sleeve. For example, FTI uses a thickness of about 0.152 mm whereas it should be thicker when a tapered pin and mating sleeve is used to avoid plastic collapse (see section 4.5).

In practice, a split sleeve is commonly used and the main reason for this is different depending on whether the wall thickness is thick or thin. The reason is pin pushing force because expanding a thick split sleeve seems to need less force than a closed (i.e. not split) one. The main reason, however, is that a thin sleeve can be more easily manufactured using shim material.

A disadvantage of having a slit is that it leaves an untreated length at the hole surface (called a pip) and this may cause a stress concentration. In practice this "pip" is removed during final reaming of the hole.

The sleeve-included model (B_s) is analysed in the following section to investigate the effect of a sleeve on the tangential residual stress distribution. The results of this model are compared with model B (without sleeve) results to see if the sleeve has any significant effect.

4.4.1) FE model with parallel sleeve

Producing an axisymetric model with a split sleeve is not possible and so it needs a 3-D model. If the sleeve is assumed to be a complete it enables an axisymetric model to be used instead of a complicated 3-D model. In Chapter 5, though, a 3-D model of a split bush is included for comparison purposes. Looking at the 3-D result in Chapter 5 shows that this assumption does not have much effect on the distribution of residual stresses in the region of interest.

The sleeved model B_s is similar to model B, however, they have some differences. These are only limited to the tapered pin size and the sleeve presence between the hole and the pin in model B_s.

Model B_s comprises three pieces of the plate, the pin and the sleeve instead of two pieces with model B. The geometry and mesh configuration of this model is shown in fig 4.11. Plane 42 elements are used for the all three pieces and Contact 48 elements are used to transfer contact forces between pieces. Two sets of symmetric contact element (see Chapter 3) have been used in the model, one set between the plate and the sleeve and the other set between the sleeve and the pin. Also with this model, like with model B the contacting surfaces were assumed to be frictionless.

The material properties for the plate and the pin are the same as for model B (see previous chapter) and the sleeve like the pin steel is assumed to behave elastically.
The boundary constraints of this model for the plate and the pin are the same as for model B, and the sleeve is only constrained in the Z direction at its lower part (see fig 4.11).
The finite element analysis of the cold expansion process is carried out for three plate thicknesses with T=2, 5 and 10 mm and three amounts of interferences with I=2%, 4%, and 6% like with model B.
In model B_s the pin diameter has changed in comparison with the pin of model B due to the presence of a sleeve. The nominal amount of interference for this model is defined in the following equation:

$$I = \frac{(r + t_s - a)}{a} \times 100 \qquad (4.1)$$

In equation 4.1 r is the pin largest radius, t_s is the sleeve wall thickness and a is the hole radius. The sleeve wall thickness was 0.152 mm corresponding to that used on the FTI method.

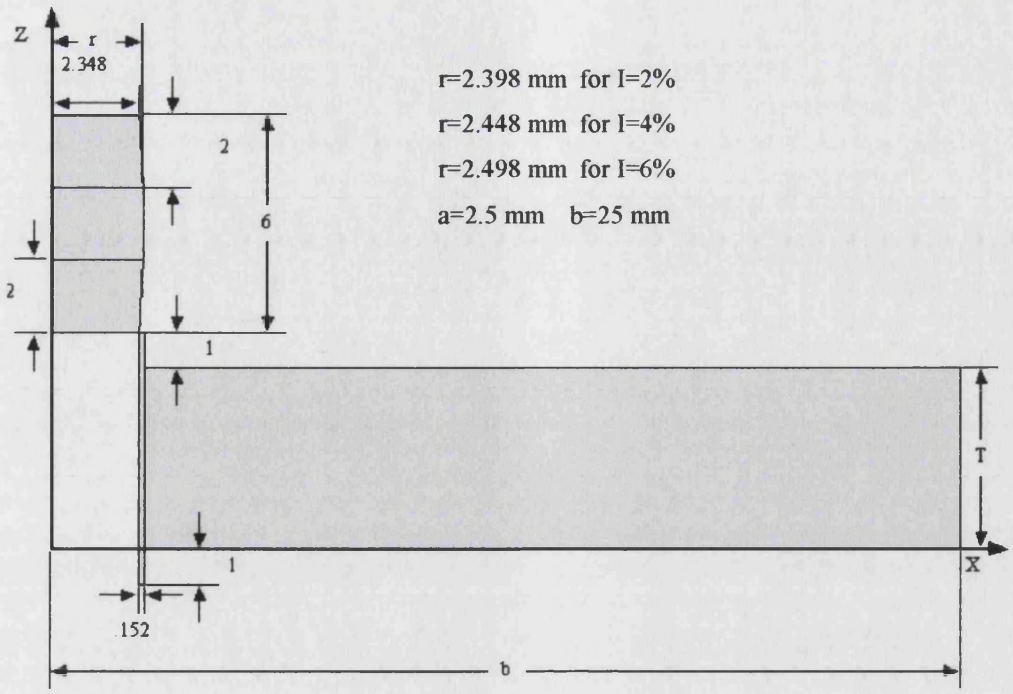

a) Projected surfaces

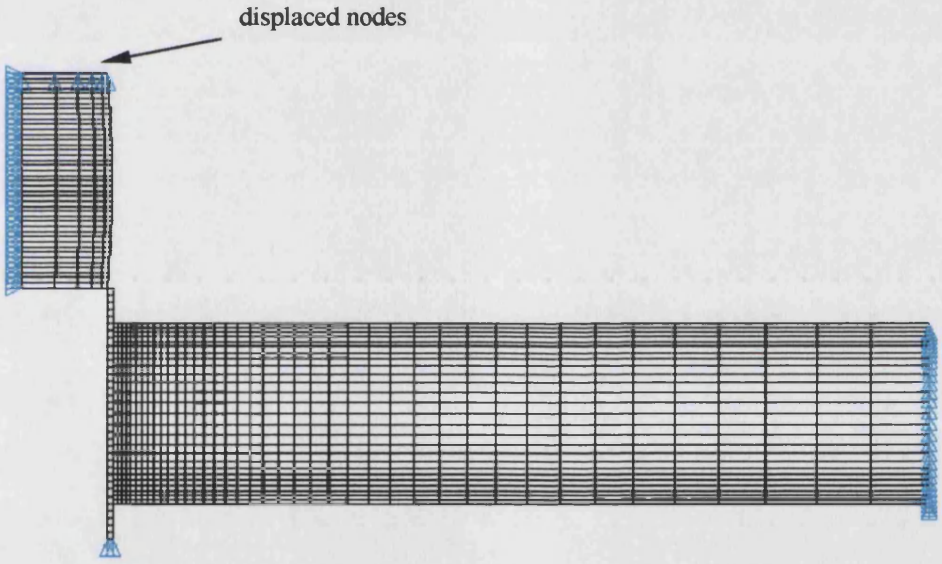

b) Axisymmetric mesh

Fig 4.11: Dimensions and mesh of a tapered pin with sleeve, model B_s

4.4.2) Discussion of results

The tangential residual stress distribution around the hole is shown in fig 4.12. The results are presented for three plate thicknesses and three amounts of interference at the pin entrance face, the mid-plane and the exit face. Comparing these results with those of model B (see fig 3.18) shows that there is virtually no difference between results for model B and B_s. Some minor differences are due to the smaller interference amount that the hole experiences in model B_s because part of the interference is taken up pressing the sleeve during cold expansion.

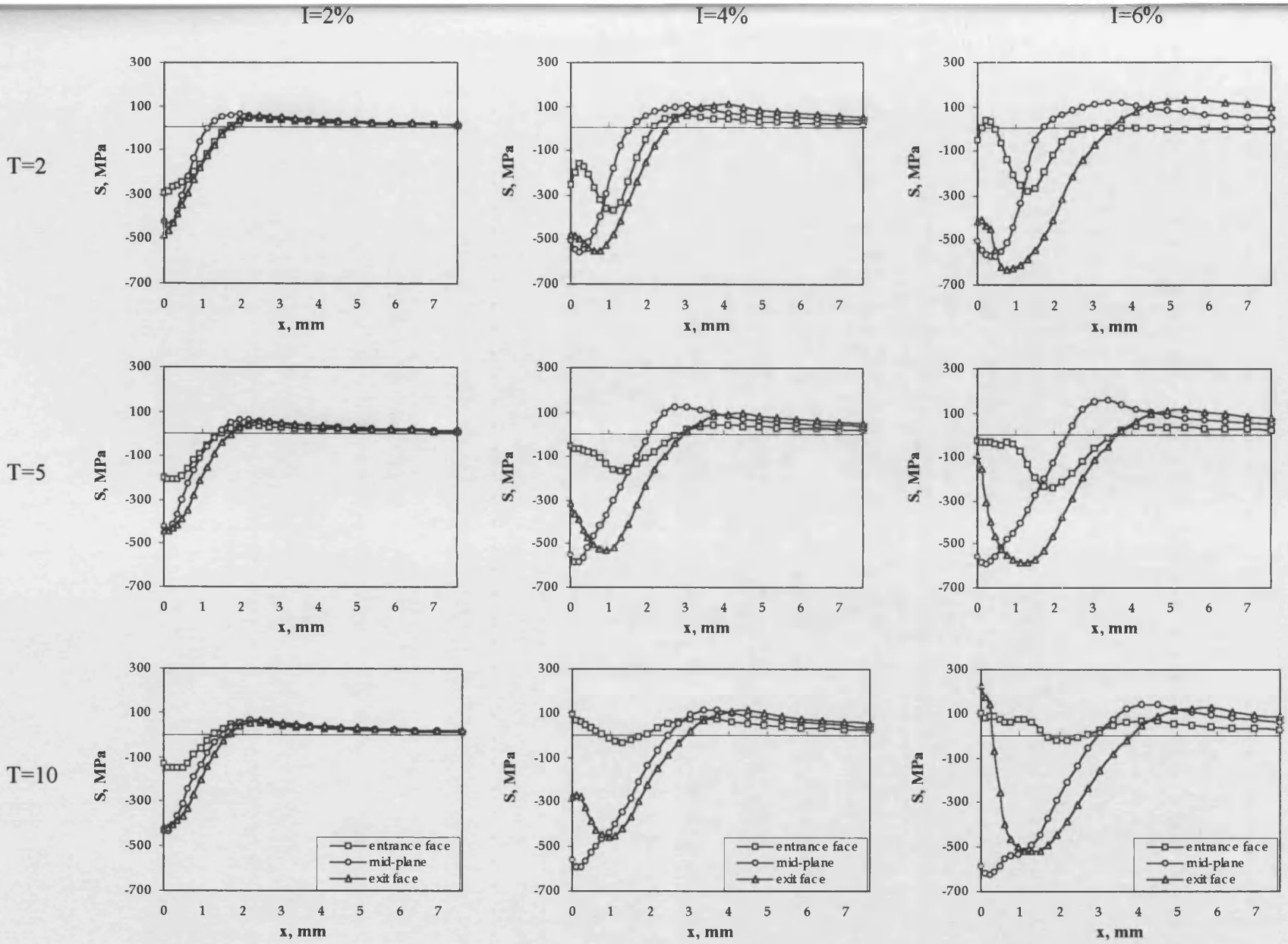

Fig 4.12: Tangential residual stress, S in method B_s for three plate thicknesses and three interference amounts

4.5) Tapered pin with mating sleeve

In chapter 3 cold expansion of a hole using a tapered pin without a sleeve was analysed and it was shown that the distribution of tangential residual stress is not uniform through the plate thickness. The FE results showed that even tensile tangential residual stress was created at the hole edge of the entrance and the exit faces for the thicker plate considered with a large interference. In this section a novel method of cold expansion which uses a tapered pin with a tapered mating sleeve is investigated in order to avoid the poor residual stress distribution which results from using previously discussed methods. With this method, unlike the tapered pin (model B) and ballising (model C) methods the hole surface is uniformly expanded and sprung back through the thickness. Therefore the residual stress distribution that is produced would be similar to the ideal method of uniform radial displacement.

4.5.1) FE model

The model geometry and its mesh are shown in fig 4.13 and it consists of three pieces - a tapered pin, the mating sleeve and the holed plate. In the model Plane 42 elements were used for all these pieces and two sets of Contact 48 elements were located between the pin and sleeve, and sleeve and the hole interface surfaces. Elastic steel properties were used for the pin and sleeve as with the parallel sleeve model B_s and elastic-plastic Al-alloy properties were applied to the plate. The sleeve was constrained at its bottom surface and the plate was constrained at its outer radius in the Z direction. The pin was constrained in the X direction at its centre line and was displaced from its top nodes during cold expansion.

The pin taper is 1:48 (i.e. when moving 48 mm from one point on its length to another point its diameter will increase or decrease 1 mm) so for producing different interference amounts the pin must be displaced different distances. The interference amount in this model is defined as:

$$I = \frac{(d/48)}{2a} \times 100 \qquad (4.2)$$

Where d is the tapered pin axial displacement.

The model described in this section was only completed for I=6% in 10 mm thick plate because the tangential residual stress distributions for other plate thicknesses and interference amounts are very similar to the results of the ideal model (A) presented in Chapter 3.

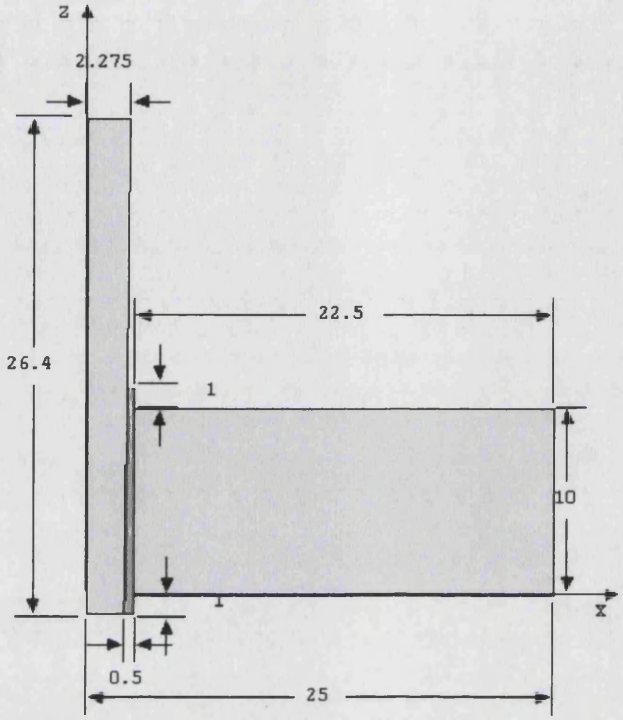

a) projected surfaces (all lines are straight despite resolution limitation)

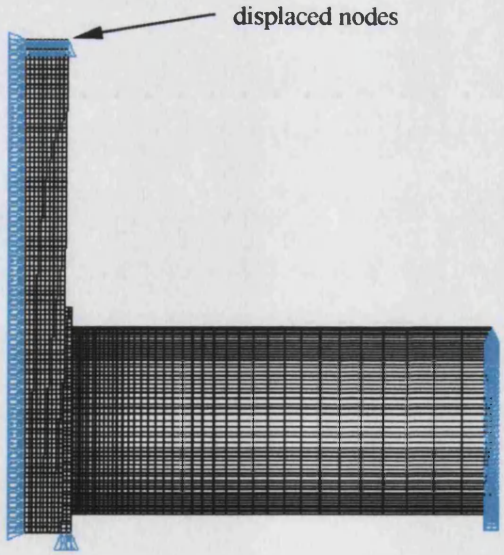

b) axisymmetric mesh

Fig 4.13: Tapered pin and mating sleeve dimensions and mesh

Loading was carried out in two stages, initially the pin was pushed down in about 400 sub-steps from the entrance face and then in the second stage it was pulled back from the entrance face using the same numbers of sub-steps. With this model the pin entrance face is the same as the exit face, however, for consistency with other models, the rear face is later referred to as the exit face.

4.5.2) Discussion of results

The tangential residual stress contours for this model are shown in fig. 4.14 and the distributions are displayed as curves for the entrance face, mid-plane and the exit face in fig 4.15. As can be seen, the residual stress distribution is not uniform through the plate thickness and is virtually symmetrical about the mid-plane. As the results show, the tangential residual stress in this model is compressive at the hole edges of the entrance and exit faces which is unlike what occurs with the ballising and tapered pin models. The results for this model are very similar to the results of model A in Chapter 3 as can be seen by comparing fig 4.15 with the equivalent chart of fig 3.17.

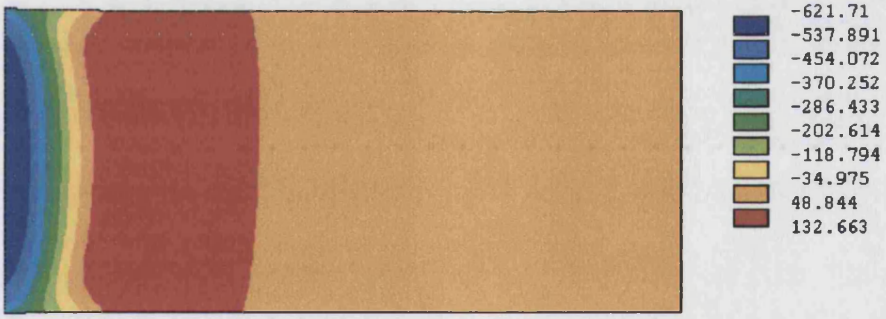

Plate thickness, T=10 mm Interference, I=6%

Fig 4.14: Tangential residual stress contours for tapered pin and mating sleeve

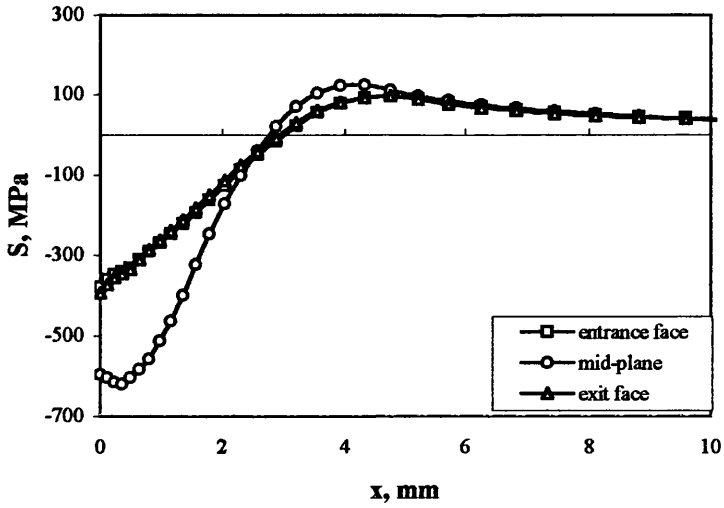

Plate thickness, T=10 mm Interference, I=6%

Fig 4.15: Tangential residual stress distribution for tapered pin and mating sleeve

Chapter 5

3-D FE models of cold expansion

5.1) Introduction

Chapters 3 and 4 two-dimensional (2-D) axisymmetric models were used for simulating cold expansion process. These models were relatively easy to generate and appropriate for symmetric models, however, there are some situations where they are not appropriate and so 3-D models must be used instead. For example, to investigate the effect of a sleeve slit on residual stresses or to find the final distribution of stresses due to loading after cold expansion, a 3-D model is needed.

In Chapters 3 and 4, the effect of cold expansion method, plate thickness, amount of interference, coefficient of friction and support location on tangential residual stress were studied. In this chapter the effect of a slit in the sleeve on the tangential residual stress distribution and also the force needed to push a pin in cold expansion process are investigated. Also, the distribution of longitudinal stress around the hole in the cold expanded plate when it is subjected to a longitudinal load is studied. This chapter only concentrates on three cold expansion techniques and these have been carried out experimentally as discussed in Chapter 6. These three techniques are the tapered pin with mating split sleeve (called CC), the tapered pin with split parallel sleeve (called BB) and the tapered pin without sleeve (called DD) (see fig 5.1). The 3-D computer simulations are completed for just one plate thickness (T=6.32 mm), one coefficient of friction (μ=0.1) and just one support type.

This chapter follows the simpler 2-D models of the previous two chapters and more accurately simulates the cold expansion practical techniques that are described in the

next chapters. Therefore, this chapter is a bridge that links the previous theoretical chapters to the next two experimental chapters.

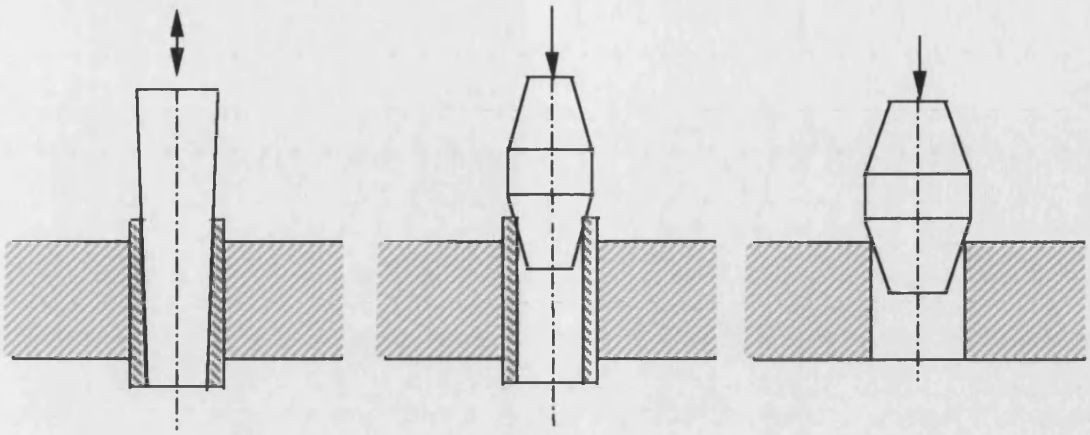

a) technique CC b) technique BB c) technique DD

Fig 5.1: Three cold expansion techniques

5.2) General explanation of models

This section describes on the common features of the three models thus avoiding repetition. The techniques are explained in greater detail in the next chapter and the common features are as follows:

1) The name of a model corresponds to the name of a technique (see Chapter 6)
2) The size of holed plate for all three models is the same. Due to the different boundary conditions, half of the plate is considered for models CC, BB and a quarter of the plate for model DD.
3) The plate is the same as used for the fatigue test specimen but only the central part is necessary for the FE models (see fig 5.2).
4) The nominal amount of interference for the models is 4.6% (see equations 3.2, 4.1 and 4.2 for definition of nominal interference)
5) The dimensions of the pins and sleeves are the same as have been used in practice for performing cold expansion (see Chapter 6), but only the engaged part of them is considered for the FE model. The dimensions of pins and sleeves are given in Chapter 6.
6) The widths of the sleeve slit in models CC and BB are not considered.

7) In models BB and CC the sleeve length is 0.5 mm longer than the plate thickness (0.25 mm of sleeve has protruded at either side of the plate). These protrusions are needed to make sure that the hole surface is in contact with the sleeve during cold expansion.
8) The material that is used for the plate is aluminium alloy 7075-T6 (using elastic-plastic behaviour) and for the pin steel (using elastic behaviour) see Chapter 2. The material that is used for the sleeve is an En 24 grade steel (using elastic-plastic behaviour) see fig 5.3.
9) The element type used for the plate, pin and sleeve is Solid 45 [43] (which is a 3-D version of Plane 42). Solid 45 has 8 integration points and 8 nodes; each node has three degrees of freedom (in the x, y and z directions).
10) Contact 49 elements [43] are used on the hole, the pin and the sleeve surfaces. This element is a 3-D version of Contact 48. Contact 49 has one contact node and four target nodes, each node has three degrees of freedom (in the x, y and z directions). The model type for friction is Elastic Coulomb with a normal stiffness, $KN=10^9$ N/m and a surface sliding stiffness, $KT=10^6$ N/m which is applied to contact elements.
11) In practice when carrying out all three cold expansion techniques, a contact washer was used to support the plate (see fig 6.9 in Chapter 6). In the FE models, the plate nodes which are in contact with the washer are constrained in the Z direction instead of using ground contact elements for the purpose of reducing the model's size.

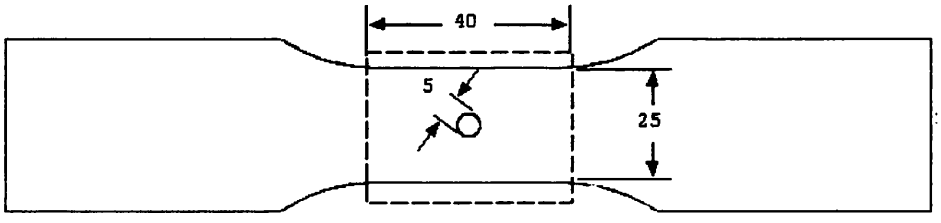

Fig 5.2: Central part of fatigue specimen which is chosen for FE models (plate thickness, T= 6.32 mm)

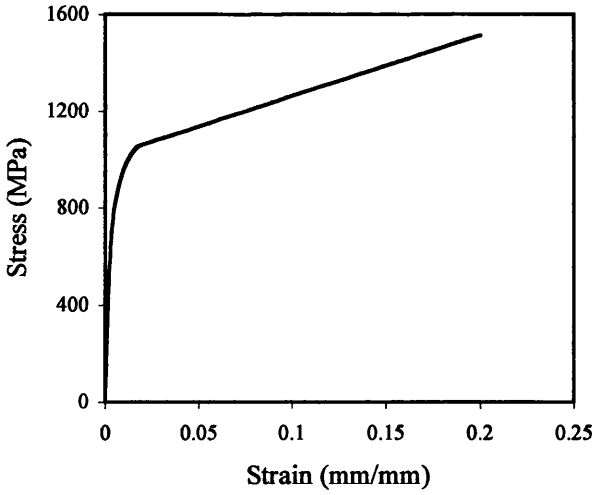

Fig 5.3: Stress-strain diagram for En 24 steel

5.3) FE model and results for technique CC

5.3.1) Model configuration

Technique CC was designed to expand the hole uniformly through the plate thickness in order to create near uniform compressive tangential residual stress around the hole. The FE model for this technique includes a plate, a tapered pin and a mating sleeve (see fig 5.4). In order to transfer contact force from the pin to the sleeve and from the sleeve to the hole surface, two sets of Contact 49 elements are used along the contacting surfaces. Due to the slit sleeve half of the plate, pin and sleeve are included in the model. Therefore, symmetrical boundary constraints were applied to the pin and the plate where they were cut from the removed parts. Also, a symmetrical boundary constraint was applied only to the left part of the sleeve (where there was no slit) see fig 5.4.

In order to constrain the model in the Z direction, the sleeve was constrained at its lower surface and the plate nodes (those which are located between two concentric circles 14 and 24 mm diameters) were constrained at its exit face. This boundary condition in the plate is needed to simulate the presence of the contact washer at the exit face as mentioned previously.

In the plate also, the two farthest nodes from the hole were constrained in the X and Z directions. This boundary condition does not affect the result, but it is helpful to avoid

pivot error in the solution process. The pin centreline nodes were also constrained in the X direction to avoid any possibility of pin oscillation (and thus avoid an equilibrium convergence problem).

Loading was considered in three steps (pin insertion, pin removal and sleeve removal) in readiness for other loading (i.e. longitudinal). In the first step the pin was pushed down 11.05 mm by incrementally displacing its upper nodes. In the second step the pin was pulled back. The pin positions and tangential stress for the first and second load steps are shown in fig 5.5. Before starting the second load step, the constraints of the plate nodes at the exit face were released because the contact washer operates only in the first load step when the plate is pushed onto the washer. In the third load step the sleeve was removed by nullifying it's elements (i.e. the elements stiffness were reduced to a very small value). The nullifying of sleeve elements did not have much effect on the residual stresses. This was because the radial stress at the hole surface, after the second load step was small and this shows that the sleeve had almost separated from the hole. To obtain residual stress the first and second load steps were sufficient, however, the third load step was required for future loading of the model (i.e. longitudinal loading see sub-section 5.3.3).

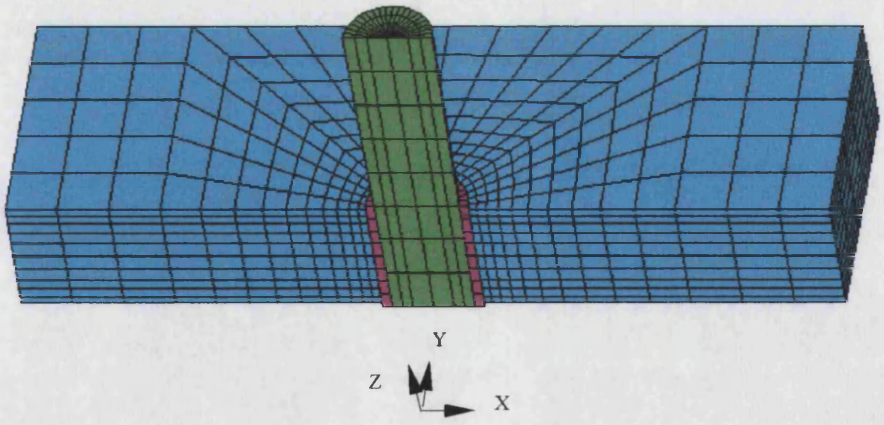

(see fig 6.3 and 6.4 in Chapter 6 for the pin and sleeve dimensions)

Fig 5.4: FE mesh for technique CC

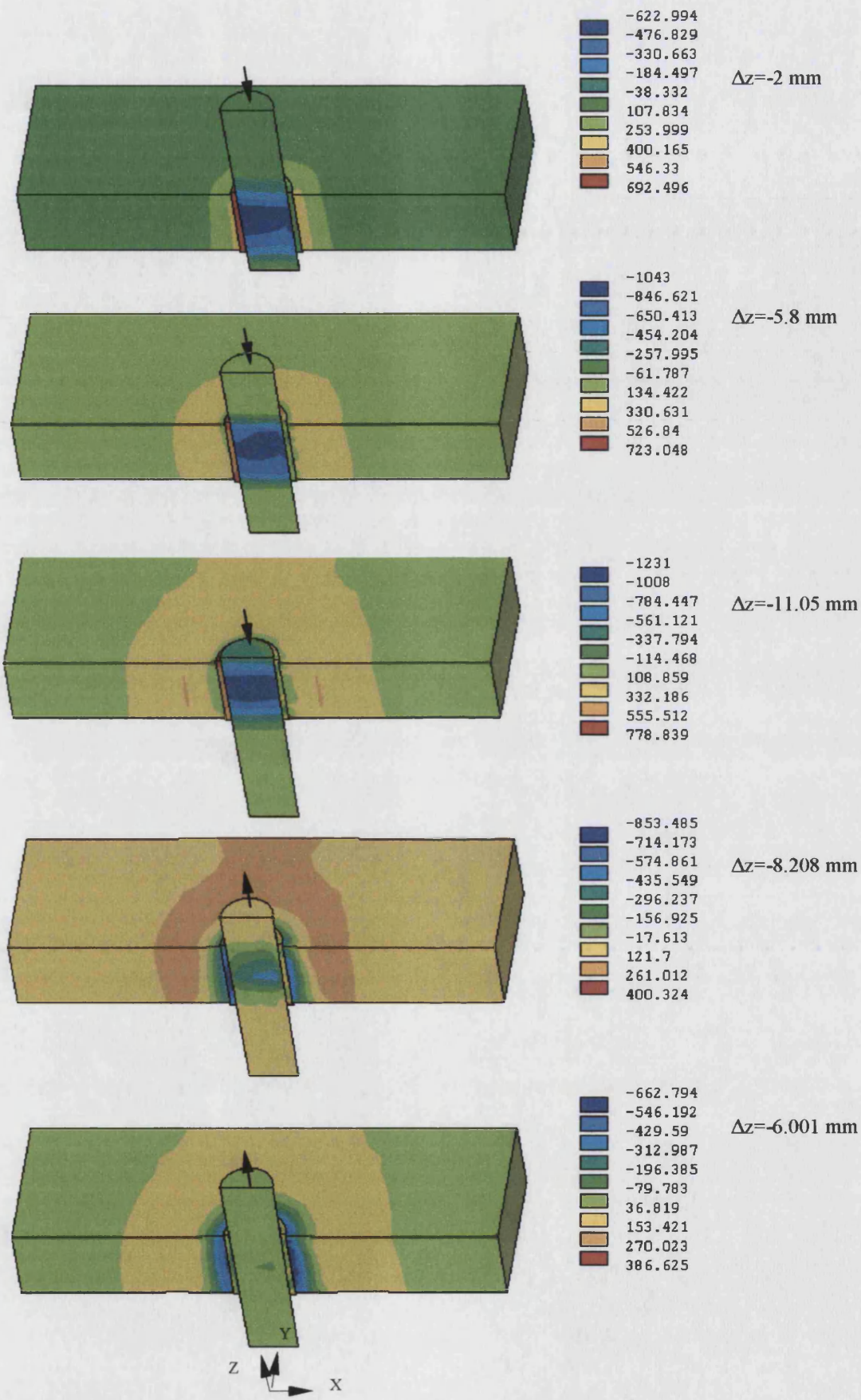

Fig 5.5: The pin positions and tangential stress in the first and second load steps

5.3.2) Tangential residual stress results

The tangential residual stress distribution after sleeve removal is shown in fig 5.6 for this model. It shows that the residual stress is almost uniform through the plate thickness (especially at the smallest section where the hole is located). Unlike the 2-D axisymmetric model, the 3-D model shows the effect of sleeve slit on the tangential residual stress. As fig 5.6 shows the effect of slit on the tangential residual stress is not appreciable through the plate thickness except for localized regions at the plate entrance and the exit faces. In these small regions the compressive tangent residual stress is a little less than at the other region of the hole surface.

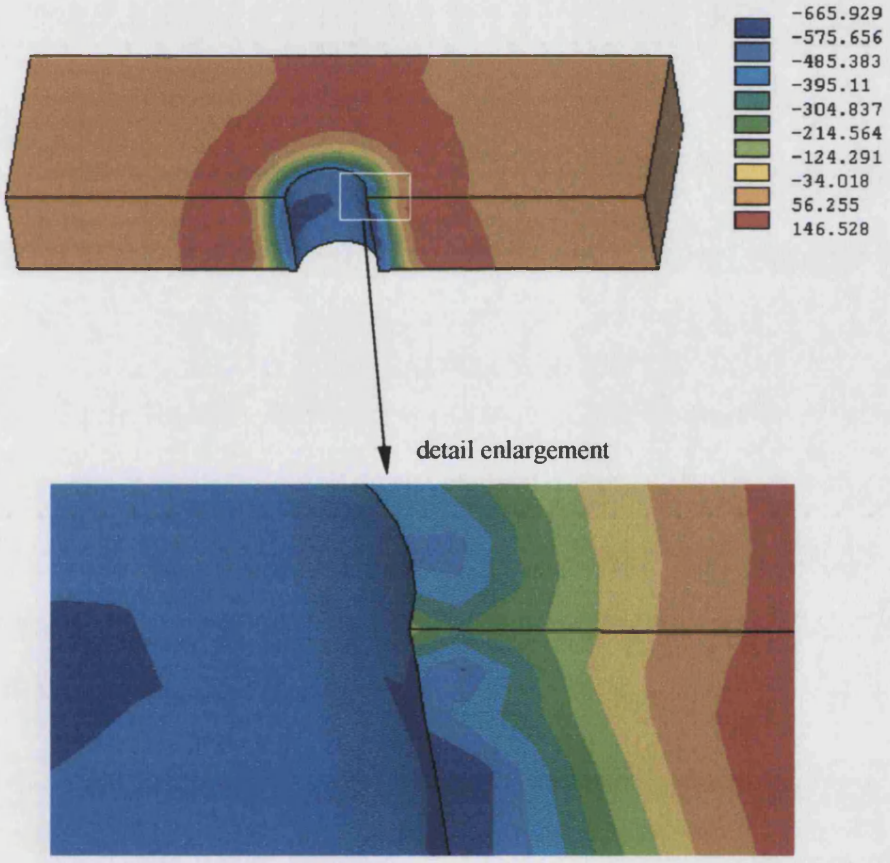

Fig 5.6: Distribution of tangential residual stress in technique CC

In addition to the tangential residual stress contours, the distribution for the three planes at the smallest cross section in the plate is shown in fig 5.7. As the curves show, the compressive tangential residual stress is almost the same at the entrance and exit faces, but it is larger in the mid-plane at the hole edge.

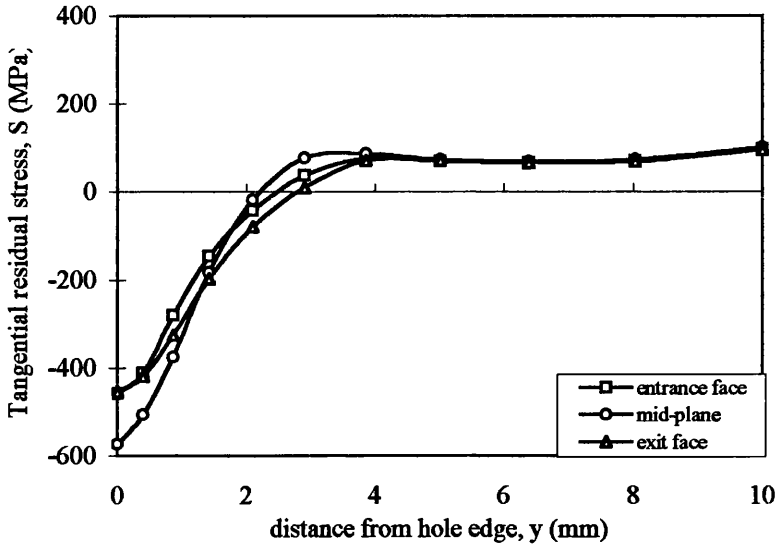

Fig 5.7: Tangential residual stress distributions at the smallest cross section for model CC

5.3.3) Combined stress under remote longitudinal stress

After creating residual stress around the hole, a longitudinal remote tensile load was applied to the cold expanded plate to investigate the distribution of combined stresses at the smallest plate cross section. This tensile load (referred to as the fourth load step) was applied incrementally (5 MPa in each sub-step) of remote stress. The combined results are shown for three remote stresses with the created residual stress for the plate in fig 5.8. The results of longitudinal remote stress, Sx verses the distance from the hole edge at the smallest section are shown for three planes in fig 5.9. According to this figure, even when the remote stress σ_x=150 MPa is applied, the combined longitudinal stress in the X direction around the hole is still compressive for each of the three planes. As the remote stress increases the combined stress changes from compressive to tensile. For the remote stress range that is applied to the plate

(i.e. σ_x=0-200 MPa) the magnitude of stress at the entrance and exit faces at the hole edge are almost the same. This remote stress range has also been used in fatigue tests as described in Chapter 7)

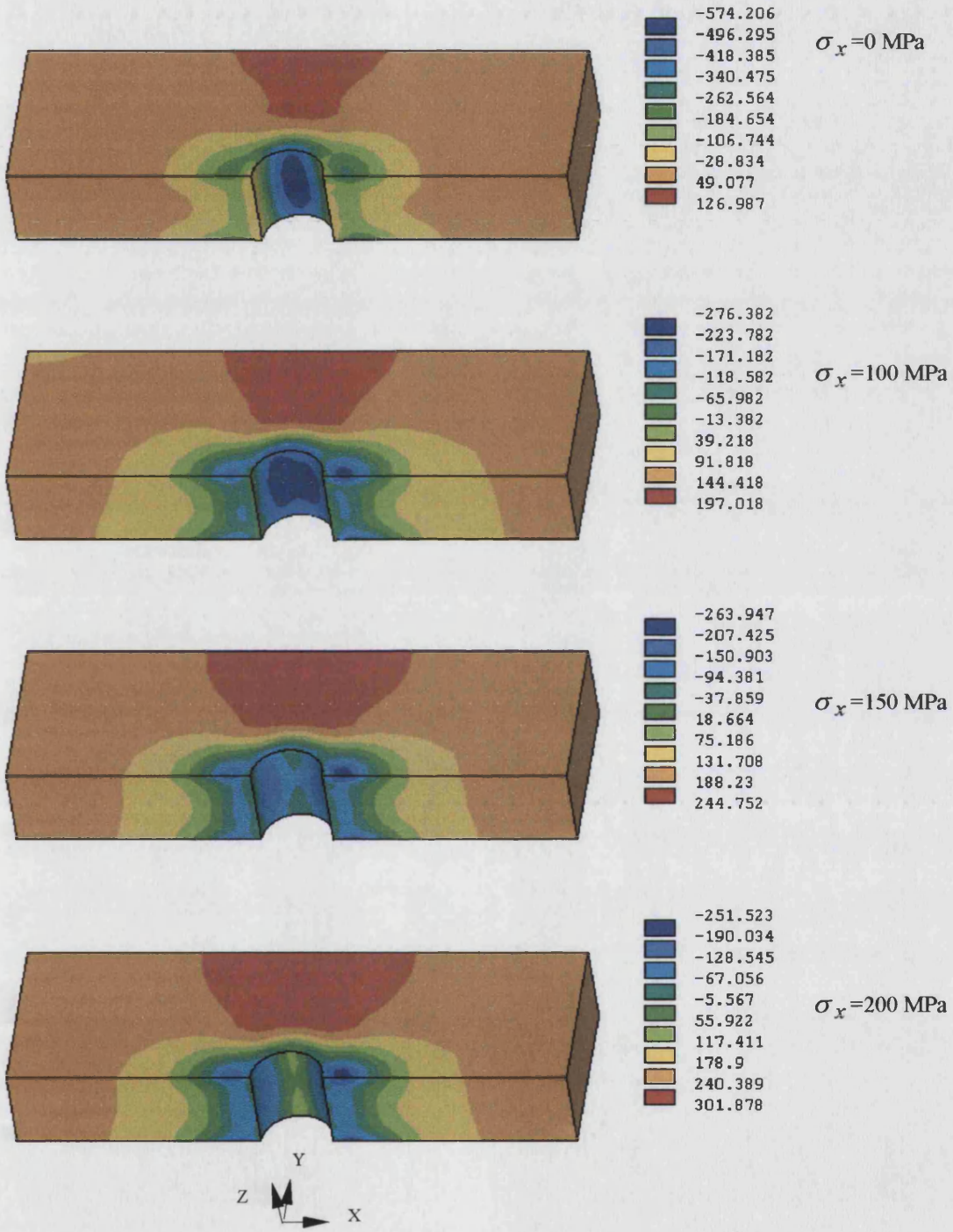

Fig 5.8: Combined longitudinal stress distributions in the plate when subjected to different remote stresses (for model CC)

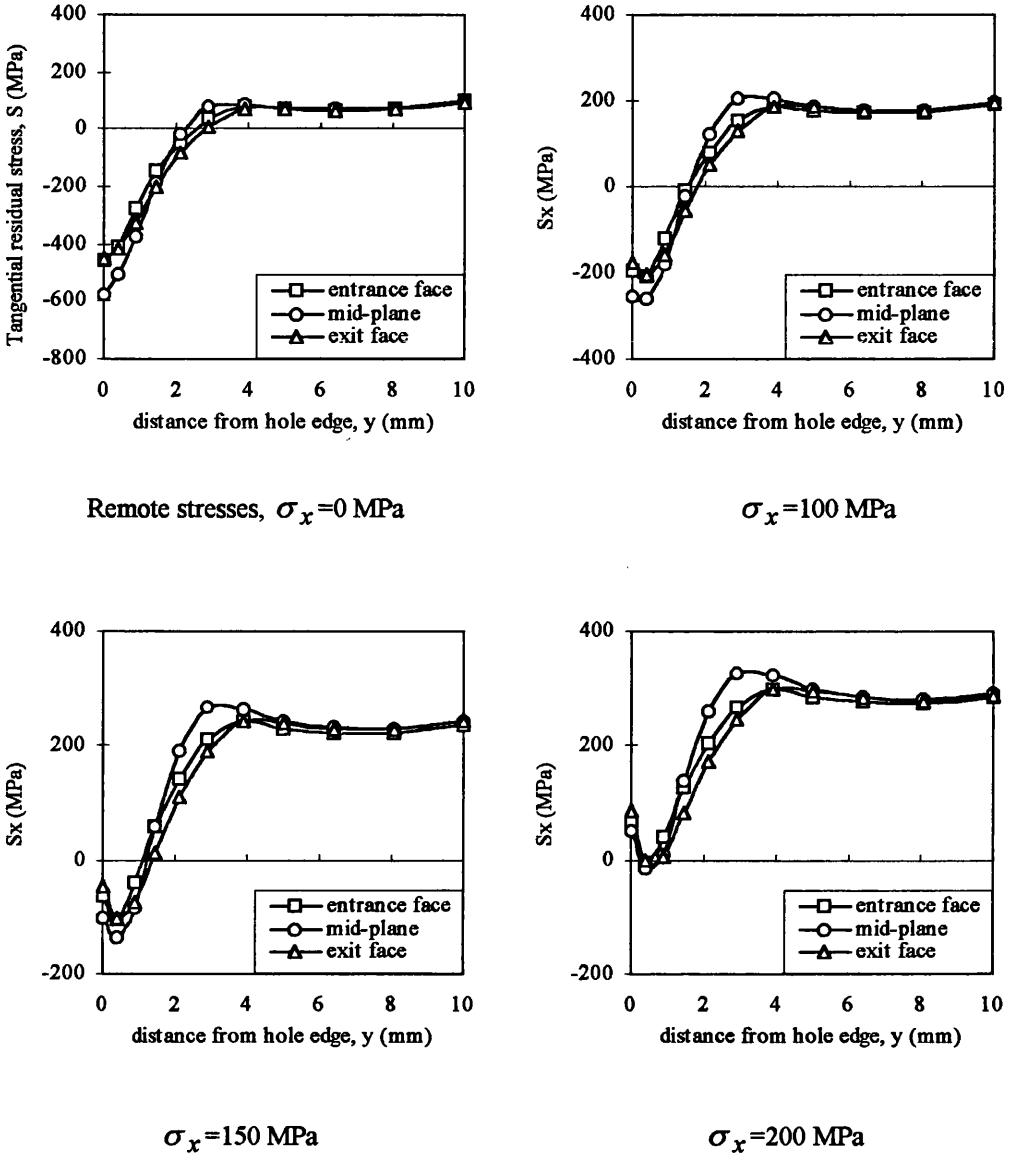

Fig 5.9: combined longitudinal stress distribution for model CC at the plate smallest cross section

5.3.4) Axial reaction force at the pin in the Z direction

The variation in the reaction force in the pin verses the pin stroke is shown in fig 5.10. It shows the force that is needed to push the pin at different pin strokes. The curve initially is linear (until the stroke is 3 mm) then the slope reduces as it reaches the maximum (about 9.5 kN) force in the total stroke. The maximum value of force is

proportional to the coefficient of friction (i.e. the larger the coefficient of friction the larger maximum reaction force).

In addition to the pin reaction force, the sleeve and the plate reaction force are shown in fig 5.11. The reaction force in the sleeve is less than in the pin because some of the applied load is supported by the plate support.

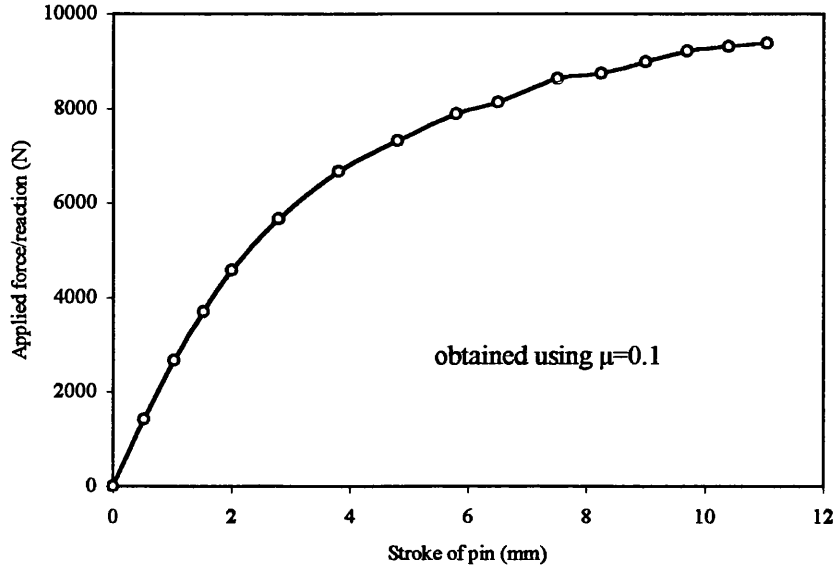

Fig 5.10: Reaction force in the pin during FE simulation of cold expansion

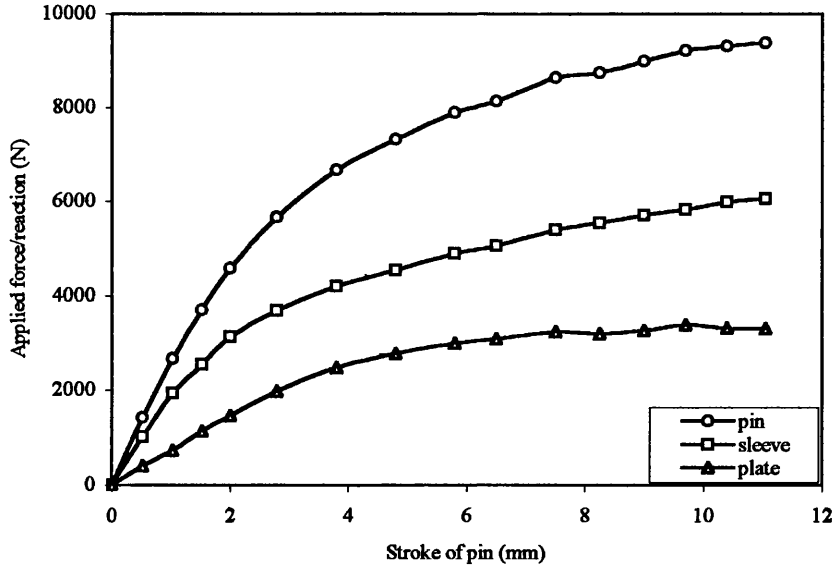

Fig 5.11: Reaction force in the pin, the sleeve and the plate during FE simulated cold expansion

5.4) FE model and results for technique BB

5.4.1) Model configuration

Model BB, which includes three half pieces (of a holed plate, a pin and a sleeve) is shown in fig 5.12. In this model for cold expanding the hole, a tapered pin and a split parallel sleeve were used. Due to this split, half of the plate, pin and sleeve were considered for the 3-D simulation. Symmetrical boundary constraints were applied to them except for the slit part of the sleeve (which is located at the sleeve right side in fig 5.12). The sleeve was also constrained at its lower surface in the Z direction and the pin was constrained at its centre line in the X direction to avoid any possibility of pin oscillation (and thus avoiding equilibrium convergence). The plate was constrained at its nodes at the exit face where the contact washer is located. The cold expansion process was considered in just two load steps. In the first step the pin was pushed down by incrementally displacing the pin upper nodes until it was passed through the hole (see fig 5.13 for five pin positions and the corresponding tangential stresses). In the second step the nodes that had been constrained in the Z direction at the plate exit face were released (these constraints were due to the presence of the contact washer). Also in the second step the sleeve elements were nullified thus simulating sleeve removal. The nullifying of sleeve elements did not have much effect on the residual stresses. This is because the radial stress at the hole surface after the first load step was small and it shows that the sleeve had almost separated from the hole surface. To obtain the residual stress, the first load step was sufficient, however, the second load step (sleeve removal) was required for future loading of the model (see next sub-section).

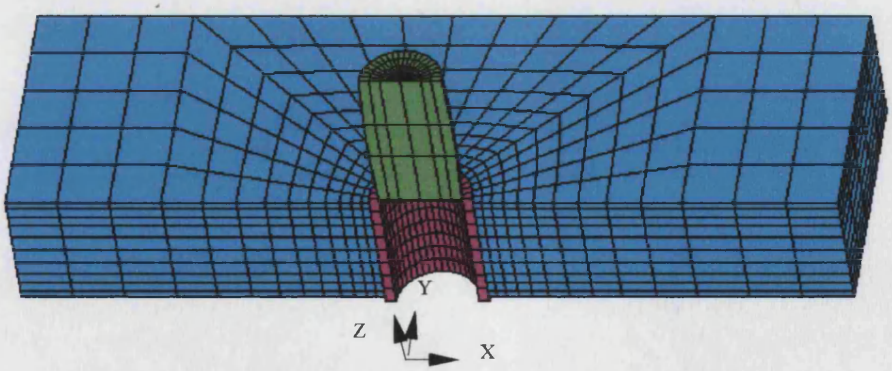

(see fig 6.13 and 6.14 in Chapter 6 for the pin and sleeve dimensions)

Fig 5.12: FE mesh for model BB

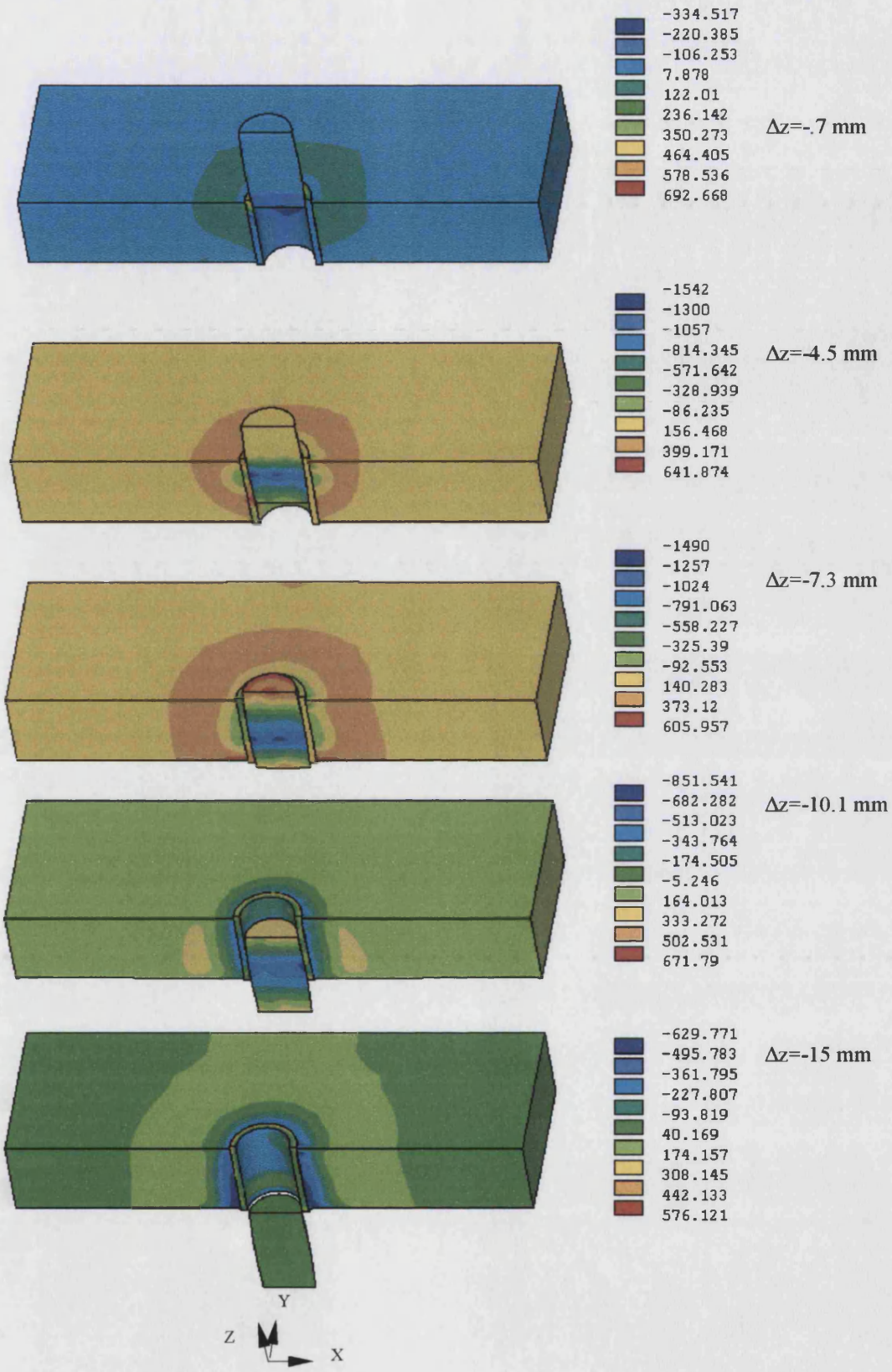

Fig 5.13: The pin position and tangential stress in the first load step for model BB

5.4.2) Tangential residual stress results

The tangential residual stress distribution after sleeve removal is shown in fig 5.14 for this model. It shows that the residual stress is not uniform through the plate thickness and it is less compressive at the plate entrance face than at the mid-plane and the exit faces. Unlike the 2-D axisymmetric model, the 3-D model shows the effect of sleeve slit on the tangential residual stress. As can be seen in the figure, the effect of the slit on the tangential residual stress is not appreciable through the plate thickness except for a localized region at the plate entrance face. In this small region the maximum compressive and the maximum tensile residual stresses are produced and the hole surface distortion is considerable compared to that produced for model CC (see fig 5.6).

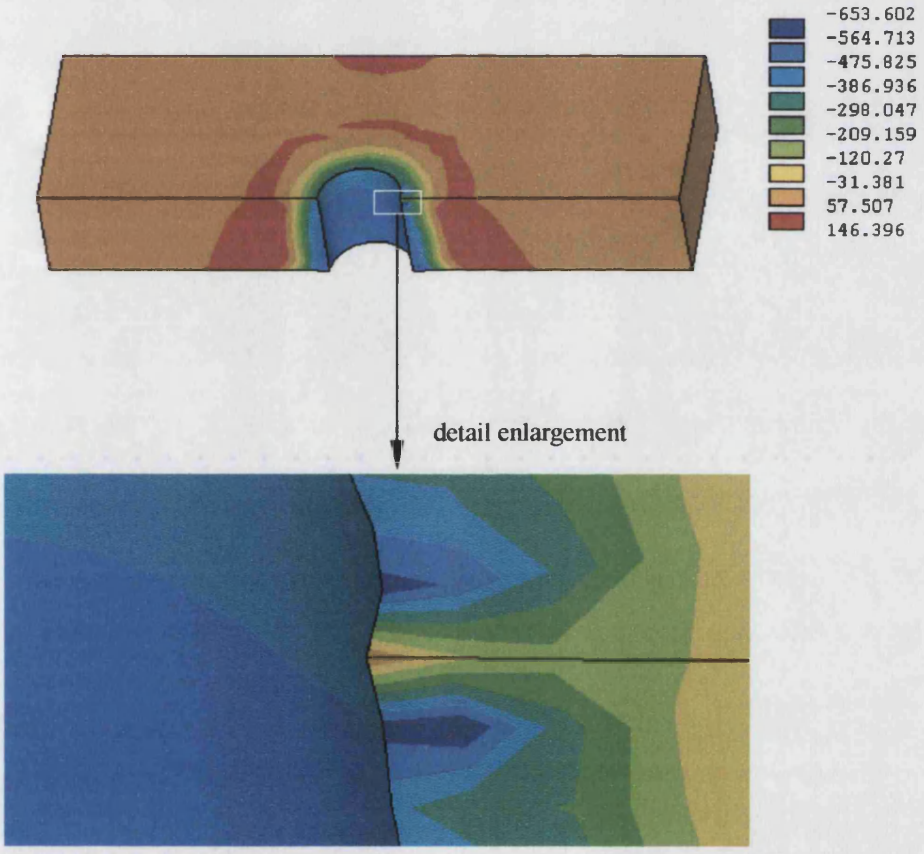

Fig 5.14: Distribution of tangential residual stress in technique BB

In addition to stress contours, the tangential residual distributions for the three planes at the smallest cross section in the plate is shown in fig 5.15. As mentioned previously, friction has been included between the sleeve and the plate and the sleeve and the pin surfaces in the model. Friction has had a positive effect in helping to compressive tangential residual stress around the hole especially at the entrance face. As shown in fig 5.15 this model doesn't show positive tangential residual stress at the hole edge of the plate entrance face (as was found with the 2-D axisymmetric model B_s in Chapter 4 fig 4.12) and this difference is entirely due to friction.

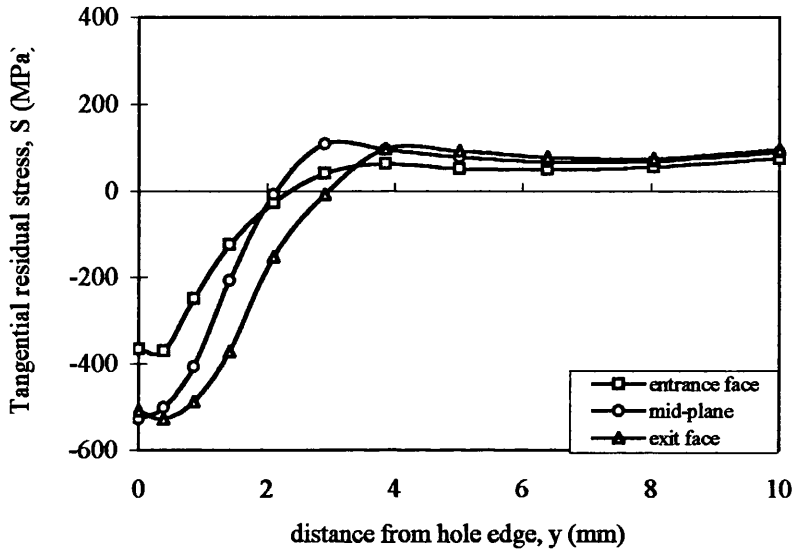

Fig 5.15: Tangential residual stress distributions at the smallest cross section for model BB

5.4.3) Combined stress under remote longitudinal stress

After creating residual stress around the hole, a remote tensile longitudinal load was applied to the plate to investigate the final distribution of stress across the smallest cross section. In the third load step tensile load was applied producing remote stress from zero to 200 MPa (incrementally with 5 MPa in each sub-step). The combined stress results are shown for different remote stress magnitudes in the plate in fig 5.16. The result of combined stress, Sx verses the distance from the hole edge at the smallest cross section is shown for the three planes in fig 5.17. According to this figure, when a remote stress, σ_x=100 MPa is combined with the residual stress, the

final stress (in the X direction) around hole remains compressive for the three planes. As the remote stress increases so the combined stress changes from compressive to tensile at the hole edge. For the remote longitudinal stress range that is applied to the plate (i.e. σ_x=0-200 MPa) the combined stress at the entrance plane is worse (from crack initiation and propagation considerations) than at the other two planes.

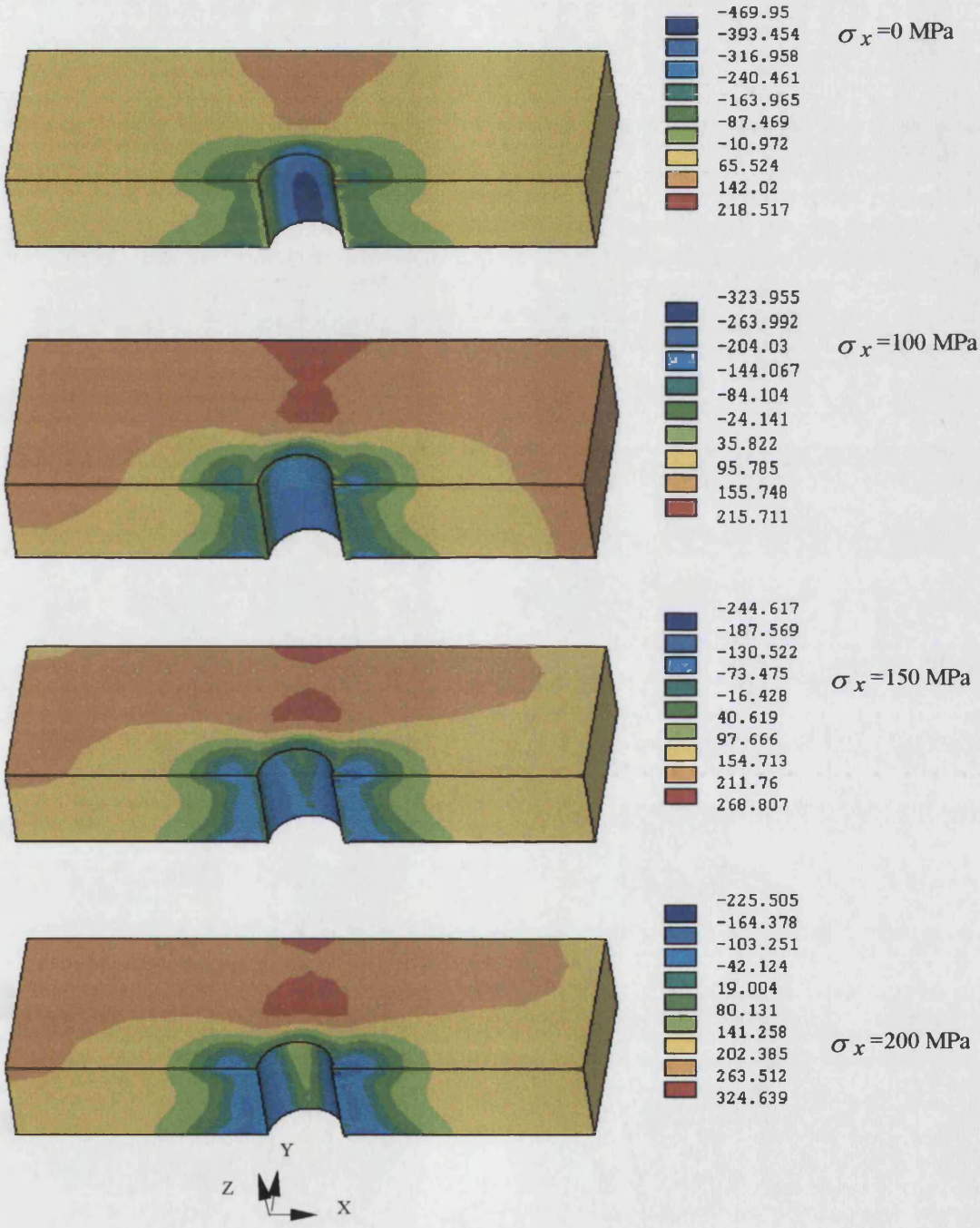

Fig 5.16: Combined longitudinal stress distributions at the plate when subjected to different remote stresses (for model BB)

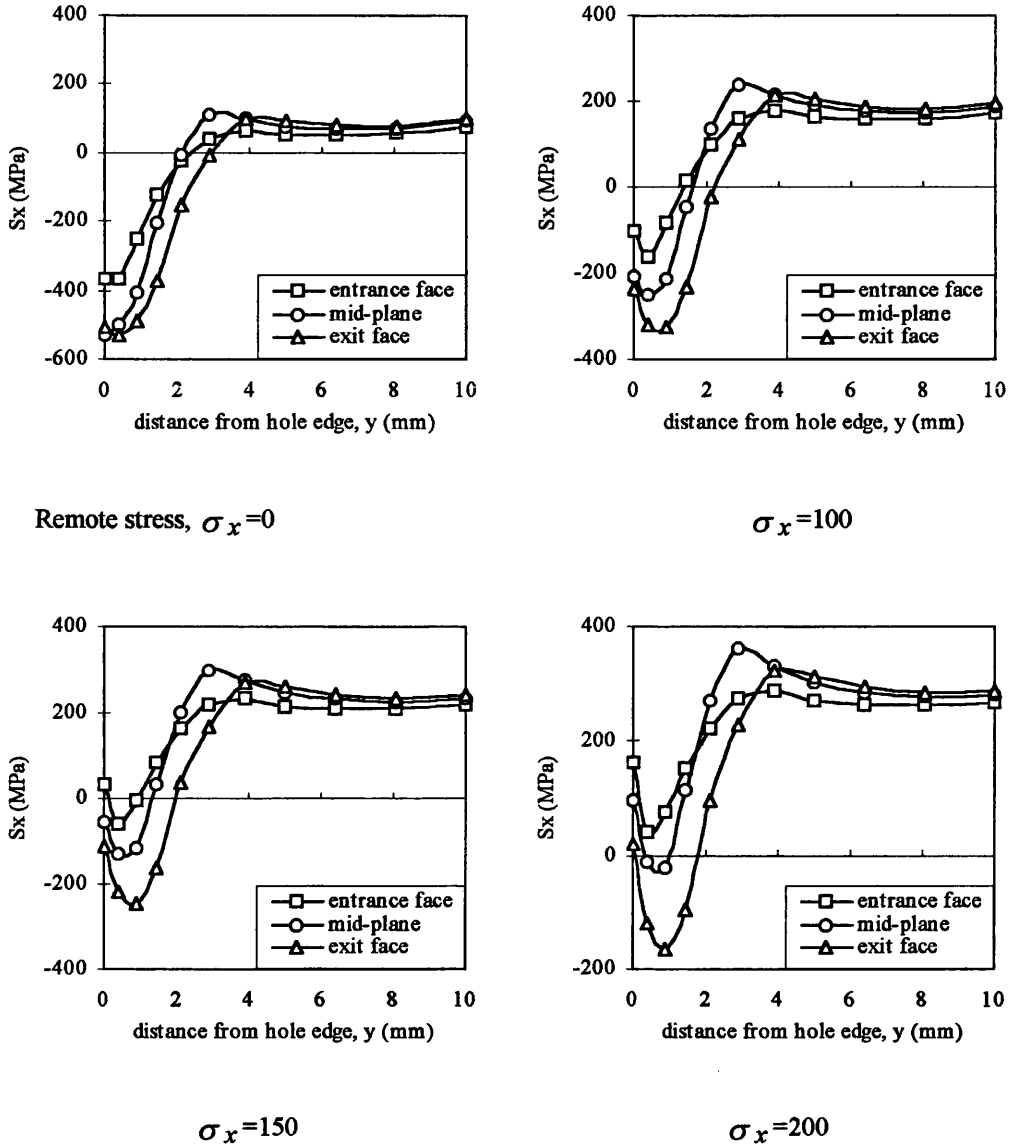

Fig 5.17: Combined longitudinal stress distribution for model BB at the plate smallest cross section

5.4.4) Axial reaction force at the pin in the Z direction

The variation in the reaction force in the pin (in the Z direction in fig 5.12) verses pin position (stroke) is shown in fig 5.18. The curve is approximately linear (until about 3 mm) then the slope reduces as it reaches the maximum load in the first half of the total stroke. In the second half of the stroke the force decreases almost linearly from the maximum (about 7.5 kN) to zero. It is found that the maximum value of the force is virtually proportional to the coefficient of friction.

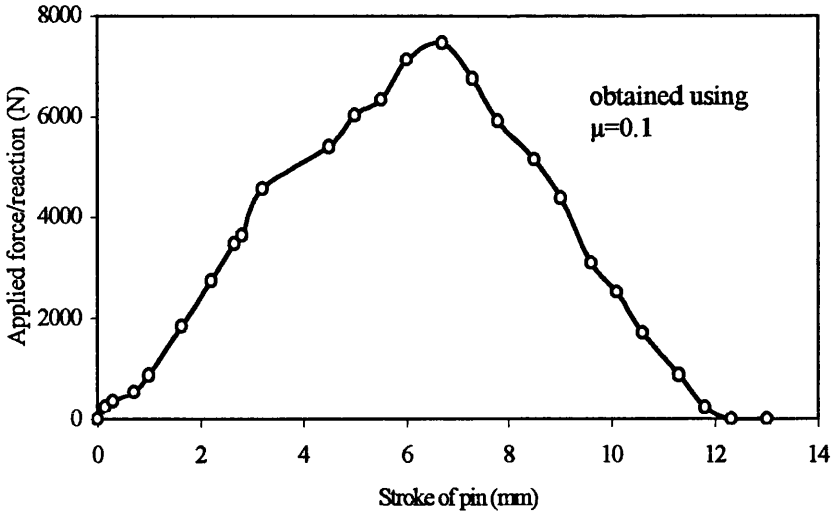

Fig 5.18: Reaction force in the pin during FE simulated cold expansion

In addition to the pin reaction force, the sleeve and plate reactions are shown in fig 5.19. The reaction force in the sleeve is less than in the pin until about the mid-stroke position but it is larger than the pin reaction force for the rest of the stroke. The maximum reaction forces in the pin and the sleeve are almost identical, however, they occurred in different stroke position.

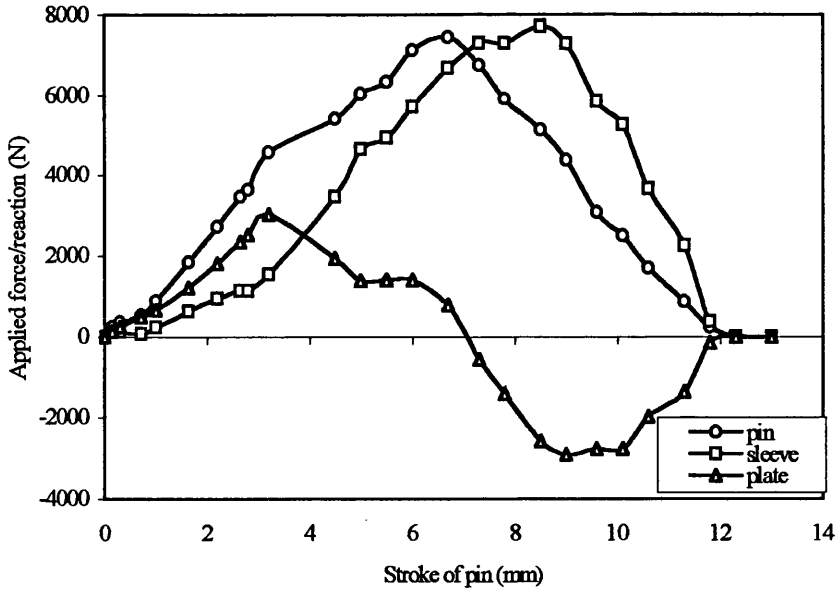

Fig 5.19: Reaction force in the pin, the sleeve and the plate during FE simulated cold expansion

5.5) FE model and results for technique DD

5.5.1) Model configuration

This model is sleeveless and comprises only two pieces - a pin and a holed plate (see fig 5.20). Only a quarter of the plate and the pin were needed in this model due to their symmetry with respect to the X-Z and the Y-Z planes. In addition to the symmetrical boundary constraints, the plate was constrained at its exit face nodes (those which are in contact with the contact washer in the Z direction). For expanding the hole, the pin was pushed down by incrementally displacing the upper nodes in the downward (i.e. -Z direction). The pin position and the plate configurations with their tangential stresses are shown in fig 5.21.

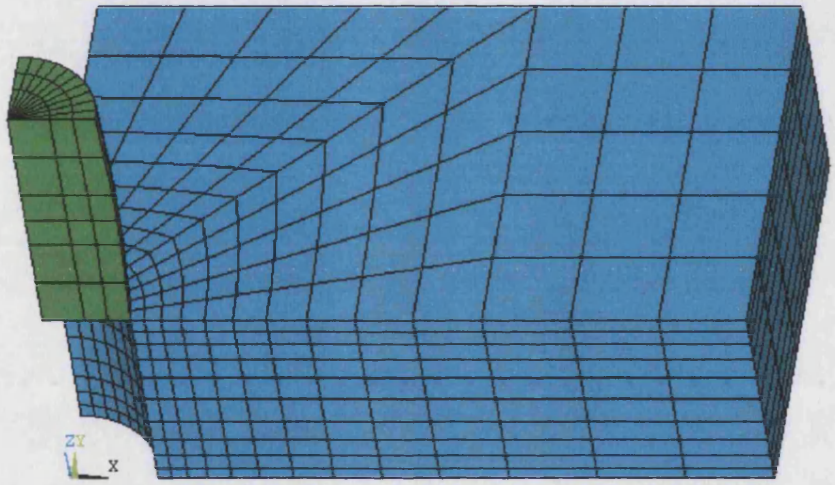

(see fig 6.19 in Chapter 6 for the pin dimensions)

Fig 5.20: FE mesh for model DD

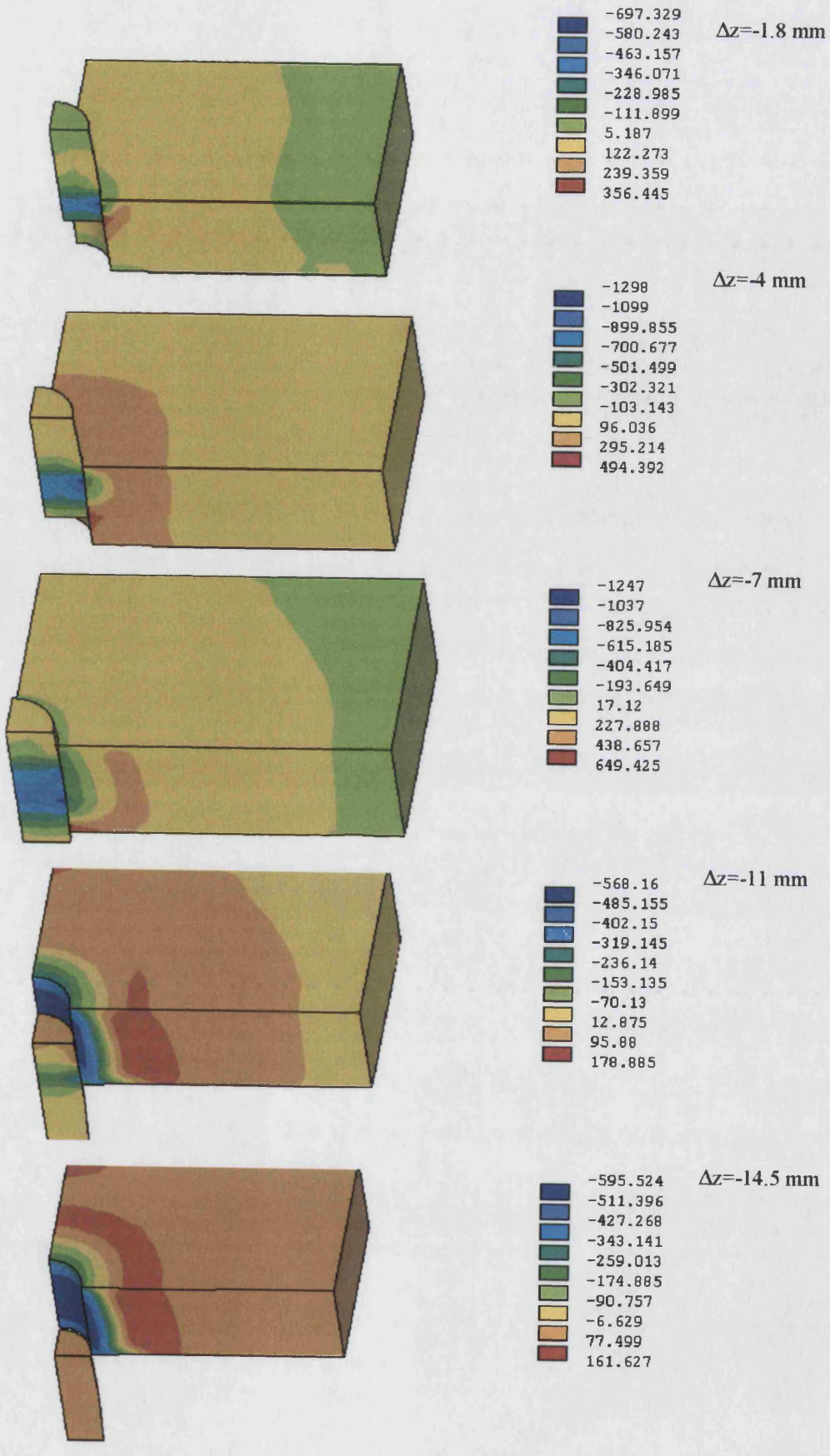

Fig 5.21: Pin positions and tangential stresses for model DD

5.5.2) Tangential residual stress results

The tangential residual stress contours are shown in fig 5.22. The stress distribution is not uniform through the plate thickness and it is less compressive at the entrance face than at the other planes. As the contours appear cylindrical it shows that using a 2-D axisymmetric model was suitable for predicting the tangential residual stress.
The tangential residual stress for the three planes is shown in fig 5.23 at the smallest cross section for comparison purpose.

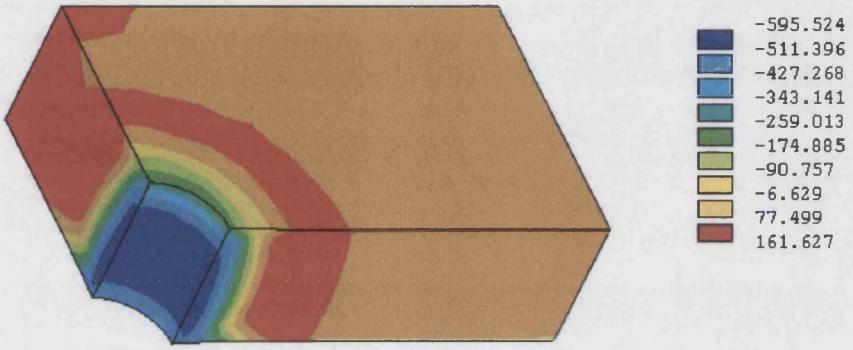

Fig 5.22: Distribution of tangential residual stress for technique DD

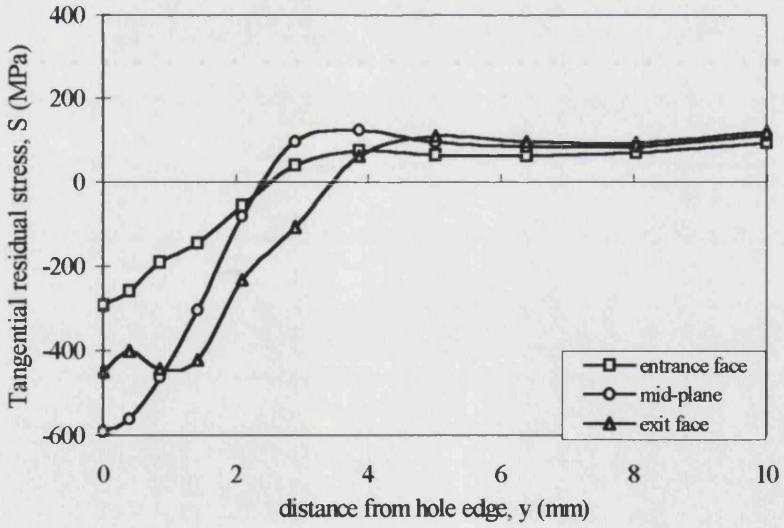

Fig 5.23: Tangential residual stress distributions at the smallest cross section for model DD

5.5.3) Combined stress under remote longitudinal stress

For model DD, as with models BB and CC, the effect of residual stress and remote longitudinal stress is shown in fig 5.24 as combined stress contours. In model DD, after creating residual stress in the first load step, a remote tensile stress was applied to the plate at the plate end in the second load step. This remote stress was increased from zero to 200 MPa in 5 MPa increments. It was found that this incremental loading was not necessary (with the remote stress range that was used here) because the region of the hole was reloaded elastically, however, it was needed to obtain the result for different remote stress values.

In addition to the combined stress contour results, the combined residual and remote stress distributions are shown as curves for the smallest cross section at the three planes in fig 5.25. According to these curves the combined stress in the X-direction remains compressive with a low magnitude of remote stress in all three planes at the hole edge. However, it can be seen that with increasing remote stress, the combined stress becomes tensile at the hole edge.

5.5.4) Axial reaction force at the pin in the Z direction

The variation in the value of the reaction force in the pin (in the Z direction see fig 20) verses pin stroke is shown in fig 5.26. It shows the force that is needed to push the pin different distances (i.e. pin strokes). The curve is virtually linear until 3 mm then its slope reduces as it reaches the maximum force in the first half of the total stroke. In the second half of the stroke the force decreases from the maximum about 6.5 kN to reach zero.

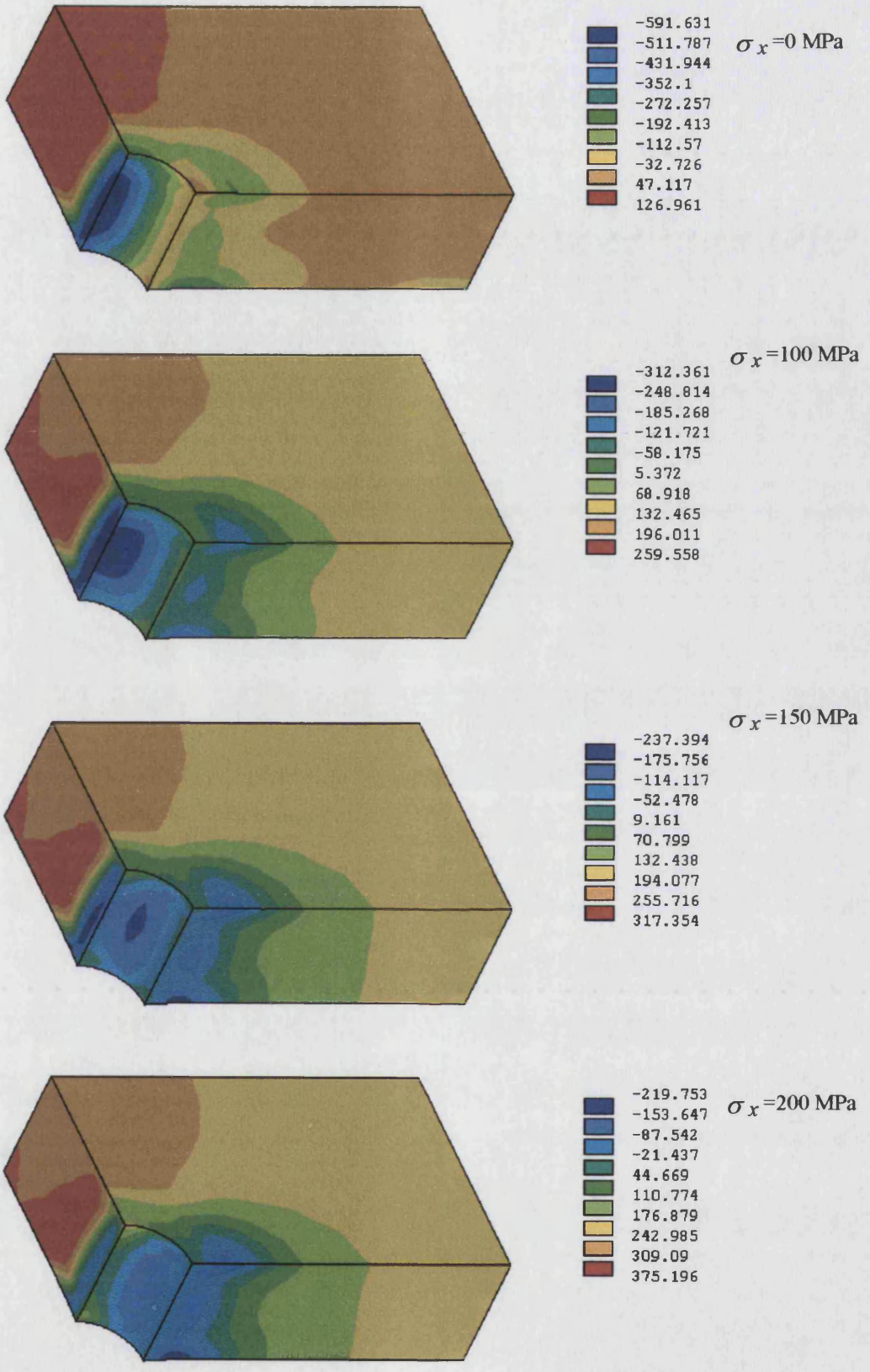

Fig 5.24:Combined longitudinal stress distributions at the plate when subjected to different remote stresses (for model DD)

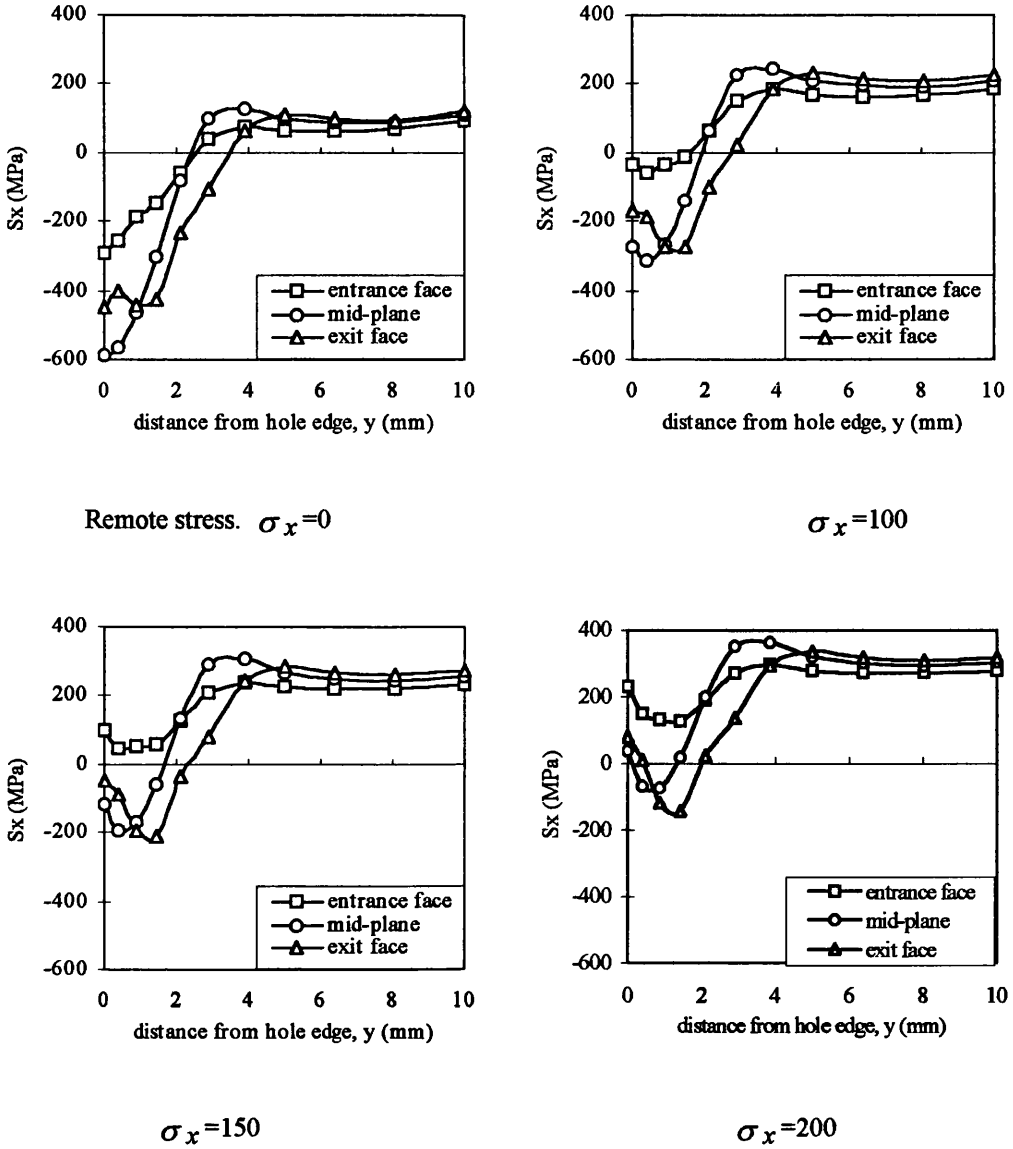

Fig 5.25: Combined longitudinal stress distributions for model DD at the plate smallest cross section

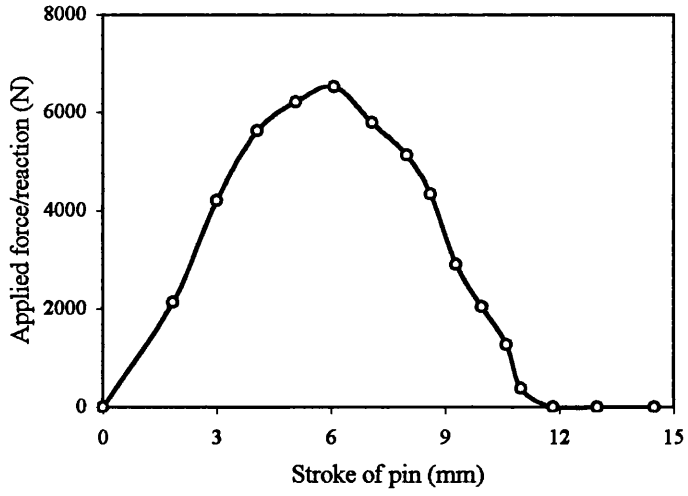

Fig 5.26: Reaction force of the pin during FE cold expansion simulation for model DD

Chapter 6

Cold expansion components and their material properties

6.1) Introduction

In this chapter the items used in three previously mentioned cold expansion techniques are described. One uses a tapered pin with mating split sleeve (called technique CC), another uses a tapered pin with a parallel split sleeve (called technique BB) and the third one uses a tapered pin without a sleeve (called technique DD). These techniques were applied to 5 mm diameter holes to expand them with 4.6% nominal interference in 6.32 mm thick aluminium-alloy 7075-T6 plates.

This chapter also explains that cold expanding a small hole such that the plate is simultaneously expanded through the thickness is practically difficult. This is because very high stresses occur in the mating surfaces of cold expansion components sometimes causing stresses beyond the yield strength of even high tensile steel.

In the following sections, the design of the expansion devices and their performances are discussed. The material properties of leading components were critical and these were obtained and are presented.

6.2) Tapered pin with mating split sleeve (technique CC)

Practical challenges have been faced to expand the hole uniformly and simultaneously throughout the plate thickness in order to create a uniform or nearly uniform compressive tangential residual stress distribution. As the results of the computer models from Chapter 4 and 5 show this is theoretically possible using a tapered pin and a mating sleeve.

In the computer models, different nominal pin diameters and bush wall thicknesses were tried in order to see the effect on the residual stress distribution around the hole. The models do not show that the chosen configuration is possible in practice. For example, the model does not have the capability to predict plastic collapse or buckling (or a combination of both) that can happen in the pin or the sleeve; this maybe possible if the problem was analysed in a different field of study. To overcome this shortcoming a trial of practical methods has been carried out to check the suitability of different configurations for the pin and the sleeve. In this trial, parameters such as the nominal sleeve wall thickness, sleeve length, number of slits in sleeve (or bush), nominal pin diameter and pin length were investigated.

6.2.1) Design of tapered pin and mating sleeve)

Designing the tapered pin and mating bush so it performed as required was difficult and challenging. Because it is a new technique and a number of problems were experienced, these were:

1) It was not known what type of steel should be used for the pin and bush. To get an idea about the magnitude of the stresses that the pin and the sleeve experience during cold expansion, several computer simulations were examined. In these simulations, elastic behaviour was considered for the pin and the sleeve material. In all simulations very high stresses were observed for the pin and the sleeve, for example the Von Mises stress was usually greater

than 800 MPa. Therefore, a high strength steel was needed for the pin and the sleeve

2) It was not known what would be the best taper angle in the pin (and the sleeve). However the simulations showed that for bigger taper angles, a large amount of force is needed to push the pin sufficiently into the hole. Fortunately the solution to this problem was straightforward because there are only a few standard sized reamers available for making the mating sleeve, otherwise it would be necessary to order a special (i.e. non standard) reamer that is more expensive. Therefore, considering the pin pushing force and the amount of the pin stroke for a desired interference (I=4.6%), a standard 1/48 taper reamer was chosen.
3) Because of the small pin diameter buckling could happen so the pin had to be designed as short as possible, however it could not be shorter than the required stroke. Besides the pin length L_p (see fig 6.1), the pin diameter d_p is also important from buckling considerations. The Euler equation [53] relates the pin diameter, the pin length and critical load. This equation can be used to estimate the diameter as the pin length is limited to the required stroke and the critical load is the pin pushing force. Generally a bigger diameter is preferable to avoid buckling but it is limited here because the pin together with the mating sleeve must fit in the 5 mm hole diameter. Therefore the bigger the pin diameter that is used the thinner the sleeve wall thickness.
4) The sleeve wall thickness, along length, L_b (see fig 6.2) is an important parameter and must be carefully considered. A thin sleeve is vulnerable against plastic collapse during cold expansion due to the axial compressive force. Also, there is a limitation in the sleeve thickness (see problem 3) so there is a trade-off between pin diameter and the sleeve wall thickness.
5) The number of slits used in the mating sleeve affects matters. A complete sleeve (i.e. without slits) is preferred from economic and manufacturing considerations but with such a sleeve the amount of interference achievable is limited because of possible plastic collapse. A double slit sleeve is more costly if unacceptably large clearance gaps are to be avoided because two bushes are needed to make one close fitting sleeve. The cost of manufacturing a single slit sleeve is a compromise solution.

In order to carry out cold expansion technique CC that would be practically easy and economically of low cost, several trial configurations of the tapered pin and mating sleeve (bush) have been designed and tested. These configurations and the problems faced are explained briefly in table 6.1.

In the table the first column shows the trial number and in the parenthesis the number of the tests that have been conducted. The other columns show the bush and the pin dimensions, the number of sleeve slits, the plate support (in some trial tests the holed plate has not been supported) and the pin surface treatment. In some tests no surface treatment had been done on the pin and this resulted in surface damage to the pin. In some tests, to overcome this problem the pin was quenched and tempered. The problems, which were encountered in the trial tests, have been explained in the last column of table 6.1.

As shown in the table, some of the pin and the sleeve configurations had practical problems such as buckling of the pin (i.e. trials TR1) or plastic collapse in the bush in the case of TR6. Also, the configurations used in trials TR1, TR2 and TR3 were found to be expensive. For these reasons the pin and sleeve configuration (shown in fig 6.3 and fig 6.4) used in Trial TR5 was chosen for cold expansion of subsequent specimens because it was more practical and economic.

In order to attach the tapered pin and mating sleeve to the testing machine jaw fixtures (see next sub-section) some shouldered parts were designed at the bottom of the pin and the bush (see fig 6.1-6.4).

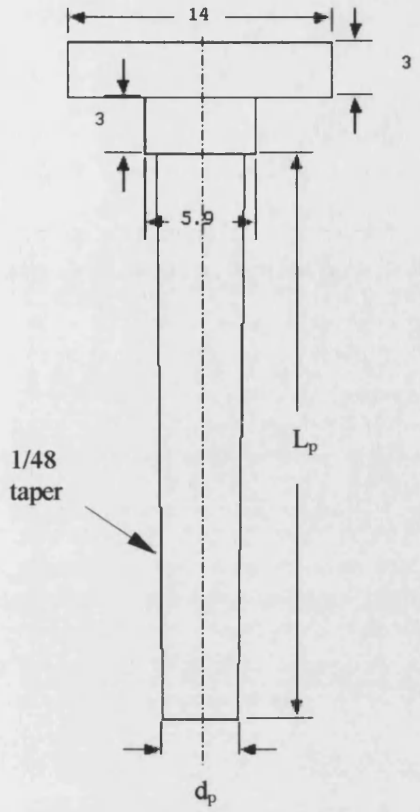

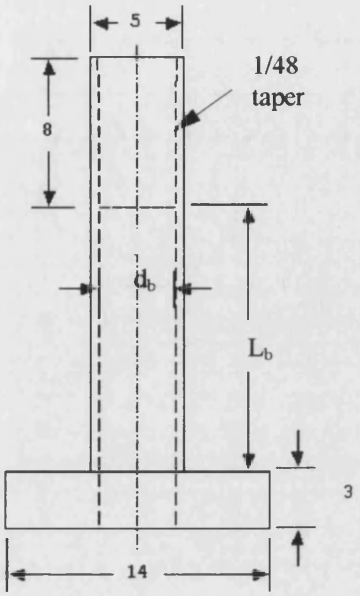

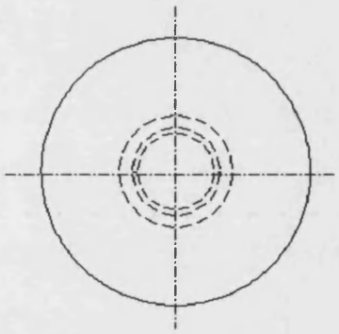

d_p=3, 4

L_p=30, 40

See table 6.1

Fig 6.1: Tapered pin dimensions for technique CC

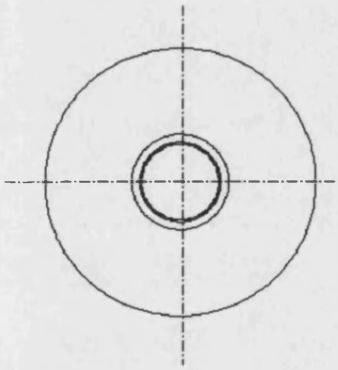

T_b=0.5, 1

L_b=5, 14

See table 6.1

Fig 6.2: Mating sleeve (bush) dimensions for technique CC

Table 6.1: Tapered pin and mating sleeve trial results (see figs 6.1 and 6.2 for geometry dimensions)

Trial No. (No. of tests)	Bush Dimensions (mm) wall thickness, T_b	length, L_b	Number of slits in bush	Pin Dimensions (mm) diameter, d_p	Length, L_p	Plate support	Pin surface treatment	comments
TR1 (3)	1	5	2	3	40	none	No surface treatment	Buckling of the pin
TR2 (2)	1	5	2	3	30	none	No surface treatment	Surface damage of the pin and the bush. Practically difficult due to lack of plate support and thickness of shoulder (in sleeve).
TR3 (2)	1	14	2	3	30	yes	Quenched and tempered	No practical problem faced. Cold expansion is not efficient due to the large wall thickness compression in the bush (the hole experiences a smaller interference)
TR4 (3)	1	14	1	3	30	yes	"	No practical problem, cold expansion is not efficient
TR5 (3)	0.5	14	1	4	30	yes	"	No practical problems, cold expansion is efficient (negligible wall thickness compression in bush)
TR6 (2)	0.5	14	No slit	4	30	yes	"	Plastic collapse at the bush base

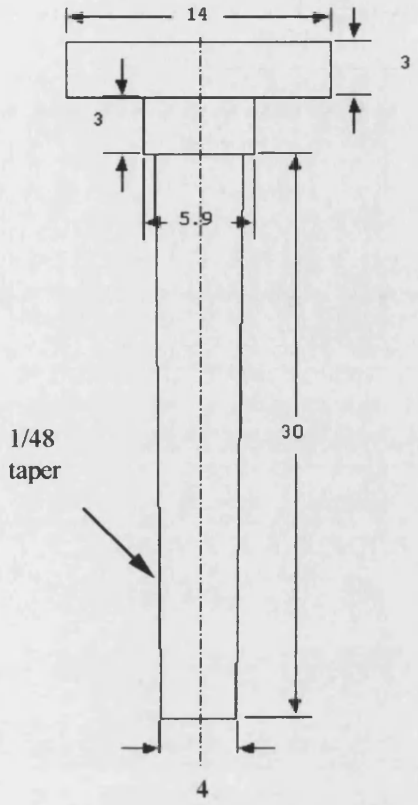

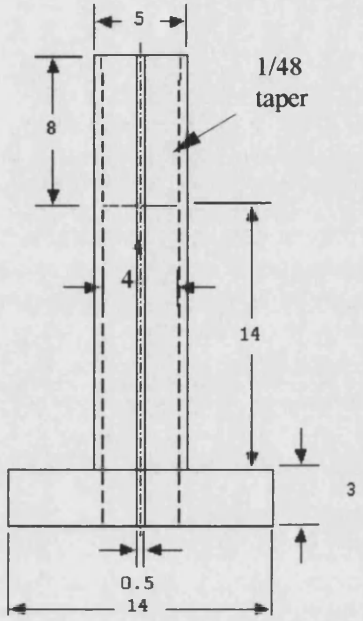

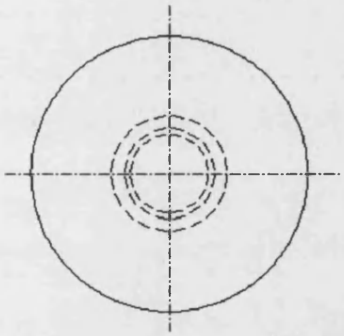

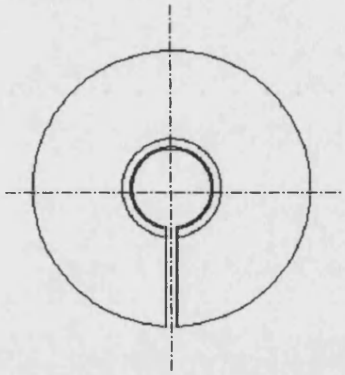

Fig 6.3: Tapered pin dimensions in technique CC

Fig 6.4: Mating single slit sleeve in technique CC

6.2.2) Design of testing machine jaw fixtures for technique CC

In the practical process of cold expansion, in addition to the sleeve and pin problems there are other problems such as applying load to the pin and also designing support for the sleeve and the plate specimen. In applying the load to the pin, a testing machine fixture was designed to push the pin into the hole for the required stroke (to give the desired amount of interference I=4.6%) and then pull it back from the same side. The sleeve support should have the capability to apply force in both axial directions as shown in the computer model (see Chapter 5).

In order to apply force to the pin and provide support for the bush, two almost identical testing machine fixtures were designed (see figs 6.5-6.7). As figs 6.5-6.7 show, the fixtures include two separate parts, a connector and a locking nut.

The connector has a hole that enables it to be fastened to the Instron machine jaw with a securing pin. Also, the smaller diameter part of the connector has been threaded to hold the pin or bush when it is screwed to the fixture.

The fixture locking part is open at one end and closed at the other end. In the closed end there is a central hole to enable the bush or pin to pass through. The two-part fixture can therefore support the bush or the pin in either direction when a force is applied in opposite directions.

The specimen also needs to be supported around the hole so a simple support ring was designed to be put on the Instron machine's lower jaw (see fig 6.8). In order to have contact between the support ring and specimen, a washer was placed between them (see figs 6.9 and 6.11).

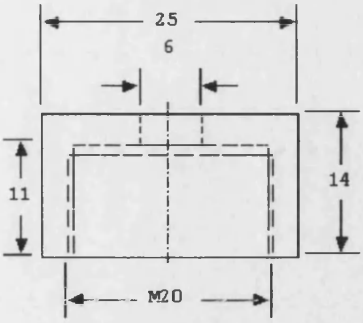

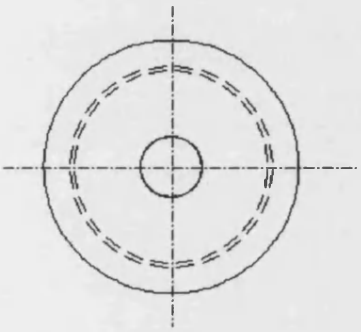

Fig 6.5: Locking nut

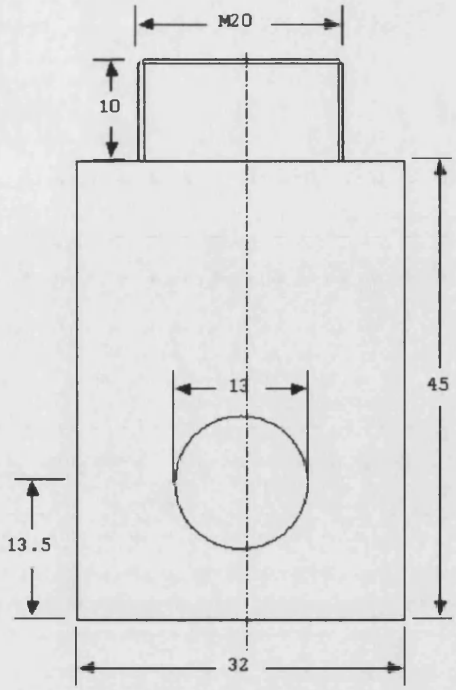

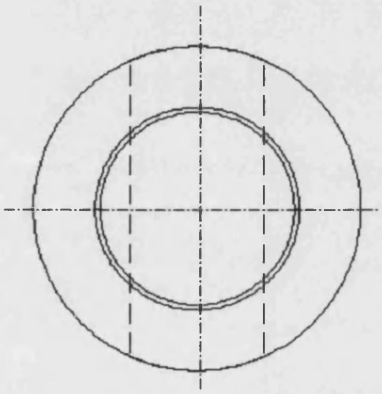

Fig 6.6: Connector

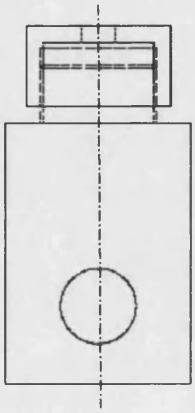

Fig 6.7: Testing machine fixture (Locking nut and connector)

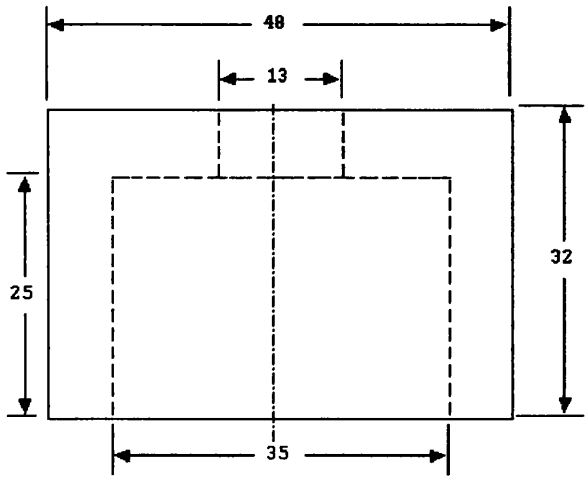

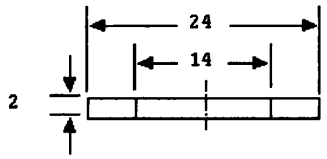

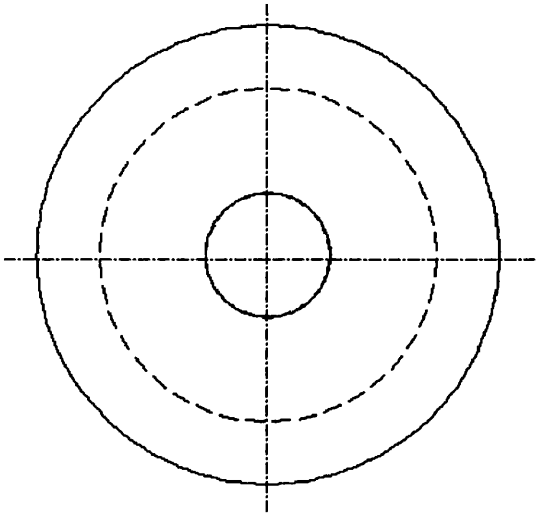

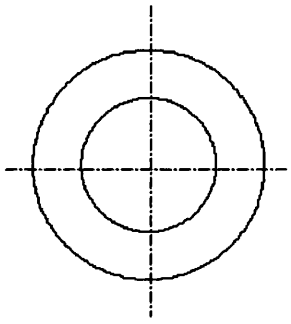

Fig 6.8: Support ring

Fig 6.9: The contact washer

6.2.3) Performing of technique CC and force-displacement graph

After having chosen the best configuration for the tapered pin and mating bush and designing the fixtures, the specimen (holed plate see fig 6.10) maybe prepared for cold expansion prior to fatigue testing. Before carrying out cold expansion, the tapered pin and mating bush (inside and outside) were lubricated with Tallow

lubricant to reduce the coefficient of fiction between the interacting surfaces and thus reduce the pin pushing force. The outside of the bush (which contacts with the hole surface) was lubricated in order to reduce the removal force after the test.

Cold expansion was carried out using a 10 kN Instron tensile and compression testing machine. In preparing for a test, the pin and the connector were fastened to the Instron machine upper (i.e. moving) jaw and the bush and its connector were fastened to the machine lower (i.e. fixed) jaw. The support ring was also placed on the lower jaw then the specimen was placed on its support so that the free end of the sleeve would pass up through the specimen hole (see fig 6.11).

During the first stage of cold expansion the pin (i.e. upper jaw of the machine) was brought down so that the pin was located inside the sleeve. At the second stage the pin was pushed down about 11 mm into the sleeve to achieve the desired I=4.6% of interference. During the third stage, the upper jaw of the Instron machine was raised thus extracting the pin from the hole. Finally the specimen was removed from the sleeve by hand ready for fatigue testing.

During cold expansion the pin was pushed down and pulled back with a speed of 4 mm/min and the force-displacement graph was recorded (a typical graph is shown in fig 6.12). All graphs had the same shape although the maximum axial forces varied slightly (about 4%). The maximum extraction (pull back) force after cold expansion was recorded and was about 5 kN.

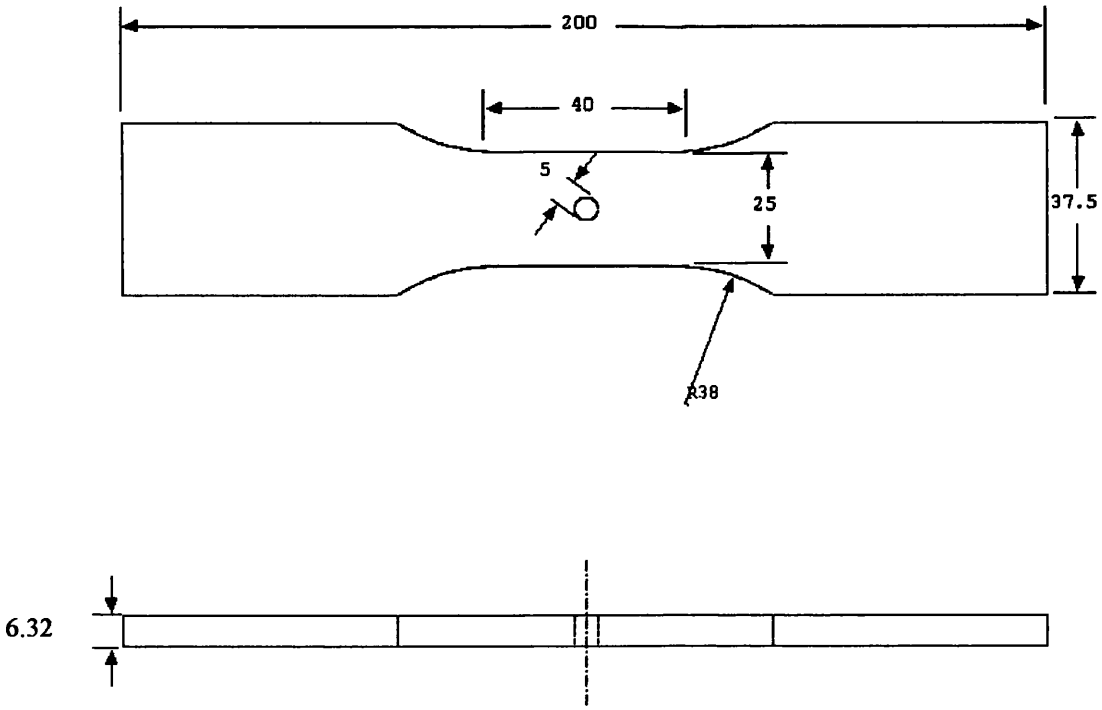

Fig 6.10: Fatigue specimen

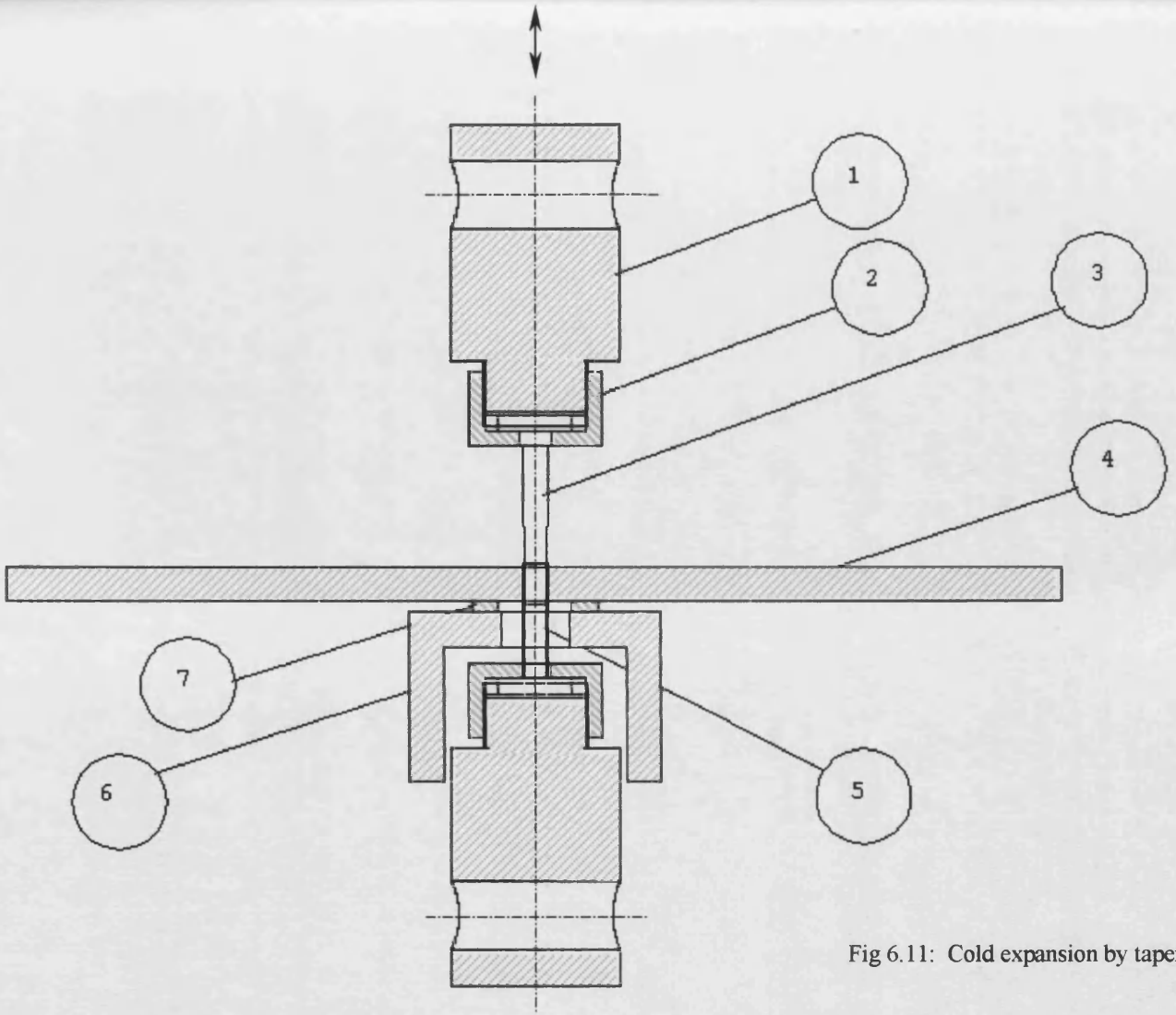

1) Instron Jaw connector (see fig 6.6)
2) The fixture locking nut (see fig 6.5)
3) The tapered pin (see fig 6.3)
4) The holed plate (see fig 6.10)
5) The mating sleeve (see fig 6.4)
6) The support ring (see fig 6.8)
7) The washer (see fig 6.9)

Fig 6.11: Cold expansion by tapered pin and mating sleeve (technique CC)

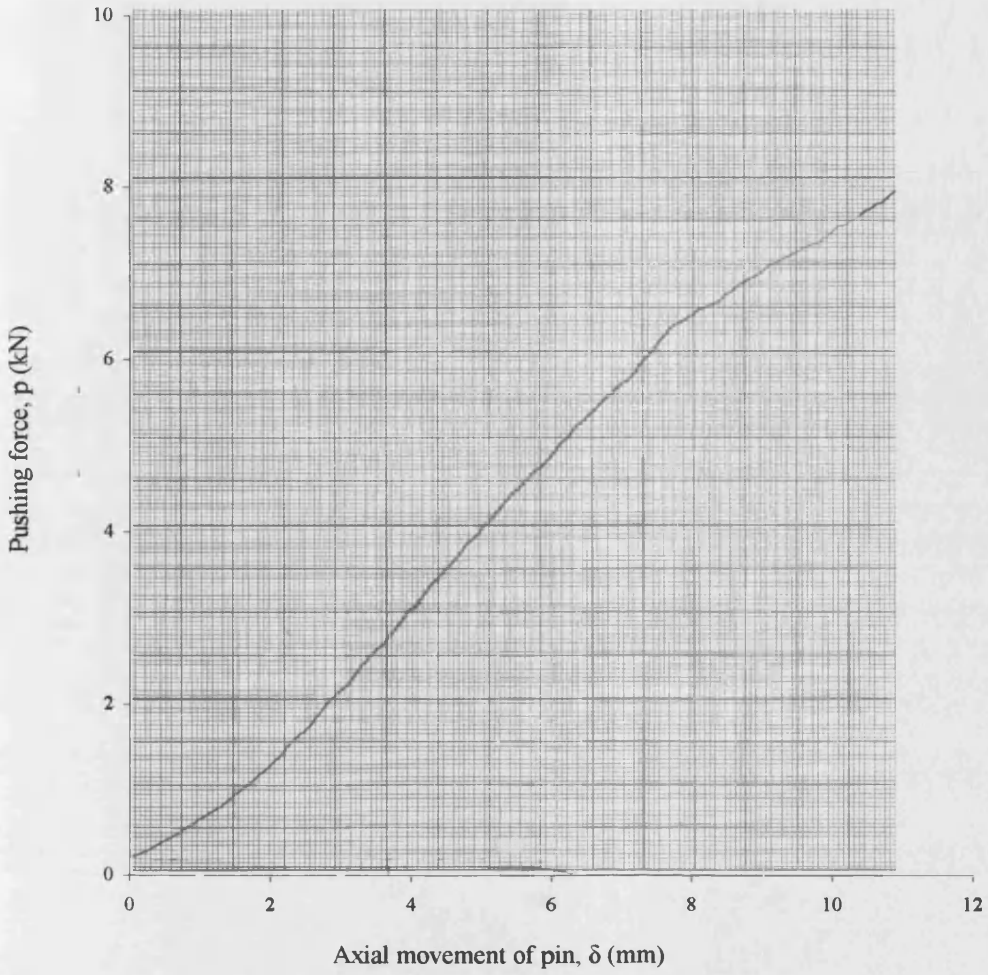

Fig 6.12: Force-displacement diagram for technique CC

6.3) Tapered pin with parallel split sleeve (technique BB)

This technique is similar to the FTI method in which a single slit sleeve and an oversized mandrel (or pin) with tapered head is used. With this technique, the sleeve is located inside the hole and the mandrel is pushed (or pulled) from one side of the holed plate and removed from the other side. The FTI technique needs a special tool but as one was not available a special tool was designed using a 10 kN Instron testing machine.

6.3.1) Design of parallel split sleeve and pin

The pin that was designed for technique BB has an oversized diameter at one end and is uniform at the other end (fig 6.13). The oversized end is tapered with a small angle in order to avoid damaging of the hole during cold expansion. The maximum diameter of the pin at the oversized end was designed so that it makes a nominal interference the same as with technique CC (I=4.6%). The overall length of the pin was chosen to be long so that it can be removed easily. To avoid surface damage to the pin surface it was surface hardened by quenching and tempering.

The sleeve used in the FTI method is thin and so will not support a large axial force. However, the sleeve that has been designed in this research is thicker and thus able to support greater axial force. This was necessary because of the comparative nature of the research so maximum effort has been taken to maintain similarity between techniques and includes material, testing machine, test environment, interference amount, geometry and dimensions.

The sleeve used in technique BB (see fig 6.14) is cylindrical (i.e. parallel walled) and is similar to the mating sleeve of technique CC. Both sleeves have the same nominal wall thickness, the same overall length and the same size of slit. Technique CC, however, has a tapered sleeve wall with very small internal angle at one end (see fig 6.4). Another minor difference between the parallel sleeve (used in technique BB) and the mating sleeve (used in technique CC) is their guide collars. With the mating sleeve the guide collar is combined with the sleeve but with the parallel sleeve it is separate (see next sub-section).

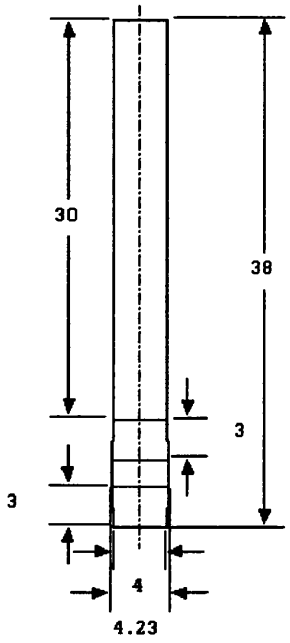

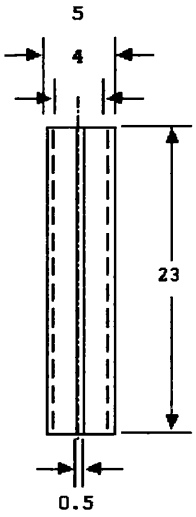

Fig 6.13: Tapered pin for technique BB

Fig 6.14: Parallel split sleeve used for technique BB

6.3.2) Testing machine fixtures and support rings

As with technique CC, the pin and sleeve of technique BB needed to be fastened to the Instron machine jaws in order to apply load during cold expansion and so the same fixtures were used (see fig 6.5-6.7).

In order to hold the pin and the sleeve straight during the expansion stage, special guide collars were designed for each of them (fig 6.15-6.16) so that the pin and the

sleeve fit tightly. During cold expansion, the guide for the pin was fastened to the upper fixture at one end and was supported to the pin at the other end. Also, the guide for the sleeve was fastened to the lower fixture at one end and supported the sleeve at the other end. Therefore, force could transfer from the fixtures to the pin and sleeve through their guides.

With technique BB, like technique CC, the holed specimen (see fig 6.10) must be supported at its exit side and the support ring and washer (see fig 6.8 and 6.9) were used for this purpose.

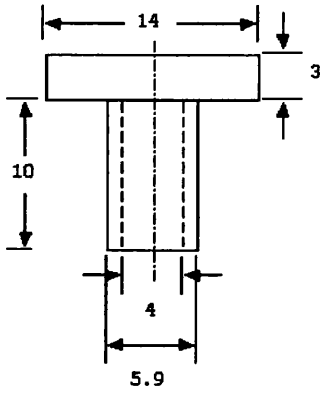

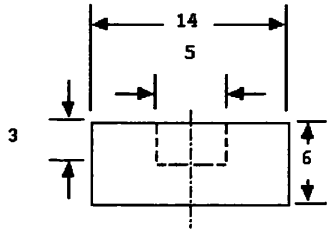

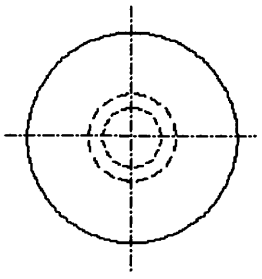

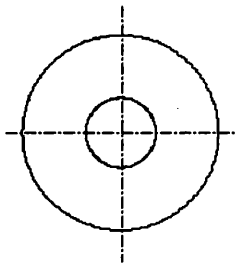

Fig 6.15: Guide collar for pin

Fig 6.16: Guide collar for parallel sleeve

6.3.3) Performing cold expansion and the force-displacement relationship

Having prepared the bush, the pin, the plate support and the fixtures the conditions are ready for carrying out technique BB. Performing this cold expansion technique is very similar to technique CC, however, it is unidirectional with the pin entering the hole from one side and exiting from the other side.

In preparing for this method, the fixtures were fastened to the Instron machine jaws then the pin and its guide were assembled to the upper fixture, the parallel sleeve and its guide were assembled to the lower fixture. As with technique CC, the support ring was placed on the Instron machine lower jaw. Then all contact surfaces (including the sleeve outside and inside, the hole surface and the pin surface) were lubricated with Tallow. Finally, the specimen was located on the support ring by pushing it into its hole on the free end of the parallel sleeve (fig 6.17).

During the first stage the pin was brought down so that it touched the sleeve. Secondly the pin was pushed down about 15 mm through the sleeve to expand the hole. At the third stage the sleeve guide, lower fixture and plate support ring were removed and the pin was taken out at the other side of the specimen. In the final stage, the parallel sleeve was extracted from the specimen hole by hand.

The pin was pushed down with a speed of 4 mm/min (as with technique CC). The force-displacement graph for the pin was recorded for all specimens and these graphs had the same shape but the maximum axial force varied in each diagram slightly by less than 4% (a typical graph is shown in fig 6.18).

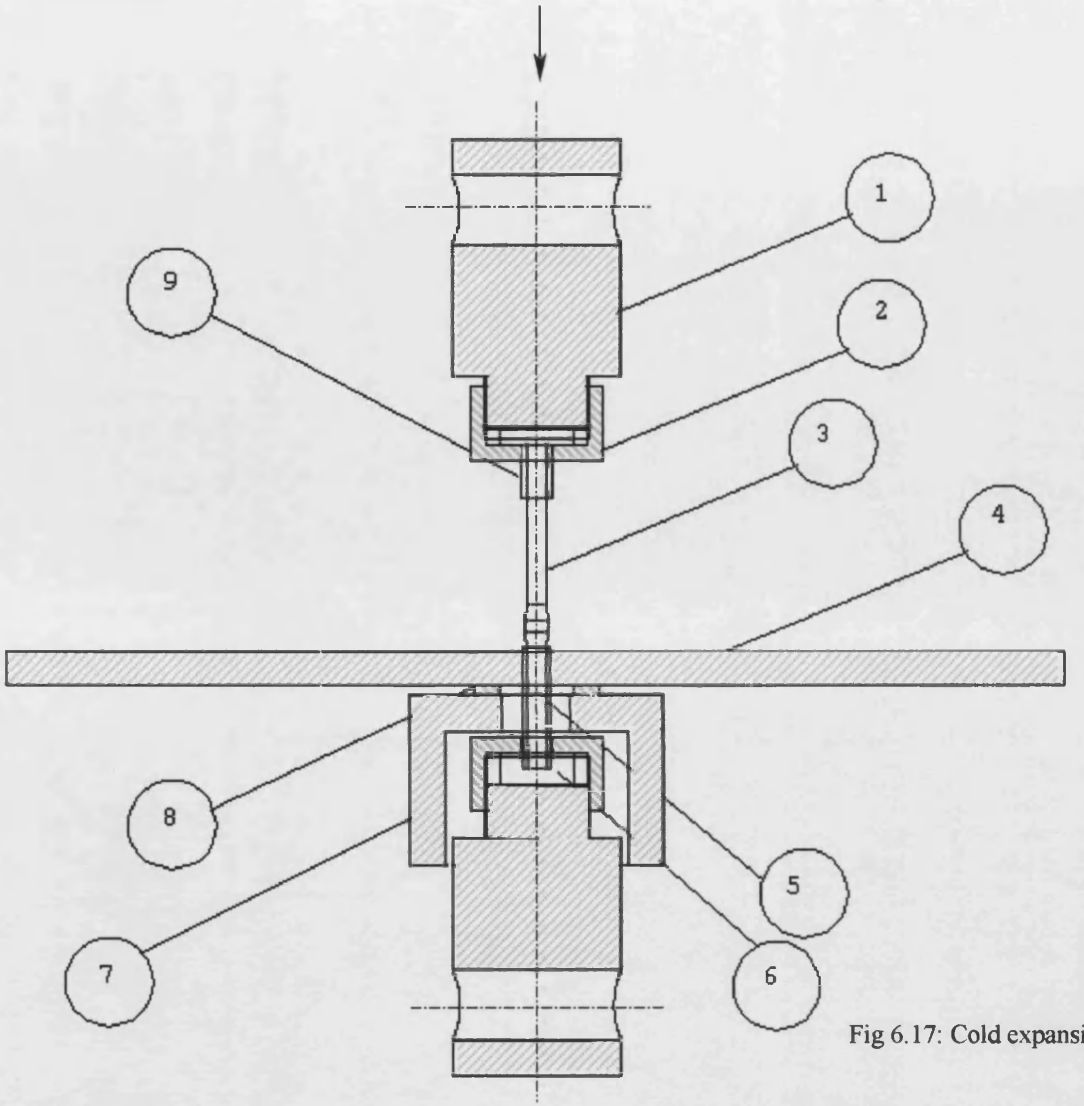

1) Instron jaw connector (see fig 6.6)
2) The fixture locking nut (see fig 6.5)
3) The tapered pin (see fig 6.13)
4) The holed plate (see fig 6.10)
5) The parallel sleeve (see fig 6.14)
6) The parallel sleeve guide (see fig 6.16)
7) The support ring (see fig 6.8)
8) The washer (see fig 6.9)
9) The pin guide (see fig 6.15)

Fig 6.17: Cold expansion by tapered pin and parallel sleeve (technique BB)

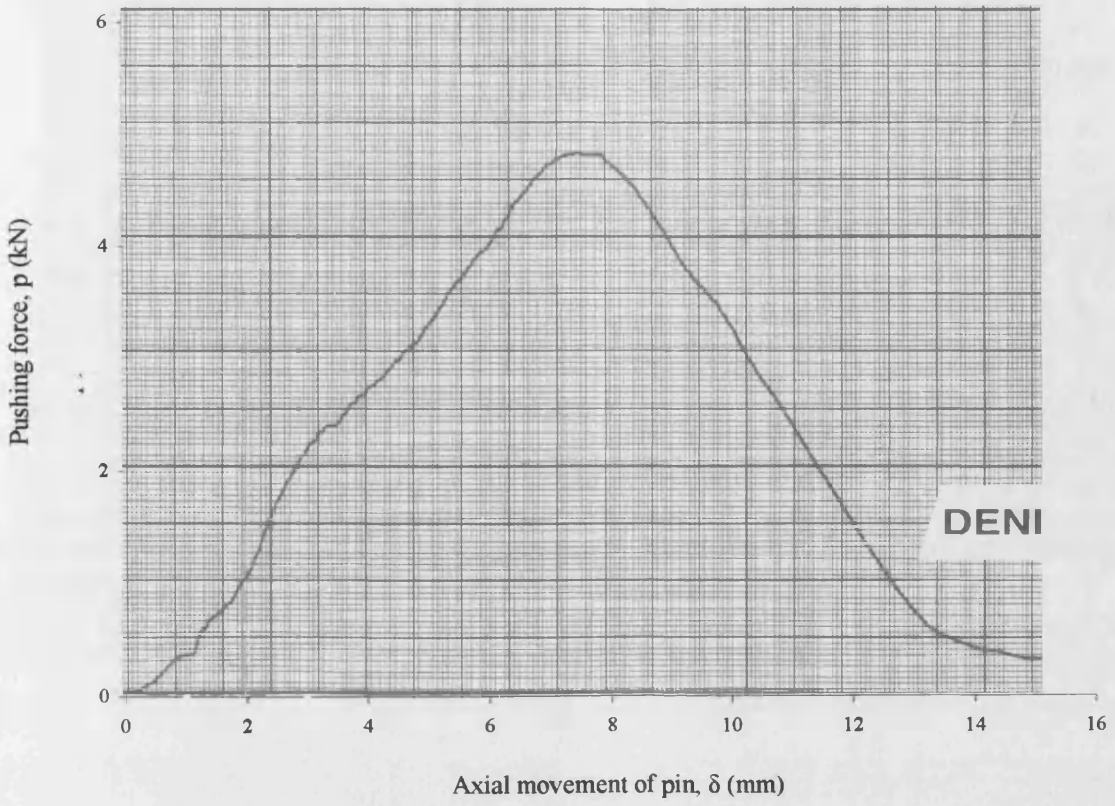

Fig 6.18: Force-displacement diagram for technique BB

6.4) Tapered pin without sleeve (technique DD)

Unlike with techniques BB and CC, this technique did not use any sleeve and during cold expansion the pin was in direct contact with the hole surface. With techniques CC and BB split sleeves were used to avoid direct contact between the pin and the hole, which can cause surface damage and thus have a negative effect on the fatigue life of a cold expanded specimen [4, 6, 7, 28]. As discussed in Chapter 4 the computer simulation shows that friction has a good effect on the distribution of compressive tangential residual stress around the cold expanded hole, especially at the pin entrance face and thus a positive effect on fatigue life. In order to investigate the effect of these two effects together on the fatigue life, technique DD has been included for comparison purpose.

Because this technique does not need a sleeve it is the easiest and cheapest of the three.

6.4.1) Design of tapered pin

The tapered pin designed for technique DD is very similar to the pin used for technique BB. It has an oversized diameter at one end and a uniform diameter at the other end (see fig 6.19). The maximum diameter of the pin at the oversized end was designed so that it makes the same nominal amount of interference as technique CC and BB (i.e. I=4.6%). The uniform end of the pin was designed long in order to be removed easily after cold expansion. In order to avoid any possibility of surface damage to the pin surface, like the previous pins, its surface was heat treated by quenching and tempering.

6.4.2) Fixture and collar guide for the pin

The cold expansion device for this technique needed only one fixture. This was fastened to the upper jaw of the Instron machine to hold the tapered pin guide that was designed to hold the pin in straight. The fixture was the same as that used for technique CC. The shape of the pin guide is similar to the shape of pin guide used for technique BB but has a different inner diameter as shown in fig 6.20. This difference is due to the larger diameter of the pin that is used for technique DD.

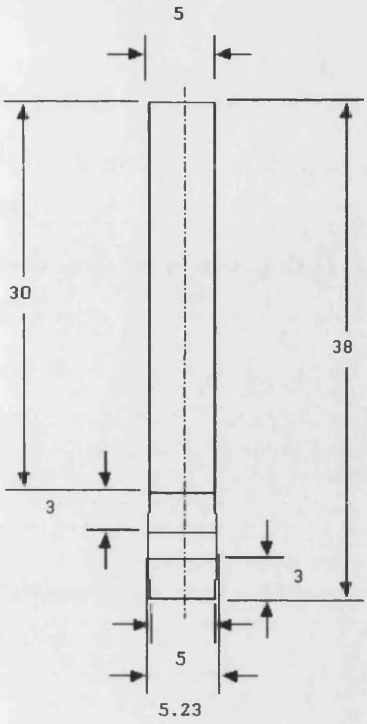

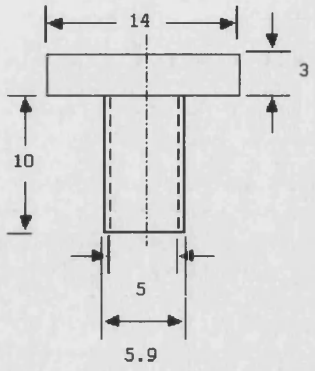

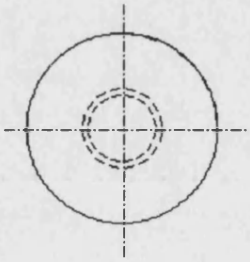

Fig 6.19: Pin used for technique DD

Fig 6.20: Collar guide for the tapered pin in technique DD

6.4.3) Performing cold expansion and force-displacement graph

In performing technique DD, the pin guide and the fixture were attached to the upper jaw of the Instron machine (the same machine that was used in technique CC and BB). Also, the holed specimen and its support were placed on the lower jaw of the machine then the pin was located in its guide (see fig 6.21).

The hole and the pin were lubricated with Tallow before commencing cold expansion. At the beginning of the test the upper jaw was brought down until the pin reached the hole entrance face. During cold expansion the machine upper jaw was moved down with a speed of 4 mm/min until the pinhead came out of the specimen. As with techniques BB and CC, the force-displacement graph of the pin was recorded for each specimen (a typical graph is shown in fig 6.22). All force-displacement curves for technique DD were similar but the maximum force varied slightly by 5%.

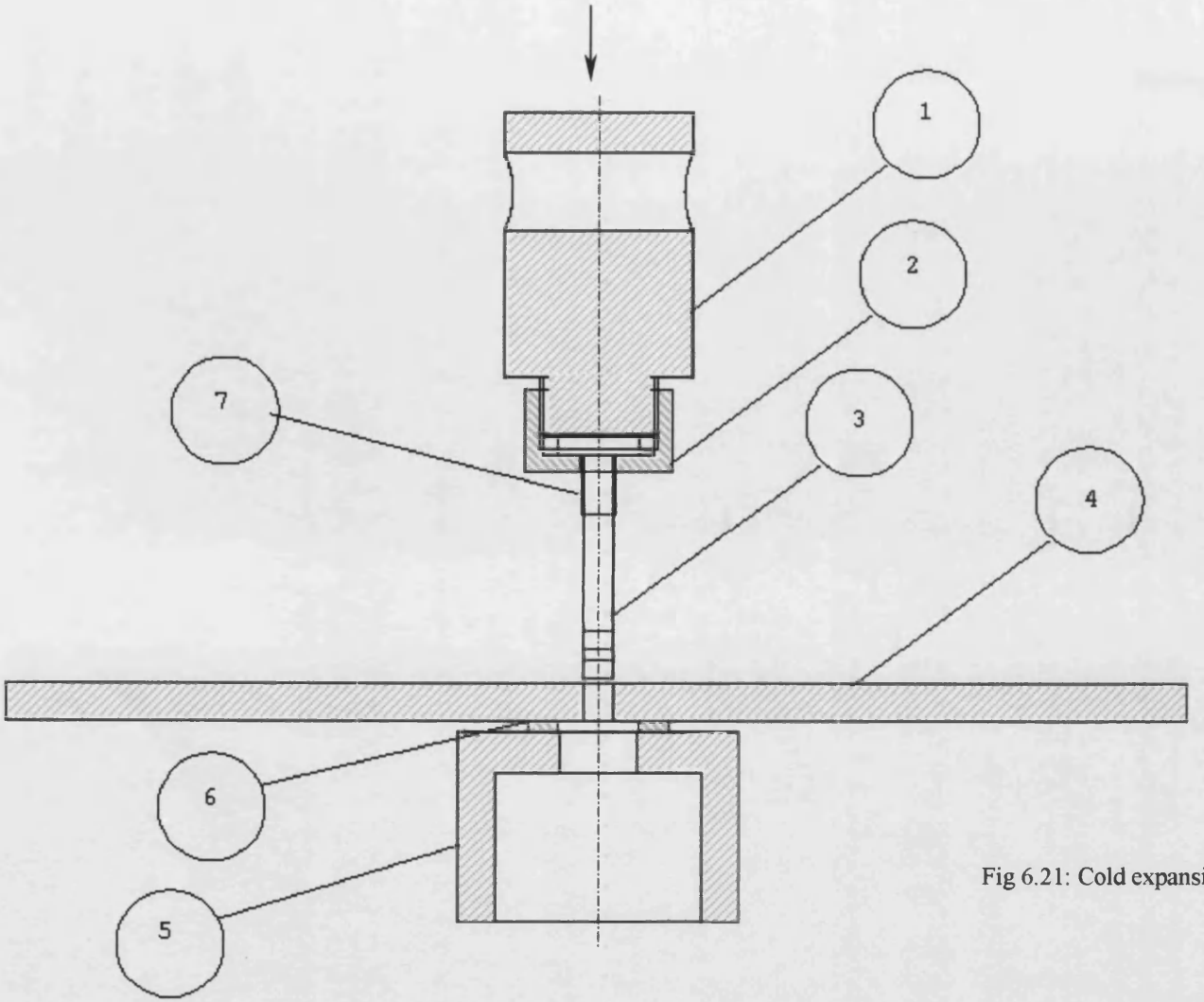

1) Instron jaw connector (see fig 6.6)
2) The fixture locking nut (see fig 6.5)
3) The tapered pin (see fig 6.19)
4) The holed plate (see fig 6.10)
5) The support ring (see fig 6.8)
6) The washer (see fig 6.9)
7) The pin guide (see fig 6.20)

Fig 6.21: Cold expansion by tapered pin (technique DD)

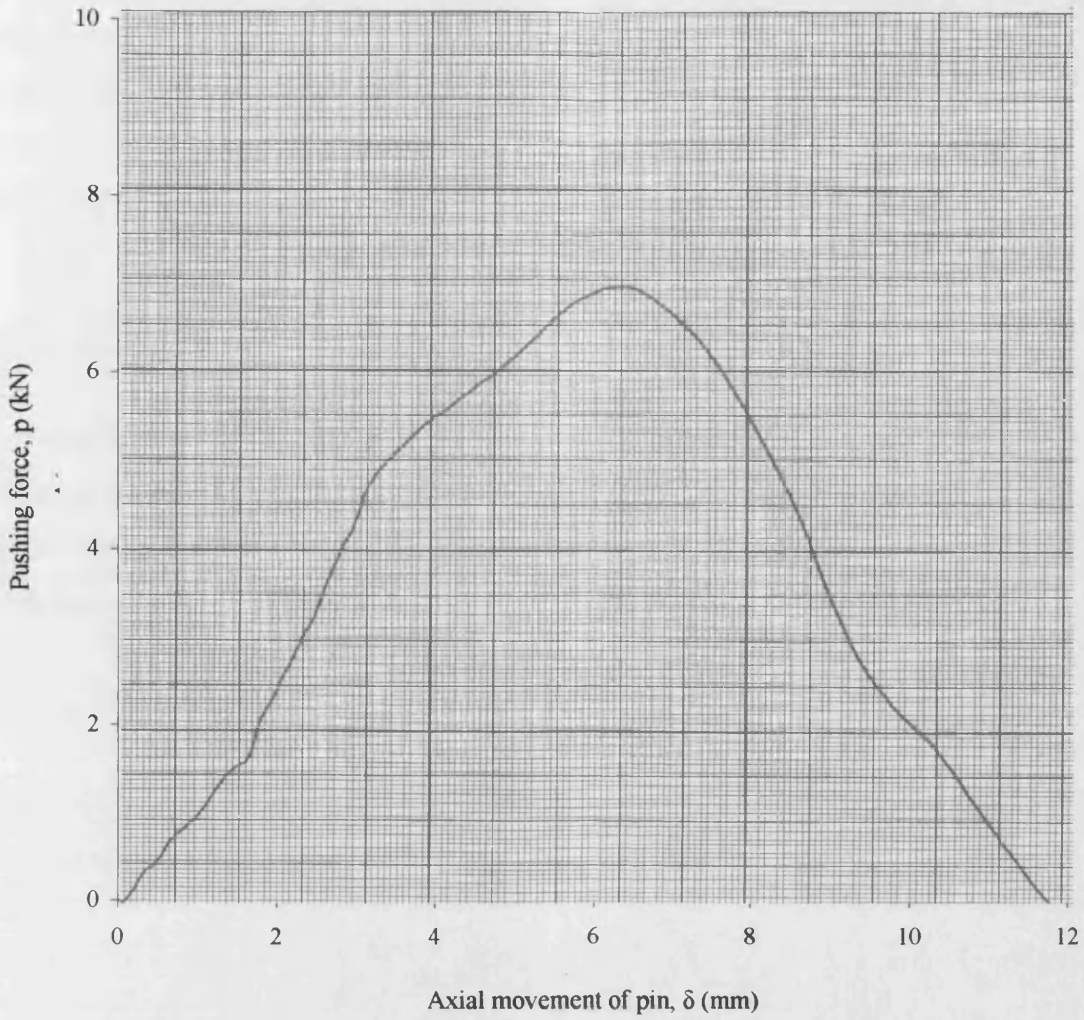

Fig 6.22: Force-displacement graph for technique DD

6.5) Materials used and their mechanical properties

Different materials have been used for the different components, for example, mild steel (En 1) was used for the fixtures, the support ring and the washer. High tensile steel (En 24) was used for the pins, the sleeves and the guide collars (for all techniques). Finally, aluminium alloy (7075-T6) was used for the holed (i.e. fatigue) specimen. This section describes the experimental tests which were carried out to obtain the mechanical properties that were needed for the finite element analyses.

These properties include the Poisson's ratio and the stress-strain diagram (and thus the elastic modulus). Although most of these properties are available in publications [i.e. 44, 54] in order to have accurate data, tests have been conducted on En 24 and aluminium alloy 7075-T6. No tests were carried out for mild steel because this material was not used in the FE models.

6.5.1) Mechanical properties of aluminium alloy 7075-T6

To obtain the mechanical properties of aluminium alloy 7075-T6 two different experimental tests were carried out. These tests were a tensile test (to obtain the stress-strain diagram and E) and a Poisson's ratio test (to obtain ν). These tests, as with the cold expansion tests, were carried out at room temperature.

6.5.1.1) Tensile test

This was carried out on a plate type specimen (as shown in fig 6.23) in a 100 kN Instron testing machine. The dimensions were chosen from the ASTM standard book [$55_{E\text{-}8}$] for a simple tension test and the length of the specimen was chosen to be along the rolling direction.

The test speed was 0.5 mm/min and is within the speed range, which the ASTM standard recommends. Two tests were carried out and the force-elongation (displacement) diagrams were almost identical (fig 6.24). Also the ultimate tensile strength and elongation were the same as the manufacture had reported (600 MPa).

As explained in Chapter 3, the stress-strain diagram was obtained from the force-displacement (p-δ) curve. In this test the elastic modulus was calculated from the initial linear part of the curve and found to be E=71.5 GPa.

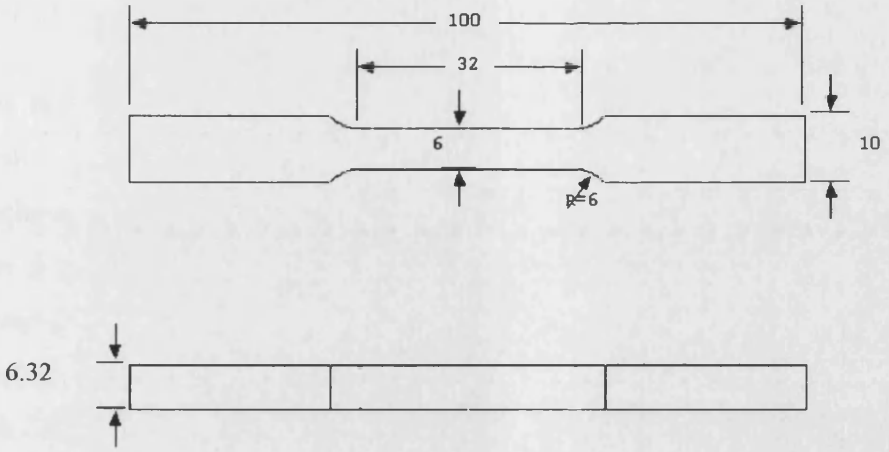

Fig 6.23: Simple tension test specimen for Al alloy 7075-T6

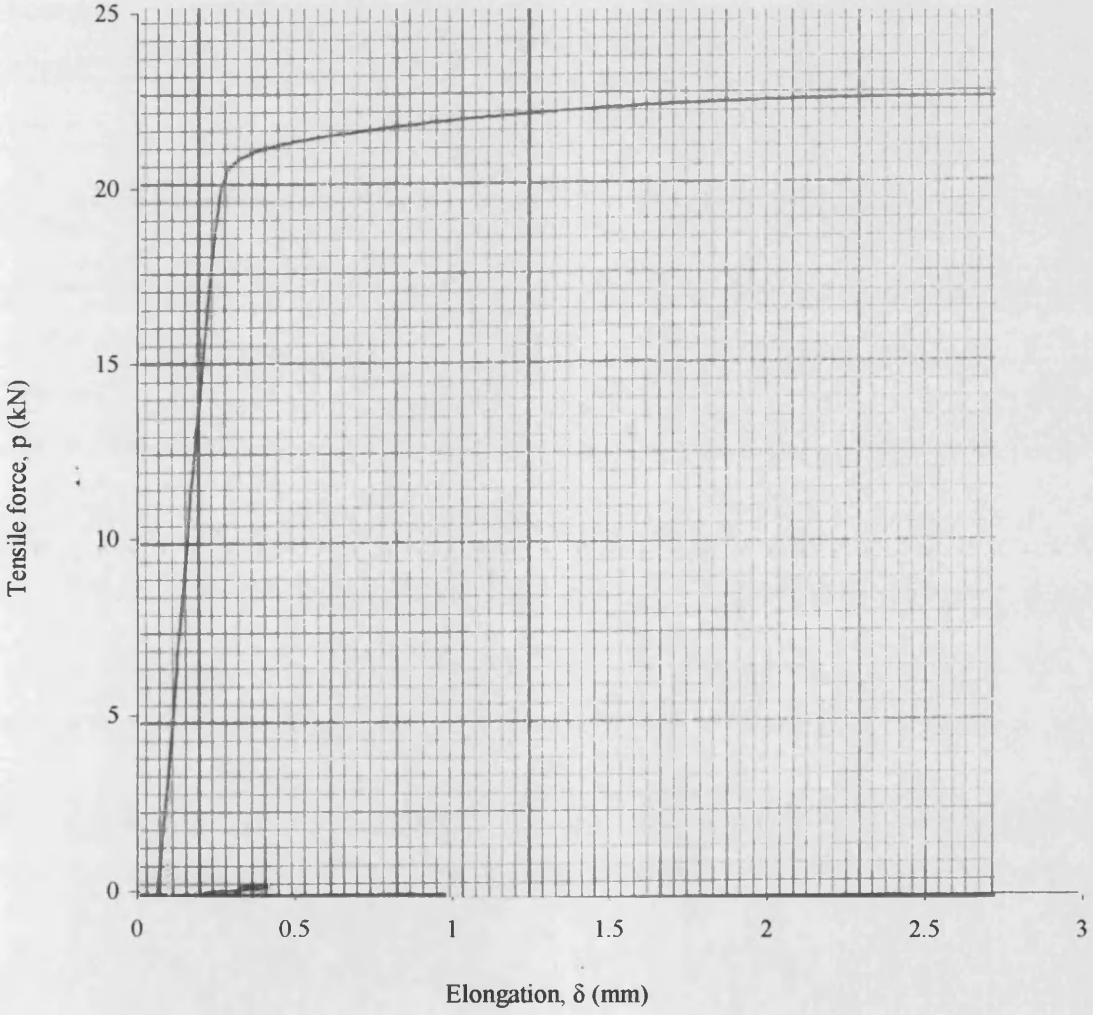

Fig 6.24: Force-elongation diagram in simple tension test for Al alloy 7075-T6

6.5.1.2) Poisson's ratio test

This test was carried out on the same specimen type that was used for the simple tension test (fig 6.23). However, instead of using a100 kN Instron machine a 10 kN machine was used. To measure the strains in longitudinal and transverse directions, four strain gauges were used as shown in fig 6.25. With this configuration it is possible to measure the Poisson's ratio in the both perpendicular planes. This was done in order to investigate if aluminium alloy 7075-T6 has any anisotropy.

The ASTM standard [55_{E-132}] recommends that strain gauges to be located on opposite sides of the specimen in order to avoid any possible bending effect because of misalignment of the specimen. This was not done here because of limited funds, however, maximum care was taken to avoid bending by achieving good specimen alignment before the final test. Several times the position of the specimen in the jaws has been readjusted in order to have the same strain in the longitudinal strain gauges for the different load increments.

After aligning the specimen in the machine jaws, load was applied incrementally and for each load increment the strains from the four gauges were recorded. The results of this test are presented in fig 6.26 in which the strains in the longitudinal direction are labelled in the horizontal axis and the strains in the transverse direction are labelled in the vertical axis. As fig 6.26 shows the transverse strains are not identical and this could be a sign of anisotropy.

The Poisson's ratio, ν were obtained from the slope of the lines and they are 0.325 and 0.335.

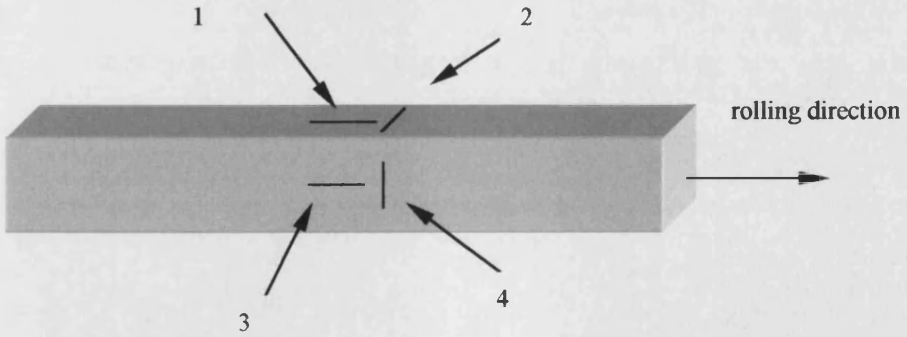

Fig 6.25: Strain gauge locations and their directions

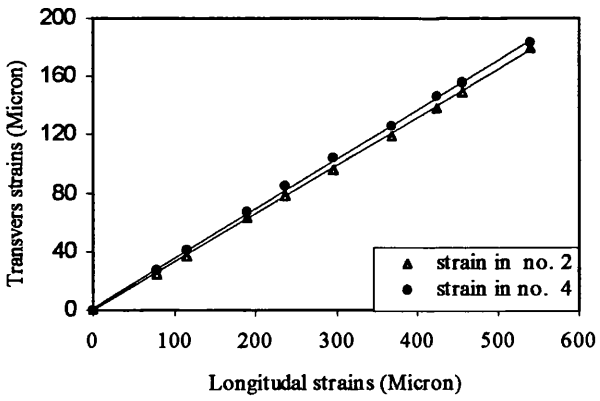

Fig 6.26: Strain gauge results

6.5.2) Mechanical properties of high strength steel (En 24)

As mentioned previously, all pins and sleeves were made of En 24 steel and the properties of this material (like aluminium alloy 7075-T6) were needed for the FE analysis. For this material only a simple tension test was carried out to obtain the stress-strain diagram and for determining the elastic modulus (the Poisson's ratio was taken from reference [44]).

This test was carried out on a round specimen (fig 6.27) as the En 24 was available in round bar form, and was conducted at the same load speed and on the same Instron machine as the aluminium alloy tests.

In this test the force-elongation curve (fig 6.28) was obtained then converted to a stress-strain diagram (see chapter 5).

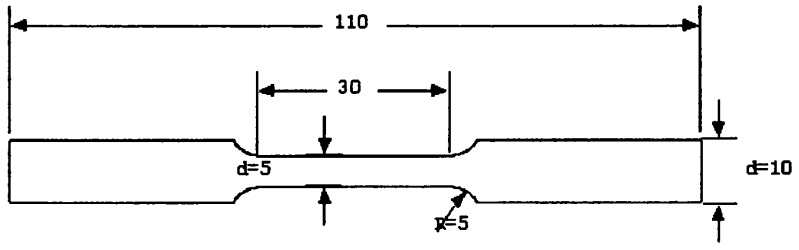

Fig 6.27: Simple tension test specimen for En 24 steel

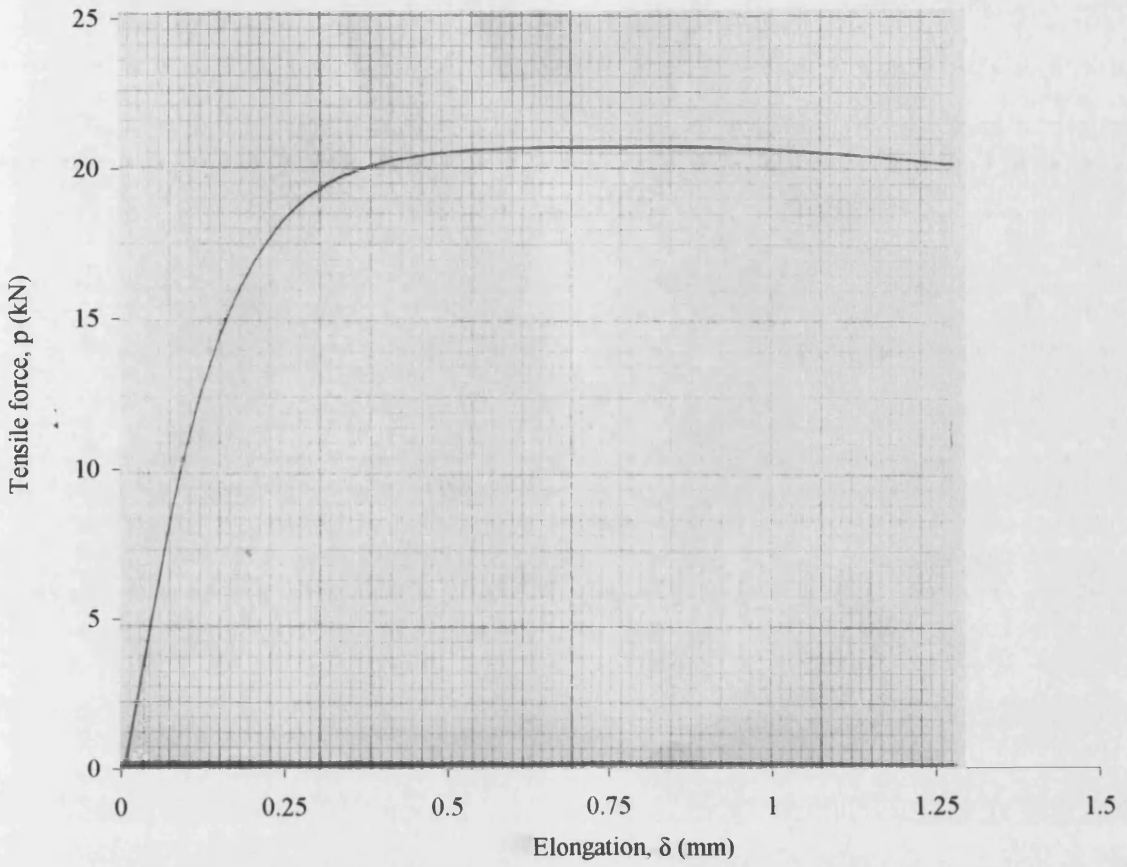

Fig 6.28: Force-elongation diagram for simple tension test on En 24 steel

Chapter 7

Fatigue test results and discussion

7.1) Introduction

This chapter describes fatigue tests carried out on four different specimen types. The fatigue specimen types include an "as drilled" specimen (type AA) and three cold expanded specimens, which were treated using the three techniques described in Chapter 6 and called CC, BB, and DD. This chapter presents the results of the fatigue tests and investigates which cold expansion technique is the more efficient in terms of increasing fatigue life when the same interference amount is used. The fatigue tests, loading machine used, the location of the fatigue crack initiation and its growth location and the S-N diagrams are explained.

7.2) Fatigue specimen material, geometry and preparation

All fatigue specimens that were tested were made from the same aluminium alloy 7075- T6. The shape and size of the fatigue specimens (see fig 7.1) were taken from the ASTM standard for constant amplitude axial fatigue tests [55_{E-466}]. The jaw grip regions were designed so that they can be fitted into the fatigue machine jaws and have enough length to avoid slipping. The grip regions were also designed wider to prevent fatigue fracture in the jaws.

The specimens were cut from a specially ordered 1m x 1m piece of aircraft specification aluminium alloy 7075-T6 plate and sawn into 40 mm x 200 mm rectangular pieces. The 40 mm width and fillets were machined using a milling cutter to achieve the designed size (see fig 7.1). A 5 mm diameter hole was drilled in the middle of the specimen and then reamed to remove any burrs and make its surface smooth. The specimen side where drilling started was marked with ink to identify whether crack initiation is affected by the face where drilling starts. After preparing all specimens some of them were used directly for "as drilled" fatigue specimens (type AA) and the rest were cold expanded using the three techniques described in the previous chapter. Any specimens that had scratches were not used.

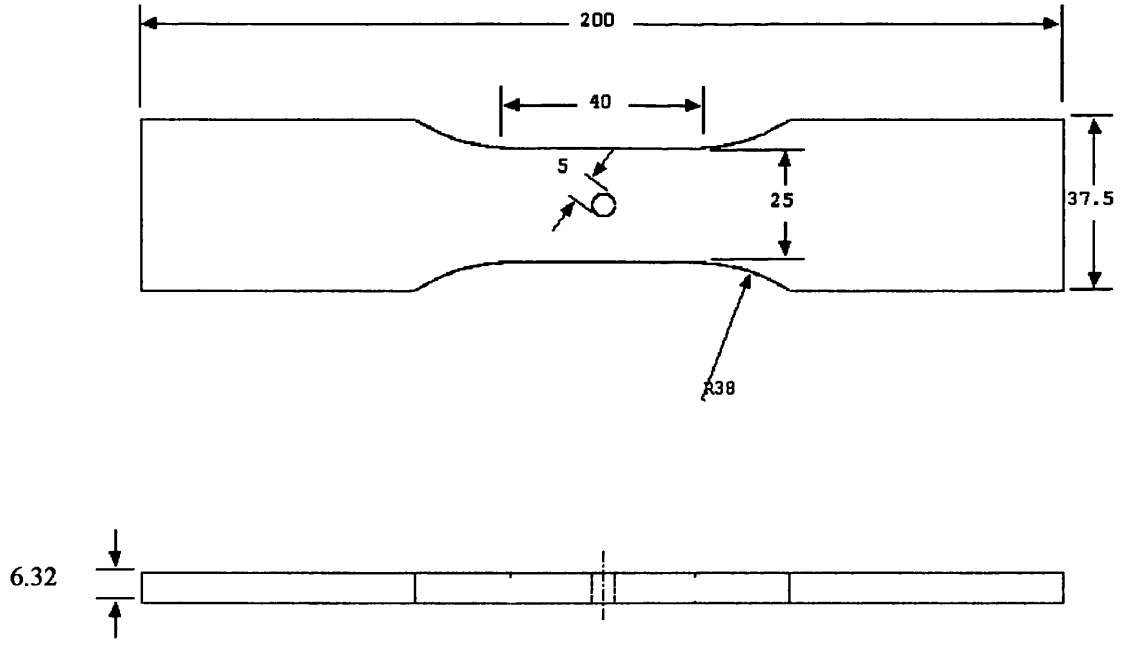

Fig 7.1: Fatigue specimen and dimensions

7.3) Fatigue test machine used

A servo hydraulic Instron axial machine (model 1332), which is capable of doing both static and dynamic test, was used for the fatigue tests. The machine capacity for static and dynamic test is 250 kN and 125 kN (in pulling and pushing) respectively. The machine is automatic and the required parameters for the fatigue test can be set using the Function Generator and the Controller Modules.

The Function Generator is used to provide the varying component of the signal controlling the hydraulic actuator (the moving machine jaw) via the servo amplifier and servo valve. The Function Generator panel provides a variety of waveforms including sinusoidal, ramp, triangular and square wave. It provides the frequency and amplitude of the wave which can be set. The Function Generator also has an option to choose whether a fatigue test is started with tension or compression.

The Controller Modules include Position, Load and Strain Controllers and also a selector panel. The Position Controller is used to displace the machine moving jaw while the other two are used to apply the desired load and strain. All the controllers have four potentiometers; two of these set minimum and maximum limits, which stop the machine when the limit parameters are overridden. The other two potentiometers are used to input mean level and amplitude of the parameters (load, strain and position). When performing a fatigue test usually the Position Controller is used either with Load or with Strain Controller. The selector panel enables a chosen parameter's mean level, maximum or minimum value to be read on the machine indicator.

7.4) Fatigue test process

This section explains how the fatigue tests were carried out. Due to the comparative nature of the project maximum effort has been taken to maintain the same test condition for all types of specimens (AA, BB, CC, DD).

1. Fastening a specimen to the machine jaws: initially a straight line was marked on the grip region of each specimen perpendicular to the longitudinal direction. They were used as a guide for alignment in the machine jaws to avoid bending. With the specimen fastened to the machine upper jaw in the grip region it was then lowered (by moving the

upper jaw) so that the other grip region entered the lower jaw. The lower jaw was set to zero mean level before it was fastened.

2. Setting Position Controller limits: An 8 mm limit was set either side of the zero mean level. This means that if the lower jaw goes up or down by as much as 8 mm from its zero mean level the machine will stop. This setting has duel benefits, one is to stop the machine, after the fatigue specimen breaks and the other is to prevent machine damage if something goes wrong during the test. Choosing position limits needs care as the amount should not be less than the specimen elongation or contraction under maximum and minimum loads of the test otherwise the machine would stop at the initial stage.
3. Setting waveform and frequency: A sinusoidal waveform was used because it is widely favoured and used. Choosing a suitable running frequency is important it governs the time that the test will last and frequency may affect the relaxation of the residual stress caused by cold expansion. Intuitively it appears that at low frequency a cold expanded specimen has a shorter fatigue life than at higher frequency. This can happen because of residual stress relaxation. Understanding the effect of frequency on fatigue life in cold expanded specimens needs more research and is not included in this research. Unfortunately only in a few published research papers has test frequency been mentioned. In addition to the effect of frequency and test time, the maximum attainable dynamic load is important. This is limited by the machine power and so the frequency was chosen to be 20 Hz. Although attempts to test at higher frequency were made but they were found unreliable.
4. Load setting: all fatigue tests were carried out under constant amplitude cyclic loading. The loading varied between a minimum of P_{min} (=0 kN) to a maximum amount P_{max}. This loading is a combination of mean P_{ave}(= $P_{max}/2$) and the alternating load amplitude, P_a (= $P_{max}/2$). When applying load to the specimen the machine control was changed from Position Controller to Load Controller. As with the Position Controller, at the first stage the minimum and maximum limits have been set (to -3 kN and P_{max} +3 kN respectively). Therefore, if the minimum load and maximum load fluctuate more than these limits the machine will stop. These limits are

necessary for machine safety and also test accuracy. After setting the load limits, the mean level load was applied to the specimen using the mean level potentiometer then after starting the fatigue test the alternating load was applied using the amplitude potentiometer.

7.5) Fatigue test results for "as drilled" specimen (type AA)

The test results for these specimens are given in table 7.1 and shown fig 7.2. In this figure the fatigue results are displayed in a log-linear chart with the alternative remote stress on the linear Y-axis and the fatigue life (number of cycle that specimens have taken to break) on the logarithmic X-axis. As fig 7.2 shows, generally the specimens have shorter fatigue life under high alternating stress and longer fatigue life with low alternating stress.

In addition to the information given in table 7.1 and fig 7.2 some other observations from the test are discussed below:

1. All specimens broke at the smallest cross sectional area where the 5 mm diameter hole is located.
2. The broken section includes two distinct light and dark coloured regions. The light region, which is near the hole surface, is smooth and shows where the crack started and propagated. The dark region, which is rough, shows where the final fracture occurred (see fig 7.3).
3. Specimens with high alternating stress have a small light region at the broken section unlike with lower stressed specimens. This is to be expected because with a large load the specimen would fracture after only small crack growth.
4. Only 2 of the 10 specimens broke symmetrically with respect to the hole and mid-plane.
5. A study of broken sections shows that with 3 of the10 specimens, the crack started at the drill entrance face and 3 from the exit face of the hole edges. In the rest of the specimens the crack propagation is symmetric about the mid-plane so it is difficult to identify in which plate face the crack has started. This observation shows that the drill and reamer entry and exit surface has virtually no effect on the crack initiation location.

6. In the specimens that cracks propagated symmetrically, the crack shape is semi-elliptical with its major axis in the mid-plane (X-axis). The corner crack, which starts from the plate faces at the hole edge, is quarter-elliptical and propagates through the plate thickness (inwards) and outwards from the hole (see fig 7.3 (a)).

Table 7.1: Fatigue test results for specimen type AA

specimen reference	P_{min} (KN)	P_{max} (KN)	N (number of cycles)	Fracture state
AA1	0.1	26.0	111420	Broken at smallest section
AA2	0.3	30.1	13570	"
AA3	0.0	22.0	75320	"
AA4	-0.2	20.1	643090	"
AA5	0.1	26.1	35180	"
AA6	-0.3	30.0	22630	"
AA7	-0.1	22.0	53820	"
AA8	0.0	20.1	247670	"
AA9	0.1	28.1	18550	"
AA10	0.1	24.1	58920	"

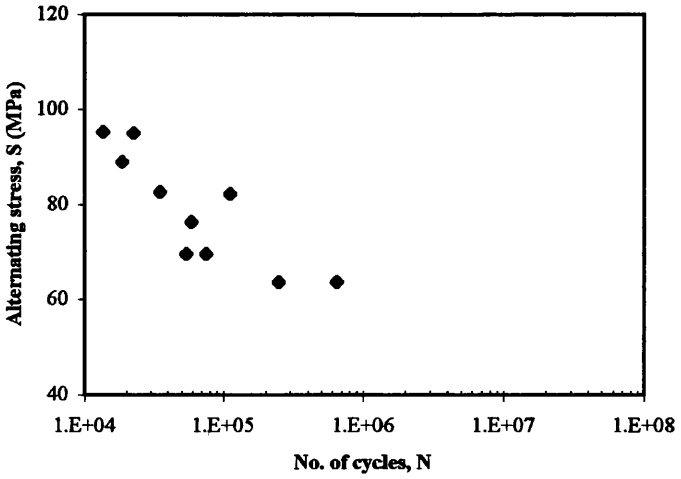

Fig 7.2: S-N diagram for "as drilled" specimen (type AA)

a) Fatigue crack growth from drill entrance in AA8

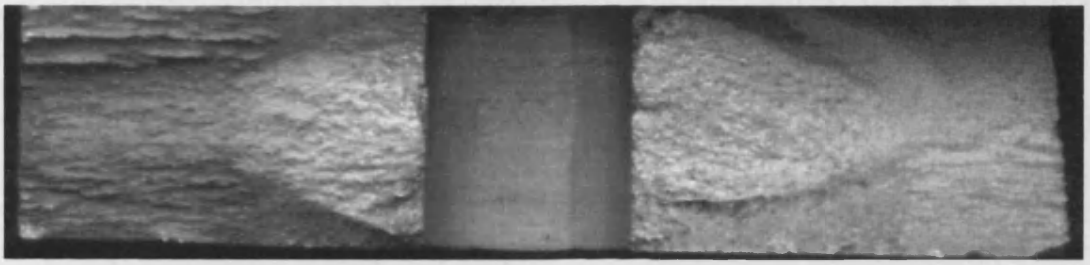

b) Fatigue crack growth from both edges of hole in AA6

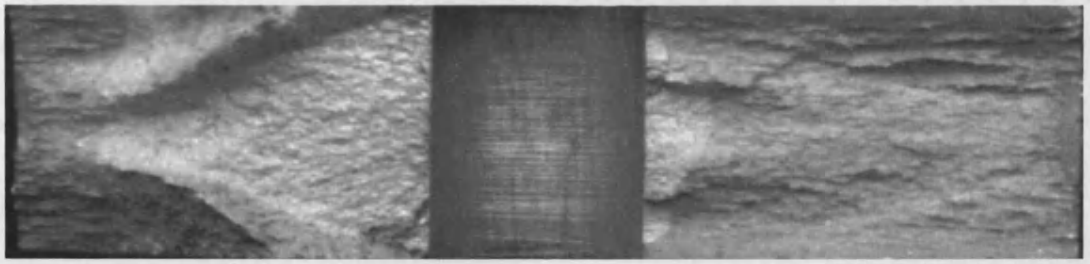

c) Fatigue crack growth initially from one side of hole in AA2

Fig 7.3: fatigue crack region for " as drilled" specimen (type AA)

7.6) Fatigue test results for cold expanded specimen type BB

The holes of these specimens were cold expanded using a tapered pin and parallel split sleeve. After cold expanding a small "pip" remains inside the hole due to the slit of the sleeve. In practice this pip is removed by reaming the hole [6, 41] but in this research no attempt was made to remove it, because it was kept away from the fracture section.

The applied loads, fatigue lives and fracture locations for these specimens are presented in table 7.2. The fatigue test results are displayed on a log - linear chart in fig 7.4 as for specimen type AA.

Close examination of the broken specimens shows that:

1. All specimens (when under identical loading) have a better fatigue life than those of type AA. The fatigue life increase is significant at lower alternating stresses and under the lowest alternating load applied the specimen did not break even after ten million cycles.
2. 8 of the 9 specimens broke and this was at the smallest cross section area where the 5 mm diameter hole is located.
3. The broken section of the specimens includes two distinct regions with light and dark coloured. The light region is smooth and shows that the crack started and propagated at the hole edge. The dark region is rough and shows the final fracture area (see fig 7.5).
4. As with specimen type AA, all the specimens with high alternating remote stress have a smaller fatigue crack region at the broken section than the lower stressed specimens.
5. No specimen broke symmetrically about the hole.
6. In 6 of the 8 broken specimens, the crack started from the hole edge at the pin entrance face (in cold expansion process) and in the other two, the broken region is symmetrical with respect to the mid-plane and so it is difficult to identify where the crack started. This observation shows that when cold expanding a hole with a tapered pin and parallel split sleeve, the crack is more likely start from the pin entrance face.
7. The fatigue crack propagation region with this type of specimen is very similar to type AA. However, with most corner cracks, propagation did not

grow inwards through the plate thickness and final fracture occurs near the hole at the pin exit face (see fig 7.5).

Table 7.2: Fatigue test results for specimen type BB

specimen reference	P_{min} (KN)	P_{max} (KN)	N (number of cycles)	Fracture state
BB1	0.1	26.1	93140	Broken at smallest section
BB2	0.4	30.0	43490	"
BB3	-0.4	22.3	1300950	"
BB4	0.2	20.3	9911000	Not broken
BB5	0.1	26.1	543120	Broken at smallest section
BB6	0.2	30.1	193780	"
BB7	-0.2	22.2	1866000	"
BB8	0.2	28.1	51200	"
BB9	0.1	29.1	578900	"

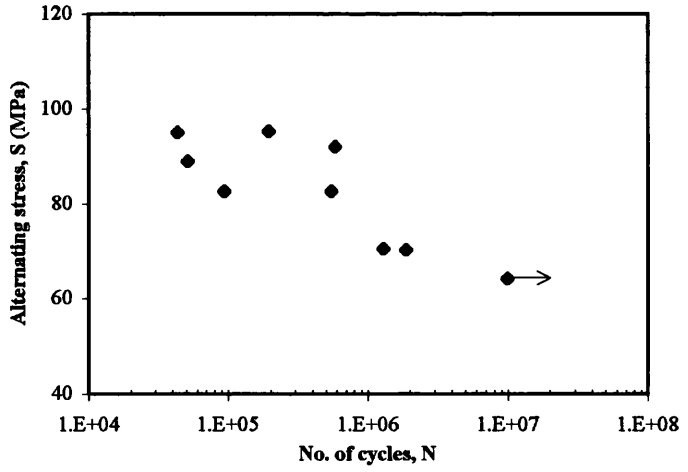

Fig 7.4: S-N diagram for specimen cold expanded by tapered pin and parallel split sleeve (type BB)

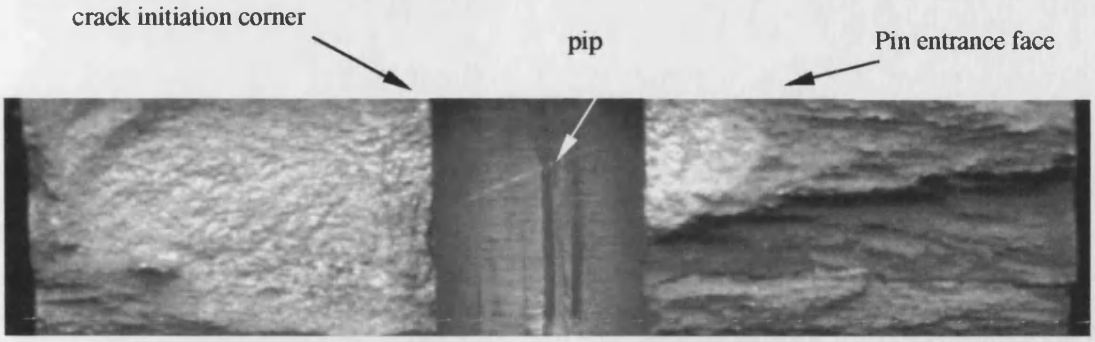

a) Crack growth at entrance and with pip visible in BB9

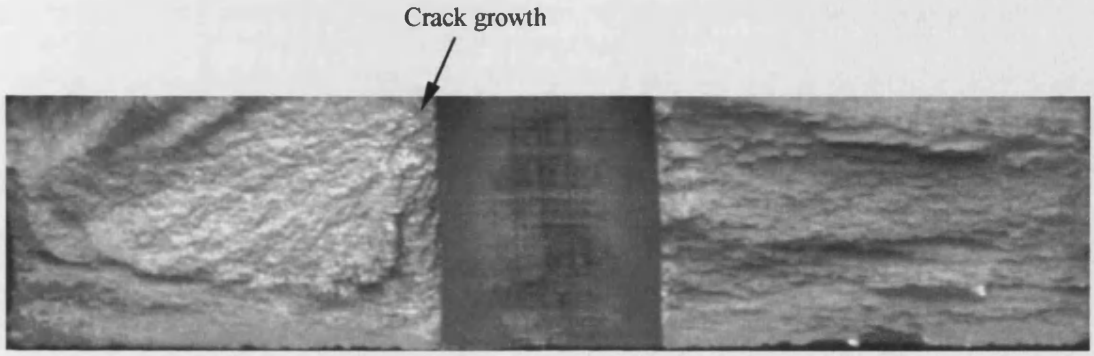

b) Crack growth at entrance corner with fracture at exit region in BB2

Fig 7.5: Fatigue crack growth and final fracture (at the exit side) for specimen type BB

7.7) Fatigue test results for cold expanded specimen type CC

This type of specimen was cold expanded using a tapered pin with mating split sleeve. Like specimen type BB a thin pip remains at the hole surface and this was not removed because it did not interfere with the fatigue test.

The applied loads and fatigue life of this specimen type are summarized in table 7.3. Like the two previous specimen types, fatigue test results for these specimens are displayed on a log-linear chart (see fig 7.6).

Close examination of broken sections of specimen type CC shows that:

1. The fatigue life of these specimens is surprising, not only because of the increase in life, but also because of the final fracture location. Three of the ten specimens did not break even until ten million cycles were reached.

Two of the ten specimens broke away from the smallest area (see fig 7.7 and 7.8) and the other five broke at the smallest cross section.

2. The broken section includes two different crack growth and final fracture regions (like specimen type AA and BB) see fig 7.9.
3. None of the specimen broke symmetrically about the hole.
4. The shape of the crack propagation region of specimens which broke at the smallest section are quarter-elliptical. This means that crack initiated at the hole edge and propagated inwards and outwards.
5. The fatigue cracks in 3 of the 5 specimens (that broke at the smallest section) initiated at the hole edge in the pin entrance face. In the other two, the crack initiated at the hole edge at the pin exit face. This is a distinct characteristic of specimen type CC that is different from those of specimen types BB and DD (see next section).

Table 7.3: Fatigue test results for specimen type CC

specimen reference	P_{min} (KN)	P_{max} (KN)	N (number of cycles)	Fracture state
CC1	0.0	26.4	478660	Broken at smallest section
CC2	0.0	30.1	256700	"
CC3	-0.3	22.4	3855600	"
CC4	-0.4	20.3	6944380	Not broken
CC5	0.0	26.1	2686630	Broken at smallest section
CC6	-0.2	30.1	345500	"
CC7	-0.2	22.2	5019410	Not broken
CC8	0.0	20.2	10000000	Not broken
CC9	0.1	28.1	184790	Broken in big area
CC10	0.1	24.1	6012510	Crack started in large section but final fracture in smaller section

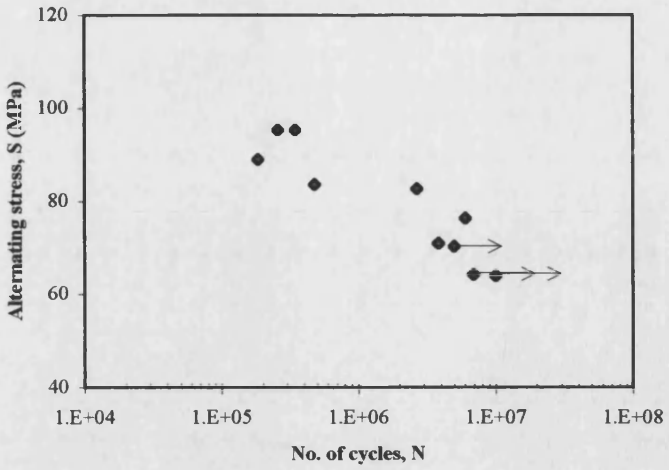

Fig 7.6: S-N diagram for specimen cold expanded by tapered pin and mating split sleeve (type CC)

Crack initiation

Fig 7.7: Fatigue fracture away from cold expanded hole in specimen CC9

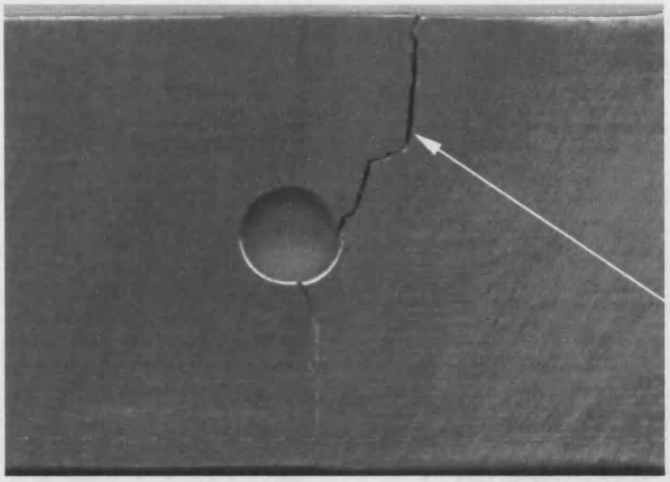

Fig 7.8: Fatigued specimen CC10 showing crack initiation away from hole edge

a) Crack growth from entrance face in specimen CC2

b) Crack growth from exit face in specimen CC3

Fig 7.9: Different plate face failures from specimen type CC

7.8) Fatigue test results for sleeveless cold expanded specimen type DD

These specimens were cold expanded with a tapered pin without using any sleeve so direct rubbing was experienced at the hole surface. This is the easiest, from practical considerations, of the three techniques. The philosophy behind using a parallel split sleeve (as in the FTI method) is to exclude the friction effect, because it is thought to be harmful to the fatigue life of a holed plate, however, the test results do not support this view. This is because specimen type BB (which is very similar to the FTI technique) did not produce a better fatigue life than specimen type DD, whereas, the interference amount (as explained in previous chapters) and the test conditions were the same. Even type DD specimen under similar loading had a better life than specimen BB in some cases.

The applied loads, fatigue lives and final fracture states for this type of specimen is presented in table 7.4. As with the previous specimen types, the fatigue test results are displayed on log-linear axes (see fig 7.10).

Close observation of the fractured sections and test results shows that:

1. The fatigue life improved in all type DD specimens, under similar loads, relative to the "as drilled" specimens.
2. Only 4 of the 6 specimens broke, the other two were loaded with low alternating stress and did not break even after several million cycles.
3. The broken area of the specimens, like other specimen types, includes two distinct regions of crack growth and final fracture.
4. No specimen broke symmetrically about either the hole or the mid-plane (see fig 7.11).
5. In all broken specimens, the shape of the fatigue crack propagation area is quarter-elliptical because in each specimen the crack has started from the hole edge at the pin entrance face (see fig 7.11).

Table 7.4: Fatigue test results for specimen type DD

specimen reference	P_{min} (KN)	P_{max} (KN)	N (number of cycles)	Fracture state
DD1	0.1	26.1	389050	Broken at the smallest section
DD2	-1.2	29.9	87410	"
DD3	-0.2	22.4	3347410	Not broken
DD4	0.0	20.3	8818550	Not broken
DD5	0.1	28.1	158550	Broken at the smallest section
DD6	0.1	24.1	500120	"

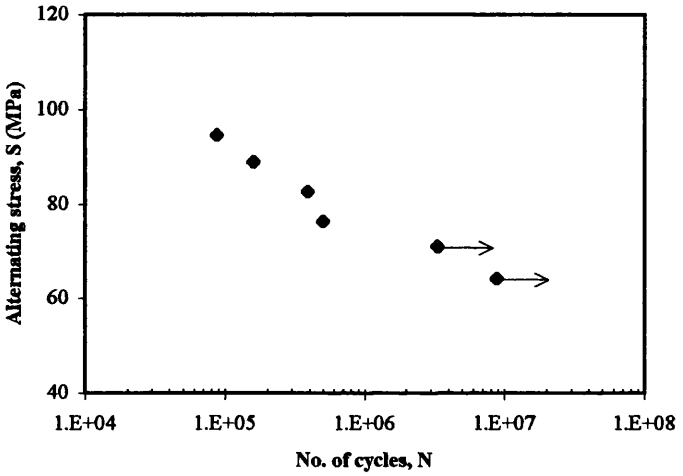

Fig 7.10: S-N diagram for specimen cold expanded by tapered pin without sleeve (type DD)

a) Crack growth from entrance face in specimen DD6

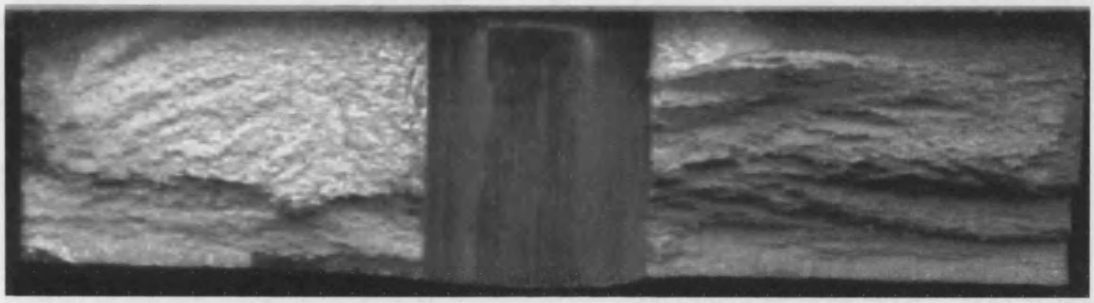

b) Crack growth from entrance face in specimen DD2

Fig 7.11: Example of single sided-crack growth for type DD specimens

7.9) Discussion of fatigue test results

Comparison of the S-N results for all four specimen types are shown in fig 7.12. It shows that all three cold expanded specimens exhibits fatigue life improvement compared with the "as drilled" specimen. However, the amount of fatigue life improvement is different for the three cold expansion techniques. The longest fatigue life was achieved using technique CC in which the hole was expanded uniformly and simultaneously through the plate thickness. The fatigue life improvement is almost the same for techniques BB and DD. With all cold expanded specimens, compressive tangential residual stress was created around the hole (as explained in chapter 5). Such stress reduces the resultant stress magnitude around the hole when it is combined with the tensile stress due to tensile longitudinal force. The cold expanded plate experiences less resultant tensile stress under longitudinal loading than the "as drilled" plate so fatigue crack initiation and/or propagation is delayed.

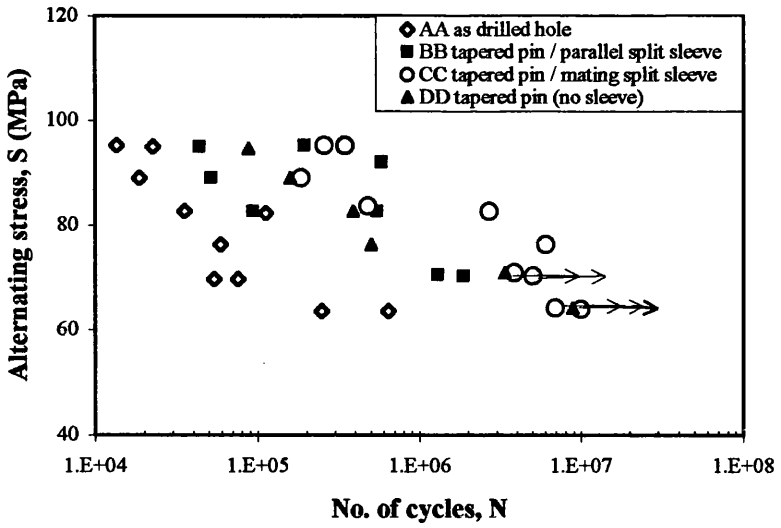

Fig 7.12: Fatigue results for all specimen types

As FE simulation of the cold expansion shows (see Chapter 5) the tangential residual stress distribution around the hole is different for techniques CC, BB and DD. The tangential stress distribution is almost uniform through the plate thickness in technique CC. However, it is non-uniform for techniques BB and DD as the compressive tangential residual stress at the entrance face is less than at the other planes. The effect of the tangential residual stress distribution was reflected in the fatigue life and also in the crack initiation location. In the specimens subjected to techniques BB and DD almost all the cracks initiated at the pin entrance face where the compressive tangential residual was least. However, in some of the specimens when using technique CC, the crack initiated at the entrance face but in others at the exit face of the hole edge.

In 2 of the 7 broken specimens of type CC the crack initiated and propagated where the cross section was greater and there was no stress concentration (see figs 7.7 and 7.8). This was not expected and shows that crack initiation not only depends on alternating stress magnitude but also on the material microstructure [56, 57]. Therefore if voids or inclusions exist at a location a crack can initiate from there. With technique CC, the area around the hole is so strengthened due to the presence of compressive residual stress, that the weakened region (with respect to crack initiation) has shifted to on other place.

As fig 7.12 shows, the improvement in fatigue life is almost the same for techniques BB and DD. This was not expected because technique BB includes a sleeve which

prevents surface damage to the hole as there is no direct contact with the pin. With technique DD there is no sleeve so the hole surface is vulnerable to such damage. The reason for this unexpected result may be explained in the context of friction, surface damage and surface finish. In some papers [3, 6, 7, 41] the reason for using a sleeve is to reduce the "friction effect" but it is not explained what this "friction effect" is.
It is believed that friction has two distinct effects, one could be referred to as "the shear stress creation" (from a mathematical perspective) and the other could relate to the "abrasive effect" (from a physical perspective). Shear stress due to friction in the cold expansion process, affects the residual stress distribution (even when using a sleeve). This aspect of friction is useful because it creates compressive tangential residual stress locally at the pin entrance face where a fatigue crack initiates. The abrasive (i.e. physical) effect of friction on the hole surface is eliminated by using a sleeve but without using a sleeve, the friction can abrade the hole surface thus scratching or smoothing it. A scratched surface produces a poor fatigue life while a smoothed and polished surface improves fatigue life. The hole surface of specimen type DD is more polished than the other two specimen types BB and CC as seen in fig 7.11-a. Understanding the abrasive friction effect on fatigue life needs more investigation than covered in this research.

The FE simulation shows that, for the longitudinal load range applied to the fatigue specimen, it results in the maximum longitudinal stresses occurring a distance away from the hole edge (see figs 5.9, 5.17, 5.25). The fact that fatigue cracks initiated and propagated from the hole edge can be explained by residual stress relaxation occurring during a test; this is also discussed by other researchers [59-61]. The fatigue life improvement was found to be greater at low alternating stress than at high alternating stress and this is because residual stresses can more readily relax at the higher load.

The fatigue test results for specimen type AA reveal that the drilling direction in producing a hole is not important and does not affect the location of crack initiation. This is because either the fatigue crack initiation was symmetric about the mid-plane or because an equal number of specimens had cracks which initiated at the drill entrance and exit faces.

Chapter 8

General discussion of results

8.1) Introduction

This chapter gives explanations for the non-uniform and different tangential residual stress distributions obtained in the different FE models. A history of the changing stresses and displacements for three chosen nodes (at entrance, mid-plane and exit faces) at the hole edge are presented during cold expansion for three models - uniform radial displacement, ballising and tapered pin without a sleeve. Also the stress and displacement histories of the three chosen nodes for the model, which includes friction, are shown to establish the effect that friction has on the resulting tangential residual stress. Also in this chapter the FE results for the pin reaction forces and experimental pin pushing forces, for the different techniques, are compared. Finally, the effect of sleeve slit on the pin pushing force is discussed.

8.2) Direct cold expansion methods

The tangential residual stress distributions around a cold expanded hole by radial uniform displacement, ballising and using a tapered pin without a sleeve (models A, B and C in Chapter 3) were previously discussed. The results considered the effect of plate thickness, interference amount and the effect of the cold expansion method. It

was shown that the residual stress distribution is not uniform through the plate thickness and also that it is different for the different methods (see fig 8.1).

As the figure shows, with the uniform radial displacement method, the tangential residual stress is compressive through the plate thickness. At the hole edge, the maximum compressive stress occurs at the mid-plane position and the minimum is at the plate faces (entrance and exit). With the taper pin method, although the tangential residual stress is compressive through the plate thickness, it is much lower than with the ideal uniform radial displacement method at the pin entrance and exit faces. With ballising even a tensile tangential stress is observed at the entrance face and also at the exit face (although at a very small region of the hole edge).

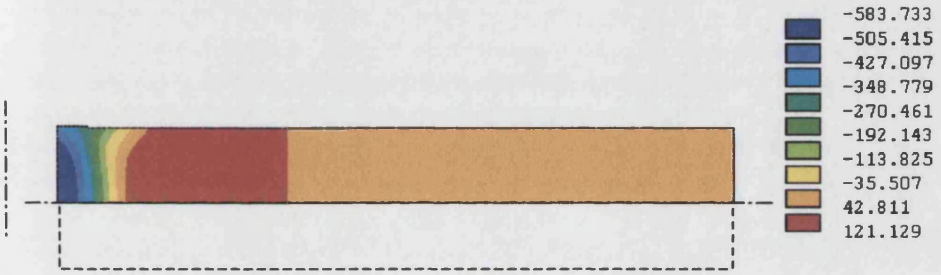

a) uniform radial displacement (model A)

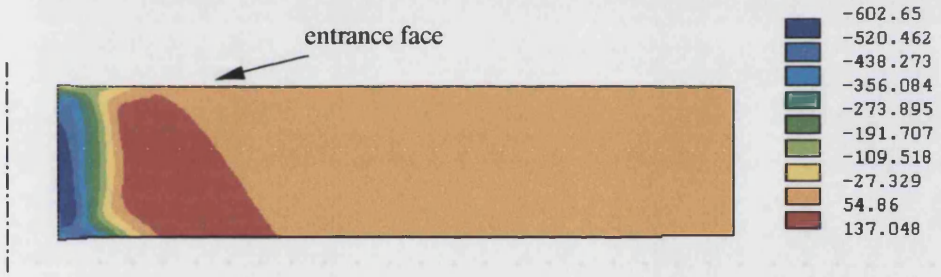

b) tapered pin without a sleeve (model B)

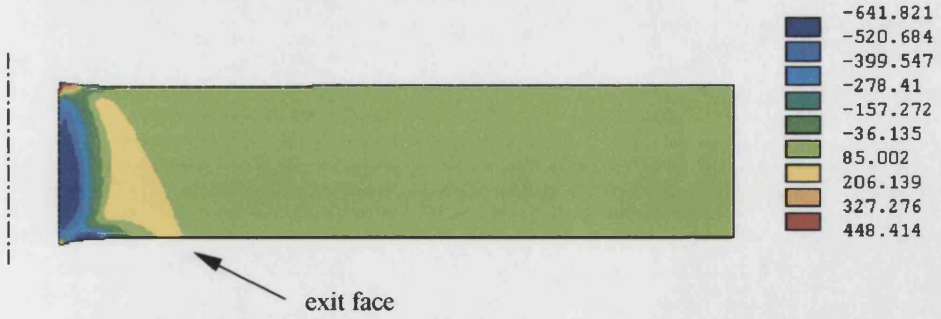

c) ballising (model C)

Fig 8.1: Tangential residual stress contours for 4% interference in 5 mm thick plate for three cold expansion methods

A question which comes to mind is "why is the tangential residual stress not uniform through the plate thickness?" An even more important question is, "why have these three methods produced different tangential residual stress distributions with the same interference amount?" Finding answers to these questions (especially the second one) is not an easy task. However, in order to understand the differences in the tangential residual stresses at the hole edge, the entrance face, the mid-plane and the exit face it is necessary to consider their stresses and displacements. The stresses are radial, effective (i.e. Von Mises) and tangential and the displacements are radial and axial. These stresses and displacements are presented for three important nodes (shown in fig 8.2) and histories are presented for 4% interference and a plate thickness of 5 mm in figs 8.3 to 8.7.

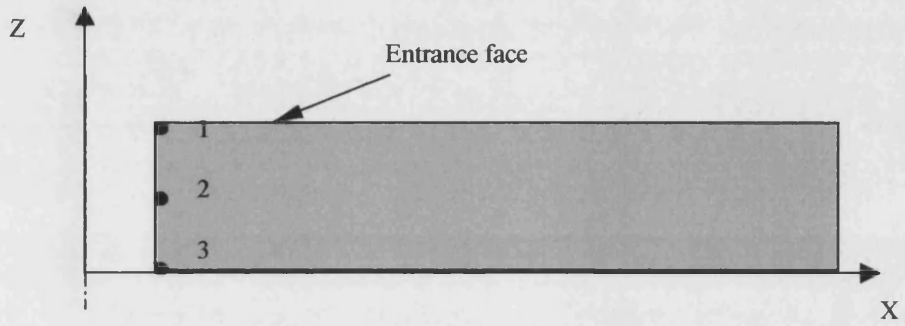

Fig 8.2: Position of chosen nodes in the three planes at the hole edge for history of stresses and displacements

8.2.1) Stress histories

Curves showing the changing radial stress history during cold expansion process are displayed in fig 8.3. This figure shows that all three nodes experience radial stress continuously with increasing load in model A (radial displacement). However, node 2 experiences a larger stress due to the plane strain state at the mid-plane. When the load is removed (i.e. the radial displaced nodes are released) the radial stress becomes zero in all the nodes considered (this is not shown in the figure).

In model B (using a tapered pin) node 1 experiences radial stress for only a short period (i.e. 2.5 mm of the pin stroke). This is surprising because it was expected to experience radial stress at least 4 mm of pin stroke due to the dimensions of the pin

(see Chapter 3). However, when the pin is pushed down more than 2.5 mm, node 1 is displaced radially more than 0.1 mm (the interference amount) and so the pin loses contact with it (see fig 8.6-b).
When the pin goes down further, node 2 experiences radial stress which is larger than at the other two nodes.
When the pin is displaced about 9 mm down, node 3 experiences radial stress but its maximum magnitude is less than the maximum radial stress at node 1. The contact between node 3 and the pin occurs for only a small time (the pin stroke). This is because of the bigger radial displacement (compared with the 0.1 mm interference amount) that occurs at node 3.

In model C (ballising), the situation of nodes 1 and 2 in experiencing radial stress is very similar to that of model B. However, these nodes experience radial stress for a shorter time (the ball stoke). The situation at node 3 is different from the other two nodes, as it never experiences any radial stress. The reason for this can be understood by considering radial displacement (see fig 8.6-c) as it shows node 3 had been radially displaced more than 0.1 mm before the ball had reached that node.

a) Model A

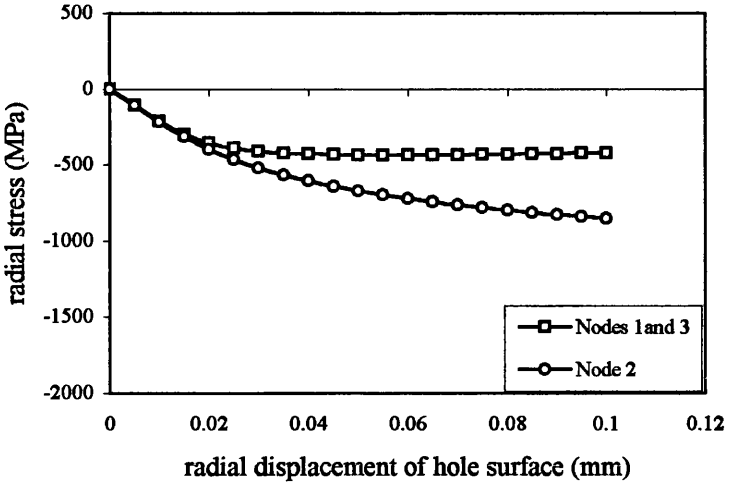

b) Model B

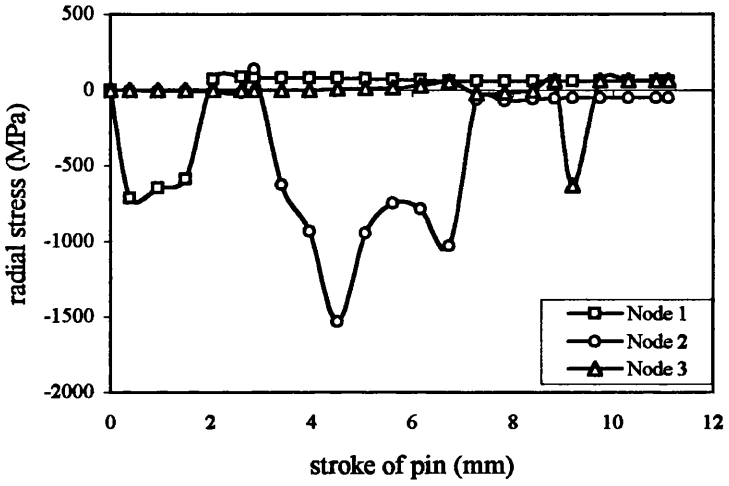

c) Model C

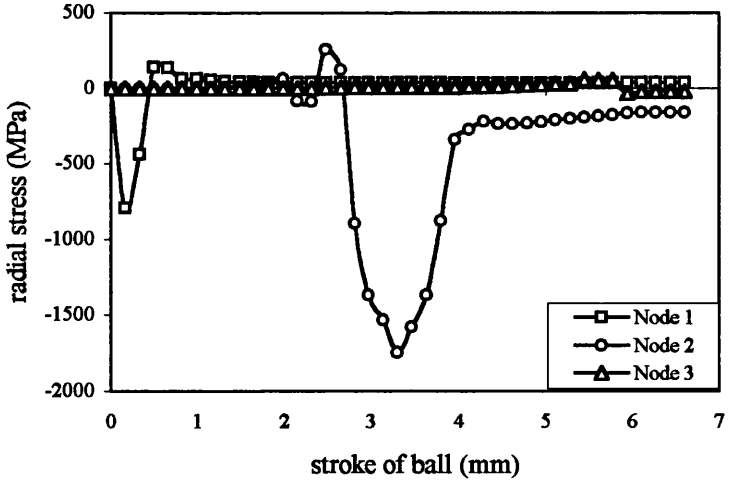

Fig 8.3: History of radial stresses, S_x curves at three nodes for models A, B and C (I=4% and T=5 mm)

The effective stress history curves during cold expansion for the models A, B and C are shown in fig 8.4. For model A the effective stress increases at three nodes with increasing radial displacement and the effective stress at node 2 is slightly larger than at the plate face nodes (i.e. nodes 1 and 3). After removing the load, the final value of effective stress decreases to 410 MPa at nodes 1 and 3 and is 508 MPa at node 2.
In model B the effective stress reaches its maximum value (620 MPa) at each node but at different pin strokes. When the pin leaves the hole the effective stress in all three nodes is reduced; the reduction is the greatest at node 1 and the least at node 2.
The history of the effective stress at the three nodes in model C is similar to those of model B. However, in ballising the hole the effective stress at node 1 rises to 386 MPa after reaching its minimum value (150 MPa) after the ball is displaced 4.5 mm

In fig 8.5 the history curves of tangential stress are shown for models A, B and C. For model A, the tangential stresses at all nodes reach their maximum values (about 280 MPa) when the hole surface is radially displaced 0.02 mm. With increasing radial displacement the tangential stress remains almost constant at nodes 1 and 3, whereas it decreases at node 2 and becomes compressive. When the radially displaced nodes at the hole are released the final tangential stress at node 1 (also 3) becomes –415 MPa and at 2 becomes –570 MPa.
In model B, the nodes experience both tensile and compressive tangential stress at different pin strokes. All three nodes experience virtually the same maximum stress at different pin displacements. However, the minimum tangential stresses in the nodes are different.
In model C, the tangential stress is compressive at node 1 for a 0.5 mm displacement of the ball. However, the stress becomes tensile for the rest of the ball stroke. At node 2, the tangential stress is initially tensile but then becomes compressive, whereas it is either zero or tensile at node 3.

a) Model A

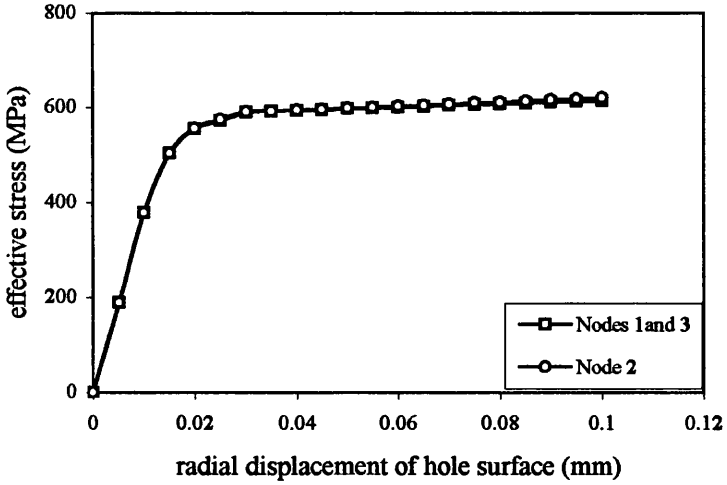

b) Model B

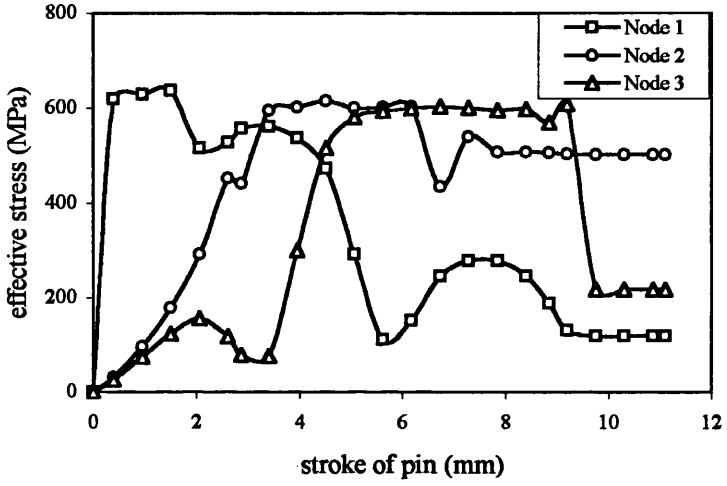

c) Model C

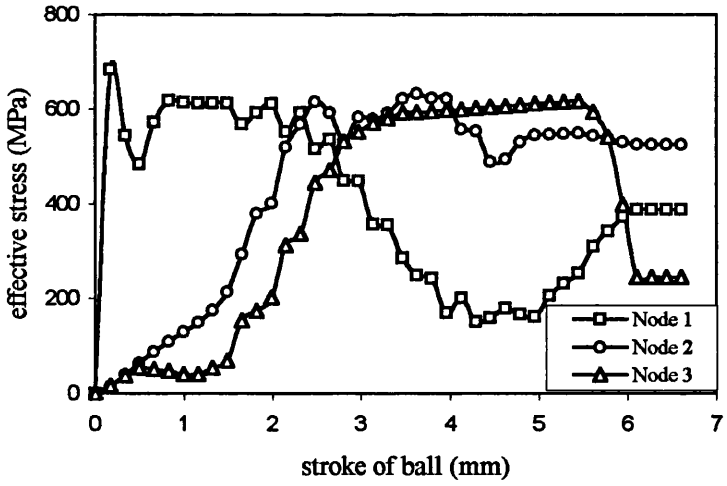

Fig 8.4: History curves of effective stresses at three nodes for models A, B and C (I=4% and T=5 mm)

a) Model A

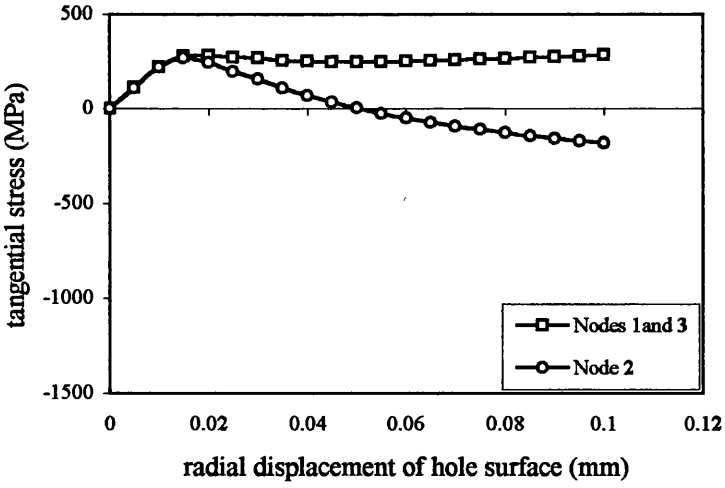

b) Model B

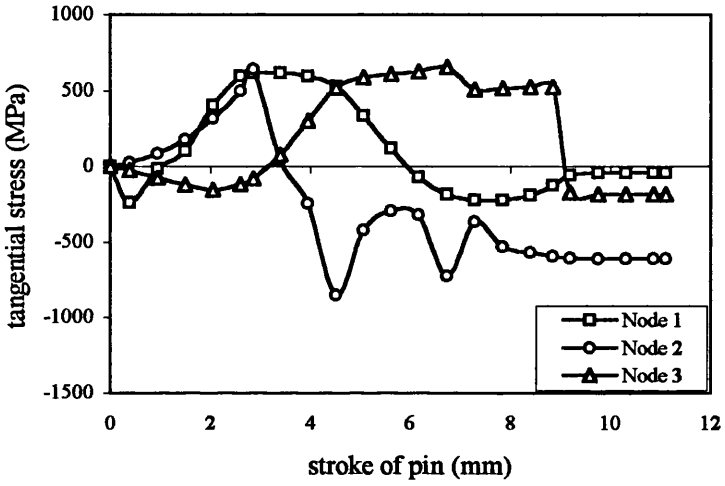

c) Model C

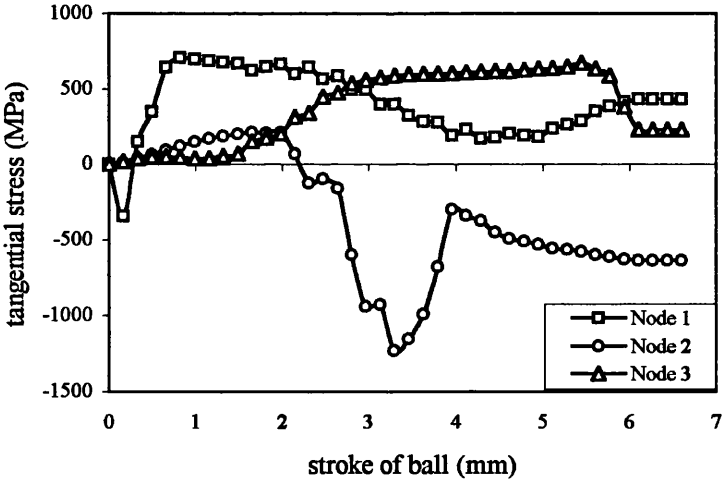

Fig 8.5: History of tangential stresses at three nodes for models A, B and C (I=4% and T=5 mm)

8.2.2) Displacement histories

The history of radial displacement, u_x for the three cold expansion models is shown in fig 8.6. For model A the radial displacements at the three nodes are, as expected, the same. However, when the load is removed, nodes 1 (also 3) and node 2 have different final radial displacements (0.0658 mm for node 1 and 3, and 0.0575 mm for node 2).
With model B, when pushing the pin down, all nodes experience a maximum radial displacement which is biggest at node 1 (i.e. 0.105 mm) and smallest at node 2 (i.e. 0.093 mm). When the pin exits the hole only small portions of these radial displacements are recovered.
With model C, node 1 is displaced radially when the ball is pushed down through the hole and reaches a maximum (i.e. 0.134 mm) after 2 mm stroke of the ball. After that the displacement fluctuates slightly and remains at 0.127 mm when the ball leaves the hole. This displacement is larger than the interference amount (i.e. 0.1 mm) and this shows that node 1 does not spring back and even moves away from the hole centre.
The radial displacement of node 2 increases from zero to 0.095 mm (with some fluctuations) and when the ball exits from the hole, it decreases to 0.07 mm. At node 3 the radial displacement increases smoothly from zero to a maximum value of 0.146 mm when the ball is moved about 5.6 mm from its initial position. Further movement of the ball causes a loss of contact and the radial displacement of node 3 decrease to 0.133 mm; this is still more than the interference amount.

The history of axial displacement, u_z for the three models is shown in fig 8.7. In model A during loading, node 1 rises in the Z direction (see fig 8.2) and node 3 moves down (by up to-0.0361 mm). When the load is removed these two nodes are displaced axially even more, for example, node 1 is displaced from 0.0361 to 0.0394 mm.
In model B, the three nodes have maximum axial displacements at the same pin stroke (i.e. 2.5 mm) and the largest of these occurs at node 1. When the pin is pushed down the axial displacements fluctuate and then remain level. The final axial displacement of node 1 is positive (the hole has bulged up at the entrance hole face), whereas, it is negative for node 3 (the hole has bulged down at the exit hole face).
In model C, the axial displacement curves at the nodes are similar to those of model B. However, the axial displacement is positive for node 1 and it is negative for nodes

2 and 3. This model shows greater bulging at the hole edges compared with models A and B.

a) Model A

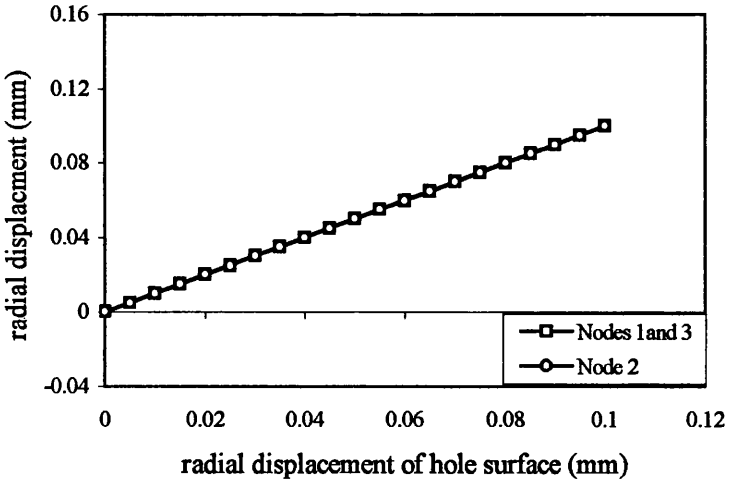

b) Model B

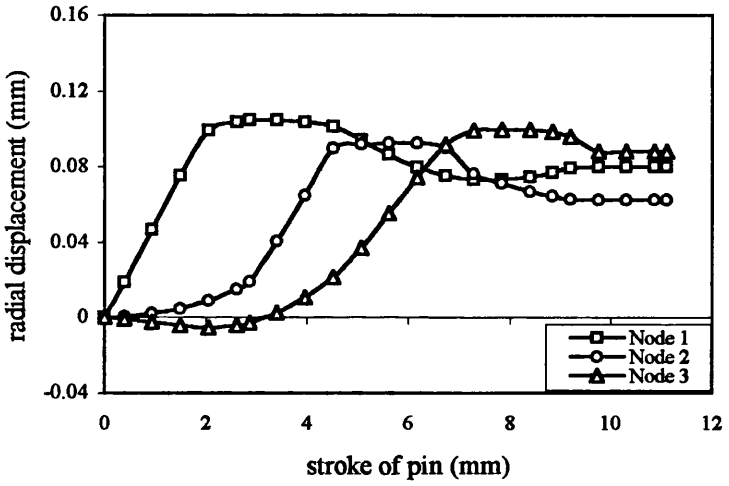

c) Model C

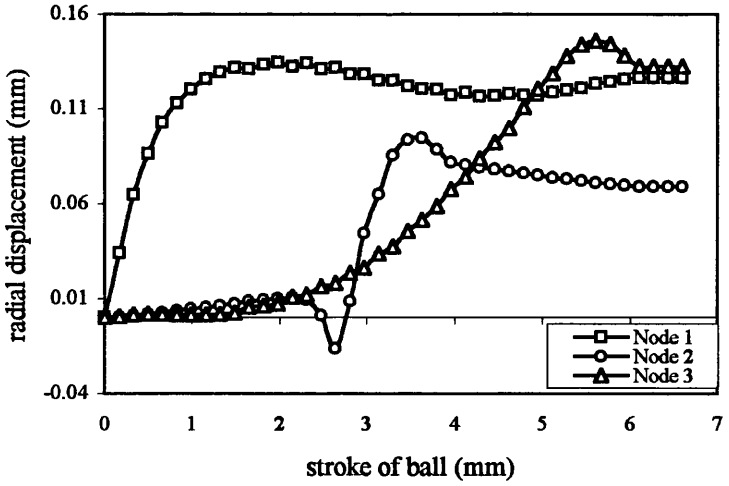

Fig 8.6: History of radial displacement, u_x at three nodes for models A, B and C (I=4% and T=5 mm)

a) Model A

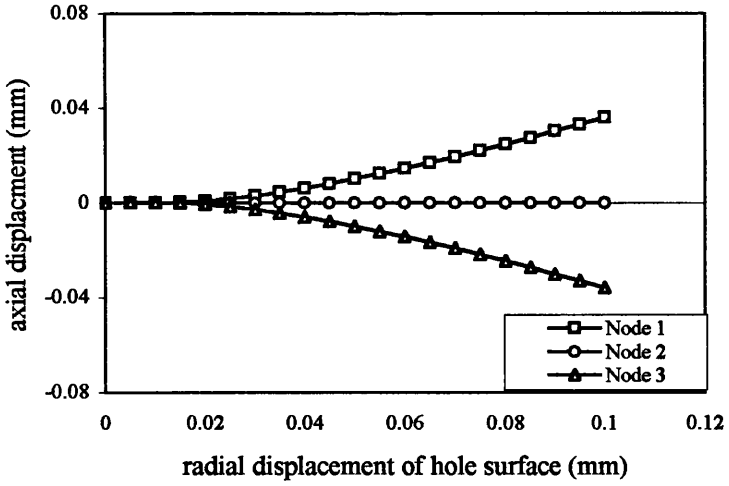

b) Model B

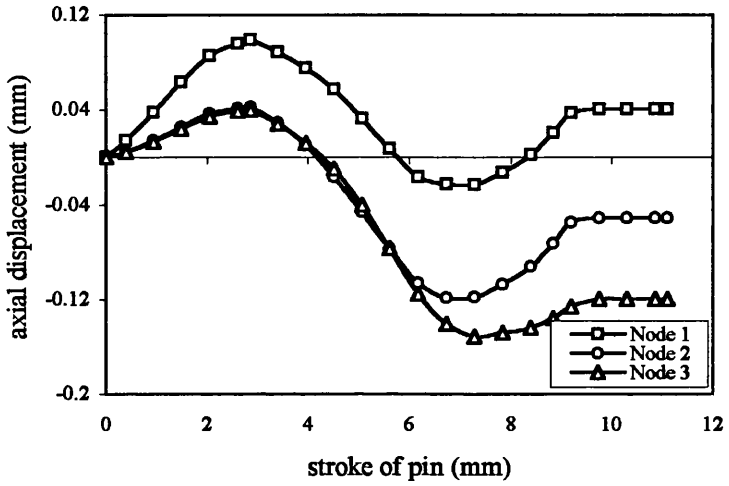

c) Model C

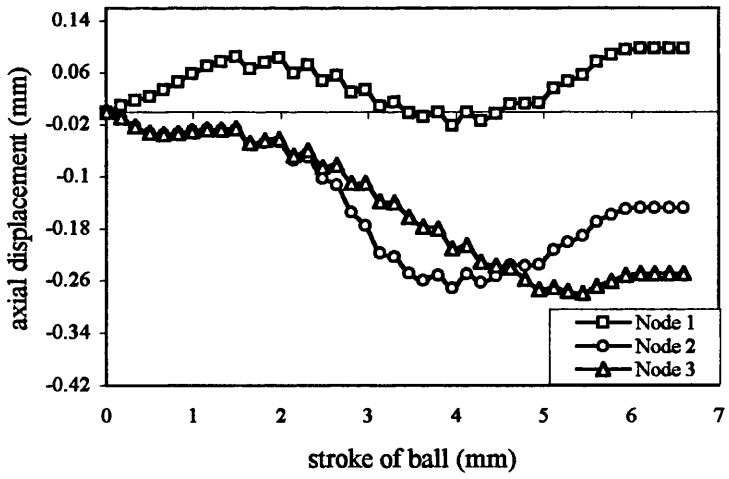

Fig 8.7: History of axial displacement, u_z in the nodes for models A, B and C (I=4% and T=5 mm)

Having presented the histories of stresses and displacements for the three nodes, it is now easier to find an explanation to the questions which were posed in the earlier part of this section. However, it is helpful to mention the circumstances for compressive tangential residual stress to be created around a hole. In theory, a hole is expanded by applying a pressure (or pushing an oversized pin) so that a plastic region, which is surrounded by an elastic region, is produced. When the pressure is removed the elastic region tries to return to its original position so it shrinks the plastic region and produces compressive tangential residual stresses. As shrinking does not occur uniformly the creation of compressive tangential residual stress will not be uniform.
In model A the plastic region at the entrance face is larger than at the mid-plane (see fig 8.8) and shrinking this thicker plastic region is more difficult than the smaller plastic region at the mid-plane. This is one explanation why the tangential residual stress at the plate face is smaller than at the mid-plane. However, the principal reason for the smaller compressive tangential residual stress is the bulging at the hole edges of the plate faces. This is because during loading (and even unloading) the hole edge spreads out as it is not laterally constrained (see fig 8.9) and so there is no material behind to cause shrinking. The less shrinkage at the plate faces (in comparison with the mid-plane) is clear where the final radial displacement is 0.0658 mm at plate faces whereas it is 0.0575 mm at the mid-plane (as explained previously in sub-section 8.2.2).

In model B plastic yielding occurs fully for all three nodes (see fig 8.4-b). However, shrinking the plastic region at the hole edges at the plate entrance and exit faces is not completed effective due to the even greater bulging in comparison with model A.
At node 1 unloading occurs when the pin is pushed about 2 mm into the hole (see figs 8.3-b and 8.4-b) and at this point a decrease in radial displacement would be expected whereas it actually increases (see fig 8.6-b). At this stage the effective stress decreases and the tangential stress and axial displacement increase as the hole edges bulge (see figs 8.5-b and 8.7-b).
At node 3, unloading occurs after about 9 mm of pin stroke (see fig 8.4-b) and at the same time shrinking takes place. However, due to the large downward bulge at this node (again because of a lack of material behind), shrinkage strength is weak resulting in a decrease in the tangential stress from about 500 MPa to –100 MPa. Slightly away

from the hole edge at the exit face there is a region with a large compressive tangential residual stress (see fig 8.1-b) and in this region bulging is smaller.

In model C, like model B, plastic yielding occurs fully at all three nodes (see fig 8.4-c). However, shrinking of the plastic region at the hole edge at the plate entrance and exit faces is not completed effectively due to even larger bulging in comparison with model B.

At node 1 unloading occurs at about 0.4 mm of the ball stroke (see fig 8.4-c) and a decrease in radial displacement would be expected. However, the radial displacement (see fig 8.6-c), axial displacement (see fig 8.7-c) and tensile tangential stress (see 8.5 c) increase with further insertion of the ball. As the radial and axial displacement and stress histories show, when the ball is pushed from 2 mm to 4 mm, all three parameters decrease temporarily and then increase. They also show that virtually no shrinking occurs; this is supported by the fact that even the radial displacement after unloading increases.

At node 3 unloading occurs at about 5.5 mm of ball stroke (where shrinking occurs) unfortunately, the amount of shrinking is small and cannot produce compressive tangential residual stress. The shrinkage is so weak that it can reduce the radial displacement by only about 0.02 mm. The reason for this may be explained by the lack of material radially behind this node as it moves down about 0.25 mm.

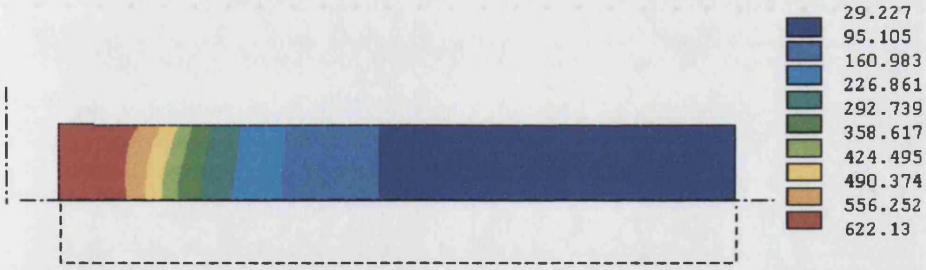

Fig 8.8: Effective stress contours for model A (for I=4% and T=5 mm)

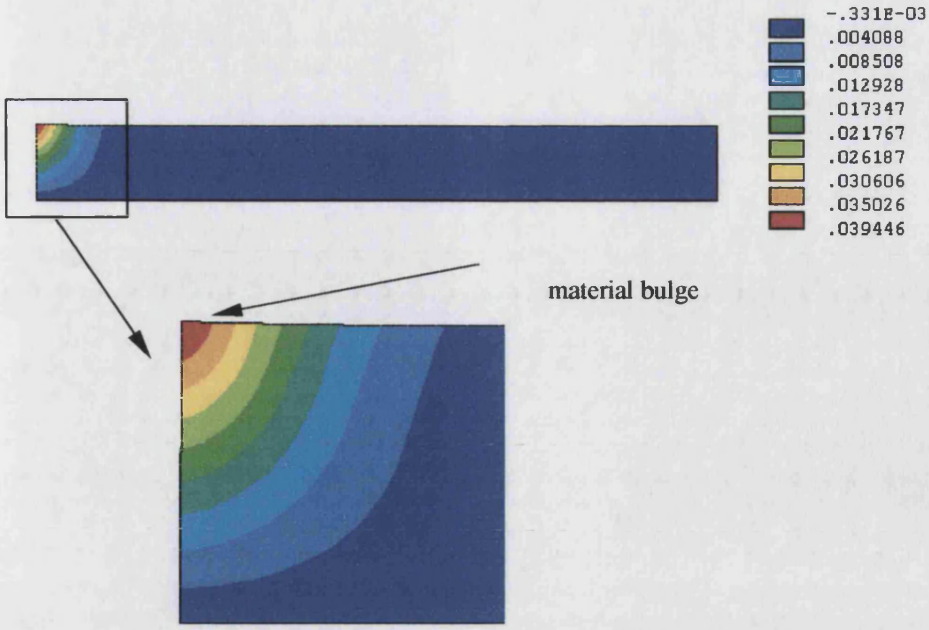

Fig 8.9: Axial displacement contours for model A (for I=4% and T=5 mm)

8.3) Effect of friction on tangential residual stress

As discussed in chapter 4 when friction is included between a pin and the hole surface (i.e. model B_f), it was found that the compressive tangential residual stress at the entrance face of the holed plate is improved. In order to see the effect of friction, the stress and displacement histories for the friction model B_f (see figs 8.10 and 8.11) are compared with the model B results without friction (see section 8.2).

With models B and B_f the histories of radial stress at nodes 1 and 2 are generally very similar in shape except that radial stress is greater in model B_f. In model B_f (unlike model B) node 3 does not experience radial stress during expansion of the hole.

Both models have similar effective stress histories for the three nodes, except for node 1, where there is a sharp fall when contact between the node and the pin is lost.

Comparing the histories of tangential stress in these two models shows that for the 2 mm stroke of the pin, node 1 experiences negative then positive stress in model B (see fig 8.5-b) whereas it experiences only negative stress in model B_f (see fig 8.10-c). When the pin is inserted further, the entrance node in model B has a large positive stress until 4 mm of the pin stroke then it deceases to about zero and remains almost zero. However node 1 in model B_f has a very small positive stress value when the pin

moves from 2 mm to 4 mm but then the stress decreases to a large negative stress magnitude.

The tangential stress histories are similar at the exit node (i.e. node 3) in both models but the reduction of stress is greater in model B than in model B_f when the pin leaves the hole.

The histories of radial displacement are also very similar in shape for the three nodes in models B and B_f but the maximum values (especially of nodes 1 and 3) are different. The maximum radial displacement at node 1 is less in model B_f than for model B, however, it is bigger at node 3 in model B_f. When the pin moves from 7 mm to 9 mm the greater radial displacement at node 3 is even clearer in fig 8.10-a where there is no radial stress at this node.

The final radial displacement of node 1 is less in model B_f than model B and this shows that shrinking is greater in model B_f. The grater shrinkage results in more compressive tangential residual stress at the entrance face when friction is included. However, the final radial displacement of node 3 is bigger in model B_f and this shows less shrinkage and a tensile tangential residual stress at the exit face of the hole edge.

Shrinking at nodes 1 and 3 can be explained by the entrance and exit face bulging and the absence of material behind these nodes. Bulging at node 1 is smaller for model B_f compared with model B (see figs 8.11-b and 8.7-b) and is due to friction dragging down the node during cold expansion. Therefore, when unloading occurs at this node, there is still material radially behind it trying to push it back thus causing compressive tangential stress at the hole edge of the entrance face. Shrinking is less at node 3 in model B_f compared with model B due to the larger bulge (see figs 8.11-b and 8.7-b). This large bulge has very little material behind to assist shrinking and results in a tensile tangential residual stress. In model B_f, friction causes all three nodes to move down relative to model B as can been seen from comparing fig 8.7-b with fig. 8.11-b.

a) radial stress

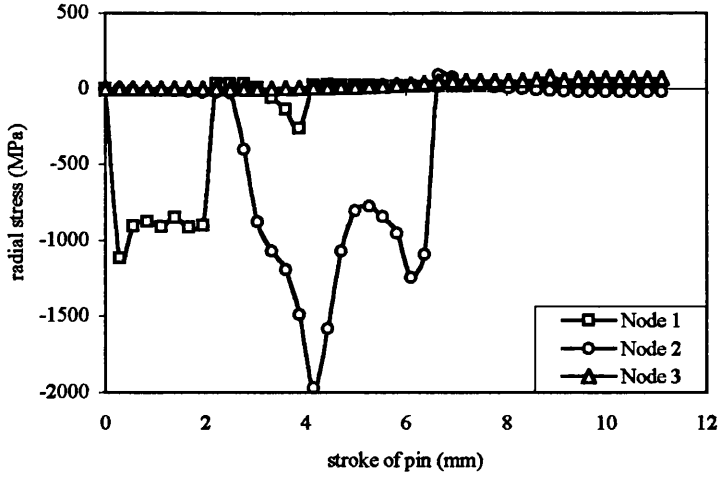

b) effective stress

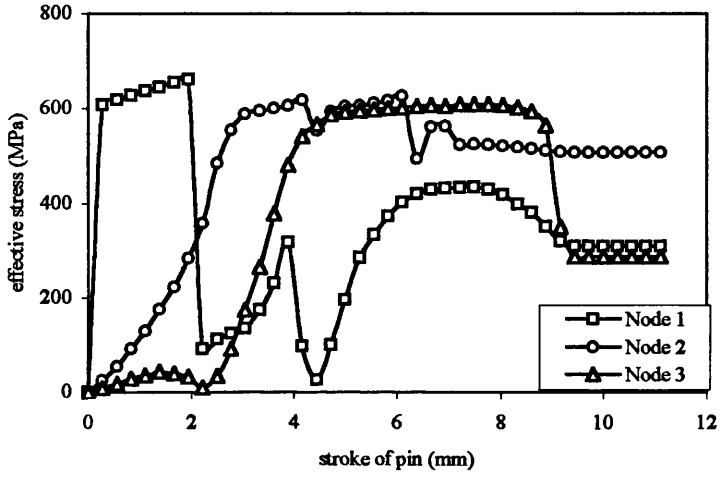

c) tangential stress

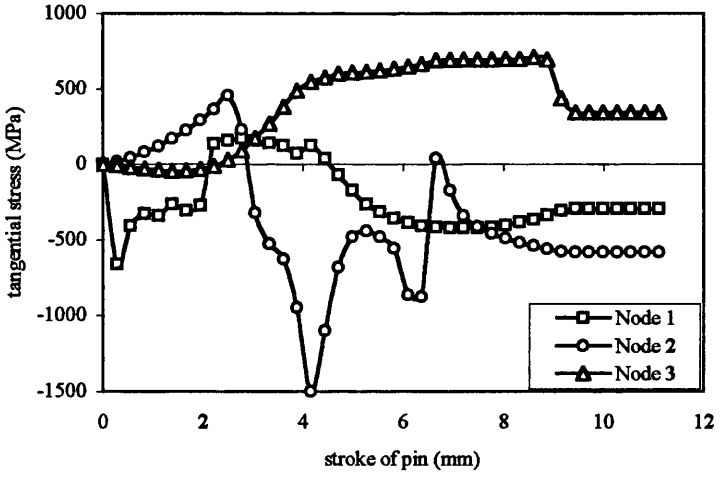

Fig 8.10: Histories of stresses at three nodes for model B_f (I=4%, T= 5mm, μ=0.15)

a) radial displacement

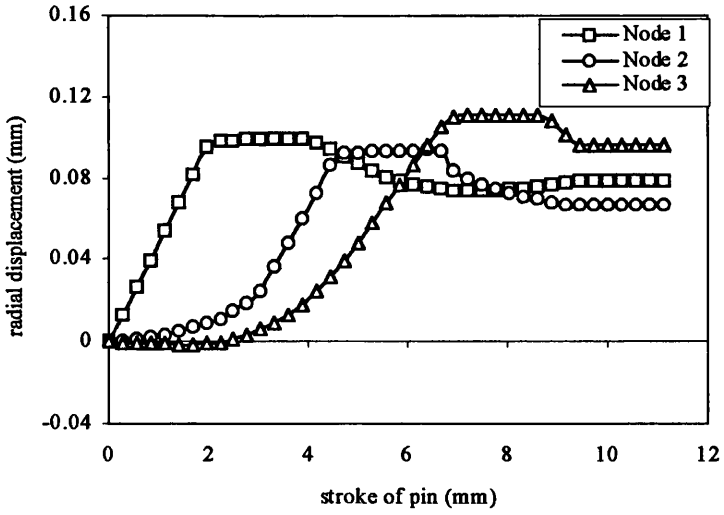

b) axial displacement

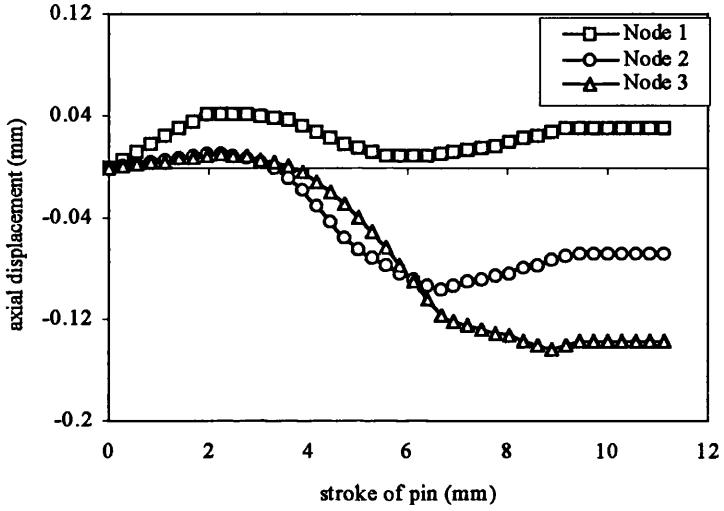

Fig 8.11: Histories of displacements at three nodes for model B_f (I=4%, T= 5mm, μ=0.15)

8.4) Comparison of simulation and experimental pin pushing force

The pin reaction force relationships obtained from the FE simulation of cold expansion for three techniques (CC, BB and DD) are given in Chapter 5. Also typical curves for the pushing forces of the pins during experimental cold expansion (for the same three techniques) are shown in chapter 6. In this section the experimental and FE results are compared to assess the accuracy of the simulation predictions. In figure 8.12 it shows that the experimental and simulation curves are very similar to each other, however, the simulation curves show a bigger force except in the case of model DD. The reason for this maybe due to the higher coefficient of friction that is used between steel pin and steel sleeve in the FE models of CC and BB. The coefficient of friction used for all surfaces was 0.1 but it appears that the actual value is less between lubricated steel components and is thought to be about 0.08.

Several 2-D axisymmetric and 3-D models (with different coefficients of friction) were run and they showed that the reaction force of the pin change in proportion with the magnitude of the coefficient of friction.

The comparison of FE results for the pin reactions shows that the pin pushing force for technique CC is largest and for technique DD is the smallest of the three techniques considered.

a) technique CC

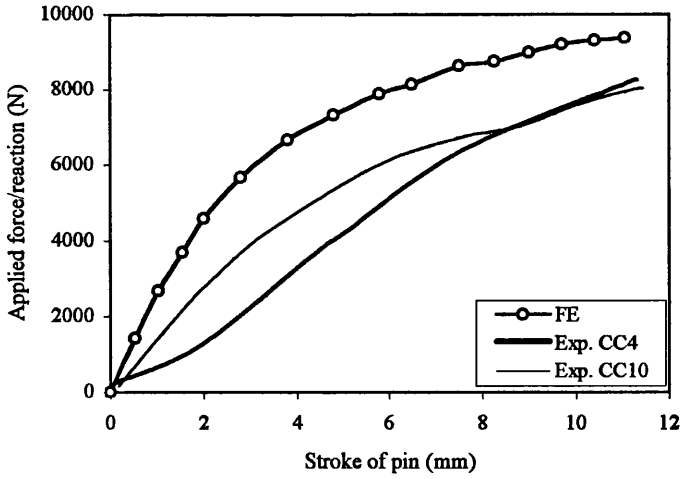

b) technique BB

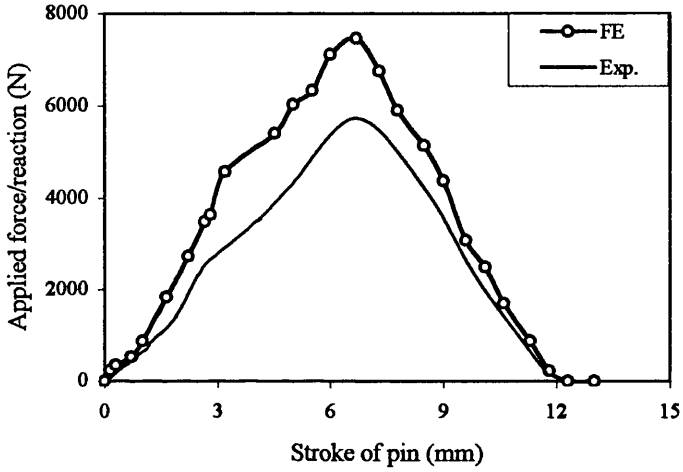

c) technique DD

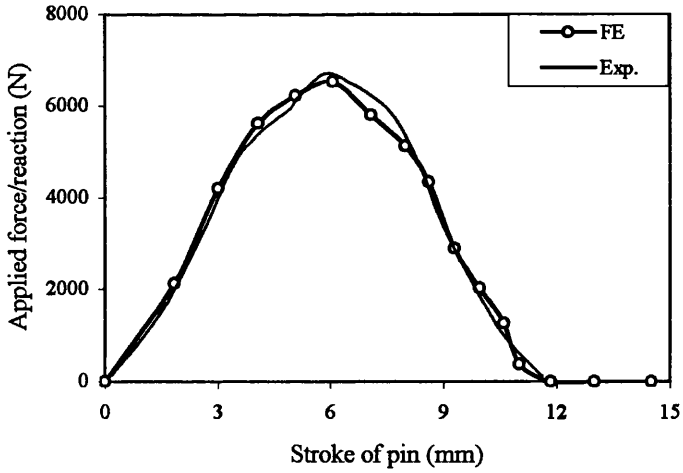

(μ=0.1 in FE)

Fig 8.12: FE and experimental pin pushing forces for techniques CC, BB and DD

8.5) Effect of sleeve slit on the pin pushing force

In order to investigate the effect of a slit on the pin pushing force two models were studied one with slit and the other without slit. The model that includes a slit is 3-D model BB (as explained in chapter 5) and the model without a slit is effectively the same model BB but with one difference, the parallel sleeve does not have any it. As mentioned previously, when the sleeve is complete (i.e. no slit) an axisymetric model can be used with good accuracy instead of using a 3-D model, so the model without a slit is an axisymmetric one and it is correspondingly called the axisymmetric version of model BB (see appendix A).

The results for the pin reaction of the 3-D model of technique BB and also the corresponding axisymmetric model are shown in fig 8.13. The difference in the pushing force in these two models is slight and this indicates, perhaps surprisingly that the sleeve slit does not have a significant effect on reducing the pin pushing force. This was an unexpected result because it appeared that the presence of the slit would mean that there would be no hoop stress in the sleeve and so all the pin force expands the holed plate. This expectation would be correct if there were no friction, however, friction exists and this was found to be the reason for this unexpected result. When the split sleeve is expanded it tries to move circumferentially but friction between the sleeve and pin, and also the sleeve and plate, will not allow the sleeve to move freely (as shown fig 8.14). Therefore, a large hoop stress is created in the sleeve. In the 2-D axisymmetric model the sleeve cannot move circumferentially but there is a hoop stress in the sleeve due to sleeve expansion.

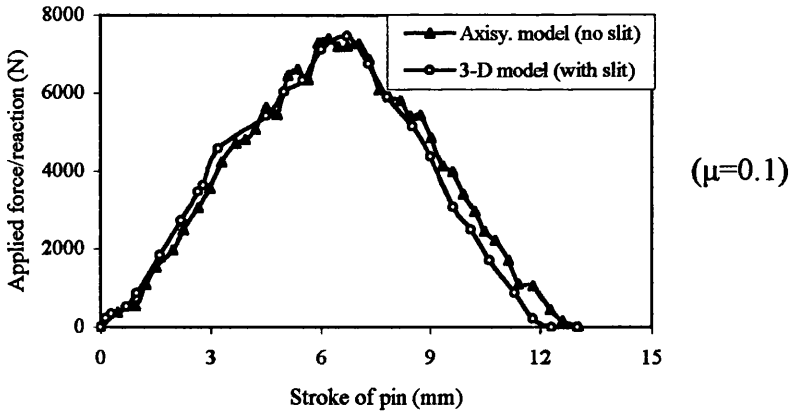

Fig 8.13: Comparison of pin pushing forces in 3-D and axisymmetric FE models

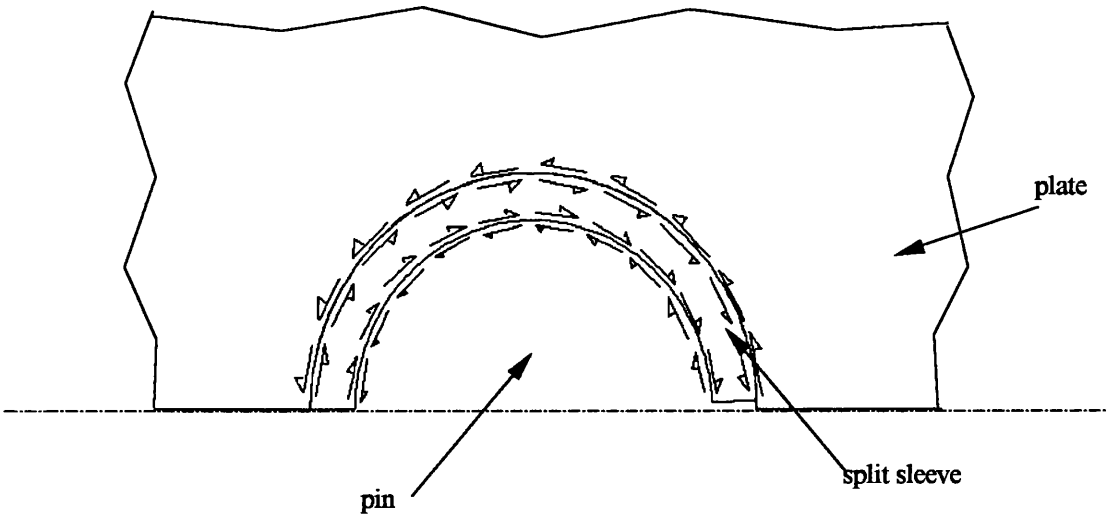

Fig 8.14: Effect of friction on hoop stress in slit sleeve

Chapter 9

Conclusions

A number of findings have resulted from this extensive theoretical and practical programme of research cold expanding fastener holes. The major findings are summarized as follows:

1. The tangential residual stress distribution found by FE analysis is not uniform through the plate thickness even in the ideal situation of expansion by "uniform radial displacement". In the FE model, the compressive tangential residual stress at the plate faces is less than at the mid-plane position. It was found that the residual stress distribution is a function of interference amount and plate thickness.
2. The shape of the oversized object to cold expand a hole is important and different object shapes (such as a ball or taper pin) create different residual stress distributions.
3. When the hole is cold expanded by a tapered pin, the tangential residual stress distribution is not uniform through the thickness and also depends on plate thickness and interference amount. The tangential residual stress at the entrance face is less compressive than at the mid-plane and the exit face. It is even tensile when a large interference amount is used in a thick plate.
4. Ballising a hole often produces high tensile tangential residual stress at the entrance face. This tensile stress increases in magnitude and the region in which it acts with increasing plate thickness and interference. Also, with the thicker plate considered (T=5, 10 mm) the tangential residual stress at the exit side of the hole edge was tensile.

5. When cold expanding a hole using a tapered pin, the location of the plate support affects the residual stress distribution at the entrance face when the plate thickness is thin (i.e. T=2 mm). The closer the support to the hole edge the more compressive becomes the tangential residual stress. The plate support location did not alter the residual stress distribution for the thicker plates considered (i.e. T=5, 10 mm).
6. Including friction in the FE models improves the tangential residual stress distribution - making it more compressive locally at the entrance face. This improvement is related to the magnitude of the coefficient of friction between the hole and the pin.
7. The tangential residual stress distribution obtained from the 2-D axisymmetric FE model using a tapered pin and thin parallel sleeve, is almost the same as the distribution obtained from the 2-D axisymmetric model using a tapered pin without a sleeve (based on the same nominal interference amount).
8. Using a tapered pin with a mating sleeve expands the hole uniformly throughout the plate thickness and creates almost a uniform compressive tangential residual stress through the thickness - provided that the pin is pushed and removed from the same plate face.
9. 3-D FE models show that a slit sleeve creates tensile (or less compressive) tangential residual stress locally at the entrance face in the region of the slit in the plate compared to away from the slit region.
10. FE models can predict accurately the pin pushing force during the cold expansion process as long as an accurate coefficient of friction is used.
11. The pin pushing force is not reduced appreciably by including a slit in the sleeve.
12. The drilling direction when producing a hole in the fatigue specimens (i.e. hole entrance and exit faces) did not have any effect on the initiation and propagation of fatigue cracks.
13. Cold expanded holes generally produced much longer fatigue lives than the "as drilled holes"
14. Although the maximum resultant stress in cold expanded specimens occurs far from the hole edge, the fatigue cracks generally start and propagate from the hole. It is believed that such phenomenon is related to residual stress relaxation that occurs during fatigue testing.

15. The tangential residual stress distribution affects fatigue life so when it is nearly uniform through the plate thickness (as occurs when cold expanding with a tapered pin with mating split sleeve) the fatigue life is longer than when it is not uniform (for example using a tapered pin and parallel split sleeve or a tapered pin without a sleeve).
16. Fatigue cracks usually start and propagate at the hole edge of the entrance face as the tangential residual stress is less compressive than at the mid-plane and the exit face. This occurs when the hole is cold expanded by using a tapered pin and parallel split sleeve or a tapered pin without sleeve.
17. Under certain cold expansion circumstances, fatigue crack initiation and propagation can occur away from the hole edge. This was observed to occur occasionally when creating large and near uniform compressive tangential residual stress by using a tapered pin and mating split sleeve with large interference.
18. Using a parallel sleeve itself with cold expansion does not improve fatigue life. It was found that the holes were cold expanded using a tapered pin with a parallel split sleeve and a tapered pin with no sleeve produced virtually the same fatigue lives. It is believed that the sleeve prevents the pin from scratching the hole, as might occur with direct contact, whereas the friction rubbing (as occurs with direct contact) can produce a smooth polished surface finish which is desirable.

References

[1] **M. O. Lai and Y. H. Siew,** *"fatigue properties of cold worked holes,"* Journal of Material Processing Technology, Vol. 48, pp. 533-540, 1995.

[2] **M. O. Lai, J. T. Oh and A. Y. C. Nee,** *"Fatigue properties of holes with residual stresses,"* Engineering Fracture Mechanics, Vol. 45, No. 5, pp. 551-557, 1993.

[3] **Nopporn Chandawannich and William N. Sharpe, Jr.,** *"An experimental study of fatigue crack initiation and growth from cold worked holes,"* Engineering Fracture Mechanics Vol. 11, pp. 609-620, 1979.

[4] **R. E. Link, R. J. Sanford,** *"Residual strains surrounding split-sleeve cold expanded holes in 7075-T651 Aluminium,"* J. Aircraft, Vol. 27, No. 7, July 1990.

[5] **Kang, K. J., Song, J. H. and Earmme, Y. Y.,** *"A method for the measurement of the residual stresses using a fracture mechanics approach,"* Journal of Strain Analysis for Engineering design, Vol. 42, pp. 23-30, 1989.

[6] **A. T. Ozdemir, L. Edwards,** *"Measurement of the Three-dimensional residual stress distribution around split-sleeve cold-expanded holes,"* Journal of Strain Analysis, Vol. 31, No. 6, pp. 413-421, 1996.

[7] **A. T. Ozdemir, R. Hermann,** *"Effect of expansion Technique and plate thickness on near-hole residual stresses and fatigue life of cold expanded holes,"* Journal of Material Science, Vol. 34, pp. 1243-1252, 1999.

[8] **M.A. Crisfield,** *"Non-linear finite element analysis of solids and structures,"* Vol.2: Advanced topics, Chichester: Wiley, pp 308-337, 1997.

[9] **Swanson Analysis Systems Inc. ANSYS,** *" Structural nonlinearities, User's Guide for Revision 5,"* Vol. 1, Chapter 6 and 7, 1993.

[10] **H. D. Hibbitt, P.V. Marcal and J.R. Rice,** *"A finite element formulation for problems of large strain and large displacement,"* Int. J. Solid and Structures, vol. 6, pp. 1069-1086, 1970.

[11] **M.A. Crisfield,** *"Non-linear finite element analysis of solids and structures,"* Vol.1: Essentials, Chichester: Wiley, pp 152-200, 2001.

[12] **E. Hinton,** *"NAFEMS introduction to nonlinear finite element analysis,"* Glasgow: National Agency for Finite Element Methods and Standards, pp 103-163, 1992.

[13] **R. Hill,** *"The mathematical theory of plasticity,"* Oxford: Clarendon Press, pp14-69, 1985.

[14] **W. Johnson and P.B. Mellor,** *"Engineering plasticity,"* New York: Van Nostrand Reinhold, pp 55-123, 1973.

[15] **D. R. J. Owen and E. Hinton,** *"Finite elements in plasticity, theory and practice,"* Pineridge Press Limited Swansea, pp 215-270, 1981.

[16] **George E. Mase,** *"Schaum's outline of theory and problems of continuum mechanics,"* New York: McGraw-Hill, pp 175-195, 1970.

[17] **George E. Dieter,** *"Mechanical metallurgy,"* London: McGraw-Hill, pp 69-99 1988.

[18] **Fung, Y.C,** *"Foundations of solid mechanics," Englewood* Cliffs, NJ. : Prentice-Hall, pp127-153, 1965.

[19] **R. J. Asaro,** *"Crystal plasticity,"* Journal of Applied Mechanics, Vol. 50, pp. 921-934, December 1983.

[20] **Swanson Analysis Systems Inc. ANSYS,** *" Structural nonlinearities, User's Guide for Revision 5,"* Vol. 2, Chapter 9, 1993.

[21] **A. Curnier,** *" A theory of friction,"* Int. J. Solid and Structures vol. 20, No. 7, pp. 637-647, 1984.

[22] **A. Francavilla and O.C. Zienkiewicz,** *" A note on numerical computation of elastic contact problem,"* International Journal For Numerical Methods In Engineering, Vol. 9, pp 913-924, 1975.

[23] **Ted belyschiko and Mark O. Neal,** *"Contact-impact by the pinball algorithm with penalty and lagrangian methods,"* International Journal For Numerical Methods In Engineering, Vol. 31, pp 547-572, 1991.

[24] **Panayiotis papadopoulos, Reese E. Jones, And Jerome M. Solberg,** *" A novel finite element formulation for frictionless contact problems,"* International Journal For Numerical Methods In Engineering, Vol. 38, pp 2603-2617, 1995.

[25] **Djordje Peric and D.R.J. Owen,** *"Computational model for 3-D contact problems with friction based on the Penalty methods,"* International Journal For Numerical Methods In Engineering, Vol. 35, pp 1289-1309, 1992.

[26] **R. W. Smith, M. H. Hirschberg and S. S. Manson,** *"Fatigue behavour of materials under cyclic and intermediate life rang,"* NASA Tech. Note D-1574, National Aeronautics and Space Administration, April 1963.

[27] **L. Schwarmann,** *"On improving fatigue performance of a double-shear lap joint"* Tech. Note, Int. J. Fatigue, Vol. 5, No. 2, pp. 105-111, April 1983.

[28] **R. Hermann,** *"Three-dimensional stress distribution around cold expanded holes in Aluminium alloys,"* Engineering Fracture Mechanics Vol. 48, No. 6, pp. 819-835, 1994.

[29] **Y. C. Hsu, R. G. Forman,** "*Elastic-plastic analysis of an infinite sheet having a circular hole under pressure,*" Journal of Applied Mechanics, pp. 347-352, June 1975.

[30] **Guo Wanlin,** "*Elastic-plastic analysis of a finite sheet with a cold-worked hole,*" Engineering Fracture Mechanics Vol. 46, No. 3, pp. 465-472, 1993.

[31] **Nadai A.,** "*Theory of expanding of boiler and condenser tube joints through rolling,*" Transaction of the American Society of Mechanical Engineers, Vol. 65, pp. 865-880, Nov. 1943.

[32] **Taylor, G. I.,** "*The formation and enlargement of a circular hole in a thin plastic sheet,*" Quarterly Journal of Mechanics and Applied Mathematics, series 7, No. 1, pp. 103-124, 1947.

[33] **Mangasarian, O. L.,** "*Stresses in plastic range around a normally loaded circular hole in an infinite sheet,*" Journal of Applied Mechanics, Vol. 27, pp. 65-73, 1960.

[34] **Alexander, J. M., and Ford, H.,** "*On expanding a hole from zero radius in a thin infinite plate,*" Proceedings of the Royal Society of London, Series A, No. 226, pp. 543-561. 1954.

[35] **Rich, D. L., and Impellizzeri, L. F.,** " *Fatigue analysis of cold worked and interference fit fastener holes,*" Cyclic stress-strain and plastic deformation aspect of fatigue crack growth, American Society for Testing and Materials, ASTM STP 637, pp. 154-175, 1977.

[36] **Carter, A. E., and Hanagud, S.,** "*Stress corrosion susceptibility of cold worked and interference fit fastener holes in air craft structures,* " AIAA Journal, Vol. 13, No. 7, pp. 858-863. 1975.

[37] **Hoffman, O., and Sachs, G.,** " *Introduction to the theory of plasticity for engineers,*" McGraw-Hill, New York, 1953.

[38] **M. Priest, C.G. Poussard, M.J. Pavier and D.J. Smith,** "*An assessment of residual stress measurements around cold-worked holes,*" Experimental Mechanics, pp. 361-366, Dec. 1995.

[39] **C. Poussard, M.J. Pavier and D.J. Smith,** "*Analytical and finite element predictions of residual stresses in cold worked fastener holes,*" Journal of Strain Analysis, Vol. 30, No. 4, pp. 291-304, 1995.

[40] **P. Papanikos and S. A. Meguid,** "*Three-dimensional finite element analysis of cold expansion of adjacent holes,*" Int. J. Mech. Sci., Vol. 40, No. 10, pp. 1019-1028, 1998.

[41] **M.J. Pavier, C.G. Poussard, D.J. Smith,**" *A finite element simulation of the cold working process for fastener holes,*" Journal of Strain Analysis, Vol. 32, No. 4, pp. 287-300, 1997.

[42] **Swanson Analysis Systems Inc. ANSYS,** *" Ansys User's Guide for Revision 5-Theory,"* Vol. 4, Chapter 14 pp 154-155, 1993.

[43] **Swanson Analysis Systems Inc. ANSYS,** *" Ansys User's Guide for Revision 5-Elements,"* Vol. 3, Chapter 4 pp 147-269, 1993.

[44] **Norman E. Dowling,** *"Mechanical behavior of materials, engineering methods for deformation, fracture and fatigue,"* Englewood Cliffs, NJ. : Prentice-Hall, pp 139-200, 1993.

[45] **Swanson Analysis Systems Inc. ANSYS,** *" Ansys User's Guide for Revision 5-Procedures,"* Vol. 1, Chapter 9 pp 71-78, 1993.

[46] FTI *Extending the Fatigue of Metal Structures, Material testing*, Fatigue Technology Inc., 150 Andover Park West, Seattle, Washington 1991.

[47] **Erik Oberg, Franklin D. Jones and Holbrook L. Horton,** *"Machinery's hand book,"* Industrial Press Inc., New York, pp 2201-2215, 1989.

[48] **W. F. Carroll,** *" A primer for Finite Elements in Elastic Structures,"* John Wiley & Sons, Inc., pp 225-287, 1999.

[49] **M.J. Fagan,** *"Finite Element Analysis, Theory and Practice,"* Prentice Hall, pp 169-220, 1992.

[50] **Klaus-Jurgen Bathe,** *"Finite element procedures in engineering analysis,"* Englewood Cliffs, NJ. : Prentice-Hall, pp 194-300, 1982.

[51] **Frank L. Stasa,** *"Applied finite element analysis for engineers,"* New York: Holt, Rinehart and Winston, pp 508-576, 1985.

[52] **Segerlind,L.J,** *"Applied finite element analysis,"* New York: John Wiley and sons Inc., pp 287-333, 1976.

[53] **T. H. G. Megson,** *"Aircraft structures for engineering student,"* Arnold and John Wily and sons Inc., pp 152-207, 1999.

[54] **Robert B. Ross,** *"Metallic materials specification handbook"* New York: E. & F. N. Spon Ltd, pp 1-85, 1980.

[55] *"Annual book of ASTM standards American Society for Testing and Materials,"* Philadelphia: ASTM, Vol. 01.03, 1994.

[56] **Fuchs,H.O. & Stephens,R.I,** *"Metal fatigue in engineering"* New York: John Wiley and sons Inc., pp 1-36, 1980.

[57] **S. Suresh,** *"Fatigue of materials,"* Cambridge: Cambridge University Press, pp 97-125, 1992.

[58] Swanson Analysis Systems Inc. ANSYS, Revision 5.7.1.

[59] **Kewe Xu, Naisai Hu and Huijiu Zhou,** *"Prediction of notch fatigue limit in a compressive residual stress field,"* Engineering Fracture Mechanics, Vol. 54, pp 171-176, 1996.

[60] **Kewe Xu, Jiawen He and Huijiu Zhou,** *"Effect of residual stress on fatigue behaviour of notches,"* International Journal of Fatigue, Vol. 16, pp 337-343, July1994.

[61] **Zhang Dingquan, Xu Kewei, He Jiawen,** *"Aspect of residual stress field at a notch and its effect on fatigue,"* Material Science and Engineering, A136, pp 79-83, 1990.

Appendix A

The axisymmetric version of model BB

The model BB comprises of three components - a single slit parallel sleeve, a tapered pin and a holed plate: this was taken from the central part of the fatigue specimen (see Chapter 5). The model that is called "the axisymmetric version of model BB" has the same components as model BB, however, the sleeve is assumed to be complete (i.e. no slit). In addition to this assumption the holed plate is assumed to be annular with an outer diameter equal to the fatigue specimen central part width as shown in fig A.1. With these assumptions a small 2-D axisymetric model, which has no slit in the sleeve, can be used to compare the pin pushing force with the model which has a slit in the sleeve (see fig A.2 for 2-D model).

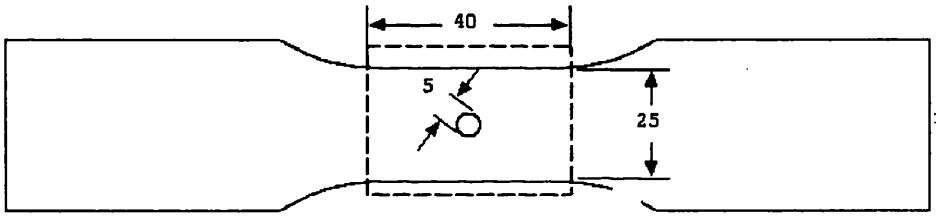

a) fatigue specimen

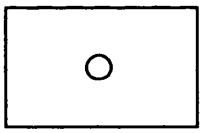

b) fatigue specimen central part chosen for model BB

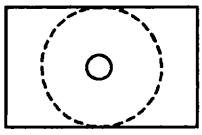

c) annular plate from central part of the fatigue specimen for the axisymetric model of BB

Fig A.1: Holed plate used for the axisymmetric model of BB

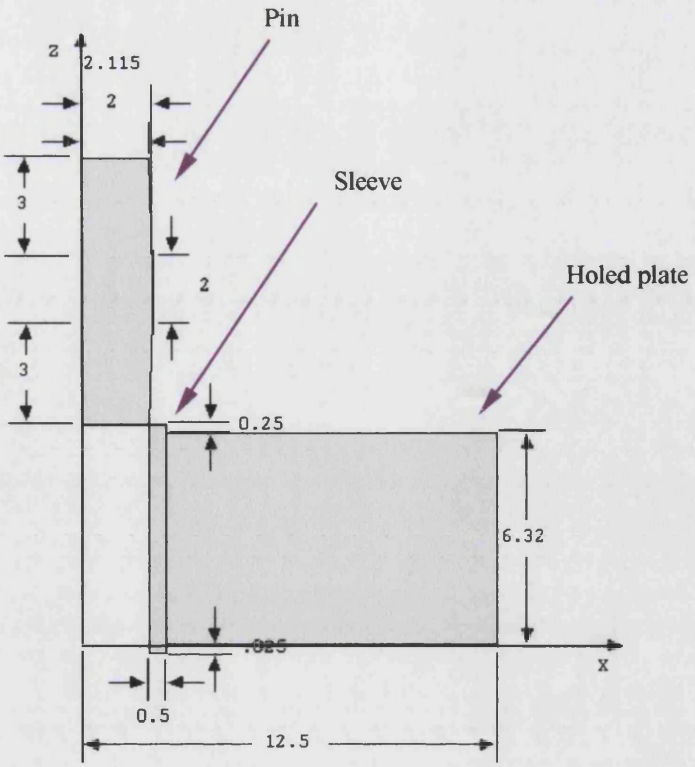

a) Projected surfaces

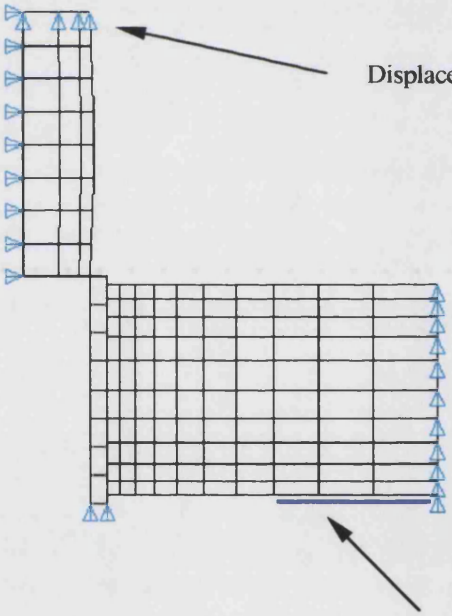

Ground Contact element location simulating contact washer

b) The model mesh

Fig A.2: The axisymetric model of BB (see Chapter 5 and 6 for material properties used in model BB)